Universidade de Aveiro
2022

Diana Andreia Gomes Branco

Estudo da melhoria da lavação de rolhas de cortiça

Study of improvement upon cork stoppers washing

Universidade de Aveiro
2022

Diana Andreia Gomes Branco

Estudo da melhoria da lavação de rolhas de cortiça

Study of improvement upon cork stoppers washing

Dissertação apresentada à Universidade de Aveiro para cumprimento dos requisitos necessários à obtenção do grau de Doutor em Engenharia Química- Especialização de Engenharia de Produtos e Processos Químicos realizada sob a orientação científica do Doutor Dmitry Victorovitch Evtyugin, Professor Associado com Agregação do Departamento de Química da Universidade de Aveiro e com auxílio do coordenador empresarial Doutor Luís Manuel Estevão Cabrita, responsável da Divisão de Engenharia de Produto da Amorim Cork, S.A.

Apoio financeiro do projeto NEWASCORK (POCI-01-0247-FEDER-0340048) financiado pela ANI e cofinanciado pela FEDER e CICECO- Aveiro Instituto de materiais.

Dedico este trabalho à minha família por todo o apoio.

O júri

presidente

Prof. Doutor Carlos Manuel Martins da Costa
professor catedrático da Universidade de Aveiro

vogais

Prof. Doutora Helena Margarida Nunes Pereira
Professora catedrática da Universidade de Lisboa

Prof. Doutora Nereida Maria Abano Cordeiro
Professora associada da Universidade da Madeira

Prof. Doutor Miguel Freire de Albuquerque Ferreira Cabral
professor auxiliar da Universidade do Porto

Prof. Doutor Manuel António Coimbra Rodrigues da Silva
professor associado com agregação da Universidade de Aveiro

Prof. Doutor Dmitry Victorovitch Evtyugin (orientador)
professor associado com agregação da Universidade de Aveiro

agradecimentos

Ao meu orientador na Universidade de Aveiro, o Doutor Dmitry Evtyugin, pela oportunidade, disponibilidade, entusiasmo e orientação científica que demonstrou ao longo de todo este percurso.

Ao meu coorientador na Amorim Cork, S.A., Doutor Luís Cabrita, pela disponibilidade e por todos os conhecimentos transmitidos e debatidos.

À Telma Teixeira pela paciência e disponibilidade prestada em todos os dias de trabalho nas instalação da Amorim Cork, S.A.

Aos meus colegas de laboratório que proporcionaram boa disposição e bons conselhos: Catarina Santiago, Ana Henriques, Fernanda Vieira, Dmitry Evtyugin, Joana Campos, Marina Matos, Sandra Magina, Nuno Gama e Inês Mendes.

Um agradecimento especial a quatro pessoas que conheci durante este período e se revelaram ser amigas sempre presentes e se tornaram indispensáveis por todo o apoio prestado quer a nível profissional, quer a nível pessoal: Ana Henriques, Catarina Santiago, Fernanda Vieira e Ângela Alexandre.

Ao Ivo Azenha, pelo apoio, pela presença e pelo incentivo em querer fazer sempre algo melhor.

Gostaria ainda de agradecer à minha família, aos meus pais, irmãos, tia e sobrinhos pelo constante apoio e presença. Sem eles teria sido bem mais difícil.

Por fim, gostaria de agradecer ao programa compete 2020 pela bolsa no projeto Newashcork (POCI-01-0247-FEDER-0340048) financiado pela ANI e cofinanciado pela FEDER e CICECO- Aveiro Instituto de materiais.

Palavras-chave

Rolhas naturais de cortiça, lavação, peróxido de hidrogénio, ozono, lenhina, metodologia de resposta de superfície, brancura ISO

Resumo

A cortiça é a casca extraída do sobreiro (*Quercus suber* L.), sendo vastamente utilizada em diversos materiais devido às suas propriedades físicas únicas. As rolhas para a indústria vinícola ocupam o maior segmento do mercado da cortiça com cerca de 72%, onde as rolhas naturais ocupam uma posição de destaque com 56% da produção total de rolhas. Os principais desafios nesta área consistem em encontrar formas de melhorar o desempenho das rolhas em aplicações relacionadas com a vinificação e áreas alimentares adjacentes. O conhecimento mais aprofundado dos aspetos fundamentais da composição química da cortiça e das características estruturais dos seus principais componentes em termos do seu comportamento na transformação da cortiça é outro ponto de investigação. A lavação é o principal processo industrial responsável pela desinfecção, aparência visual e desempenho funcional das rolhas.

O principal objetivo desta dissertação, realizada na Universidade de Aveiro em colaboração com a Amorim Cork, S.A., foi estudar o processo de lavação de rolhas de cortiça natural de forma a obter o melhor aspeto visual, uniformidade de cor e desempenho técnico. Foi dada especial atenção às características estruturais dos componentes macromoleculares das rolhas naturais e à sua resposta superficial em relação à lavação. Assim, os componentes isolados da cortiça foram avaliados por métodos de química húmida, espectroscopia GC-MS, FTIR e 1D/2D RMN e difracção por espalhamento de raios-X. A morfologia da rolha natural foi estudada por SEM e a química de superfície por UV-vis DR, FTIR-ATR e espectroscopia Raman confocal. As propriedades da superfície foram avaliadas por profilometria óptica 3D e medição de ângulo de contato. As propriedades ópticas foram avaliadas pela brancura ISO e pelos parâmetros de cor CIElab.

Procedeu-se ao estudo da composição química e das características estruturais dos principais componentes macromoleculares das rolhas naturais (suberina, lenhina, celulose e xilana) e relacionou-se com as suas propriedades superficiais. A anisotropia nas propriedades superficiais e a rugosidade do topo e lateral das rolhas naturais de cortiça foi explicada pela diferença de exposição das camadas da parede celular do felogénio e pelos danos mecânicos ocorridos durante a produção da rolha. As diferenças na composição química da superfície e topologia explicam o maior índice de polaridade do topo que predetermina melhor molhabilidade com água e soluções hidroalcoólicas do que para a lateral da rolha. A lavação, sendo um tratamento agressivo com peróxido de hidrogénio em condições de forte alcalinidade, prejudica as propriedades superficiais das rolhas no que se refere à molhabilidade, que se deve à significativa degradação da suberina na superfície da cortiça. A degradação da superfície durante a lavação deteriora o processamento posterior das rolhas de cortiça e o seu desempenho funcional.

Resumo (continuação)

A otimização da lavação convencional com H_2O_2, a implementação de ozono como agente branqueador de rolhas naturais e a combinação do ozono com a otimização da lavação convencional com H_2O_2 foram propostas com o intuito de melhorar a viabilidade económica e o desempenho das rolhas de cortiça. A otimização da lavação convencional e a implementação do ozono foram realizadas utilizando um desenho de experiências fatorial fracionado e metodologia de resposta de superfície (MRS). As condições das variáveis de processo que maximizam o efeito do ozono na rolha foram escolhidas usando métodos estatísticos (ANOVA, teste de Tukey e teste T de amostras emparelhadas). Os resultados revelaram que duas variáveis da lavação convencional (concentrações de H_2O_2 e NaOH) têm um efeito superior na resposta do que as outras (por exemplo, tempo de oxidação e volume de água de lavagem). Ao aplicar a otimização do modelo numérico com um objetivo de brancura ISO (aprox. 34% ISO), foi possível obter uma melhoria significativa em termos de economia de reagente, com uma redução de 37% para H_2O_2 e 33% para NaOH e água de lavagem, respetivamente. A introdução do ozono como reagente na lavação permitiu o aumento da brancura ISO nas rolhas naturais em cerca 5%, em apenas 15 min com uma degradação mínima da superfície. A combinação de um primeiro estágio de lavação com ozono e um segundo estágio de lavação convencional otimizada com H_2O_2 permitiu a redução adicional do consumo de peróxido de hidrogénio, tempo de oxidação e volume de água de lavagem, mantendo a brancura ISO e desempenho funcional do produto final. Estes processos de lavação otimizados (com e sem tratamento de ozono) revelaram uma melhor preservação da superfície da rolha relacionada com uma menor degradação da suberina, obtendo uma molhabilidade controlada e um melhor desempenho da rolha em relação ao revestimento funcional com parafina e silicone. Por fim, foram avaliados os parâmetros básicos de qualidade aplicadas na indústria (pH, humidade, teor residual de peróxido de hidrogénio, teor de pó, migração de cor, progressão da capilaridade e absorção do vinho pelas rolhas) em rolhas provenientes dos diferentes processos de lavação. Ao comparar os resultados dos parâmetros de qualidade da lavação otimizada com a lavação convencional, verificaram-se resultados semelhantes, com um menor consumo de reagentes, menor tempo de processo e melhor desempenho funcional das rolhas.

Keywords

Natural cork stoppers, reactive washing, hydrogen peroxide, ozone, lignin, response surface methodoly, ISO brightness

Abstract

Cork is the outer bark extracted from the cork oak tree (Quercus suber L.) and is widely used in different materials due to its unique physical properties. Wine stoppers occupy the largest cork market segment with about 72%, where the natural cork stoppers have a distinct position with 56% of the total cork stoppers production. The main challenges in the area consist in finding ways to improve the performance of stoppers in winemaking applications and adjacent food areas. A better understanding of the fundamental aspects of cork chemical composition and structural features of its main components within the context of their behavior in cork processing is another research point to consider. Reactive washing (RW) is the main industrial process responsible for the disinfection, appearance and functional performance of stoppers.

The main objective of this thesis, carried out at the University of Aveiro in collaboration with the Amorim Cork, S.A., was to study reactive washing (RW) process of natural cork stoppers in order to achieve their better appearance, color uniformity and technical performance. Special attention was given to the structural characteristics of the macromolecular components of natural cork stoppers and their surface response to RW. Accordingly, the isolated cork components were evaluated by wet chemistry methods, GC-MS, FTIR and 1D/2DNMR spectroscopy and X-ray scattering diffraction. The natural cork stopper morphology was studied by SEM and the surface chemistry by UV-vis DR, FTIR-ATR and confocal Raman spectroscopy. Surface properties were assessed by 3D optical profilometry and contact angle measurements. The optical properties were evaluated by ISO brightness and CIElab color parameters.

The refinement of the chemical composition and structural characteristics of the main macromolecular components of natural cork stoppers (suberin, lignin, cellulose and xylan) were carried out and related to their surface properties. The anisotropy in the surface properties and the roughness of the top and lateral of natural cork stoppers was explained by the difference in the exposure of the phellogen cell wall layers and as a result of mechanical damage that occurred during the stopper production. The differences in the surface chemical composition and topology explain the higher polarity index of the top surface that predetermines it better wettability with water and hydroalcoholic solutions than the lateral surface of the stopper. . Reactive washing (RW), being an aggressive treatment with hydrogen peroxide under strong alkaline conditions, impairs the surface properties of cork stoppers regarding their wettability, which is due to the significant degradation of suberin on the cork surface. The surface degradation in RW deteriorates further processing of cork stoppers and their functional performance.

Abstract (continuation)

The optimization of the conventional reactive washing with H_2O_2, the implementation of ozone as a bleaching agent for the natural cork stoppers and the combination of ozone treatment and optimized conventional reactive washing with H_2O_2 were proposed to improve the economic feasibility and the quality performance of cork stoppers. The optimization of the conventional reactive washing and the ozone treatment were accomplished using a three fractional factorial design and response surface methodology (RSM). The process variables conditions that maximize the effect of ozone on the stopper were chosen using statistical methods (ANOVA, Tukey test, and paired-samples T-test). The results revealed that two variables of conventional RW (H_2O_2 and NaOH concentrations) have a greater effect on the response than the others (e.g. reaction time and volume of washing water). By applying numerical model optimization with an ISO brightness target (*ca.* 34 %ISO), it was possible to achieve a significant improvement in terms of reagent savings, with a reduction of 37% for H_2O_2, and 33% for NaOH and washing water, respectively. The introduction of ozone as RW reagent allowed the increase of *ca*. 5% ISO brightness of natural cork stoppers within 15 min with minimal degradation of their surface. The combination of a first RW stage with ozone and a second stage of optimized conventional reactive washing with H_2O_2 allowed the further reduction of hydrogen peroxide consumption, oxidation time and washing water volume, while maintaining the final natural stopper brightness and functional performance. This optimized RW processes (with and without ozone treatment) revealed better preservation of the stopper surface from suberin degradation with controlled wettability and improved performance towards functional coating with paraffin and silicone. At last, the basic quality parameters (pH, humidity, residual content of hydrogen peroxide, dust content, color migration, capillarity progression and absorption of wine by the stoppers) commonly used in the industry were evaluated for the cork stoppers from the different reactive washing processes. Similar results were obtained when comparing these quality parameters of the optimized RW with the conventional one, with lower consumption of reagents, less process time and better functional performance of stoppers.

Table of Contents

Abbreviations and Symbols

γ_L	Liquid surface tension
γ_L^d	Dispersive component of liquid surface tension
γ_L^p	Polar component of liquid surface tension
γ_S	Solid surface tension
γ_S^d	Dispersive component of solid surface tension
γ_S^p	Polar component of solid surface tension
θ_0	Corrected contact angle
θ_{app}	Apparent contact angle
^{13}C CP MAS	Carbon cross-polymerization-magic angle spinning
^{13}C NMR	Carbon nuclear magnetic resonance
^{1}H NMR	Hydrogen nuclear magnetic resonance
A	Surface area
Ac	Acetyl groups
AGPs	Arabinogalactan-proteins
ANOVA	Analysis of variance
Araf	Arabinofuranose
A_{smooth}	Nominal Area
C	Carbon
CA	Coniferyl alcohol
COSY	^{1}H-^{1}H Homonuclear correlation spectroscopy
DC	Degree of crystallinity
DCM	Dichloromethane
DF_E	Degrees of freedom of the errors
DF_M	Degrees of freedom of the model
DFRC	Derivatisation followed by reductive cleavage method
DL	Dioxane lignin
DMSO	Dimethyl sulfoxide
DoE	Design of experiments
DR	Diffuse reflectance
DS	Degree of substitution
ECF	Elemental chlorine free
ESI-MS	Electrospray ionisation-mass spectrometry
EtOH	Ethanol
FA	Ferulic acid
FFE	Fractional factorial experiment

FSE	Free surface energy
FTIR	Fourier-transform infrared spectroscopy
FTIR-ATR	Fourier-transform infrared spectroscopy- attenuated total reflection
G	Guaiacyl
GC-MS	Gas chromatography-mass spectrometry
GlcA	D-glucuronic acid
Glcp	Glucopyranosyl unit
H	Hydrogen
H	*p*-hydroxyphenyl
H_0	Null hypothesis
H_1	Alternative hypothesis
HPLC	High-performance liquid chromatography
HSQC	Heteronuclear single quantum coherence spectroscopy
HS-SPME	Headspace-solid phase microextraction
LCS	Lateral of cork stopper
MCL	Milled cork lignin
Me	Methyl ester
MeGlcA	Methyl glucuronic acid
MeOH	Methanol
M_p	Molecular weight of the highest peak
MS_E	Mean squares of the errors
MS_M	Mean squares of the model
M_w	Molecular weight
MWL	Molecular weight distribution
N	Nitrogen
NMR	Nuclear magnetic resonance
NOESY	Nuclear Overhauser effect spectroscopy
O	Oxygen
OCRW	Optimized conventional reactive washing
ORW	Ozone reactive washing
OWRK	Owens-Wendt-Roble-Kaeble model
Pc	*p*-coumaric acid
PO	Permanganate oxidation
Py	Pyrolysis
R^2adj	Adjusted coefficient of determination
R_a	Roughness average
R_p	Parametric value of maximum profile heigh peak

R_v	Parametric value of valley depth
RW	Reactive washing
RW+	Ozone reactive washing plus optimized conventional reactive washing
S	Syringyl
S_a	Arithmetical mean heigh of the surface
S_{dr}	Developed interfacial area ratio
SEC	Size-exclusion chromatography
SEM	Scanning electron microscopy
SEM-EDS	Scanning electron microscopy with energy dispersive spectroscopy
S_p	Parametric value of maximum heigh of peak
SS_E	Some of squares of the errors
SS_M	Some of squares of the model
SS_T	Total some of squares
S_v	Parametric value of valley depth
T	Procyanidins
TCF	Totally chlorine free
TCS	Top of the cork stopper
TMS	Tetramethylsilane
TOCSY	Total correlation spectrocopy
UA	Uronic acids
UV-vis	Ultraviolet-visible
W_a	Adhesion work
wt	Weight
Xylp	Xylopyranosyl unit
Y	Response

Table of Figures

Table of Tables

Chapter 1

INTRODUCTION

Content

1.1. Introduction

Cork is the outer bark extracted from the cork oak tree (*Quercus suber* L.). This tree has a high merismatic capacity allowing the periodical extraction of cork [1–3]. Cork is widely used to produce materials for food and composite industries due to its unique physical properties such as impermeability to liquids and gases, elasticity and resilience, good heat and acoustic insulation, and resistance to disease and chemical and microbial attack [4–6]. These amazing properties are due to an unusual combination of chemical composition and morphology of cork cells.

From the cork products point of view, cork stoppers for wine bottling occupy the largest market segment with about 72% [7,8]. At a national level, Amorim Cork, S.A: is the largest cork producer, being responsible for the production and distribution of a wide range of stoppers, natural and technical, for all kinds of wines, champagne, and spiritual beverages, meanwhile, the natural cork stoppers have a distinct position with 56% of the total cork stoppers production [7]. Natural cork stoppers are a natural product selected by wine producers to seal wines, liquors, and other types of generous beverages. Due to the wine market continuous growing, the demand for high-quality natural cork stoppers is growing too, which makes this industry more demanding. Accordingly, the main challenges consist in finding ways to improve the performance of stoppers in winemaking applications and adjacent food areas. A better understanding of the fundamental aspects of cork chemical composition and structural features of its main components within the context of their behavior in cork processing is another research point to consider. All these topics are in the focus of this work that was developed within the research and development collaboration between the University of Aveiro and Amorim Cork, S.A. under the scope of Portugal 2020 project "Newashcork-Novas abordagens na desinfeção e branqueamento de rolhas de cortiça".

From the cork bark until the natural cork stopper, this material has to go through several industrial steps where reactive washing (RW) plays an important role in disinfection and the final appearance of the stopper. RW is a treatment with hydrogen peroxide under strong alkaline conditions and increased temperature. All reagents are of high-grade quality according to food safety requirements, whose costs are remarkably superior to corresponding ordinary quality technical products. The RW leads to changes in the surface of the natural cork stopper, which in turn may affect their subsequent receptivity towards food-grade paraffin, silicone, and other functional coatings [9,10], which are essential in the sealing and extractions properties of the natural cork stoppers [10,11]. Thus, the overload of RW reagents is prejudicial for economic reasons but also affects the consumption properties of cork stoppers and must be tailored.

Similar to other industries, an effective and sustainable development is in the focus of natural cork stoppers producers such as Amorim Cork, S.A, besides accomplishing a high standard pattern

of quality and performance. Hence, a better understanding of the fundamentals of cork stoppers behavior in reactive washing currently applied in the industry, its optimization, and the implementation of new alternative ecologically agent for the natural cork stoppers treatment are essential goals to meet the market demands and improve the industrial competitiveness.

1.2. Contextualization, objectives, and the structure of the thesis

The main goals of this work were related to the study on the reactive washing of natural cork stoppers aiming to contribute both to the fundamental and applied aspects of this process. Particular attention was paid to the better understanding of structural features of cork components in natural stoppers because the commonly reported data on cork are related essentially to the cork planks [4–6,12–15].

In addition, practically no information is available on the surface characteristics of natural stoppers in relation to the reactive washing, and further response during coating with functional formulations (food-grade paraffin, silicone, among others). No clear approaches are available for the optimization of reactive washing. There is no knowledge of the response of cork stoppers to ozone treatment, already widely used as a bleaching agent for the cellulosic pulps [16,17], textile cotton [18–20], and for water disinfection purposes [21,22].

Accordingly, the main objectives of this thesis were as follows:

1. Refinement of the structural features of cork macromolecular components in natural cork stoppers, also with respect to their exposure stopper's surface.
2. The study of the surface properties of natural cork stoppers and their changes during reactive washing.
3. Critical analysis and optimization of the conventional reactive washing.
4. Evaluation of ozone as a new treatment agent for the reactive washing and the development of the reactive washing process of natural cork stoppers with ozone.

Hence, this thesis is divided into nine chapters in order to meet all the proposed objectives. In **Chapter 1** is provided a general introduction to the context of this thesis and is outlined the main goals of this work. **Chapter 2** reviews the morphology, chemical composition, and industrial processing of cork, with emphasis on the reactive washing of natural cork stoppers. In this chapter is also described the conventional reactive washing with hydrogen peroxide and is presented ozone as an alternative bleaching agent for the reactive washing of natural cork stoppers.

Chapter 3 deals with the chemical composition of the natural cork stoppers, where the structural features of the macromolecular components of the natural cork stoppers (suberin, lignin cellulose, and hemicelluloses) were analyzed. In **Chapter 4** is studied the changes in the surface characteristics of natural cork stoppers in relation to the conventional reactive washing with hydrogen peroxide under strong alkaline conditions and increased temperature.

Chapter 5 describes the optimization of the conventional reactive washing employing fractional factorial design and response surface methodology (RSM). **Chapter 6** is devoted to the study of the

implementation of ozone as a bleaching agent for the reactive washing in natural cork stoppers, and the analysis of the surface characteristics of the stopper after the ozone treatment.

Chapter 7 combines the ozone reactive washing with the conventional reactive washing with hydrogen peroxide that is optimized using the fractional factorial design and response surface methodology (RSM). In **Chapter 8** is disclosed the study of the surface of the natural cork stoppers that had the different optimized reactive washing processes, evaluating the changes provoked by each process.

Chapter 9 handles the industrial quality tests that were performed in the natural cork stoppers from the different optimized reactive washings. Finally, in **Chapter 10** the main conclusions of the work are presented, together with some perspectives for future work.

1.3. References

[1] S.P. Silva, M.A. Sabino, E.M. Fernandes, V.M. Correlo, L.F. Boesel, R.L. Reis, Cork: properties, capabilities and applications, Int. Mater. Rev. 50 (2005) 345–365. https://doi.org/10.1179/174328005X41168.

[2] A. Costa, H. Pereira, A. Oliveira, Variability of radial growth in cork oak adult trees under cork production, For. Ecol. Manage. 175 (2003) 239–246. https://doi.org/10.1016/S0378-1127(02)00145-7.

[3] A. Caritat, M. Molinas, E. Gutierrez, Annual cork-ring width variability of *Quercus suber* L. in relation to temperature and precipitation (Extremadura, southwestern Spain), For. Ecol. Manage. 86 (1996) 113–120. https://doi.org/10.1016/S0378-1127(96)03787-5.

[4] H. Pereira, Variability of the chemical composition of cork, BioResources. 8 (2013) 2246–2256. https://doi.org/10.15376/biores.8.2.2246-2256.

[5] H. Pereira, Chemical composition and variability of cork from *Quercus suber* L., Wood Sci. Technol. 22 (1988) 211–218. https://doi.org/10.1007/BF00386015.

[6] E. Conde, E. Cadahía, M.C. García-Vallejo, J.R. González-Adrados, Chemical characterization of reproduction cork from spanish *Quercus suber*, J. Wood Chem. Technol. 18 (1998) 447–469. https://doi.org/10.1080/02773819809349592.

[7] APCOR, APCOR's Cork Yearbook 2020, 2020.

[8] APCOR – Estatísticas, (n.d.). http://www.apcor.pt/media-center/estatisticas/ (accessed September 10, 2021).

[9] D.G. Branco, C.A. Santiago, F.J. Oliveira, L. Cabrita, D. V Evtuguin, Surface properties of cork in relation to reactive washing, Colloids Surfaces A Physicochem. Eng. Asp. 624 (2021). https://doi.org/10.1016/j.colsurfa.2021.126762.

[10] J.R. Gonzalez-Adrados, M.C. Garcia-Vallejo, M.J. Caceres-Esteban, J.L. Garcia De Ceca, F. Gonzalez-Hernandez, R. Calvo-Haro, Control by ATR-FTIR of surface treatment of cork stoppers and its effect on their mechanical performance, Wood Sci. Technol. 46 (2012) 349–360. https://doi.org/10.1007/s00226-011-0403-5.

[11] C. Ortega-Fernández, J.R. González-Adrados, M.C. García-Vallejo, R. Calvo-Haro, M.J. Cáceres-Esteban, Characterization of surface treatments of cork stoppers by FTIR-ATR, J. Agric. Food Chem. 54 (2006) 4932–4936. https://doi.org/10.1021/jf0529823.

[12] H. Pereira, Cork : Biology, production and uses, 1st ed., Elsevier B.V., Lisboa, 2007.

[13] H. Pereira, Studies on the chemical composition of virgin and reproduction cork of Quercus suber L ., An. Do Inst. Super. Agron. 25 (1981) 17–25.

[14] P.J. Holloway, The composition of suberin from the corks of *Quercus suber* L. and *Betula*

pendula roth, Chem. Phys. Lipids. 9 (1972) 158–170. https://doi.org/10.1016/0009-3084(72)90011-4.

[15] N. Parameswaran, W. Liese, H. Günzerodt, Characterization of wetcork in *Quercus suber* L., Holzforschung. 35 (1981) 195–199. https://doi.org/10.1515/hfsg.1981.35.4.195.

[16] A. Seisto, K. Poppius-Levlin, A. Fuhrmann, Effect of ozone bleaching on the fibre properties of pine and birch kraft pulp, Cellul. Pulps, Fibres Mater. (2000) 137–147. https://doi.org/10.1533/9781845698546.137.

[17] N.A. Mamleeva, S.A. Autlov, N.G. Bazarnova, V. V. Lunin, Delignification of softwood by ozonation, Pure Appl. Chem. 81 (2009) 2081–2091. https://doi.org/10.1351/PAC-CON-08-10-11.

[18] M. Prabaharan, R.C. Nayar, N.S. Kumar, J.V. Rao, A study on the advanced oxidation of a cotton fabric by ozone, Color. Technol. 116 (2000) 83–86. https://doi.org/10.1111/j.1478-4408.2000.tb00024.x.

[19] F. Arooj, N. Ahmad, I.A. Shaikh, M.N. Chaudhry, Application of ozone in cotton bleaching with multiple reuse of a water bath, Text. Res. J. 84 (2013) 527–538. https://doi.org/10.1177/0040517513499429.

[20] M. Prabaharan, J.V. Rao, Study on ozone bleaching of cotton fabric-process optimisation, dyeing and finishing properties, Color. Technol. 117 (2001) 98–103. https://doi.org/10.1111/j.1478-4408.2001.tb00342.x.

[21] W. Ding, W. Jin, S. Cao, X. Zhou, C. Wang, Q. Jiang, H. Huang, R. Tu, S. Han, Q. Wang, Ozone disinfection of chlorine-resistant bacteria in drinking water, Water Res. 160 (2019) 339–349. https://doi.org/10.1016/j.watres.2019.05.014.

[22] R. Chand, D.H. Bremner, K.C. Namkung, P.J. Collier, P.R. Gogate, Water disinfection using the novel approach of ozone and a liquid whistle reactor, Biochem. Eng. J. 35 (2007) 357–364. https://doi.org/10.1016/j.bej.2007.01.032.

Chapter 2

BIBLIOGRAPHY REVIEW

CORK: MORPHOLOGY, COMPOSITION, AND INDUSTRIAL PROCESSING

Contents

2.1. Cork origin

Cork material is 100% natural, reusable, recyclable, and sustainable [1]. Cork is the outer bark of the cork oak tree (*Quercus suber* L.), which is stripped with a periodicity of 9/10 years, according to the growth conditions and geographical area traditions [2]. This period allows the tree to produce cork with enough thickness for industrial processing. In Portugal, cork extraction is regulated by the law decree Nº169/2001 [3]. *Quercus suber* L. has, on average, a longevity of 170 to 200 years, which corresponds to about 17 stripping's [4].

Quercus suber L. is a singular tree that has existed for more than 60 million years, it requires water availability, sunlight, and mild temperatures being predominantly present in the western Mediterranean (Portugal, Spain, southern France, and part of Italy), North of Africa and China [5–8]. Europe contains almost 67% of the total production area and manufactures more than 80% of worldwide cork [9–12]. Portugal takes lead concerning the global cork oak tree area (denominated "*montado*") with about 34% which corresponds to an area of 720 thousand hectares representing approximately 22% of the national forest [12,13].

Cork is extracted from the trunk and branches of the cork oak tree, in the form of large convex planks, very light and still moist from the sap of the tree. The value of cork for the industry depends on two factors: the caliber of the plank, which is related to the annual growth of cork, and the cork quality, which covers the porosity given by the lenticular channels and biotic or abiotic defects [14–16].

Cork can be divided into virgin, secondary, and reproduction cork (denominated "*amadia*"). Virgin cork is the cork from the first stripping (denominated by "*desbóia*"), which is made when the tree reaches 25 years old and has a perimeter of 70 cm when measured 1.3 m from the ground [3,17,18]. This cork has an extremely irregular outer surface and undesired hardness to produce natural cork stoppers, being used for other applications such as floors, insulation products, technical stoppers, etc. Secondary cork, called "*secundeira*", comes from the second stripping and, despite having a more regular and less stiff structure, it still is unsuitable to produce natural cork stoppers possessing similar uses to those of virgin cork. It is only after the third stripping that the cork, reproduction cork, has enough quality for the production of natural cork stoppers [3,9,19].

The consecutive cork debarking from the same tree without injuring the tree allows the sustainable manufacture of products with high added value maintaining the intrinsic characteristics of the raw material, cork. The fact that no cork oak tree is cut is very interesting in terms of economic and social sustainability. In fact, *Quercus suber* L. tree is a protected species, being forbidden its cut.

2.2. Cork morphology

2.2.1. Macroscopic structure

Cork has a brownish homogeneous aspect, with growth rings along with its thickness, distinguished by different cell dimensions and cell wall thickness, formed either in Spring/Summer or Autumn/Winter [8,9]. When the cork oak undergoes stripping, the outer part of the tree, the bark, is exposed. This, in turn, is pushed by the successive layers of new cells formed externally (phellem) by the cork oak's phellogen and, in a smaller quantity, cells of phelloderm, formed into the cork oak, giving rise to a suberous tissue called cork [9,20].

The newly formed cells still do not have the final dimensions and, thus, they undergo growth in the protoplasm (inside the cell), which implies a continuous expansion of the phellogenic tissue and, consequently, the diameter of the tree. Phellogen activity is higher in the 2-3 years immediately after stripping, decreasing its activity until the next stripping [6,9].

The scrape (denominated "*raspa*"), which forms the outer layer of cork, dries, contracts, and hardens, cracking due to the increase in the outer perimeter in relation to the inner perimeter, as a result of the growth. Virgin cork does not show scrape, as this is the thickest layer present in the suberous tissue, with an irregular dark brown appearance [21].

The annual addition of layers causes a lenticular evolution along the radial direction, thus forming lenticular channels, these are channels/pores that make contact between the environment and the interior of the tree [16]. Figure 2.1 shows what was previously described, as well as the different components in an axial section of an adult cork oak.

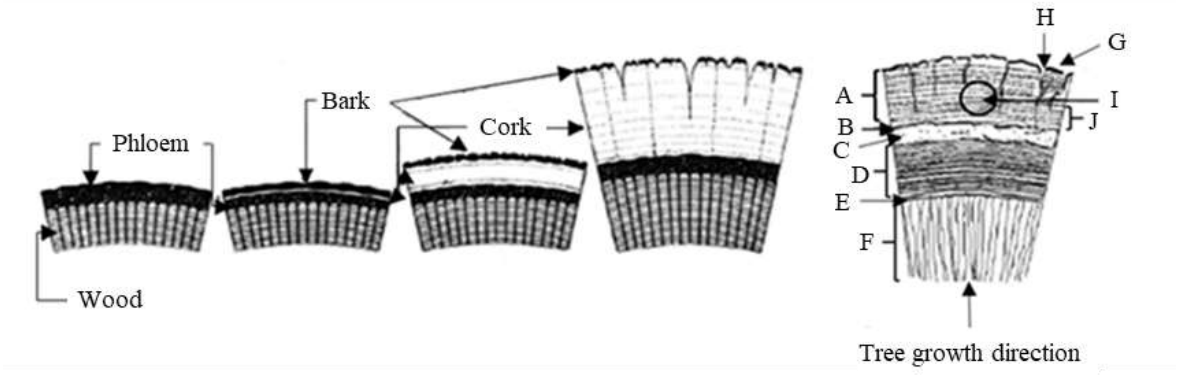

Figure 2.1- Schematic representation of axial section growth in cork oak tree. (A) cork (suberose tissue); (B) subero-phellogenic change; (C) phellogen; (D) phloem; (E) cambium; (F) wood; (G) bark; (H) lenticular channels; (I) area for stopper production; (J) annual growth rings [9,14,21].

2.2.2. Microscopic structure

Cork is defined as a homogeneous tissue made up of thin-walled cells grouped in a characteristic alveolar structure, resembling a honeycomb, usually without intercellular space. The cells can be described as rectangular prisms, placed parallel in the radial direction of the tree (Figure 2.2) [9,20,22].

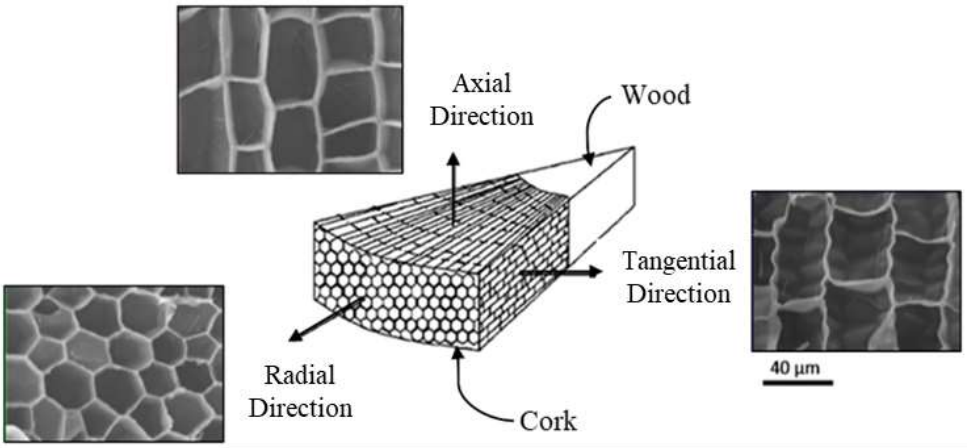

Figure 2.2- Schematic representation of the cell layout in the cork growth section and the respective scanning electronic microscopy images [9,163,164].

In the tangential direction, the formation of new cells by the phellogen occurs through cellular division, while along the radial direction there is an elongation of them, causing the successive increase in the diameter of the cork oak [14].

On average, one cork cell is between 30 and 40 µm wide and 35 to 45 µm high, with each cubic centimeter of cork containing about 40 million cells arranged in perpendicular rows to the trunk of the cork oak, in this way, a natural cork stopper has approximately 800 million cells [4,21].

Each annual ring comprises 50 to 200 cell layers wide (1-6 mm), in which tissue growth is less pronounced during Autumn/Winter and increases during Spring/Summer, with growth rings being observed by the distinct cells with different sizes and thickness, whether formed in one season or another [6,21]. The cells communicate with each other by microchannels, called plasmodesms (cross sectional diameter of 100 nm), that cross the cell wall [21,23].

Cork cell walls are constituted by a structural base of suberin, lignin, cellulose, hemicelluloses and polyphenols, waxes, and extractives. Cork cells walls have three layers: a thin layer of cellulose and hemicelluloses, that line the cell cavities corresponding to the tertiary wall, a thick secondary cell wall composed alternating between suberin and waxes that provide impermeability to the cell, and a lignified medium layer, called the middle lamella or internal primary wall, that gives the rigidity and stiffness [9,11,14,17,24]. However, this scheme for the cell wall appears somewhat incompatible

with the extent of lignification found for cork, so it can be speculated that the lignin and the suberin macromolecules can be paired within the secondary wall assembly [17,23,25]. The different layers specified can be seen in Figure 2.3.

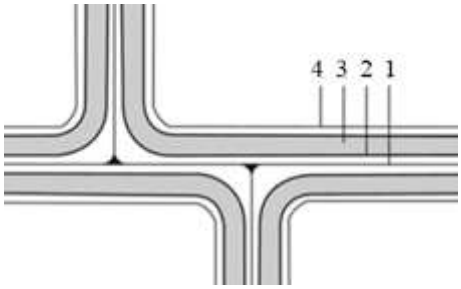

Figure 2.3- Schematic representation of cork cell walls: 1- Medium lamella; 2- Primary wall; 3- Secondary wall; 4- Tertiary wall [14].

2.3. Cork chemical composition

The cork chemical composition has been widely studied over the past years by different scientists, however, the structural features of its components are far to be completely disclosed. It has already been proven that the chemical composition of cork varies significantly and depends on too many factors such as geographic position, climate, soil conditions, genetic origin, tree dimensions, age (virgin or reproduction), and growth conditions [9,26]. Even in the same tree, depending on the collected sample location, the chemical composition may have significant variations [17].

Cork cells are composed of two types of components: structural and non-structural, that are subdivided according to the classification presented in Figure 2.4.

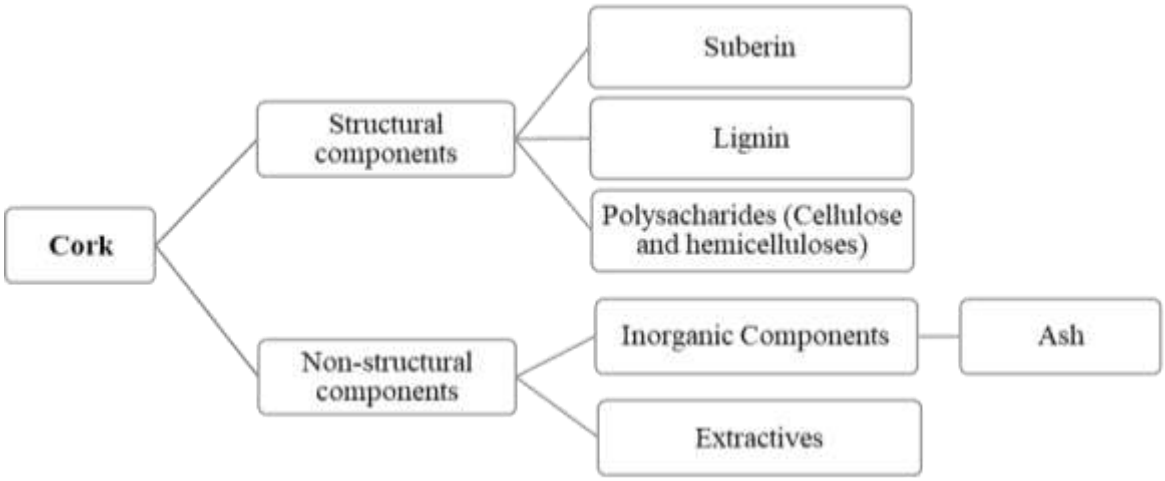

Figure 2.4- Cork chemical composition.

The structural components are macromolecules of a polymeric nature, and they provide support and rigidity to the cell wall, these components are molecules whose removal is only possible through chemical reactions that transform them into smaller units, thus allowing them to become soluble and

more easily extracted. The non-structural components are organic compounds of low molecular weight, which can be solubilized using appropriate solvents [14].

The structural components are the most representative compounds in the cell wall, where suberin plays the greatest role, followed by lignin and polysaccharides (cellulose and hemicelluloses). In the non-structural components, the extractives have a significant amount and comprise mostly lipophilic and polyphenolic compounds. Despite the non-structural components being in minor quantity in relation to the structural components, they are unbounded or loosely bounded to the cell wall, being easily extracted when in contact with ethanol solutions, since the most important use of cork is as wine closure, these compounds must be taken in consideration. These compounds may alter the organoleptic properties of wine such as color, flavor, astringency, and bitterness, and also, they have an important role in wine oxidation processes [27,28].

A detailed study of the chemical composition of cork is imperative to understand how cork materials behave in the face of chemical changes during their processing. As already mentioned, depending on the cork sample analyzed, the chemical components on the suberous tissue vary, giving rise to the appearance of different proposals for the chemical composition of cork, as shown in Table 2.1.

Table 2.1- Results of quantitative analysis of chemical composition of cork from *Quercus suber* L.

Cork age	Reference	Suberin	Lignin	Polysaccharides	Extractives	Ash
Virgin cork	[29]	45.3	21.1	12.8	19.2	1.2
	[17]	35.2	22.4	21.3	16.9	0.91
Reproduction cork	[30]	37.8	14.8	-	15.8	-
	[29]	34.1	26.3	26.1	13.7	2.6
	[31]	33.2	13.1	6.3	24.0	-
	[17]	39.4	23.0	19.9	14.2	1.2
	[32]	60.9[1]	22.7	25.8	-	-
	[14]	~50	~20-25	~20	~14-18	-
	[5]	42.8	22.0	-	16.2	-

Table 2.1 shows that virgin cork, on average, has higher percentages of extractives and suberin and less lignin, polysaccharides, and ash than reproduction cork. The reduction in suberin in reproduction cork can be related to a decrease in the thickness of the secondary wall, after the first stripping [29].

According to Table 2.1 it can be seen that the main components of cork are suberin and lignin, being these two polymers responsible for the major properties of cork cells such as resistance to

[1] Suberin content is overvalued by about 20% due to the high difficulty in eliminating the solvent in the rotary evaporator [32].

compression, high elasticity and relaxation properties, permeation and diffusion of liquids and gases through cork [5,17,32]. Cellulose comprises about half of the total polysaccharides of cork, which implies that cellulose does not play such a leading role in defining cell wall chemistry and properties of cork, as it does in the wood [17]. On the other hand, hemicelluloses, especially xylans, due to their relatively high percentage, have more influence on cork properties than in other lignocellulose materials [32].

2.3.1. Suberin

Suberin is the macromolecular compound present in cork in a highest percentage (Table 2.1). Suberin is a biopolymer, that can be found in underground plants, periderms, and the bark of several tree species [14,33]. Suberin is placed in the cell walls and plays a fundamental role as a protective barrier between the environment and the core of the tree, so the distribution of suberin in the cell wall suggests that its formation occurs whenever and where there is a need to reduce the transport of water, dissolved salts, and gases towards the tissues of the tree [34]. Electron microscopic analysis shows that suberized layers in the cell wall have a characteristic lamellar appearance, with light and dark bands, most probably due to wax layers intercalated with suberin polymer [35,36].

Suberin is responsible for properties such as elasticity, low density, impermeability to liquids and gases, low thermal and sound conductivity, among others [37]. This polymer is believed to be characterized by the presence of two distinct domains: an aliphatic domain and a phenolic or aromatic domain that are covalently linked, whose compositions are not yet fully disclosed due to the high complexity in the extraction of this compound from the cork structure [38].

Suberin in its natural state is insoluble in every solvent and it's only possible to solubilize it after its depolymerization. Depolymerization can be carried out by three different methodologies: alkaline hydrolysis, transesterification with BF_3 or sodium methoxide with methanol; and hydrogenolysis with $LiAlD_4$ [32–35]. These methodologies despite not having the ability to isolate suberin in its purest state are considered as quantitative methods as they allow the depolymerization of the aliphatic component and in turn the solubilization of its products. The method of isolation and quantification of suberin will impact the results of suberin obtained [41]. Gas chromatography coupled with mass spectrometry (GC-MS) has been the technique most used for the analysis of monomer composition of suberin, after the adequate chemical derivatization of suberin cleavage products. Table 2.2 compiles the chemical composition of cork suberin from different previous studies.

Table 2.2- Chemical composition of cork suberin from *Quercus suber* L.

Reference	[42]	[43]	[44]	[45]	[41]	[46]	[47]
1-alkanols	0.0-2.2	4.7-8.3	1.3-2.4	0.4	1.8-6.1	4.2	1.8
C16:0	-	0.1-0.6	-	-	0.1-0.9	0.3	-
C18:1 (9)	-	0.2-0.3	-	Trace	-	-	-
C18:0	-	0.3-0.7	-	-	-	-	-
C20:0	-	0.4-1.3	-	0.1	0.3-0.4	0.3	0.1
C22:0	0.0-1.7	1.8-5.1	0.6-1.2	0.2	1.4-4.2	3.1	0.7
C24:0	0.0-1.5	1.0-1.6	0.7-1.2	0.1	0.0-0.6	0.5	0.8
C26:0	-	0.0-0.5	-	-	-	-	0.2
1-alkanoic acids	2.5-8.4	2.6-10.1	3.9-5.6	1.1	1.6-7.0	5.4	3.3
C16:0	-	0.2-0.4	-	Trace	0.5-3.3	2.3	0.1
C18:0	-	0.0-0.2	1.1-2.0	Trace	-	-	Trace
C18:1 (9)	-	0.0-0.3	-	-	-	-	Trace
C18:2 (9,12)	-	0.0-0.1	-	-	-	-	-
C20:0	-	0.0-0.3	-	0.1	0.0-0.5	0.3	-
C22:0	1.8-6.3	1.3-5.2	1.6-2.0	0.9	0.8-2.3	1.8	2.1
C24:0	0.5-4.1	1.1-3.6	1.2-1.6	-	0.3-0.9	1.0	1.0
ω-hydroxyalkanoic acids	0.0-36.1	50.8-74.1	37.4-46.6	26.3	37.0-57.1	37.3	64.2
C16:0 16-OH	0.0-0.7	0.4-1.1	0.3-0.7	0.4	0.5-0.8	0.7	1.2
C16:0 di-OH	-	0.9-2.6	0.8-1.5	-	-	-	-
C18:0 18-OH	-	0.0-0.3	0.5-0.7	0.1	0.3-0.5	0.5	Trace
C18:1 (9) 18-OH	0.0-12.8	2.6-8.8	5.2-6.3	5.4	8.1-11.5	8.4	17.5
C18:0 9,10-epoxy, 18-OH	0.0-5.5	0.7-1.4	-	7.3	1.2-3.1	2.7	-
C18:1 di-OH	-	0.3-1.3	-	-	-	-	-
C18:0 9, 18 -OH, 10-OCH_3	-	0.8-3.8	7.0-8.0	2.2	-	-	-
C18:0 9, 10, 18-OH	-	3.0-12.7	6.6-7.4	-	7.7-11.8	9.5	10.3
C18:0 9,10-epoxy + 9-oxo	-	0.5-0.9	-	-	-	-	5.8
C18:0 9-OH, 10-OCH_3	-	0.5-0.9	-	-	-	-	-
C18:0 9, 10-OH	-	5.0-13.0	-	-	-	-	-
C20:0 20-OH	0.0-0.7	1.1-2.5	0.7-1.6	0.5	0.8-0.9	1.0	-
C20:1 (10) 20-OH	-	0.2-1.2	-	-	1.0-2.3	-	-
C20:0 di-OH	-	0.9-10.1	-	-	-	-	-
C21:0 21-OH	-	0.0-0.3	-	-	-	-	-
C22:0 22-OH	0.0-17.4	14.5-16.3	13.7-17.1	7.9	11.0-12.4	12.2	24.8
C22:1 (11) 22-OH	-	-	-	-	1.5-1.6	-	-
C23:0 23-OH	-	0.0-0.2	-	2.4	-	-	-
C24:0 24-OH	0.0-1.6	4.2-6.0	2.6-3.3	-	2.4-4.4	0.2	4.3
C26:0 26-OH	-		-	0.1	2.5-7.8	2.1	Trace
α, ω- dicarboxylic acids	53.3-91.6	17.3-29.4	45.4-54.5	45.5	10.9-21.6	14.9	20.6
C16:0	2.2-3.3	1.6-2.9	1.9-2.5	2.0	0.3-0.6	0.7	1.8
C18:0	-	0.0-1.0	-	0.5	-	-	-
C18:1 (9)	7.7-13.8	3.6-50.0	6.6-7.5	6.2	1.5-2.4	2.3	4.9
C18:0 9,10-epoxy	37.8-46.6	-	-	22.9	1.0-4.4	2.9	3.6
C18:0 9, 10-OH	0.0-2.5	-	6.4-8.0	7.7	5.4-7.6	6.8	6.8
C18:0 9-OH, 10-OCH_3	-	-	18.4-21.5	-	-	-	-
C20:0	1.1-3.5	2.6-3.6	1.0-1.9	1.0	2.5-6.2	2.0	0.5

Reference	[42]	[43]	[44]	[45]	[41]	[46]	[47]
α, ω- dicarboxylic acids							
C20:1	-	0.3-5.0	-	-	-	-	Trace
C20:0 9,10-OH	-	-	0.5-1.2	-	-	-	-
C22:0	1.7-22.4	7.1-10.4	10.0-10.6	4.5	-	-	2.7
C24:0	0.3-2.0	1.1-2.5	0.6-1.3	0.7	0.2-0.4	0.2	0.2
Aromatic	0.0-3.9	0.0-1.3	0.4-1.1	1.1	5.3-9.1	5.1	4.5
Ferulic acid	0.0-3.9	0.0-1.3	0.4-1.1	0.5	5.3-9.1	5.1	4.5
Quinic acid	-	-	-	0.1	-	-	-
Coniferyl alcohol	-	-	-	0.3	-	-	-
Vanillin	-	-	-	0.1	-	-	-
3,4- di- hydroxybenzoic acid	-	-	-	0.1	-	-	-
Glycerol	-	-	-	14.2	-	-	4.3
Unidentified	0.0-2.1	0.0-1.6	-	10.0	-	19.9	-

Undertaken studies (Table 2.2) demonstrate that the aliphatic component of suberin is composed mainly of long-chain (C16-C26) fatty acids ω-hidróxi and α, ω-dicarboxylic and, in less extent carboxylic acids and aliphatic alcohols, while in the aromatic domain it is possible to identify compounds such as glycerol and ferulic acid [41–47]. However, how the aliphatic components are linked together still is a matter of study, considering the type of monomers existing on suberin, a linear polymer composed of ω-hydroxyl acids can be made. Still, one can predict that probably linear polymers cannot produce a stable three-dimensional structure with a fine and regular lamellation [48,49].

Studies show no free carboxylic groups detected which imply that the alkanoic acids, with only one functional group, have to be esterified to the polymer in the terminal position and the α, ω-dicarboxylic acids must be esterified in suberin by both end groups [42].

Gas chromatography-mass spectrometry (GC-MS) analysis allowed the better understanding on the potential linking groups that led to the concept of a linear interesterification of the aliphatic monomers, further linked to the abundant aromatic fraction of suberin, where ferulic acid is the compound most frequently detected [50,51]. Ferulic acid is believed to be esterified to the acyl groups in suberin, giving some indication on the linking points between the aliphatic monomers and the polymeric phenolics in the cell wall [42,45,51]. Whether ferulic acid can be a constituent of suberin or not has been a subject of controversy. In some of the reported studies of cork extracts removed by methanolysis, ferulic acid was found as the only aromatic compound. This would indicate that this acid is associated directly with the fatty acids in the suberin polymer [40]. Besides ferulic acid, glycerol was also detected in suberin depolymerization extracts and it is considered that plays an important role as a key suberin building block.

Most of the suberinic acid monomers were found esterified to middle and terminal carbon positions of glycerol, thus indicating that glyceryl-acyl linkages are a general structural feature in the suberin [51,52]. Moreover, the number of glycerol hydroxyls is enough to esterify most of the available carboxylic groups from aliphatic acid monomers demonstrating that α, ω- dicarboxylic acids may act as the bridges between different glycerol molecules (and of ω-hydroxy alkanoic acids) allowing the cross-linking of the polymer [42,53,54]. Also, glycerol allows the covalent linking between aliphatic and aromatic domains and linkages among the structural components in the cell wall: suberin with carbohydrate and/or lignin [55,56]. Figure 2.5 demonstrates the model proposed by Bernards obtained through the suberin present in a potato periderm.

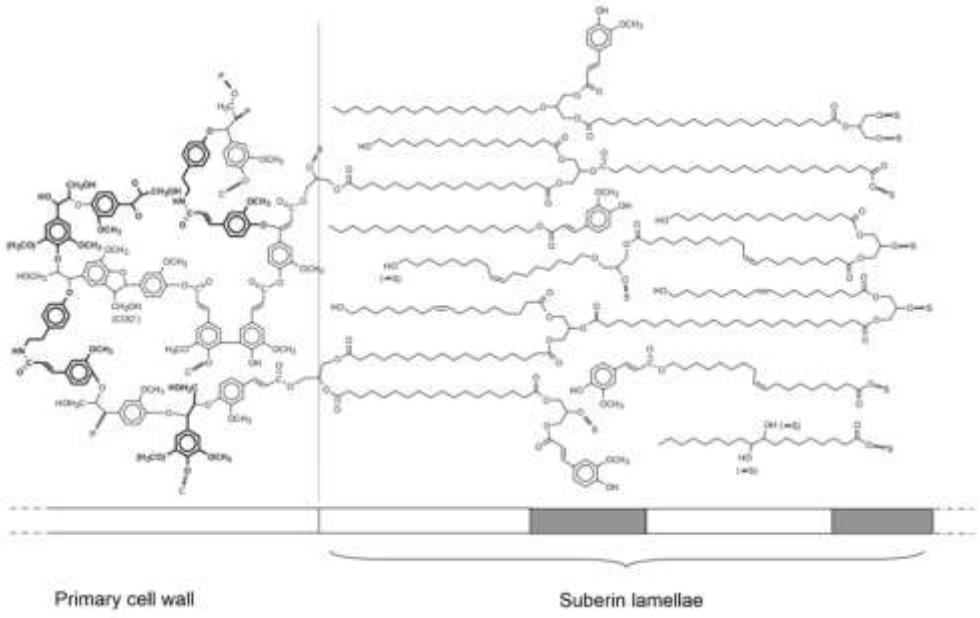

Figure 2.5- Model of macromolecular structure of suberin proposed by Bernards [38]. Connections are to the following: C, carbohydrate; P, phenolic; S, suberin.

According to features in Figure 2.5, it appears that the macromolecular proposal of suberin consists of a cross-linked polyester, composed of aliphatic and aromatic covalently linked to a phenolic matrix. In this way, there are three types of monomers: glycerol, long-chain aliphatic compounds, and aromatic compounds.

2.3.2. Lignin

Lignin is a structural compound of aromatic origin and the second most abundant in suberous tissue. Lignin together with suberin contribute to the physical behavior of the cells, since lignin is a rigid and hard polymer with strong covalent bonds in a 3D-network, it is responsible for the mechanical support and rigidity of the cork cell wall, being these two polymers responsible for the

compression resistance and dimensional recovery after stress relief [5,14,17,57]. Lignin is not an exclusive component of cork, being present in most vascular plants.

Lignin is a non-regular cross-linked heteropolymer, formed by the polymerization of three phenylpropane monomers, the *p*-hydroxy cinnamyl alcohols (*p*-coumaryl, coniferyl, and sinapyl alcohols), which vary in the degree of methoxyl substitution in C3 and C5 of the aromatic ring (Figure 2.6) [14,23,58]. The different chemical types of lignins are based on the ratio (H:G:S) of the aromatic rings of these alcohols that are named respectively *p*-hydroxyphenyl (H), guaiacyl or 3-methoxy-4-hydroxyphenyl (G), and syringyl or 3,5-dimethoxy-4-hydroxyphenyl (S).

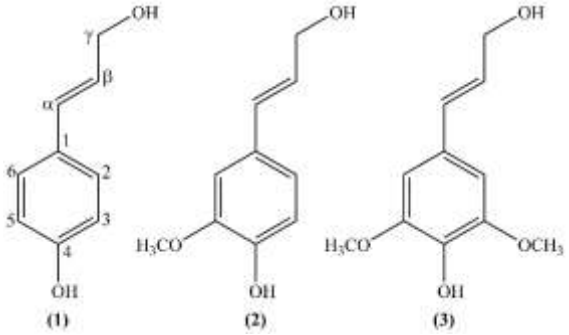

Figure 2.6- Lignin precursor alcohols. *p*-coumaryl alcohol (1), coniferyl alcohol (2), and sinapyl alcohol (3).

The polymerization between the three monomers is initiated via enzymatic dehydrogenation of the alcohol group that leads to the formation of phenoxy radicals [23]. These are resonance stabilized structures with a radical character on the phenolic oxygen, but also on the ring carbons 1, 3, and 5, and on the β carbon of the aliphatic chain, that through a random coupling reaction form dimeric structures (dilignols) [14]. Depending on the positions reactivity, the inter-unit linkages in the polymer can be as follows: β-O-4', α-O-4', β-β', β-5', 5-5', 4-O-5' or β-1', among others (Figure 2.7) [59].

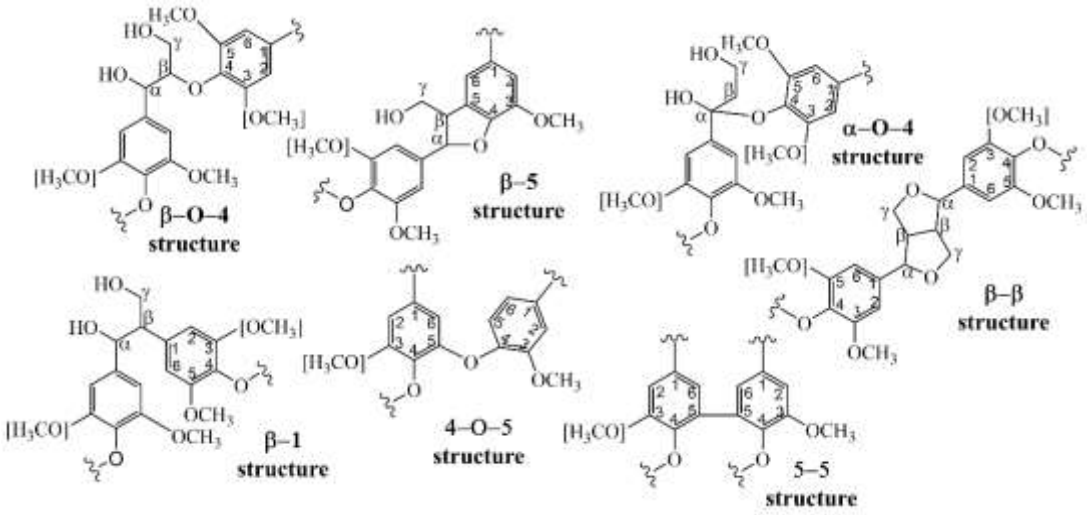

Figure 2.7- Main inter-unit linkages in the lignin polymer.

The most frequent bond is β-O-4' [23]. After dilignols formation, the polymerizations continue and this dilignol can react either with a monomeric or other dilignol radical arising another molecule that may react with another one. The polymerization proceeds by random coupling giving rise to a three-dimensional macrostructure called lignin [14].

The chemical structure of cork lignin and its organization on the cell wall still isn´t completely understood and several attempts have been made to isolate and characterize cork lignin. Zimmerman *et al.* in 1985 used a Björkman isolation procedure but did not find any lignin alcohol precursor or typical dilignol units which suggest that wasn't lignin present in the cork extracts examined [60]. On the other hand, Marques *et al.* (1994) using the same isolation procedure was able to isolate a material called Milled Cork Lignin (MCL), which was characterized using chemical methods, Py/GC/FID and FTIR. The results showed that the FTIR spectrum fulfills only partly the spectral requirements of lignin obtaining a "lignin-like polymer" with some impurities namely long-chain acids and alcohols of suberin and sugars, but it was also showed that the aromatic moiety contained a large amount of guaiacyl (G) lignin units, small amounts of *p*-hydroxyphenyl (H) units and traces of syringyl (S) units [61]. Although it was proved the existence of lignin polymer, the fact that the sample was not desuberized constituted a problem, therefore affecting their subsequent quantification [57].

Then Marques *et al.* (1996, 1999) applied also the Björkman isolation procedure to determine Milled Cork Lignin (MCL) composition from previous saponified cork using chemical methods such as elemental analysis, HPLC chromatography, FTIR, and Py/GC/FID [62,63]. The elemental analysis allowed infer the average molecular weight of MCL through C_{900} formulae which was $C_{900}H_{874}O_{282}OMe_{85}$ with a methoxyl content of about 14% and a molecular weight with a monomodal distribution pattern with a maximum around 7000-8000 Da that correspond to a mean degree of polymerization of approximately 40 [62]. FTIR analysis demonstrates that MCL is essentially constituted by G-units, which was proven by Py/GC/FID analysis that gave a composition of 0.8% of H-units, 97.6% of G-units, and 1.6% S-units [62]. Marques and Pereira (2013) also confirm the major presence of guaiacyl units in lignin-like cork polymer with an H:G:S ratio of 3.6:93.7:2.7 beyond this they compare the results of Py/GC/FID of different corks from the barks of *Betula pendula*, *Quercus suber*, and *Quercus Cerris* [64].

Pascoal Neto *et al.* (1996) used a different approach for the isolation of the aromatic fraction of cork, named "lignin-like polymer", they used an organosolv-based technique, with an ethanol/water mixture as solvent, at high temperature, in the presence of an acidic catalyst. Then, the material obtained was characterized by elemental analysis, functional analysis, nitrobenzene oxidation followed by HPLC analysis of the oxidation products, FTIR, and ^{13}C NMR. Through the results achieved it was possible to confirm that the lignin-like polymer of cork has guaiacyl (G) units as the

major component, it was also detected syringyl (S) units although in small quantities and no *p*-hydroxyphenyl (H) units were identified [65].

The inter-unit linkages on cork lignin were evaluated by Marques *et al.* (1999) applying thioacidolysis and permanganate oxidation techniques on Milled Cork Lignin (MCL) and Milled Cork Lignin previously saponified (MCL_{sap}) and they were able to identify arylglycerol- β-aryl ether linkages as the main linkage on the lignin structure, besides this linkage, were also recognized β-5', α-5', 5-5' and 4-O-5' linkages but in smaller extent [66]. In 2016, Marques *et al.* via Py-TMAH and 2D-HSQC-NMR were able to confirm that around 80% of the detected inter-unit linkages in cork lignin are β-O-4' alkyl aryl ether bonds, 18% are β-5' phenylcoumaran, 2% are β-β' resinols and 1% are 5-5' type dibendioxocins linkages [67]. Moreover, was found 3% of ferulic acid was linked by ether linkages into the suberin and lignin structures [67].

Lourenço *et al.* (2016) compared lignins between xylem, phloem, and phellem in *Quercus suber L.* using different analytical methodologies (Py-GC/MS, NMR, and DFRC) besides the confirmation of a cork lignin polymer being predominantly a G-lignin (ratio G/S/H ratio of 85/13/2), they also observed the presence of condensed structures such as phenylcoumaran (β-5', 20%) and dibenzodioxocins (5%) [68]. On the other hand, on the phloem and xylem of *Quercus Suber* L. the content of G-units it's smaller with a ratio H:G:S of 1:58:41 and 1:45:55, respectively [68].

One of the biggest issues pointed in all the studies presented above was that all the samples used were not subjected to the previous desuberization, making the identification in all the analysis more difficult, since it was present a large amount of aliphatic structures as well as carbohydrates among the lignin structures [63,65–67]. This suggests that lignin is covalently linked to suberin but also to hemicelluloses [9,14,29,57]. In addition, the representativeness of isolated lignin preparations raises questions, because less than 20% of lignin from the total in cork have been analyzed.

2.3.3. Polysaccharides (cellulose and hemicelluloses)

The chemical composition of cork also includes cellulose and hemicelluloses, however in lower amounts when compared to those found in wood xylem from other species, which translates to a lesser influence of these components to physiological functions in the cell wall. Polysaccharides provide structural rigidity and prevent the collapse of cork cells [9].

Cellulose (Figure 2.8) is a linear polymer composed exclusively of β-D-glucopyranose units (or D-glucose), with β-(1-4') glycosidic bonds. In the cellulosic chain, each β-D-glucopyranose contains three hydroxyl groups, two secondary (in C2 and C3) and one primary (in C6) [69]. The hydroxyl groups at the ends of the chain have distinct chemical properties, being one reducer (reducing terminal) and another non-reducer (non-reducing terminal). Cellulose possesses a regular structure,

being an amorphous-crystalline polymer, either there is higher or lower organization. The molecular weight of cellulose can reach up to 10^6 Da or even higher [70].

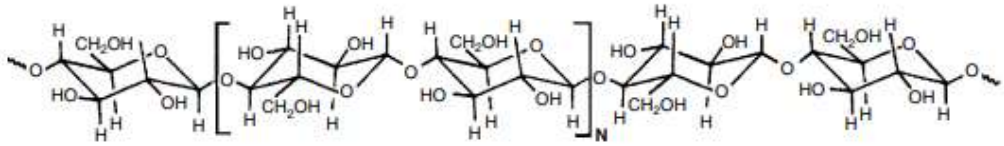

Figure 2.8- Partial structure of cellulose [69].

Hemicelluloses are non-cellulosic polysaccharides with an amorphous, branched structure, with a molecular weight substantially lower than cellulose, and they cooperate with lignin and cellulose concerning the support and rigidity to cork cells [71,72]. Hemicelluloses are made of different sugar units, such as D-glucose, D-mannose, D-galactose, D-xylose, L-arabinose, D-glucuronic acid, and in less abundance other sugars such as L-rhamnose or D-fucose (Figure 2.9) [69,70].

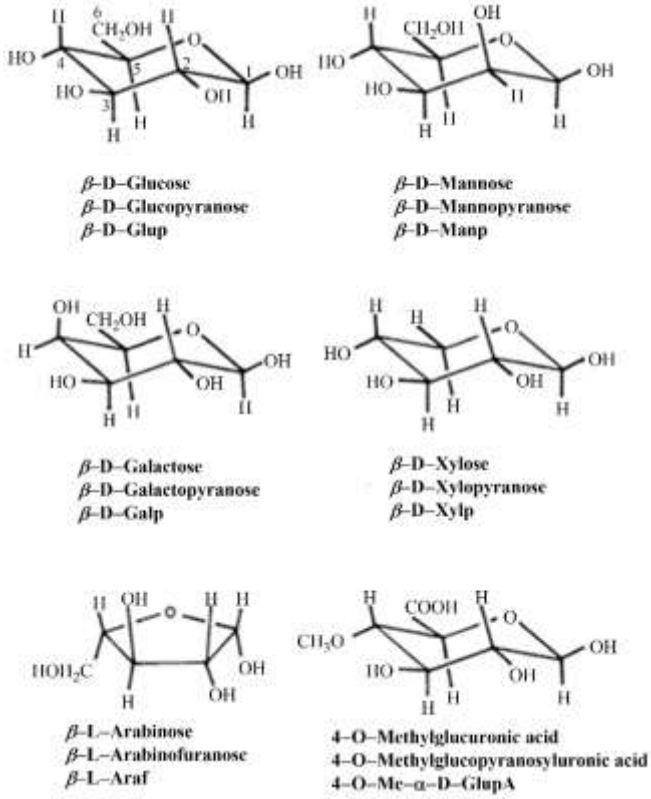

Figure 2.9- Sugar monomers from hemicelluloses. The designations D (dextrogyre) and L (levogyre) describe the standard configurations for the two optical isomers of glyceraldehyde (the simplest carbohydrate) and define the conformation of the hydroxyl group at carbon 4 (C-4) for pentoses (xylose and arabinose) and C-5 for hexoses (glucose, galactose, and mannose). The Greek letters α and β designate the configuration of the hydroxyl group on C-1 (adapted from [69]).

There are several types of hemicelluloses, and their constitution could be one sugar or the combination of more. The designation of each hemicellulose is often formulated in agreement with their predominant sugar monomers, for example, galactoglucomannans, arabinoglucuronoxylans, glucomannans, glucuronoxylans (Figure 2.10) [69,70,73]. Depending on the type of wood (softwood

or hardwood) the hemicelluloses have different predominancy, however in cork there are no relevant studies showing the type of hemicellulose present.

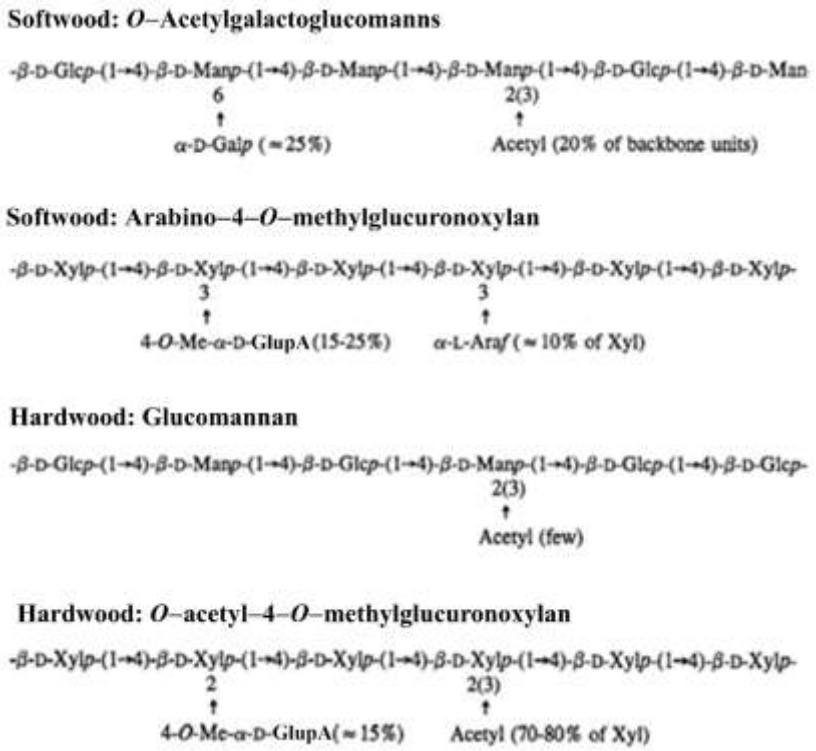

Figure 2.10- Representative structures of the predominant hemicelluloses (adapted from [73]).

Table 2.3 shows the results obtained by Pereira in 1988 in a study that sought to define the total percentage of monosaccharides present in virgin and reproduction cork. The results correspond to an average of 40 distinct samples of virgin cork and 10 different samples of reproduction cork and the respective standard deviation.

Table 2.3- Composition of monosaccharides after acid hydrolysis of virgin and reproduction cork [17].

Monosaccharides	% Total of monosaccharides	
	Virgin cork	Reproduction Cork
Glucose	50.7 (6.4)	45.4 (6.2)
Xylose	34.0 (5.1)	32.3 (5.5)
Arabinose	6.4 (0.8)	13.2 (2.3)
Galactose	3.6 (0.9)	5.1 (2.6)
Manose	3.7 (0.7)	3.2 (1.1)
Ramnose	1.7 (0.4)	0.8 (0.1)

According to Table 2.3, it appears that in cork, hemicelluloses have a more significant role than in xylem cells of woody matter, since xylan provides the structural compatibility between structural components of the cell wall, this function in the cork cell wall must be especially important.

Regarding the total percentage of monosaccharides from virgin and reproduction cork is proved that there are no significant changes.

2.3.4. Extractives

Extractives are the non-structural compounds in a higher percentage, which are found unbounded or loosely bound in the cell walls and can be removed by extraction with suitable solvents without causing changes in cell structure and mechanical properties of cork [14,17]. Extractives are divided into two major groups: lipophilic and phenolic compounds. Lipophilic compounds comprise aliphatic and terpene compounds, which influence the waterproofing characteristics of cork and can be extracted with nonpolar or low polar solvents such as chloroform, benzene, hexane, or dichloromethane [9]. Aliphatic compounds in cork include n-alkanes (chains between C16-C34), fatty acids (monoacids, diacids, hydroxy acids), and fatty alcohols (all even chains between C20 and C26) [14,21]. The composition of this fraction varies between 3.5 and 7.9% due to factors intrinsic to the cork oak and the industrial process of reproduction cork itself [74,75]. The terpenic compounds constitute about 50% of the lipophilic compounds of cork and are mainly triterpene compounds. Some examples of triterpene compounds found in cork are disclosed in Figure 2.11 [76–78].

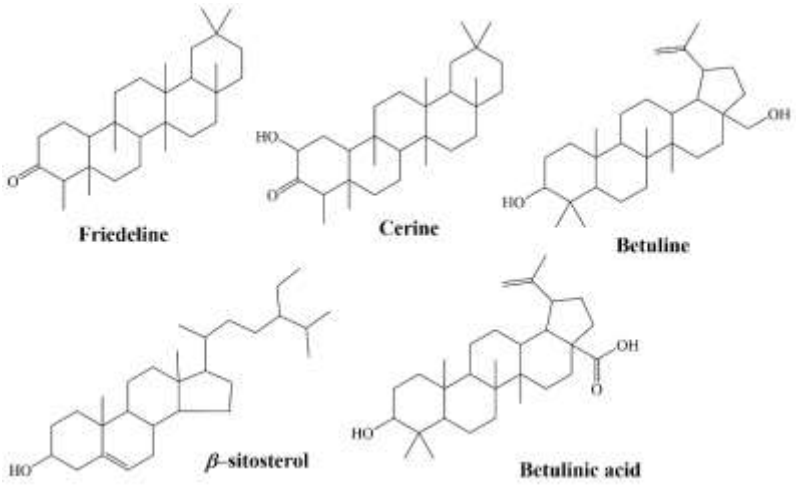

Figure 2.11- Some triterpene compounds found in cork.

Phenolic compounds are one of the most diverse groups and are part of the secondary metabolism of plants. These metabolites are fundamental for the growth and development of plants, performing protective functions against attacks by pathogens and predators, in addition to contributing to color and sensory characteristics [14,79–82]. In general, the phenolic compounds present in cork can be divided into flavonoids, simple phenolic compounds, and hydrolyzable tannins, which can be extracted with polar solvents, such as methanol:water and ethanol:water solutions, and water itself. Within this set of compounds, greater emphasis should be placed on

hydrolyzable and condensed tannins (subclass of flavonoids), since these, when in contact with beverages with alcoholic content, contribute to organoleptic properties, namely color, astringency, and bitterness of the final product [83].Some examples of these type of compounds are featured in Figure 2.12.

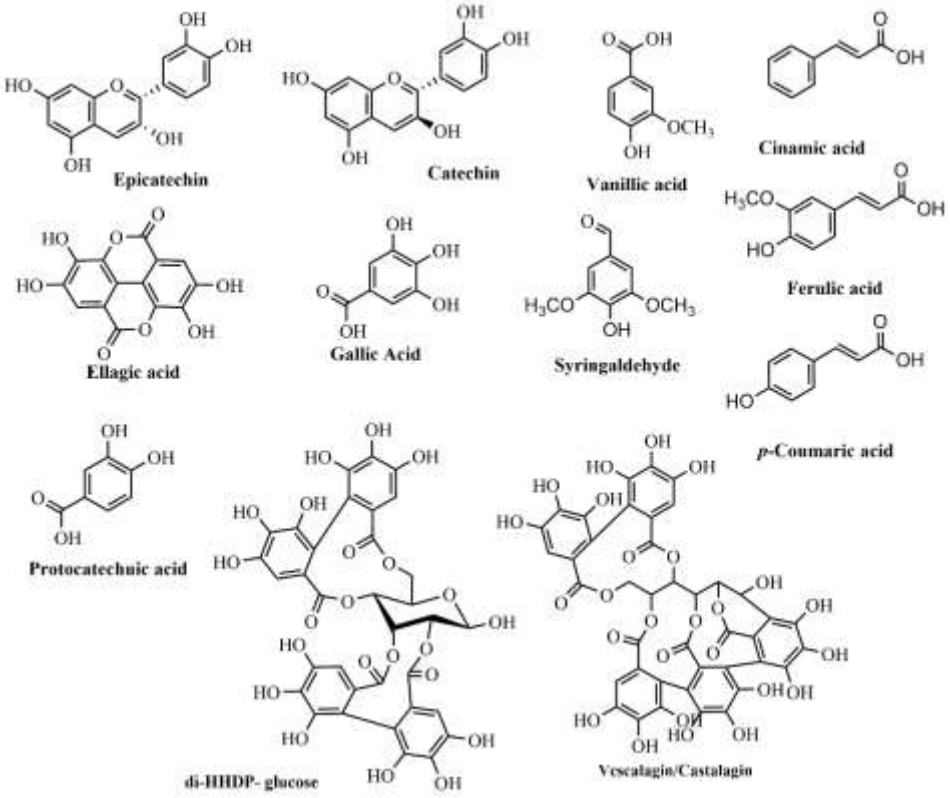

Figure 2.12- Examples of flavonoids (monomeric structure of the condensed tannins: epicatechin and catechin), simple phenolic compounds (vanillic acid, cinnamic acid, ferulic acid, gallic acid, syringaldehyde, *p*-coumaric acid, and protocatechuic acid), and hydrolyzable tannins (di-HHDP-glucose, vescalagin/ castalagin, and ellagic acid) present in cork.

These natural phenolic compounds have a wide variety of physiological properties that make them a target of study, such as radical scavenger, anti-allergic, anti-inflammatory, antimicrobial, antioxidant, and anticancer properties, among others that have potential effects on human health [79,84,85].

2.4. Physical and mechanical properties of cork

The structure of the suberous tissue and the chemical composition of the cell walls provides to cork a wide range of physical and mechanical properties that make it ideal for various applications, either as a final product or as a processed product, which enables the use of cork with superior and inferior quality. Among the different properties of cork, low density, low permeability to liquids and gases, high porosity, compressibility, and elasticity stands out.

Cork has a density that can vary between 120 and 250 Kg m^{-3} because more than 50% of cork is made up of air or a gas mixture different from the air [9,86]. The variation in density can be justified by the geometry of the cells, the structure of the cell wall, the age of cork, the presence of lenticular channels, and other discontinuities [16,86]. The permeability of cork to liquids and gases is very low due to the suberin and lipophilic compounds present in the cell wall [87]. Suberin is a low polarity compound, which provides hydrophobicity to cork materials. This property is an advantage for bottle sealing.

The porosity of cork is closely related to the number of existing lenticular channels, the bigger this factor, the greater the porosity and, therefore, lower the cork quality. Hence, was created a nomenclature in the cork industry that classifies cork according to its quality, being divided into descending parameters between '*flor'*, '*extra*', '*superior*', 1º, 2º, 3º, 4º, 5º, and 6º [16,88].

Finally, compressibility and elasticity are related to the existence of suberin and lignin present in cell walls. Suberin combined with the low levels of lignin promotes the flexibility of the cork cells. By causing compression in a cork stopper, the gas inside the cells is compressed against the cell wall and its pressure increases. After relaxation, the stopper regains its original shape, thereby putting pressure on the bottleneck [23]. Cork can be compressed to about half of its width without losing any flexibility and decompresses, recovering its initial shape, allowing this material to be used as a sealant [87]. Some general physical and mechanical properties of cork are presented in Table 2.4.

Table 2.4- Generic physical and mechanical properties of cork [9,86,89,90].

Physical and mechanical properties	Range of values
Density	120-250 Kg m^{-3}
Young's modulus	E_R=10.4 MPa E_{NR}=9.2 MPa
Poisson's ratio	$\nu_{R/NR}$=0-0.097 $\nu_{NR/R}$=0-0.064 $\nu_{NR/R}$=0.26-0.5
Collapse stress and strain in compression	σ_R=0.8 MN/m^2 E_R= 4% σ_{NR}=0.7 MN/m^2 E_{NR}= 9%
Fracture stress	σ_R=1.0 MN/m^2 σ_{NR}=1.1 MN/m^2
Loss coefficients	η_R=0.1 η_{NR}=0.3
Water diffusion coefficient	D_R=1x10^{-11} m^2/s D_{NR}=4x10^{-10} m^2/s
Thermal diffusivity	α=1x10^{-6} m^2/s
Thermal conductivity	λ=0.045 W/m.K
Specific heat	C_p=350 J/Kg.K

R- radial direction, NR- non-radial direction

2.5. Types of cork stoppers

While the needs for sealing/insulation materials increases, the use of cork in different areas of activity has been growing exponentially. However, about 72% of cork products are destined for the production of stoppers for the wine industry [12,91]. Cork is the choice of the best wine cellars in the world. In the list of the 100 best wines in the world, published by the prestigious Wine Spectator magazine in 2016, cork is the leader with about 89% of wines sealed with a cork stopper and, for the wine consumers in the main world markets, this preference is superior to 85% [92]. Consumers associate the use of a cork stopper to a closure with a good and very good quality wine and this perspective is reflected in the success of the brands. Due to the high R&D investment in the stopper industry and its growing development, exist several types of stoppers with different specifications of calibers and classes, to adapt to different drinks and bottles to respond to the market demands. Currently, cork stoppers can be divided into three main groups: natural, technical, and capsulated cork stoppers, described in Figure 2.13 [93,94].

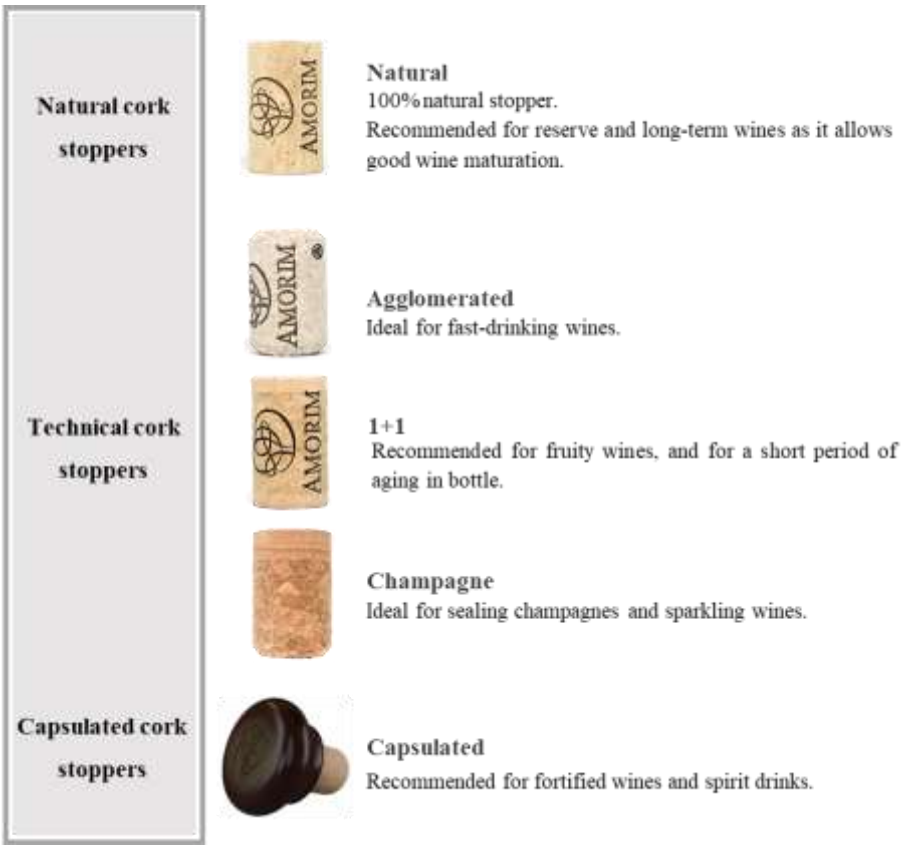

Figure 2.13- Main groups of cork stoppers produced at Amorim Cork S.A.

The natural cork stoppers are extracted directly from the cork oak and are 100% natural cork, this stopper can undergo a process where the stoppers pores are filled with a dispersion of cork powder and glue giving space to colmated stoppers. The technical cork stoppers can be subdivided

into agglomerated, 1+1, and Champagne. These stoppers have in common a body of granulated cork with solvent-based or aqueous glue, however with different sizes of cork granule for each type of technical stopper, besides this, the agglomerated cork has no disk of natural cork in its constitution, while the 1+1 has one disk at each top of the agglomerated body of the stopper, and the champagne stoppers may have one or two disks of natural cork at one of the stopper tops.

The capsulated cork stoppers can be produced from natural cork stoppers or cork micro agglomerate to which is inserted a capsule, that can be of different materials such as wood, glass, metal, among others.

2.6. The production flow of natural cork stoppers

From the cork plank to the final product, cork goes through a series of steps that differ according to the type of stopper they are intended for. Natural cork stoppers are of great importance in cork exports, constituting around 56% of the total value, while technical stoppers represent 27% [12]. Since the stoppers of interest during this study are natural cork stoppers, only this production flow will be presented (Figure 2.14).

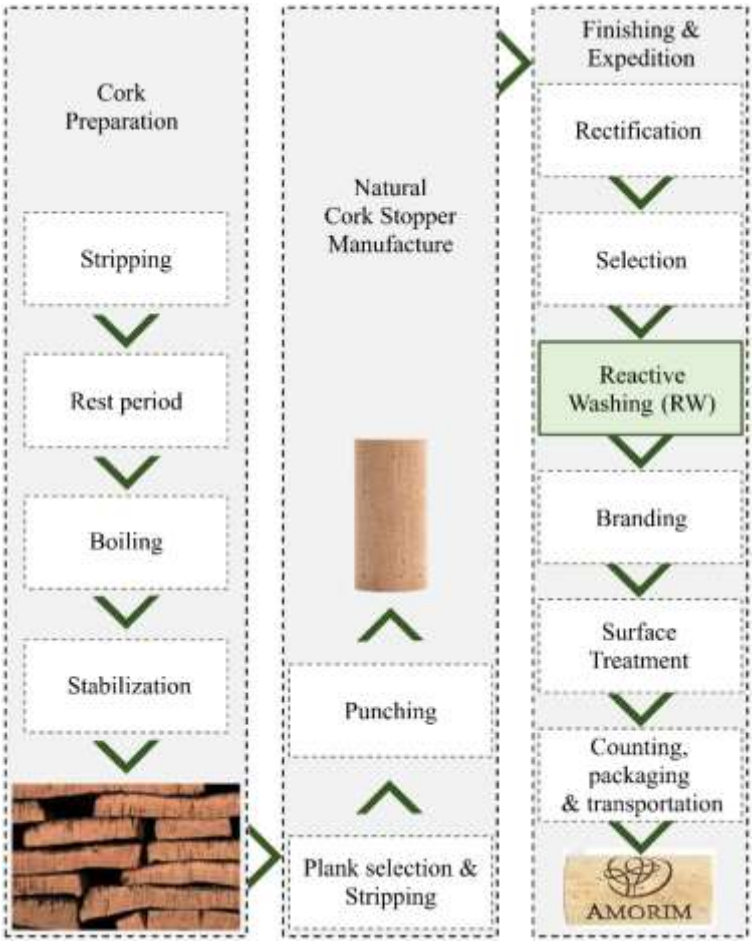

Figure 2.14- Natural cork stoppers production flow.

Figure 2.14 differentiates the three main stages to produce natural cork stoppers: cork preparation, natural cork stopper manufacture, and the finishing and expedition. The first step comprises the stripping, rest period, boiling, and stabilization, and is common to all types of stoppers.

Stripping takes place during the most active phase of cork when the phellogen is in full merismatic activity allowing the easy separation of the cork layers [95]. This occurs between mid-May and early June to mid-August, as it is easier to strip it without injuring the tree trunk [7]. Stripping is a process carried out by specialized professionals, who use an ax. In Portugal, this process is specified in Decree-Law Nº169/2001. For stripping to be allowed, it is necessary that the cork oak is 25 years old and has a perimeter of 70 cm when measured 1.3 m from the ground [3]. Stripping is executed in six steps: opening, separating, tracing, extracting, removing, and marking. It should be noted that the thinner boards are intended to produce discs for technical stoppers or other materials.

In the **rest period**, the extracted cork planks are stacked on open-air on stainless steel structures in large, cemented areas, built on an inclined plane for a minimum of 6 months. This procedure prevents the cork from remaining in contact with the soil and has very significant results in reducing microbial contamination. The piles allowed the maximization of water flow and air circulation [96]. These piles are formed following the rules defined in CIPR and have as main objective stabilize and develop a uniform moisture content [97].

Boiling is the first step in the industrial process of stopper production. The cork planks, that have already completed the rest period, are placed in clean water at about 100 ℃ for a period of 1 hour, contributing to microflora decrease. This procedure aims to clean the cork, extract water-soluble substances, and increase the thickness of the planks by about 20%, which contributes to a density reduction, in addition, to make them softer and more elastic. This situation occurs because, before the boiling, the cork cells are compressed irregularly, however during this process, the gas contained within the cells expands [98].

Stabilization has a duration of one to four weeks, the planks rest and the boards are flattened, allowing them to reach the ideal moisture content (8-16%) to obtain the necessary consistency for their transformation into stoppers [96].

The second stage of the flow diagram (Figure 2.14) is exclusive to natural cork stoppers and includes two fundamental steps: plank selection and stripping and punching.

In the **plank selection**, the edges of the planks are prepared, and the corners trimmed. Then a manual evaluation is carried out where the planks are separated by quality classes according to thickness, porosity, and appearance. **Stripping** consists in cutting, from the planks previously selected, strips slightly wider than the length of the stopper to be manufactured [98].

Punching is a manual or semi-automatic process that consists of perforating the strips with a drill to obtain the desired dimensions for the stopper. Drilling waste is used to produce cork granulate. After punching, a statistically significant sample from each batch is subjected to gas chromatographic analyses to detect undesirable components, such as TCA precursors. The lots are subjected to treatment with ROSA Evolution® ("Rate of Optimal Steam Application"), which uses water vapor and controlled temperature conditions. Whenever the results reveal the minimum TCA percentage, the lot is immediately returned to the source, so that corrective measures can be applied.

The third stage of production (Figure 2.14) is common to all stoppers, which includes the final procedures such as rectification, selection, reactive washing (RW), branding, surface treatment, and counting, packaging and transportation.

In the **rectification**, the stopper acquires the final dimensions previously specified, by correction of the diameter and length through abrasive agents.

The **selection** procedure consists of the separation of finished stoppers into different classes through visual inspection, or automatic artificial inspection of stopper surfaces. Stoppers with possible defects are eliminated.

The **reactive washing (RW)** process is a set of operations that aims to clean, disinfect, and give the desired color to the stoppers. The washing programs are defined by equipment and chosen color. Currently, this stage uses hydrogen peroxide in the presence of sodium hydroxide and increased temperature. The volumes of the reagents and the oxidation periods vary in accordance with the program chosen. Once the oxidation period is completed, the cork stoppers are washed with water, sodium bisulfate, and then again water. The sodium bisulfate is used to reduce the surface alkalinity, and then the stoppers pass through a drying cycle. After this process, the moisture content is stabilized, thus obtaining an optimization of the performance of the cork as a sealant and reducing microbiological contamination [96]. The RW process is further analyzed in section 2.8- Reactive Washing (RW) process.

After RW, an optional process that gives rise to colmated cork stoppers may occur, this operation consists in filling the lenticular channels of the washed cork stoppers with a mixture of cork powder, from the rectification, with a solvent-based or aqueous glue, thus allowing their fixation. This step provides a better visual appearance and performance of the stopper.

In **branding,** the stoppers are marked according to the customer's specifications. This process can be performed by heat, laser, induction, or ink approved by FDA.

In the **surface treatment**, the surface of the cork stopper is coated with a film of paraffin and/ or silicon that acts as a lubricant and contributes to the impermeabilization of the cork stopper to liquids and gases, as well as, facilitate both its introduction and subsequent extraction from the bottle and improve the sealing performance.

Finally, the stoppers are counted and packed in raffia or plastic bags and cardboard boxes, according to the order form. In the stoppers packed in polyethylene bags, a preservative of widespread use in the wine industry is introduced, sulfur dioxide (SO_2), which is a gas that inhibits microbiological development, and the packages are sealed and transported to the customer.

2.7. TCA as a cork concomitant

TCA (2,4,6-trichloroanisole) is a chemical compound that belongs to the chloroanisoles family and has the structure shown in Figure 2.15. This compound is exogenous to wine, wood, and cork stoppers. However, if it is present in the atmosphere and comes in contact with cork stopper, it is easily adsorbed, thus becoming the main responsible for what in popular language is known as "cork taint", and even in low concentrations (2-4 ng/L) of this compound, this defect is detected [99].

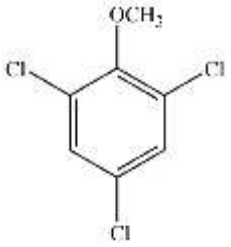

Figure 2.15- TCA chemical structure.

The microorganisms present in cork have developed a defense mechanism, which, under favorable conditions of temperature and humidity, form chloroanisoles through chlorophenols by biomethylation reaction (Figure 2.16) [96,99,100].

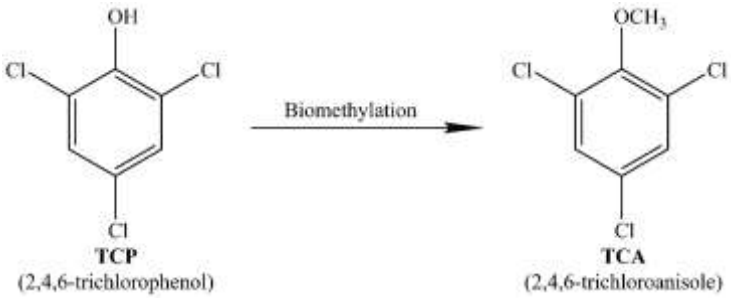

Figure 2.16- TCA formation- biomethylation reaction.

Chlorophenols existed in the chemical composition of most pesticides used industrially, and they have a high resistance to their environmental biodegradation, which causes wide contamination of waters, soils, plant matter, and atmosphere, inclusive. The reduction/elimination of microorganisms prevents the formation of additional amounts of TCA. However, this procedure does not eliminate the TCA already existing in cork.

From the cork oak tree to the stopper there are several points of contamination, including during the processing and packaging, hence the importance of good cork production practices, namely the

realization of short stabilization periods of the raw material after the boiling and the correct management of materials that come in contact with cork stoppers to reduce the possibility of TCA formation. It is also for this reason that the use of chlorinated compounds in the washing of cork stoppers is not allowed as they enhance the formation of chlorophenols and consequently the formation of chloroanisoles.

The extraction of this unwanted compound from cork presents some difficulties due to the low volatility of TCA (boiling point at 240 ℃), the intrinsic characteristics of cork, and the fact that TCA is specifically adsorbed by the structural components of cork such as cellulose, lignin, and suberin [100]. However, to eliminate TCA and other volatile organic compounds, Amorim Cork S.A. developed ROSA Evolution® technology, which uses water vapor and controlled temperature conditions. The TCA found on the surface of the cork is thus effectively extracted by entrainment by water vapor [101]. Additionally, Amorim Cork, S.A. recently launched the technologies Natury and Xpür, that aim to eliminate the detectable TCA in natural and microagglomerate cork stoppers, respectively. These technologies are based on thermal desorption principles, using pressure, temperature, purified water and time, in a non-sequential way [102]. The strategies presented allow the efficient removal of TCA to values lower than the limit accepted (0.5 ng/L).

2.8. Reactive Washing (RW) process

The reactive washing process, according to the CIPR, is a "set of operations designed to ensure the cleaning, dust removal and disinfection of the stoppers" [2], therefore the main objective of the RW process is to disinfect and increase brightness, as well as stabilize the color of the cork surface since this process takes place on the surface of the cork giving it the desired appearance. To achieve cork stoppers with high brightness values two principal reactions need to occur: (1) degradation, solubilization and removal of the colored matter, and (2) transformation of the coloring matter on the stoppers surface into colorless. For this goal, it is necessary to remove, at least partially, the chromophores, as these are the compounds that most influence the color of cork [103,104]. It is commonly accepted that lignin, polyphenolics, suberin and some extractives contribute to the color of cork material. The knowledge of these chemical structures will allow devising better approaches to effective chromophore removal, as well as help to develop strategies to reduce chromophore formation.

[2] Source- Código Internacional das Práticas Rolheiras (CIPR)- version 6.3- 2011

2.8.1. Chromophores

Chromophores or chromophore groups, which means “carrier of color”, are sets of atoms responsible for the color of a material, in this case, of cork. These compounds usually have high extinction coefficients, and even in -ppb to -ppm concentrations, they can give a yellowish appearance to the raw material [105,106]. These elements cover most of the constituents, which means that they all enhance the color of the cork, however, lignin is the constituent pointed out as the one that most influences the color of cork [104,107,108], although studies have been made that show that cellulose materials with low or zero content in lignin also presented chromophore structures, in less extent [103,106,109–111]. In wood, lignin is a light yellow or cream-colored compound, but due to its high reactivity, it has the predisposition to form chromophores groups [112]. The main chromophore units of lignin contain the combination of the carbonyl and ethylene groups and aromatic rings, as depicted in Figure 2.17.

Figure 2.17- Main compounds of chromophore groups of lignin [107].

The presence of the individual chromophore group (Figure 2.17) is unlikely to be solely responsible for the light absorption in the visible region of the electromagnetic spectrum, in this way they can be seen as chromogens (Vis-inactive compounds), nevertheless, the problem arises when they combine generating chromophores (Vis-active compounds) [105,113]. There is a wide diversity of chromophore groups. The distinction between them is based on the type of conjugated functional groups (double bonds, essentially), some examples are depicted in Figure 2.18.

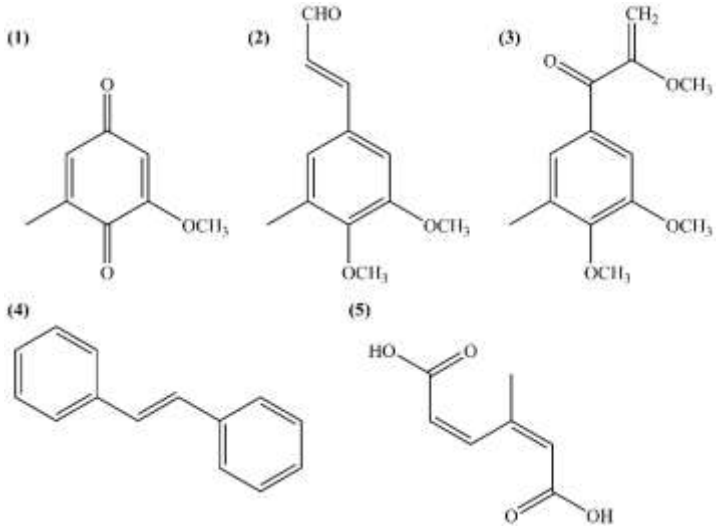

Figure 2.18- Examples of chromophore groups- (1- Quinone type; 2- Double bonds conjugated with aldehyde groups; 3- Double bounds conjugated with ketone and ethylene group; 4- Stilbene type; 5- Muconic acid type).

Chromophores and potential chromophores (chromogens) are derived from a wide variety of phenol, cathecol, and quinone-like structures conjugated to unsaturated systems of styrene, diphenylmethane, and butadiene structures. It should be noted that unsaturated structures can be eliminated either by reduction or oxidation [58].

2.8.2. Hydrogen peroxide as a bleaching agent

In the RW process it is necessary to apply a bleaching agent, currently, hydrogen peroxide in an alkaline medium. The bleaching agent in question or its reaction products with other reagents act on the stopper surface, namely on the conjugated chromophore structures, increasing brightness. Bearing the lack of information regarding the cork RW process, it is assumed that the reactions that take place occur similarly to those occurring in the pulp and paper industry, after the application of the same reagents.

The choice of bleaching agents is based on factors such as the selectivity of the agents towards chromophore and chromogens groups, degree of efficiency, handling costs and minimizing environmental pollution [114]. Historically, it was used calcium hypochlorite as a bleaching agent for cork stoppers. However, despite being efficient and economic, it left small amounts of chlorine in the form of chloro-organic compounds that caused unpleasant smells and corrupted the taste of the drink with which they were in contact [115]. This bleaching agent also has the possibility of forming dioxins and toxic substances. Given these effects, the use of calcium hypochlorite gradually decreased, and the application of hydrogen peroxide began to be more prominent.

Hydrogen peroxide as a bleaching agent is an important advance, as it is more economical and environmentally friendly, since it generates much less harmful effluents to the environment, for the same quality of RW. Hydrogen peroxide (H_2O_2) is a weak acid (pK_a 11.8) and forms salts with various metals. Under normal conditions, pure hydrogen peroxide is very stable at room temperature, however, hydrogen peroxide in the presence of small amounts of impurities or contaminants such as iron, copper, manganese, nickel, chromium ions, among others, is unstable and decomposes into water and molecular oxygen [116].

Hydrogen peroxide requires strong alkaline conditions (11<pH<12) to act as a bleaching agent. These conditions are ensured by the addition of sodium hydroxide (NaOH). The reaction of hydrogen peroxide in an alkaline medium is shown in Equation 2.1.

$$H_2O_2(aq) + OH^-(aq) \rightleftharpoons HO_2^-(aq) + H_2O(l) \quad (2.1)$$

The hydroperoxide anion (HO_2^-) which is in equilibrium with hydrogen peroxide is a strong nucleophile acting on the side chains of lignin. Its action is done through the degradation of the

double bonds of the structures of the chromophores, especially containing carbonyl groups (aldehydes, ketones, quinones, etc.), producing soluble structures, which facilitate its extraction and allows the increase in the brightness of the stopper surface [114,117,118].

During the bleaching with hydrogen peroxide, there are two competing reactions. The reaction leading to the formation of the reactive specie (HO_2^-) (Eq. 2.1) that is responsible for the increase of brightness on the stopper surface and a secondary reaction (Eq. 2.2) that consists of the decomposition of hydrogen peroxide into water and molecular oxygen, preventing the increase in brightness and as such highly undesired.

$$H_2O_2 + HO_2^- \rightarrow O_2 + H_2O + OH^- \quad (2.2)$$

The decomposition reaction depicted in Equation 2.2 is enhanced by the pH of the reaction medium. The more alkaline the reaction medium, the greater the consumption of hydrogen peroxide, which also translates into more hydrogen peroxide consumed in the secondary reaction of the hydrogen peroxide [114,117]. To avoid the secondary reaction of hydrogen peroxide, stabilizers such as magnesium silicates can be added to the reaction medium [58].

The presence of transition metals in the reaction medium can catalyze the decomposition of hydrogen peroxide through a Fenton-type reaction, as represented in Equation 2.3 [119].

$$H_2O_2 + M \rightarrow M^+ + OH^- + OH^{\cdot} \quad (2.3)$$

Other factors that influence the efficiency of hydrogen peroxide as a bleaching agent are temperature and reaction time. Thus, for temperatures above 90 °C, the degradation of hydrogen peroxide is enhanced with the release of hydroxyl radicals (OH·), according to Equation 2.4.

$$H_2O_2 \rightarrow 2\,OH\cdot \quad (2.4)$$

Hydrogen peroxide does not normally react readily with polysaccharides. However, the formation of hydroxyl radicals causes the oxidation of cellulose with subsequent breakdown of the polymer chains.

This process, despite being industrially developed, presents some parameters that must be optimized, such as the process reagents concentrations, the water volume used, and the time spent in each RW, while maintaining the visual characteristics of the stoppers and the performance quality of the final product.

2.9. New approaches in reactive washing

To fill the flaws by the current reactive washing, three different paths of study are presented. The first relates to the optimization of the conventional reactive washing currently applied in the industry using response surface methodology (RSM). This approach aims to reduce the consumption of bleaching reagents in order to cause less damage on the surface of the stoppers and improve economic efficiency. The second relates to the application of ozone as an alternative bleaching agent for the reactive washing. The third approach relates to the combination of the ozone treatment with the conventional hydrogen peroxide (H_2O_2) treatment aiming to reduce the reagent's demands and combine the positive aspects offered by each process.

The optimization of the conventional reactive washing using RSM starts by choosing the process variables that most influence the quality of the process, and, in this way eliminates possible wastes of reagents and monetize the processing time, without negatively affecting the final product.

The application of ozone as a bleaching agent is a method completely distinct from the conventional RW. This RW process is already used in other industry areas such as pulp and paper and textile. In this way, the procedures applied in these industries will serve as a basis for the study of the implementation of ozone as a bleaching agent for the reactive washing of cork stoppers.

2.9.1. Conventional reactive washing optimization

Reactive washing (RW) as is applied today reveals some drawbacks in the process since it requires high concentrations of reagents to obtain the target brightness level, besides increased temperatures with a great level of time and process water requirements. The combination of these operation aspects results in a process with high costs and time spent not only in the reactive washing itself but also as waste treatments. Additionally, the use of these strong process conditions may provoke changes in the surface of the natural cork stopper that would have implications in the subsequent processes and influence the quality of the final product [120,121]. In particular, the degradation of the stopper's surface leads to the deterioration of its ability to receive the treatment formulations containing food-grade silicone, paraffin, and other functional formulations, thus decreasing the consumer properties. In this way, the main goal is to improve the performance of the process by discovering the optimum value for the process variables for the reactive washing process without compromising the desired brightness and have minimal deterioration of the stopper surface.

Usually, the optimization of a process has been carried out by evaluating the influence of one factor at a time (OFAT) on an experimental response, where each factor corresponds to an independent variable of the process in study [122]. However, this type of approach has several disadvantages since it is necessary a large number of experiments to understand how the variables

influence the response, which translates into an increase of time and cost associated, besides, this methodology does not allow the estimation of interactive effects between the variables studied [122–125]. One way to overcome this problem is the application of a multivariate technique such as response surface methodology (RSM). RSM is a tool widely used to develop new products and processes, as well as to improve products and methodologies, optimizing the process and minimizing costs. This method is a collection of mathematical and statistical techniques that are capable of fitting experimental data to empirical models such as low-order polynomial equation via a design of experiments (DoE), creating a relationship between the response or set of responses and the independent variables (factors) [122,126–129].

Design of experiments (DoE) is an important tool for driving innovation since it is possible to obtain major information such as identifying critical parameters and the robust operating regions for each process with a smaller number of experiments performed [116]. DoE has three essential principles to ensure its applicability: randomness, replication, and blocking. Randomness implies that the order of the runs performed is random, which can protect the experiment from bias or systematic error. On the other hand, replication of the runs allows the estimation of experimental error and is used to obtain a more precise estimative for the mean response for a singular combination of factors levels in the experiment. Finally, blocking is applied to reduce or eliminate the variability supplied by nuisance factors (factors that may influence the process but are not the factors of interest), this principle is accomplished by using a set of relatively homogeneous experimental conditions [116].

Through the implementation of DoE attention should be paid to the scale where the study will be conducted. To spend fewer amounts of material is preferable to carry out the initial designs on small scale as a laboratory scale, this design provides important information about the process and helps in the scale-up process to larger scales [130].

There is a guideline set to apply DoE: (1) recognition of and statement of the problem; (2) selection of the response variable; (3) choice of factors, levels, and range; (4) choice of experimental design; (5) performing the experiment; (6) statistical analysis of the data; (7) conclusions and recommendations [131].

RSM is intrinsically linked to DoE, in fact, RSM is employed in all DoE steps: before selecting the variables and the experimental design, during the actual experiment, and after analyzing the data. This method is one of the possible linear models that can be applied in DoE. RSM is characterized by showing graphically the relation between the independent variables and the response, with which the main goal is to determine the optimum operating condition [132]. To better understand the employment of RSM its implementation is divided into three principle sequential stages: pre-

experimental planning; experimental design and statistical analysis; confirmation and optimization. All three stages have crossover similarities between the implementation of RSM in DoE.

2.9.1.1. Pre-experimental planning

Once the problem has been stated, the second step focuses on the selection of response variable which must be a variable that provides valuable information about the process in the study, being preferably a continuous variable with appropriate units (absolute or relative units) and should be obtained by non-destructive and non-damaging methods so the measure can be repeated whenever necessary [133]. Then it is necessary to choose factors, levels, and range, that should be selected according to process knowledge through practical studies and/or theoretical understanding. Factors are process variables that can be changed independently from each other into specific levels of interest that must be properly controlled [122,134]. The levels chosen delimitates the region of interest, which should be relatively large while maintaining the robustness of the process. These three steps represent the pre-experimental planning and even though the application of this methodology requires to be initiated by the statement of the problem, the subsequent steps could be performed in reverse order or at the same time.

Once the pre-experimental planning is correctly achieved, usually is used software that would help provide a matrix of experiments to conduct the study. Depending on the number of factors and levels there will be a different number of runs in the experiment. The simplest factorial design experiment is 2 factors with 2 levels each, which corresponds to 2^2, that equals to 4 runs. The realization of the four runs results in a full factorial experiment since all the possible runs are performed, however, if there are four or five factors with more than two levels each, the application of full factorial experiment becomes unsuited in terms of time and costs consumed, so its preferably to perform a fractional factorial experiment (FFE). FFE also performs a combination of factors levels, but only a subset of runs is used [134].

2.9.1.2. Experimental design and statistical analysis

The experimental design chosen in the fourth step is the election of an empirical model, which relates the response Y to the factors $x_{1,}x_2, \dots, x_k$ (Eq. 2.5).

$$Y = f\left(x_{1,}x_2, \dots, x_k\right) + \varepsilon \tag{2.5}$$

The function f usually is a low-order polynomial function (first or second-order) and ε is the statistical error associated with the experimental design and is assumed to have a normal distribution

(mean zero and constant variance σ^2) [125,129]. If the empirical model is a first-order polynomial function, Equation 2.5 becomes Equation 2.6, considering that the study has two factors.

$$Y = b_0 + b_1 x_1 + b_2 x_2 + \varepsilon \tag{2.6}$$

The parameters b_0, b_1, and b_2 are unknown and will be estimated from the data in the experiment using the method of least square. This model is also recognized as the main effects model since it only considers the main effects of each variable and does not allow the evaluation of factors interaction. In this way, a second-order model (Equation 2.7) is widely used, because, besides the prediction of interaction effects between factors, it also can adopt a large variety of functional forms that frequently work well in solving real problems.

$$Y = b_0 + b_1 x_1 + b_2 x_2 + b_{12} x_1 x_2 + b_{11} x_1^2 + b_{22} x_2^2 + \varepsilon \tag{2.7}$$

The next step is running the experiment, which should be done carefully and ensuring that all runs are performed accordingly to the plan to diminish experimental error. Then is necessary to analyze the statistical data and validate the model. Through the residual values, it's possible to verify the difference between the experimental data and the values predicted by the model, if this difference is small it means that the mathematical model is well fitted [122].

To validate the adequacy of the fitted model to the experimental data is commonly used analysis of variance (ANOVA) and coefficient of determination (R^2). ANOVA is a statistical method that is based on the sum of squares determination, whose total sum of squares (SS_T) corresponds to the total variability of the experiment. This total variability is partition into the sum of squares of the model (SS_M), which describes the systematic variation between the combination of a set of levels of each factor (treatment) to another combination, with the sum of squares of the errors (SS_E), that represents the random variation between replicates within each treatment (Equation 2.8) [135].

$$SS_T = SS_M + SS_E \tag{2.8}$$

The SS_M is then decomposed into the sum of squares of main effects and interaction effects. The ratio of the mean of squares of the model (MS_M) with the mean of squares of the errors (MS_E) follows the F-distribution, assuming that the error terms are normally distributed with constant variance [136]. The *F*-value (Equation 2.9) helps to draw conclusions about the model validation. The mean of squares of the model (MS_M) is calculated as the sum of squares of the model (SS_M) divided by its degree of freedom (DF_M), and the same is applied for the mean of squares of the errors (MS_E).

$$F - value = \frac{MS_M}{MS_E} = \frac{\frac{SS_M}{DF_M}}{\frac{SS_E}{DF_E}} \quad (2.9)$$

The *F*-value obtained for the model is compared with the *F*-value tabulated (in a defined level of confidence, usually 95%) and then two hypotheses are imposed: null hypothesis (H_0) that states that all the parameters b_i are equal to zero and the alternative hypothesis (H_1) that predicts that at least one of the parameters b_i is non-zero. If the model F-value is higher than the F-value tabulated, the null hypothesis is false, i.e., the model has significance, and the response has a surface associated.

The coefficient of determination (R^2) reflects the amount of variability in the response, *Y*, which can be explained by the empirical model chosen and is described by Equation 2.10.

$$R^2 = \frac{SS_M}{SS_T} = 1 - \frac{SS_E}{SS_T} \quad (2.10)$$

This parameter (R^2) varies between 0 and 1, whose value close to 1, usually, indicates a good fitness of the model to the experimental data, however, in this case, a higher value of the coefficient of determination does not automatically mean that the model is fitted because the addition of new variables to the model will always increase the value of R^2[129]. In this way to assure that the model will give a good prediction, it is also evaluated the value of adjusted R^2 (Equation 2.11).

$$R^2_{adj} = 1 - \frac{MS_E}{MS_T} = 1 - \frac{\frac{SS_E}{DF_E}}{\frac{SS_T}{DF_T}} \quad (2.11)$$

The adjusted R^2, in general, increases with the addition of more model variables, if there exist non-significant terms in the model the adjusted R^2 will decrease. Therefore, to validate the quality of the model is necessary to have values of coefficient of determination (R^2) and adjusted R^2 near to 1.

Once the model is duly approved, the next phase is evaluating the importance/significance of each process variable in the model obtained, to achieve this objective is employed the testing hypothesis for each model coefficient. The null hypothesis (H_0) states that the parameter b_j is equal to zero and the alternative hypothesis (H_1) claims that the parameter b_j is different from zero. If the null hypothesis is true, then x_j can be withdrawn from the model, if not statistics tests such as *t*-value or *p*-value are commonly used to define the significance of the factor's effects. *p*-value consists of the probability, under the assumption of no influence of one of the variables in the response, of obtaining a result equal to or more extreme than what was obtained [137]. For small *p*-values (*p*-

value≤0.05) the null hypothesis can be rejected at a 5% or less significance level in favor of the alternative hypothesis [138]. This study helps understand the value of each effect in the model, which translates into the inclusion or exclusion of variables to obtain a more effective model.

2.9.1.3. Confirmation and optimization

Once all the data is analyzed, is fundamental to proceed with the confirmation testing of the model, to achieve this step are chosen a set of final tests to be performed. The predicted response values given by the empirical model are compared with the experimental values obtained, if there are no significant differences the graphical representation of the data leads to a linear equation with a high coefficient of determination (R^2).

Optimization is a well-recognized step in RSM implementation since this methodology is characterized by showing the response surface graphically. The main goal of this step is to find the optimum levels for each input variable to obtain the most desirable response. If the desirable or optimal response values are accomplished in the limits of the experiment, the following step is to perform additional experiments within the region where the desirable response values are presumed to be found [136,139]. In this way is possible to obtain a better combination of process variables to achieve the desired response with a high degree of confidence.

The application of RSM enables to obtain: more information about the process in the experimental design; conclusions about the study done and recommendations for future steps, without having to carry out a large number of experiments, which can be very time and cost consuming.

2.9.2. Ozone as a bleaching agent

Ozone was discovered in 1839 by C.F. Schonbein and was applied commercially for the first in 1907 in the treatment of municipal water in Nice. However, it was only in 1992 that ozone was used as a bleaching agent at an industrial level [140,141]. The application of ozone as a bleaching agent has grown exponentially due to environmental needs and market demands [116].

Ozone concentrations below $0.2\,mg/m^3$ are tolerated by humans, however higher concentrations carry risks. Nevertheless, its strong odor allows it to be detected before it becomes dangerous (0.01-0.02 ppm) [114,140]. Ozone is an allotropic form of oxygen formed by adding free oxygen radical to the oxygen molecule, according to Equation 2.12.

$$O_2(g) + O \cdot \rightarrow O_3(g) \qquad (2.12)$$

Ozone is a bluish color gas, however, as it is in low concentration in the environment, it is practically colorless, and has a strong and characteristic smell described as “fresh air after a storm” [142]. In liquid state boils at 111.3 ℃ and in the solid-state its melting point is -192.5 ℃. The ozone molecule has four resonance hybrids shown in Figure 2.19.

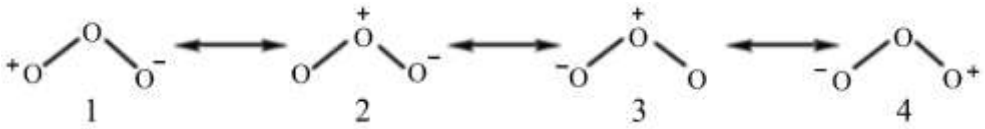

Figure 2.19- Ozone allotropic form.

Structures 1 and 4 are responsible for the electrophilic character of ozone, belonging to 1,3-dipolar compounds and, therefore, follow the typical reaction mechanisms of this class of compounds [71]. The three oxygen atoms in the ozone molecule are rearranged with an obtuse angle, where the central oxygen atom is equidistant to the other two oxygen atoms (the angle is approximately 116°49' and the distance of the connection is 1,278 Å) [140].

Ozone has a high oxidation potential that allows it to react with a wide range of organic compounds, including lignin and its derivatives [140,141,143]. When the standard oxidation potential of ozone (2.07 V, 25 °C) is compared with that of hydrogen peroxide (1,77 V), it is concluded that this is a promising bleaching agent [144]. The standard oxidation potential of ozone in an aqueous solution is expressed by Equation 2.13.

$$O_3 + 2H^+ + 2e^- \rightarrow O_2 + H_2O \qquad E^0 = 2{,}07\ V \qquad (2.13)$$

2.9.2.1. Reaction of ozone with cork components

Ozone allows an increase in the brightness of the stopper surface by acting on unsaturated lignin areas, including those found in aromatic rings [108]. Figure 2.20 shows some of the reactions of ozone with lignin structures (hydroxylation, dimethoxylation, cleavage of the aromatic ring and vinyl moieties, among others).

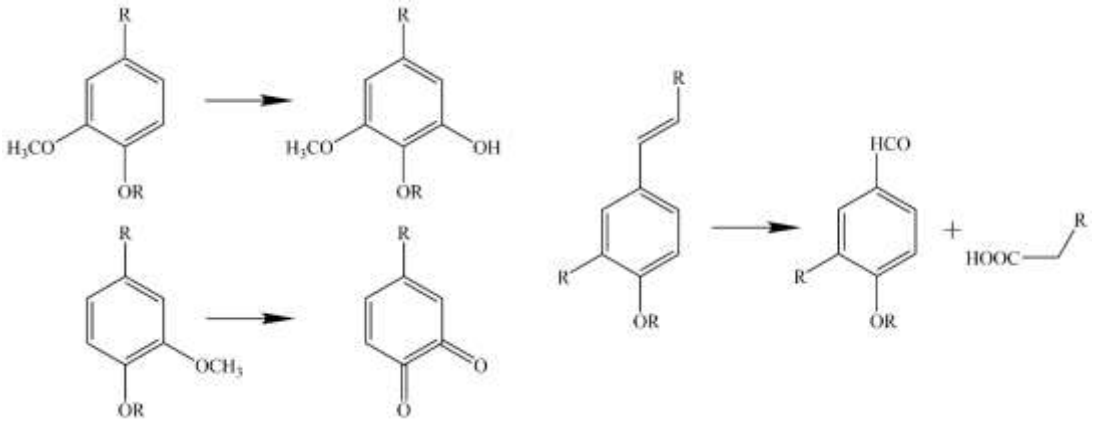

Figure 2.20- Ozone reactions with structural features present in lignin.

Thus, the breaking of aliphatic carbons pairs favors the formation of aldehydes and ketones, which occurs according to the Criegee mechanism via ozonation, and originates dicarboxylic acids from the aromatic rings (Figure 2.21) [108].

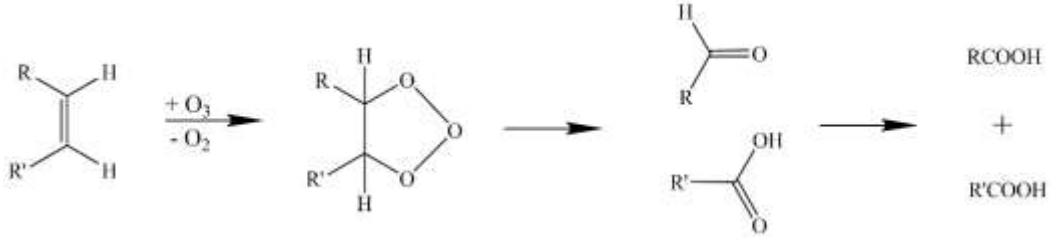

Figure 2.21- Ozone reaction with double bounds.

Ozone is not selective towards the lignin, thus, the application of this compound in the stoppers must be carried out under an efficient agitation, avoiding the local excess of ozone on the surface of the stoppers, which initially leads to delignification, a situation that increases the stopper surface brightness, but in greater quantity also causes the breakdown of double bonds in suberin, which reduces the stopper quality.

The ozone bleaching capacity is enhanced by the slightly acidic pH of the reaction medium [145,146]. As previously discussed, cork has about 12.0% hemicelluloses, the major being xylan, that in alkaline medium give rise to hexenuronic acids from uronic moieties. These acids when present at the end of reactive washing promotes brightness reversion [147]. The slightly acidic medium of this bleaching agent prevents the formation of these undesirable unsaturated structures, in addition to the fact that even if this formation occurs, ozone can eliminate them, giving this agent high brightness stability.

The use of ozone as a bleaching agent translates into several advantages such as the efficient removal of chromophores in extractives and unsaturated acids, thus improving the brightness of the cork without causing stains and blistering in the cork. The direct application of ozone in the gaseous state does not require an effluent treatment system, since ozone rapidly decomposes into molecular oxygen which can be reused to produce ozone again. At the same time, ozone is known as a powerful widely used disinfecting agent [148,149].

2.9.2.2. Ozone in aqueous solution

When the reaction of ozone with chromophores groups occurs in an aqueous medium, three factors must be taken into account: the solubility of ozone in water, the decomposition of ozone in water, and the mass transfer of ozone. These three points are closely related and the efficiency of reactive washing in an aqueous medium depends on them.

There is a competition between the solubility of ozone in an aqueous medium and ozone decomposition reactions and likewise, the dynamic equilibrium of the water/ozone solution depends

on the quality of the mass transfer of ozone in water and the kinetics of the reactions ozone decomposition [150].

2.9.2.2.1. Solubility of ozone in water

The solubility of ozone in water is a crucial parameter regarding the capacity of ozone as a bleaching agent. The solubility of ozone in equilibrium with its partial pressure is usually defined by Henry's law, according to Equation 2.14.

$$x_{O_3} = \frac{P_{O_3}}{k_H} \tag{2.14}$$

Where x_{O_3} is the molar fraction of dissolved ozone (mol mol^{-1}), P_{O_3} is the partial pressure of ozone (atm) and k_H is Henry's constant (atm molar fraction^{-1}).

Henry's constant is shown in Equation 2.15 and relates it to temperature.

$$\frac{dLnk_H}{d(1/T)} = -\frac{\Delta H}{R}$$
$$k_H = k_H^0 \cdot Exp\left(-\frac{\Delta H}{R}\left(\frac{1}{T} - \frac{1}{T^0}\right)\right) \tag{2.15}$$

Where R is the gas constant, ΔH is the enthalpy of the solution, and the parameters k_H^0 and T^0 refer to k_H and T under standard conditions.

Equation 2.14 and Equation 2.15 show that the increase in temperature causes a decrease in the concentration of ozone dissolved in water. The reduced solubility of ozone at high temperatures can be explained by the drop in the driving force of the liquid phase and an increase in the rate of the decomposition of the ozone [71]. The degree of ozone solubility in water depends on the ozone concentration in the gas phase and this is related to the partial pressure. Other factors that influence solubility are the pH and the concentration of ions present in the water.

The pH is a determining parameter concerning the stability of ozone in water and consequently in its solubility, thus the concentration of ozone dissolved in water increases with decreasing pH [71]. Quederni *et al*. determined Henry's constants for the solubility of ozone in water as a function of temperature for different pH values, presented in Equation 2.16 [150].

$$k_H = exp\left(20{,}7 - \frac{3547}{T}\right)\ (pH = 7)$$
$$k_H = exp\left(18{,}1 - \frac{2876}{T}\right)\ (pH = 2) \tag{2.16}$$

In general, the solubility of ozone in water can be improved by increasing the concentration of ozone in the gas mixture, compressing the gas, decreasing the water temperature, decreasing the pH of the reaction medium, and reducing the impurities present in water.

2.9.2.2.2. Decomposition of ozone in water

Ozone tends to decompose in the presence of water, favoring the formation of very reactive radicals with low selectivity (Figure 2.22). Hydroxyl ions catalyze the ozone decomposition reaction and promote the formation of hydroxyl radicals [71,151].

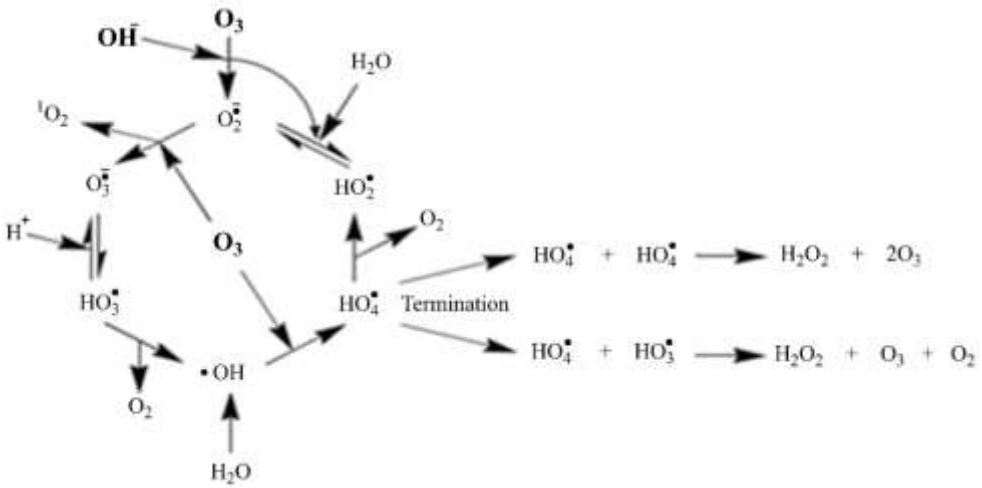

Figure 2.22- Cyclical mechanism of ozone decomposition in water according to Staehelin *et al.* [165].

Figure 2.22 demonstrates the main species present in the ozone decomposition, which is initiated by the presence of hydroxyl ions (OH^-) (Equation 2.17).

$$O_3 + OH^- \rightarrow HO_2 \cdot + \cdot O_2^- \tag{2.17}$$

The ozone consumption rate due to its decomposition increases by raising the alkalinity of the reaction medium (greater amount of hydroxyl groups), according to Equation 2.18.

$$\frac{d[O_3]}{dt} = -k \cdot [O_3]^a \cdot [OH^-]^b \tag{2.18}$$

Where k is the reaction constant, and a and b are reaction orders of ozone and hydroxyl anion, respectively. The value of a varies between 1 and 2 and the value of b between 0.12 and 1.0 [152]. Nevertheless, studies have shown that for pH values between 4 and 8, a equals to 2, that is, the reaction is of second order for ozone, for pH values above 8, the reaction order for ozone is higher, which causes an increase in its decomposition rate [152,153].

The set of reactions from the first propagation step of ozone decomposition in an aqueous medium is presented in Equation 2.19. The reaction of ozone with the superoxide ionic radical ($\cdot O_2^-$) is one of the main propagation reactions, because it reacts quickly with ozone, giving rise to the formation of the intermediates $\cdot O_3^-$ and $HO_3\cdot$ [154].

$$\begin{aligned} O_3 + \cdot O_2^- &\rightarrow \cdot O_3^- + O_2 && k = 1{,}6 \times 10^9\ M^{-1}s^{-1} \\ \cdot O_3^- + H^+ &\overset{a}{\rightarrow} HO_3\cdot && k_a = 1{,}6 \times 10^9\ M^{-1}s^{-1} \\ HO_3\cdot &\overset{b}{\rightarrow} \cdot O_3^- + H^+ && k_b = 3{,}7 \times 10^4\ M^{-1}s^{-1} \\ HO_3\cdot &\rightarrow HO\cdot + O_2 && k = 1{,}1 \times 10^5\ M^{-1}s^{-1} \end{aligned} \tag{2.19}$$

The second propagation step, as well as the reaction constants, are depicted in Equation 2.20.

$$\begin{aligned} HO\cdot + O_3 &\rightarrow HO_4\cdot && k = 2{,}0 \times 10^9\ M^{-1}s^{-1} \\ HO_4\cdot &\leftrightarrow HO_2\cdot + O_2 && k = 2{,}8 \times 10^4\ M^{-1}s^{-1} \\ HO_2\cdot &\leftrightarrow \cdot O_2^- + H^+ && pKa = 4{,}8 \end{aligned} \tag{2.20}$$

The specie $HO_4\cdot$ has a longer half-time than its accumulation rate and, therefore, is an important specie concerning termination reactions (Equation 2.21) of the ozone decomposition cycle [71].

$$\begin{aligned} HO_4\cdot + HO_4\cdot &\rightarrow H_2O_2 + 2O_3 \\ HO_4\cdot + HO_3\cdot &\rightarrow H_2O_2 + O_3 + O_2 \end{aligned} \tag{2.21}$$

The reactions present in Equation 2.21 are dominant in the presence of high concentrations of ozone. Some factors influence the decomposition of ozone in water, such as temperature, pH, the existence of UV light, among others.

Depending on the pH of the reaction medium, ozone acts not only by direct reaction but also on the formation and reaction of hydroxyl radicals, one of the most reactive oxygen species. Hydroxyl radicals are more reactive than ozone because they have an standard oxidizing power of 2.80 V, however, they are less selective also attacking the functional groups of polysaccharides [151,153].

2.9.2.2.3. Mass transference

The effectiveness of ozone as a bleaching agent depends on the presence of water that limits the ozone mass transference and, as such, higher ozone charges are required for similar levels of efficiency when compared to the absence of water in the reaction medium [155].

In the presence of water, ozone bleaching is a complex mass transfer process that includes stages of chemical absorption by cork, gas-liquid mass transfer, accompanied by ozone decomposition, and oxidation reactions [156]. The determining step in this process is controlled by the mass transfer of

the oxidizing species towards the reaction site with chromophore groups of cork [71]. Osawa & Schuerch proposed the model shown in Figure 2.23.

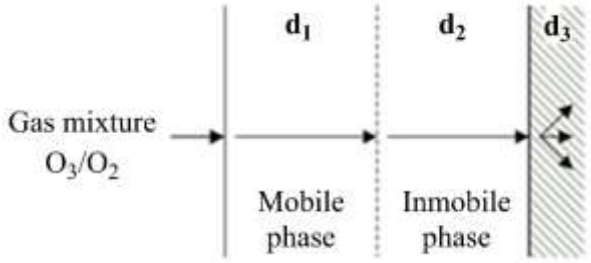

Figure 2.23- Scheme of ozone mass transfer into aqueous medium proposed by Osawa & Schuerch [166].

The first step of ozone in a gaseous state is the dissolution of ozone in the mobile phase of water that occurs by convection (d_1). The dissolved ozone (and its decomposition products) is then transported through an immobile phase of water by diffusion (d_2). This step is crucial since this process is slower than convection transport [71].

The mass transfer of ozone from the gas phase to the liquid phase can be explained by the two films theory which assumes that there are hypothetically two laminar films in each of the fluids (Figure 2.24) [156,157].

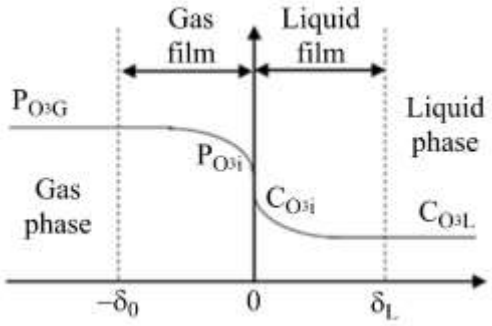

Figure 2.24- Two-film theory model.

The mass of ozone transferred from the gas phase to the liquid phase over time is described in Equation 2.22.

$$\frac{dN}{dt} = K_G a \left(P_{O_3G} - P_{O_{3_i}}\right) V = K_L a \left(C_{O_{3_i}} - C_{O_3L}\right) V \quad (2.22)$$

Where N is the ozone mass transfered (kg), K_G is the global mass transfer coefficient for the gaseous film $\left(\text{m s}^{-1}\right)$, a is the interfacial area per volume unit (m^2m^{-3}), P_{O_3G} is the partial pressure of ozone in the gas phase (Pa), $P_{O_{3_i}}$ is the partial pressure of ozone at the gas-liquid equilibrium interface (Pa), V is the volume $\left(\text{m}^3\right)$, K_L is the global mass transfer coefficient for the liquid phase $\left(\text{m s}^{-1}\right)$, $C_{O_{3_i}}$ is the concentration of ozone in the liquid phase $\left(\text{mol L}^{-1}\right)$.

At constant temperature, the thermodynamic equilibrium between the two phases in contact can be described by Henry's Theory, presented in Equation 2.23.

$$C_{O_3L}{}^{*} = k_H\, P_{O_3}$$
$$C_{O_3L} = k_H\, P_{O_3} \quad (2.23)$$

In this way, the amount of ozone transferred can be calculated by Equation 2.24.

$$\frac{dN}{dt} = K_L a\left(C_{O_3}{}^{*} - C_{O_3L}\right)V \quad (2.24)$$

There is a relationship between the global mass transfer coefficient for the liquid film (K_L) and the mass transfer coefficient for the liquid (k_L) and gas film (k_G), according to Equation 2.25 [156,157].

$$\frac{1}{K_L} = \frac{1}{k_L} + \frac{k_H}{k_G} \quad (2.25)$$

Since ozone is slightly soluble in water, mass transfer is controlled by the liquid phase, so in aqueous systems with ozone the value of $1/k_L$ is much higher when compared with the value of k_H/k_G which demonstrates that $K_L \approx k_L$ and, thus, it would be necessary to decrease the resistance of the liquid film to improve the mass transfer rate of ozone [156]. Thus, and considering that $N = C/V$, the concentration of ozone in the liquid phase over time can be exposed by Equation 2.26.

$$\frac{dC_{O_3L}}{dt} = k_L\, a\, C_{O_3}{}^{*} \quad (2.26)$$

2.9.2.3. Processual variables

The efficiency of the cork stopper reactive washing process with ozone depends on variables such as the presence or absence of water in the reaction medium, temperature, pH, and reaction time.

2.9.2.3.1. Presence of water in the reaction medium

As previously described, the presence of water in the ozone bleaching influences its efficiency. The half-life time of ozone in the gaseous state is longer than that found in an aqueous solution. Additionally, the purity of the water in the aqueous solution affects the stability of the ozone, the presence of transition metals promotes spontaneous decomposition of ozone (Equation 2.27) [71,140,142].

$$2O_3 \xrightarrow{M^{n+}/H_2O} 3O_2 \quad (2.27)$$

The presence of transition metals in the reaction medium act as catalysts for the decomposition of ozone according to the reactions in Equation 2.28.

$$\begin{gathered} O_3 + M^{n+} + H^+ \rightarrow HO\cdot + M^{(n+1)+} + O_2 \\ HO\cdot + O_3 \rightarrow HO_2\cdot + O_2 \\ HO_2\cdot \leftrightarrow O_2\cdot + H^+ \\ O_2\cdot + M^{(n+1)+} \rightarrow M^{n+} + O_2 \end{gathered} \tag{2.28}$$

2.9.2.3.2. Temperature

This bleaching agent is highly sensitive to temperature. The efficiency of ozone is compromised by the increase in temperature, if the value recorded is above 60°C, ozone decomposes into oxygen, and therefore decreases its delignification capacity. On the other hand, if the reaction is in the presence of water, reactions occur, forming the hydroxyl radicals (Equation 2.29) and hydroperoxide (Equation 2.30) that are extremely reactive and have low selectivity towards polysaccharides [71,116].

$$O_3 + H_2O \rightarrow 2HO\cdot + O_2 \tag{2.29}$$

$$O_3 + HO\cdot \rightarrow HOO\cdot + O_2 \tag{2.30}$$

In this way, the bleaching temperature must be as low as possible, which means that the temperature of the ozone generation and the reaction medium must be maintained between 30°C and 60°C [71,116].

2.9.2.3.3. pH effect

Ozone has a good performance when the reaction medium pH is between 5.4 and 6.15, because at this level of acidity ozone is quite stable [158,159]. The more alkaline the medium, the greater the concentration of hydroxyl ions which, as already mentioned, promote the decomposition of ozone, and thus reduce the reactive washing capacity of this agent. Additionally, the formation of hydroxyl and hydroperoxide radicals occurs, which are not very selective and also react with polysaccharides, and other components of cork, which reduces the efficiency of the process [145].

2.9.2.3.4. Time reaction

The increase in ozone concentration and reaction time causes an increase in brightness. However, for longer reaction times, cellulose and suberin degradation may occur, which causes a decrease in the quality of the stoppers [143]. The brightness rise of the stopper surface will be more

pronounced in the first moments since ozone can react almost spontaneously with the double bonds of the functional groups of the chromophores [158].

2.9.2.4. Ozone generation

Because of its high reactivity, ozone cannot be stored and does not accumulate without continuous production. Ozone is not added individually, thus using a carrier gas, the most common being oxygen and air [160]. However, the use of pure oxygen allows the formation of ozone in higher concentrations. Currently, ozone can be generated commercially by three different methods: corona discharge; UV radiation (at a wavelength of 188 nm); and electrolysis, being the most used the discharge corona [140,142].

In the corona discharge, ozone is generated when the carrier gas passes through two electrodes (one with high and one with low voltage) slightly separated, where one of them is coated with a dielectric material. When voltage is applied between the two electrodes arranged concentrically, and this voltage exceeds the ionization potential of the dielectric material, electrons go through the passage zone of the carrier gas providing enough energy to dissociate the oxygen molecules (Equation 2.31), then the oxygen atoms interact with oxygen molecules present, promoting the formation of ozone (Equation 2.12) [71,140]. This method is outlined in Figure 2.25.

$$O_2(g) + e^- \rightarrow 2O(g) + e^- \quad (2.31)$$

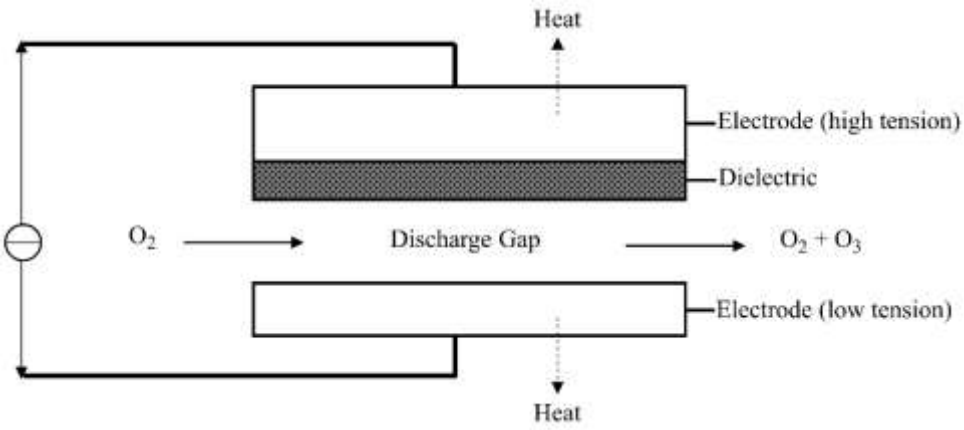

Figure 2.25- Scheme of ozone generation by the corona discharge method.

Through this ozone generation method, an exothermal physical-chemical reaction occurs and since ozone decomposition increases with rising temperature and ozone concentration, the ozone generator must have an adequate cooling system [71].

This method allows the production of between 1 and 3% of ozone when the carrier gas is air, while if using high purity oxygen a formation of up to 16% of ozone can be reached, this concentration can be increased if the gaseous mixture is compressed [58,142]. Although production

costs on a larger scale are low, the energy consumption required by this method is high, which is a disadvantage of this method [58,142]. To keep the energy consumption as low as possible, the gases used as raw material in the ozone generator must be dry since the ozone production yield decreases considerably even with low moisture levels [161]. The electrical potential used to maintain the corona discharge for ozone generation is normally greater than 10000V [162].

As previously described, the ozone molecules formed are very unstable, so the ozone generator must be directly connected to the reactor where the reactive washing will take place to prevent it from decomposing into oxygen before reacting.

2.9.2.5. Process and equipment

Given the similarity with the pulp and paper industry, an industry where ozone bleaching is already well established, Figure 2.26 shows the generalized ozone bleaching process for the pulp and paper industry.

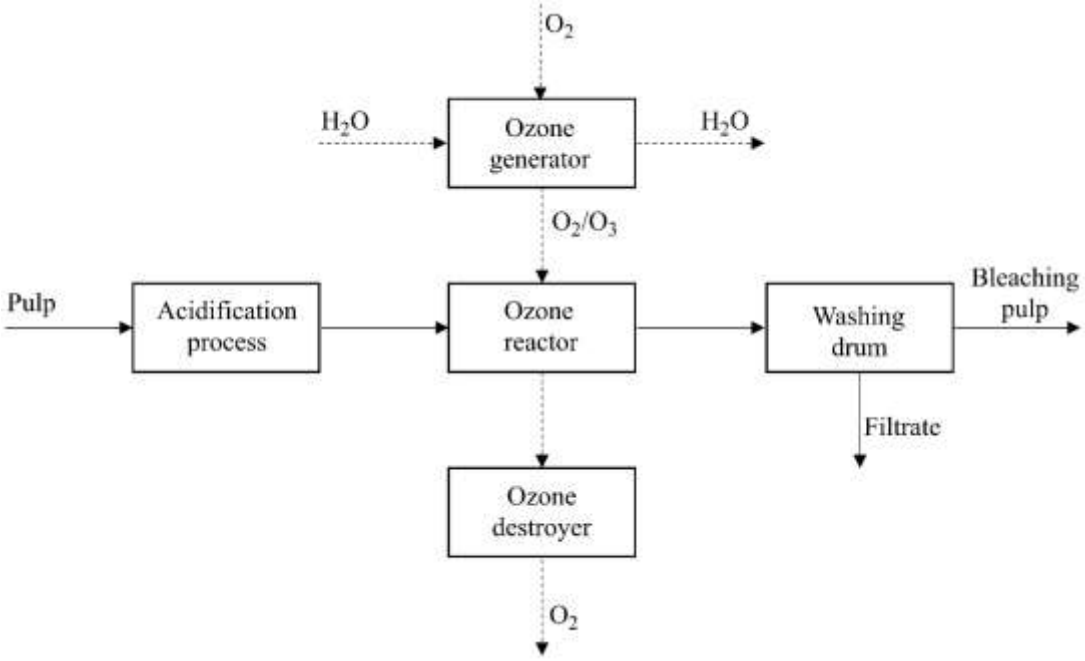

Figure 2.26- Schematic representation of the ozone bleaching process.

As can be seen from Figure 2.26, in general, the pulp before coming in contact with ozone in the reactor goes through an acidification stage that aims to improve the ozone stability in the subsequent equipment and, consequently, increase bleaching efficiency. The pulp after the reactor is already bleached and passes to a drum where it is washed to remove impurities from the process. In these industries, these systems operate continuously, contrary to what is expected for the cork industry. The bleaching process requires different equipment whether the application of ozone as a bleaching agent is directly on cork stoppers or in the presence of water in the reaction medium.

In Amorim Cork, S.A. there are three types of equipment prepared for the RW process, with different volume capacities, such as 3000 (3k), 20 000 (20k), and 100 000 (100k) stoppers (45 x 24 mm, length x diameter). The pilot-scale equipment is the smaller one with the capacity to 3000 stoppers recognized by 3k equipment, the other two are of industrial scale. The equipment features are presented in Figure 2.27.

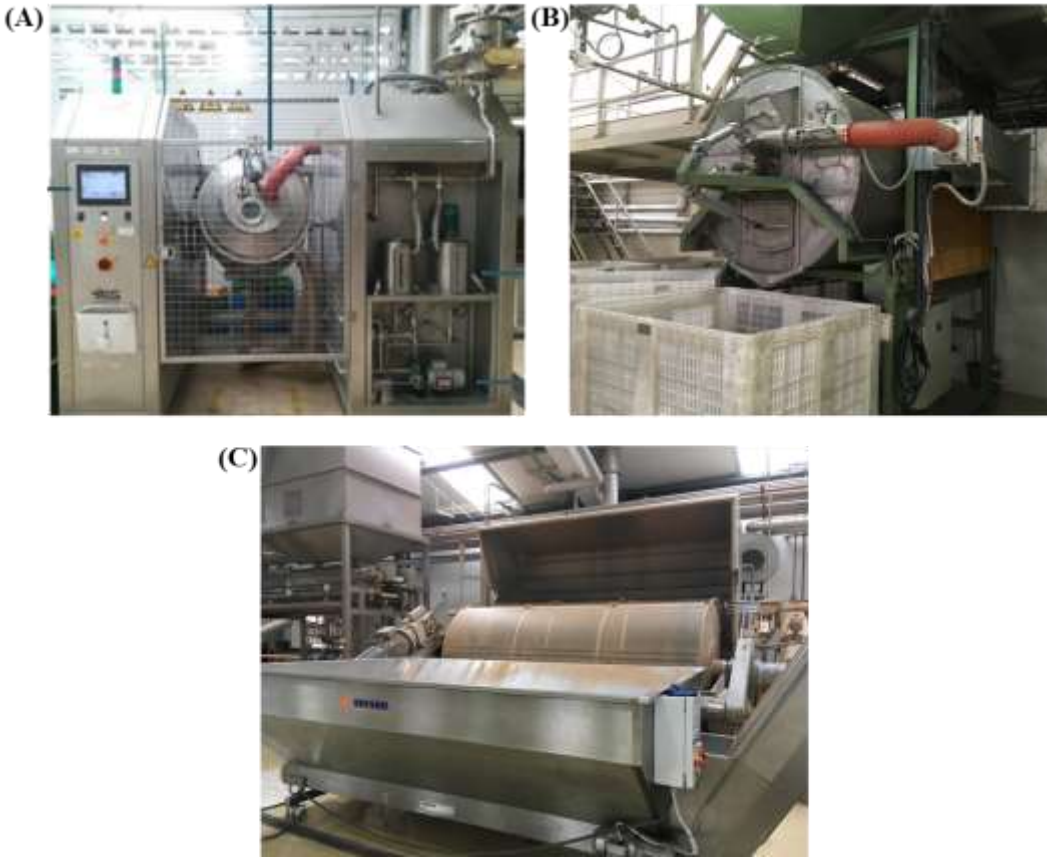

Figure 2.27- RW equipment's present in Amorim Cork, S.A. Pilot equipment- 3k (A), and industrial equipment (B) 20k, and (C) 100k.

The smaller equipment, the 3k, has two tanks for the reagent input in the reactor drum, and the loading and unloading of the stoppers are realized by the operator, there are no automatisms associated with these actions. On the other hand, the industrial types of equipment (20k and 100k) have scales that allow the entrance of the desired volume of reagents into the reactor's drums. The reagents enter in contact with the stoppers by sprayers located inside the drum, and the drying process is done by the passage of air heated by collectors. The load and unload of stoppers in these reactors are made by a supply system that has more automatisms than the 3k equipment. All the reactors have a console associated that allows the input of the RW process program and the change of the conditions of the steps of the reactive washing.

All the reactors in Amorim Cork are prepared for the conventional RW with hydrogen peroxide. However, they are not adapted for the introduction of ozone as a bleaching agent. The implementation of ozone requires equipment hermetically sealed to avoid any ozone leakage, besides an ozone generator and destroyer to eliminate the ozone that did not react when in contact with the stoppers. Additionally, the equipment for the implementation of ozone treatment in stoppers requires access to an air or oxygen line, as well as, a water line, for the input on the ozone generator and the refrigeration of the same equipment, respectively. To keep ozone generation costs as low as possible, it is important that the by-product, oxygen, is fully reused. Three distinct methods can be applied, as shown in Figure 2.28.

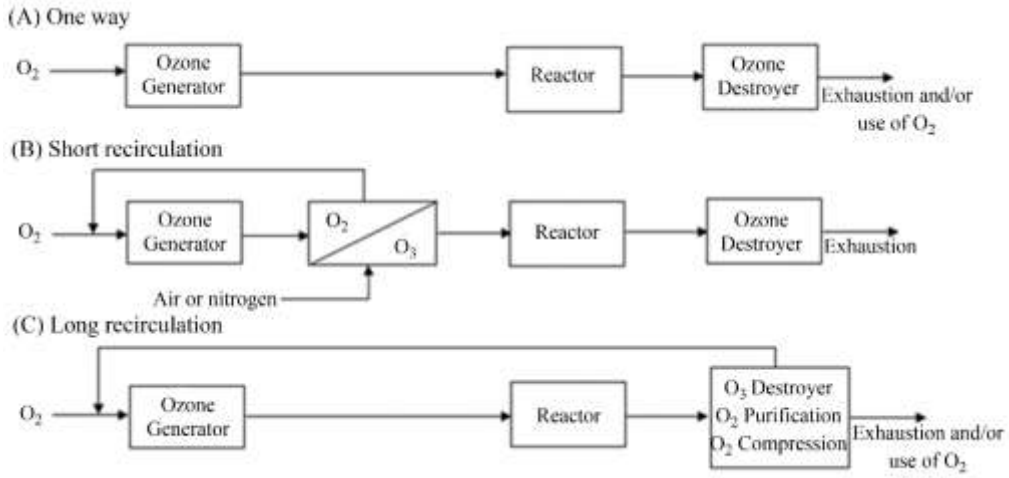

Figure 2.28- Possible ways to reuse oxygen [161].

Method (A) consists of the direct use of residual gaseous oxygen in another process without any other type of purification, of all methods this is the most economical. In the case of short recirculation (B), the gas stream that leaves the ozone generator is separated into oxygen and ozone, the oxygen is returned to the generator to be used as the supply gas. With long recirculation (C), the oxygen remaining after the ozone generator returns to the ozone generator, however, it needs to be purified in terms of moisture to maintain the performance of the ozone generator [161]. Thus, it is important to obtain a high ozone utilization rate to reduce the energy consumption used to carry out the destruction of ozone in excess [157].

In this way, the implementation of ozone as a bleaching agent for the RW on an industrial scale requires the design and construction of a new equipment that respects all the ozone handling security and process demands.

2.10.References

[1] APCOR, APCOR – O que é?, (n.d.). http://www.apcor.pt/cortica/o-que-e/ (accessed September 7, 2021).

[2] M.E. Rosa, M.A. Fortes, Recovery of used cork stoppers, Colloids Surfaces A Physicochem. Eng. Asp. 344 (2009) 97–100. https://doi.org/10.1016/j.colsurfa.2009.02.035.

[3] Decreto-lei Nº169/2001 de 25 de Maio do Ministério da Agricultura, do Desenvolvimento Rural e das Pescas, Portugal, 2001. www.dre.pt.

[4] Mitos e Curiosidades- Cortiça- Amorim Cork, (n.d.). https://www.amorimcork.com/pt/cortica/mitos-e-curiosidades/?f_tema=64 (accessed September 11, 2021).

[5] H. Pereira, Variability of the chemical composition of cork, BioResources. 8 (2013) 2246–2256. https://doi.org/10.15376/biores.8.2.2246-2256.

[6] A. Costa, H. Pereira, A. Oliveira, Variability of radial growth in cork oak adult trees under cork production, For. Ecol. Manage. 175 (2003) 239–246. https://doi.org/10.1016/S0378-1127(02)00145-7.

[7] A. Caritat, E. Gutiérrez, M. Molinas, Influence of weather on cork-ring width, Tree Physiol. 20 (2000) 893–900. https://doi.org/10.1093/treephys/20.13.893.

[8] A. Caritat, M. Molinas, E. Gutierrez, Annual cork-ring width variability of *Quercus suber* L. in relation to temperature and precipitation (Extremadura, southwestern Spain), For. Ecol. Manage. 86 (1996) 113–120. https://doi.org/10.1016/S0378-1127(96)03787-5.

[9] S.P. Silva, M.A. Sabino, E.M. Fernandes, V.M. Correlo, L.F. Boesel, R.L. Reis, Cork: properties, capabilities and applications, Int. Mater. Rev. 50 (2005) 345–365. https://doi.org/10.1179/174328005X41168.

[10] Corticeira Amorim S. G. P. S., The art of cork, 2005.

[11] A.P. Duarte, J.C. Bordado, Cork – a renewable raw material: Forecast of industrial potential and development priorities, Front. Mater. 2 (2015) 1–8. https://doi.org/10.3389/fmats.2015.00002.

[12] APCOR, APCOR's Cork Yearbook 2020, 2020.

[13] ICNF, 6º Inventário Florestal Nacional (IFN6), 2015. http://www.icnf.pt/portal/florestas/ifn/resource/ficheiros/ifn/ifn6-res-prelimv1-1.

[14] H. Pereira, Cork : Biology, production and uses, 1st ed., Elsevier B.V., Lisboa, 2007.

[15] H. Pereira, F. Lopes, J. Graça, The evaluation of the quality of cork planks by image analysis, Holzforschung. 50 (1996) 111–115. https://doi.org/10.1515/hfsg.1996.50.2.111.

[16] O. Anjos, H. Pereira, M.E. Rosa, Effect of quality, porosity and density on the compression

properties of cork, Eur. J. Wood Wood Prod. 66 (2008) 295–301. https://doi.org/10.1007/s00107-008-0248-2.

[17] H. Pereira, Chemical composition and variability of cork from *Quercus suber* L., Wood Sci. Technol. 22 (1988) 211–218. https://doi.org/10.1007/BF00386015.

[18] M.A. Fortes, M. Emília Rosa, H. Pereira, The cellular structure of cork from *Quercus Suber* L., IAWA J. 8 (1987) 213–218. https://doi.org/10.1163/22941932-90001048.

[19] APCOR – Descortiçamento, (n.d.). http://www.apcor.pt/cortica/processo-de-transformacao/descorticamento/ (accessed September 10, 2021).

[20] H. Pereira, M. Tomé, Cork oak, Non-Wood Prod. (2004) 613–620.

[21] L. Gil, A cortiça como material de construção, APCOR-Asso, Santa Maria de Lamas, n.d.

[22] L.J. Gibson, Biomechanics of cellular solids., J. Biomech. 38 (2005) 377–399. https://doi.org/10.1016/j.jbiomech.2004.09.027.

[23] H. Pereira, The rationale behind cork properties: A review of structure and chemistry, BioResources. 10 (2015) 1–23. https://doi.org/10.15376/biores.10.3.Pereira.

[24] S. Lequin, D. Chassagne, T. Karbowiak, R. Gougeon, L. Brachais, J.P. Bellat, Adsorption equilibria of water vapor on cork, J. Agric. Food Chem. 58 (2010) 3438–3445. https://doi.org/10.1021/jf9039364.

[25] R.T. Teixeira, H. Pereira, Suberized cell walls of cork from cork oak differ from other species, Microsc. Microanal. 16 (2010) 569–575. https://doi.org/10.1017/S1431927610093839.

[26] L. Yafang, J. Ting, S. Xiaozhou, Chemical composition of cork from *Quercus variablis*, Wood Fiber Sci. 44 (2012) 214–219.

[27] A. Fernandes, I. Fernandes, L. Cruz, N. Mateus, M. Cabral, V. De Freitas, Antioxidant and biological properties of bioactive phenolic compounds from *Quercus suber* L., J. Agric. Food Chem. 57 (2009) 11154–11160. https://doi.org/10.1021/jf902093m.

[28] J. Azevedo, I. Fernandes, P. Lopes, I. Roseira, M. Cabral, N. Mateus, V. Freitas, Migration of phenolic compounds from different cork stoppers to wine model solutions: antioxidant and biological relevance, Eur. Food Res. Technol. 239 (2014) 951–960. https://doi.org/10.1007/s00217-014-2292-y.

[29] H. Pereira, Studies on the chemical composition of virgin and reproduction cork of Quercus suber L ., An. Do Inst. Super. Agron. 25 (1981) 17–25.

[30] P.J. Holloway, The composition of suberin from the corks of *Quercus suber* L. and *Betula pendula* roth, Chem. Phys. Lipids. 9 (1972) 158–170. https://doi.org/10.1016/0009-3084(72)90011-4.

[31] N. Parameswaran, W. Liese, H. Günzerodt, Characterization of wetcork in *Quercus suber* L., Holzforschung. 35 (1981) 195–199. https://doi.org/10.1515/hfsg.1981.35.4.195.

[32] E. Conde, E. Cadahía, M.C. García-Vallejo, J.R. González-Adrados, Chemical characterization of reproduction cork from spanish *Quercus suber*, J. Wood Chem. Technol. 18 (1998) 447–469. https://doi.org/10.1080/02773819809349592.

[33] P.E. Kolattukudy, Biopolyester Membranes of Plants : Cutin and Suberin, Science (80-.). 208 (1980) 990–1000. https://doi.org/10.1126/science.208.4447.990.

[34] R. Franke, L. Schreiber, Suberin - a biopolyester forming apoplastic plant interfaces, Curr. Opin. Plant Biol. 10 (2007) 252–259. https://doi.org/10.1016/j.pbi.2007.04.004.

[35] W. Cottle, P.E. Kolattukudy, Biosynthesis, Deposition, and Partial Characterization of Potato Suberin Phenolics, Plant Physiol. 69 (1982) 393–399. https://doi.org/10.1104/pp.69.2.393.

[36] C.L. Soliday, P.E. Kolattukudy, R.W. Davis, Chemical and ultrastructural evidence that waxes associated with the suberin polymer constitute the major diffusion barrier to water vapor in potato tuber (*Solanum tuberosum* L.), Planta. 146 (1979) 607–614. https://doi.org/10.1007/BF00388840.

[37] A.J.D. Silvestre, C.P. Neto, A. Gandini, Cork and suberins: Major sources, properties and applications, in: Monomers, Polym. Compos. from Renew. Resour., 2008: pp. 305–320. https://doi.org/10.1016/B978-0-08-045316-3.00014-4.

[38] M.A. Bernards, Demystifying suberin, Can. J. Bot. 80 (2002) 227–240. https://doi.org/10.1139/b02-017.

[39] P.E. Kolattukudy, Biochemistry and function of cutin and suberin, Can. J. Bot. 62 (1984) 2918–2933. https://doi.org/10.1139/b84-391.

[40] M.F. Bento, H. Pereira, M.Á. Cunha, A.M.C. Moutinho, K.J. van den Berg, J.J. Boon, Thermally assisted transmethylation gas chromatography mass spectrometry of suberin components in cork from Quercus suber L., Phytochem. Anal. 9 (1998) 75–87.

[41] M.C. García-Vallejo, E. Conde, E. Cadahía, B. Fernández De Simón, Suberin composition of reproduction cork from *Quercus suber*, Holzforschung. 51 (1997) 219–224. https://doi.org/10.1515/hfsg.1997.51.3.219.

[42] M.F. Bento, H. Pereira, M.Á. Cunha, A.M.C. Moutinho, K.J. van den Berg, J.J. Boon, O. van den Brink, R.M.A. Heeren, Fragmentation of Suberin and Composition of Aliphatic Monomers Released by Methanolysis of Cork from *Quercus suber* L.,Analysed by GC-MS, SEC and MALDI-MS, Holzforschung. 55 (2001) 487–493. https://doi.org/10.1515/hf.2001.080.

[43] M.H. Lopes, A.M. Gil, A.J.D. Silvestre, C.P. Neto, Composition of suberin extracted upon gradual alkaline methanolysis of *Quercus suber* L. cork, J. Agric. Food Chem. 48 (2000) 383–391. https://doi.org/10.1021/jf9909398.

[44] N. Cordeiro, M.N. Belgacem, A.J.D. Silvestre, C. Pascoal Neto, A. Gandini, Cork suberin as

a new source of chemicals. 1. Isolation and chemical characterization of its composition, Int. J. Biol. Macromol. 22 (1998) 71–80. https://doi.org/10.1016/S0141-8130(97)00090-1.

[45] J. Graça, H. Pereira, Methanolysis of Bark Suberins: analysis of glycerol and acid monomers, Phytochem. Anal. 11 (2000) 45–51. https://doi.org/10.1002/(SICI)1099-1565(200001/02)11:1<45::AID-PCA481>3.0.CO;2-8.

[46] E. Conde, M.C. García-Vallejo, E. Cadahía, Variability of suberin composition of reproduction cork from *Quercus suber* throughout industrial processing, Holzforschung. 53 (1999) 56–62. https://doi.org/10.1515/HF.1999.010.

[47] M.F.S. Bento, H. Pereira, M.Á. Cunha, A.M.C. Moutinho, K.J. Van Den Berg, J.J. Boon, A study of variability of suberin composition in cork from Quercus suber L. using thermally assisted transmethylation GC-MS, J. Anal. Appl. Pyrolysis. 57 (2001) 45–55. https://doi.org/10.1016/S0165-2370(00)00093-0.

[48] A. Schmutz, T. Jenny, N. Amrhein, U. Ryser, Caffeic acid and glycerol are constituents of the suberin layers in green cotton fibres, Planta. 189 (1993) 453–460. https://doi.org/10.1007/BF00194445.

[49] P.E. Kolattukudy, Polyesters in Higher Plants, in: Adv. Biochem. Eng. Biotechnol., Springer-Verlag Berlin Heidelberg, 2001: pp. 1–49. https://doi.org/10.1007/3-540-40021-4_1.

[50] A. Gandini, C.P. Neto, A.J.D. Silvestre, Suberin: A promising renewable resource for novel macromolecular materials, Prog. Polym. Sci. 31 (2006) 878–892. https://doi.org/10.1016/j.progpolymsci.2006.07.004.

[51] J. Graça, H. Pereira, Glyceryl-Acyl and Aryl-Acyl Dimers in *Pseudotsuga menziesii* Bark Suberin, Holzforschung. 53 (1999) 397–402. https://doi.org/10.1515/HF.1999.066.

[52] J. Graça, H. Pereira, Feruloyl esters of ω-hydroxyacids in cork suberin, J. Wood Chem. Technol. 18 (1998) 207–217. https://doi.org/10.1080/02773819809349577.

[53] J. Graça, S. Santos, Glycerol-derived ester oligomers from cork suberin, Chem. Phys. Lipids. 144 (2006) 96–107. https://doi.org/10.1016/j.chemphyslip.2006.08.001.

[54] S. Santos, J. Graça, Glycerol-ω-hydroxyacid-ferulic acid oligomers in cork suberin structure, Holzforschung. 60 (2006) 171–177. https://doi.org/10.1515/HF.2006.028.

[55] L. Moire, A. Schmutz, A. Buchala, B. Yan, R.E. Stark, U. Ryser, Glycerol is a suberin monomer. New experimental evidence for an old hypothesis, Plant Physiol. 119 (1999) 1137–1146. https://doi.org/10.1104/pp.119.3.1137.

[56] A.M. Gil, M. Lopes, J. Rocha, C.P. Neto, A 13C solid state nuclear magnetic resonance spectroscopic study of cork cell wall structure: The effect of suberin removal, Int. J. Biol. Macromol. 20 (1997) 293–305. https://doi.org/10.1016/S0141-8130(97)00029-9.

[57] A. V. Marques, H. Pereira, On the determination of suberin and other structural components

in cork from *Quercus suber* L., An. Do Inst. Super. Agron. 42 (1987) 321–335.

[58] D. Fengel, G. Wegener, Wood-chemistry, ultrastructure, reactions, Walter de Gruyter, Berlin, 1989. https://doi.org/10.1515/9783110839654.

[59] D. Dimmel, Overview, in: C. Heitner, D.R. Dimmel, J.A. Schmidt (Eds.), Lignin Lignans-Adv. Chem., Taylor & Francis, Boca Raton, 2010: pp. 1–10.

[60] E. Zimmermann, W., Nimz, H. & Seemüller, H and ^{13}C NMR Spectroscopic Study of Extracts from Corks of Rubus idaeus, Solanum tuberosum, and Quercus suber., Holzforschung. 39 (1985) 45–49. https://doi.org/10.1515/hfsg.1985.39.1.45.

[61] A. V. Marques, H. Pereira, D. Meier, O. Faix, Quantitative analysis of cork (Quercus suber L.) and milled cork lignin by FTIR spectroscopy, analytical pyroiysis, and total hydrolysis, Holzforschung. 48 (1994) 43–50. https://doi.org/10.1515/hfsg.1994.48.s1.43.

[62] A. V. Marques, H. Pereira, D. Meier, O. Faix, Isolation and characterization of a guaiacyl lignin from saponified cork of *Quercus suber* L., Holzforschung. 50 (1996) 393–400. https://doi.org/10.1515/hfsg.1996.50.5.393.

[63] A. V. Marques, H. Pereira, J. Rodrigues, D. Meier, O. Faix, Isolation and comparative characterization of a Björkman lignin from the saponified cork of Douglas-fir bark, J. Anal. Appl. Pyrolysis. 77 (2006) 169–176. https://doi.org/10.1016/j.jaap.2006.03.003.

[64] A.V. Marques, H. Pereira, Lignin monomeric composition of corks from the barks of Betula pendula, Quercus suber and Quercus cerris determined by Py-GC-MS/FID, J. Anal. Appl. Pyrolysis. 100 (2013) 88–94. https://doi.org/10.1016/j.jaap.2012.12.001.

[65] C.P. Neto, N. Cordeiro, A. Seca, F. Domingues, A. Gandini, D. Robert, Isolation and Characterization of a Lignin-Like Polymer of the Cork of Quercus suber L., Holzforschung. 50 (1996) 563–568. https://doi.org/10.1515/hfsg.1996.50.6.563.

[66] A. V. Marques, H. Pereira, D. Meier, O. Faix, Structural characterization of cork lignin by thioacidolysis and permanganate oxidation, Holzforschung. 53 (1999) 167–174. https://doi.org/10.1515/HF.1999.028.

[67] A. V. Marques, J. Rencoret, A. Gutiérrez, J.C. del Río, H. Pereira, Ferulates and lignin structural composition in cork, Holzforschung. 70 (2016) 275–289. https://doi.org/10.1515/hf-2015-0014.

[68] A. Lourenço, J. Rencoret, C. Chemetova, J. Gominho, A. Gutiérrez, J.C. del Río, H. Pereira, Lignin Composition and Structure Differs between Xylem , Phloem and Phellem in Quercus suber L ., Front. Plant Sci. 7 (2016) 1–14. https://doi.org/10.3389/fpls.2016.01612.

[69] R.M. Rowell, R. Petterson, J.S. Han, J.S. Rowell, M.A. Tshabalala, Cell Wall Chemistry, in: R.M. Rowell (Ed.), Handb. Wood Chem. Wood Compos., Taylor & Francis, Boca Raton, 2005: pp. 33–74.

[70] E. Sjöström, Wood polysaccharides, in: Wood Chem. Fundam. Appl., 2nd Ed., Harcout Brace Jovanovich, San Diego, 1993: pp. 51–77.

[71] G. Koch, Raw Material for Pulp, in: H. Sixta (Ed.), Handb. Pulp, 1st Ed., WILEY-VCH Verlag GmbH & Co. KGaA, Lenzing, Austria, 2006: pp. 21–68. https://doi.org/10.1002/9783527619887.

[72] E. Sjöström, U. Westermark, Chemical composition of wood and pulps basic constituents and their distribution, in: R. Alén (Ed.), Anal. Methods Wood Chem. Pulping, Papermak., 1st Ed., Springer, 1998: pp. 1–20. https://doi.org/10.1007/978-3-662-03898-7.

[73] C.J. Biermann, Wood and fiber fundaments, in: Handb. Pulping Papermak., Academic Press, San Diego, 1996: pp. 13–54.

[74] E. Conde, M.C. García-Vallejo, E. Cidahía, Waxes composition of *Quercus suber* reproduction cork from different Spanish provenances, Wood Sci. Technol. 33 (1999) 271–283. https://doi.org/10.1007/s002260050115.

[75] E. Conde, M.C. García-Vallejo, E. Cadahía, Waxes composition of reproduction cork from Quercus suber and its variability throughout the industrial processing, Wood Sci. Technol. 33 (1999) 229–244. https://doi.org/10.1007/s002260050112.

[76] A.F. Sousa, P.C.R.O. Pinto, J.D. Silvestre, Armando, C.P. Neto, Triterpenic and other lipophilic components from industrial cork byproducts, J. Agric. Food Chem. 54 (2006) 6888–6893.

[77] V. Castola, A. Bighelli, S. Rezzi, G. Melloni, S. Gladiali, J.M. Desjobert, J. Casanova, Composition and chemical variability of the triterpene fraction of dichloromethane extracts of cork (*Quercus suber* L.), Ind. Crops Prod. 15 (2002) 15–22. https://doi.org/10.1016/S0926-6690(01)00091-7.

[78] V. Castola, B. Marongiu, A. Bighelli, C. Floris, A. Lai, J. Casanova, Extractives of cork (Quercus suber L.): chemical composition of dichloromethane and supercritical CO2 extracts, Ind. Crops Prod. 21 (2005) 65–69. https://doi.org/10.1016/j.indcrop.2003.12.007.

[79] N. Balasundram, K. Sundram, S. Samman, Phenolic compounds in plants and agri-industrial by-products: Antioxidant activity, occurrence, and potential uses, Food Chem. 99 (2006) 191–203. https://doi.org/10.1016/j.foodchem.2005.07.042.

[80] V.I. Kefeli, M. V Kalevitch, B. Borsari, Phenolic cycle in plants and environment, J. Cell Mol. Biol. 2 (2003) 13–18.

[81] R.N. Bennett, R.M. Wallsgrove, Secondary metabolites in plant defence mechanisms, New Phytol. 127 (1994) 617–633. https://doi.org/10.1111/j.1469-8137.1994.tb02968.x.

[82] L. Bravo, Polyphenols : chemistry , dietary sources , metabolism , and nutritional significance, Nutr. Rev. 56 (1998) 317–333. https://doi.org/10.1111/j.1753-

4887.1998.tb01670.x.

[83] M. Monagas, C. Gómez-Cordovés, B. Bartolomé, Evolution of the phenolic content of red wines from Vitis vinifera L. during ageing in bottle, Food Chem. 95 (2006) 405–412. https://doi.org/10.1016/j.foodchem.2005.01.004.

[84] S.A.O. Santos, P.C.R.O. Pinto, A.J.D. Silvestre, C.P. Neto, Chemical composition and antioxidant activity of phenolic extracts of cork from Quercus suber L., Ind. Crops Prod. 31 (2010) 521–526. https://doi.org/10.1016/j.indcrop.2010.02.001.

[85] C. Proestos, M. Kapsokefalou, M. Komaitis, Analysis of naturally occurring phenolic compounds in aromatic plants by RP-HPLC and GC-MS after silylation, J. Food Qual. 31 (2008) 402–414. https://doi.org/10.1111/j.1745-4557.2008.00208.x.

[86] O. Anjos, C. Rodrigues, J. Morais, H. Pereira, Effect of density on the compression behaviour of cork, Mater. Des. 53 (2014) 1089–1096. https://doi.org/10.1016/j.matdes.2013.07.038.

[87] Cortiça- Características, (n.d.). https://www.amorim.com/a-cortica/caracteristicas/ (accessed September 10, 2021).

[88] APCOR, Manual técnico das rolhas, (2015) 56. http://www.apcor.pt/wp-content/uploads/2016/01/ManualRolhas_PT_VF.pdf.

[89] V. Oliveira, M.E. Rosa, H. Pereira, Variability of the compression properties of cork, Woods Sci. Technol. 48 (2014) 1–12. https://doi.org/10.1007/s00226-014-0651-2.

[90] L.J. Gibson, K.E. Easterling, M.F. Ashby, The structure and mechanics of cork, Proc. R. Soc. London A. (1981) 99–117. https://doi.org/10.1098/rspa.1981.0117.

[91] APCOR – Estatísticas, (n.d.). http://www.apcor.pt/media-center/estatisticas/ (accessed September 10, 2021).

[92] Cortiça e vedantes artificiais, (n.d.). https://www.amorimcork.com/pt/a-cortica-e-o-vinho/cortica-vs-vedantes-artificiais/ (accessed September 17, 2021).

[93] APCOR – Rolhas, (n.d.). http://www.apcor.pt/produtos/rolhas/ (accessed September 10, 2021).

[94] Rolhas, Unidades de Negócio - Corticeira Amorim, Líder Mundial Setor Cortiça, (n.d.). https://www.amorim.com/unidades-de-negocio/rolhas/ (accessed September 10, 2021).

[95] C. Fialho, F. Lopes, H. Pereira, The effect of cork removal on the radial growth and phenology of young cork oak trees, For. Ecol. Manage. 141 (2001) 251–258. https://doi.org/10.1016/S0378-1127(00)00333-9.

[96] Confédération Européenne Du Liège, Código internacional das práticas rolheiras, (1999) 1–22.

[97] Matéria Prima e Processo Produtivo, (n.d.). https://www.amorimcork.com/natural-cork/raw-material-and-production-process/ (accessed September 7, 2018).

[98] APCOR - Rolhas Naturais, (n.d.). http://www.apcor.pt/artigo/242.htm (accessed December 8, 2014).

[99] J. Coque, M. Rodríguez, R. Martínez, Causas y orígenes de la contaminación del vino por haloanisoles, 2005.

[100] C. Pereira, L. Gil, O Problema do odor a mofo nas rolhas de cortiça e processos para a sua redução/eliminação, Silva Lusit. 14 (2006) 101–111.

[101] M. Cabral, Cork product system and appratuses by extraction of compounds dragged in water vapour, WO 2004014436 A1, 2004. https://patentimages.storage.googleapis.com/f8/6e/b2/bff6ce7d218a22/WO2004014436A1.pdf.

[102] Naturity e Xpur: as tecnologias anti-TCA mais inovadoras, ecológicas e eficientes do mundo, (2021). https://www.amorim.com/pt/media/noticias/naturity-e-xpur-as-tecnologias-anti-tca-mais-inovadoras-ecologicas-e-eficientes-do-mundo/2310/.

[103] T.J. Dyer, Elucidating the formation and chemistry of chromophores during kraft pulping, 2004.

[104] D.N.S. Hon, W. Glasser, On Possible Chromophoric Structures in Wood and Pulps — a Survey of the Present State of Knowledge, Polym. Plast. Technol. Eng. 12 (1979) 159–179. https://doi.org/10.1080/03602557908067670.

[105] T. Rosenau, A. Potthast, K. Krainz, H. Hettegger, U. Henniges, Y. Yoneda, C. Rohrer, A.D. French, Chromophores in cellulosics, XI: Isolation and identification of residual chromophores from bacterial cellulose, Cellulose. 21 (2014) 2271–2283. https://doi.org/10.1007/s10570-014-0289-0.

[106] P. Korntner, T. Hosoya, T. Dietz, K. Eibinger, H. Reiter, M. Spitzbart, T. Röder, A. Borgards, W. Kreiner, A.K. Mahler, H. Winter, Y. Groiss, A.D. French, U. Henniges, A. Potthast, T. Rosenau, Chromophores in lignin-free cellulosic materials belong to three compound classes. Chromophores in cellulosics, XII, Cellulose. 22 (2015) 1053–1062. https://doi.org/10.1007/s10570-015-0566-6.

[107] C.W. Dence, D.W. Reeve, Pulp bleaching: principles and practice, 1st Ed., 1996.

[108] M. Ek, G. Gellerstedt, G. Henriksson, Pulping Chemistry and Technology, 3rd Ed., De Gruyter, 2009.

[109] T. Rosenau, A. Potthast, W. Milacher, A. Hofinger, P. Kosma, Isolation and identification of residual chromophores in cellulosic materials, Polymer (Guildf). 45 (2004) 6437–6443. https://doi.org/10.1016/j.polymer.2004.07.031.

[110] T. Rosenau, A. Potthast, K. Krainz, Y. Yoneda, T. Dietz, Z.P.I. Shields, A.D. French, Chromophores in cellulosics, VI. First isolation and identification of residual chromophores

from aged cotton linters, Cellulose. 18 (2011) 1623–1633. https://doi.org/10.1007/s10570-011-9585-0.

[111] A. Schedl, T. Zweckmair, F. Kikul, M. Bacher, T. Rosenau, A. Potthast, Pushing the limits: Quantification of chromophores in real-world paper samples by GC-ECD and EI-GC-MS, Talanta. 179 (2018) 693–699. https://doi.org/10.1016/j.talanta.2017.11.049.

[112] S.M. Ghoreishi, M.R. Haghighi, Chromophores removal in pulp and paper mill effluent via hydrogenation-biological batch reactors, Chem. Eng. J. 127 (2007) 59–70. https://doi.org/10.1016/j.cej.2006.09.022.

[113] S.I. Falkehag, J. Marton, A. Erich, Chromophores in Kraft Lignin, in: J. Marton (Ed.), Lignin, Struct. React., 1966: pp. 75–89. https://doi.org/10.1021/ba-1966-0059.ch007.

[114] H.U. Suess, Pulp bleaching today, De Gruyter, 2010. https://doi.org/10.1515/9783110218244.

[115] G. Zucchini, A. Donati, Process for bleaching and sterilizing cork articles, and cork articles bleached using the said process, US 005098447A, 1992.

[116] P. Bajpay, Hot peroxide bleaching, Can. Chem. News. 50 (1998) 15–17.

[117] H.U. Süss, N.F. Nimmerfrof, J.D. Kronis, The naked truth on hot peroxide bleaching, in: CPPA 1997 Annu. Meet., Montreal, 1997: pp. 1–13.

[118] A. Wójciak, H. Kasprzyk, E. Sikorska, I. Khmelinskii, A. Krawczyk, A.S. Oliveira, L.F.V. Ferreira, M. Sikorski, Changes in chromophoric composition of high-yield mechanical pulps due to hydrogen peroxide bleaching under acidic and alkaline conditions, J. Photochem. Photobiol. A Chem. 215 (2010) 157–163. https://doi.org/10.1016/j.jphotochem.2010.08.005.

[119] P. Bajpay, Environmentally Benign Approaches for Pulp Bleaching, 1st Ed., Elsevier B.V., 2005. https://doi.org/10.1016/B978-0-444-51724-1.X5000-X.

[120] G. González-Gaitano, M.A.C. Ferrer, Definition of QC parameters for the practical use of FTIR-ATR spectroscopy in the analysis of surface treatment of cork stoppers, J. Wood Chem. Technol. 33 (2013) 217–233. https://doi.org/10.1080/02773813.2013.779715.

[121] C. Ortega-Fernández, J.R. González-Adrados, M.C. García-Vallejo, R. Calvo-Haro, M.J. Cáceres-Esteban, Characterization of surface treatments of cork stoppers by FTIR-ATR, J. Agric. Food Chem. 54 (2006) 4932–4936. https://doi.org/10.1021/jf0529823.

[122] M.A. Bezerra, R.E. Santelli, E.P. Oliveira, L.S. Villar, L.A. Escaleira, Response surface methodology (RSM) as a tool for optimization in analytical chemistry, Talanta. 76 (2008) 965–977. https://doi.org/10.1016/j.talanta.2008.05.019.

[123] F.C. Zimmer, A.H.P. Souza, A.F.C. Silveira, M.R. Santos, M. Matsushita, N.E. Souza, A.C. Rodrigues, Application of factorial design for optimization of the synthesis of lactulose obtained from whey permeate, J. Braz. Chem. Soc. 28 (2017) 2326–2333.

https://doi.org/10.21577/0103-5053.20170083.

[124] V. Czitrom, One-factor-at-a-time versus designed experiments, Am. Stat. 53 (1999) 126–131. https://doi.org/10.1080/00031305.1999.10474445.

[125] N. Hamaidi-Maouche, S. Bourouina-Bacha, F. Oughlis-Hammache, Design of experiments for the modeling of the phenol adsorption process, J. Chem. Eng. Data. 54 (2009) 2874–2880. https://doi.org/10.1021/je800959k.

[126] N.R. Domagalski, B.C. Mack, J.E. Tabora, Analysis of Design of Experiments with Dynamic Responses, Org. Process Res. Dev. 19 (2015) 1667–1682. https://doi.org/10.1021/acs.oprd.5b00143.

[127] J.U. Ani, U.C. Okoro, L.E. Aneke, O.D. Onukwuli, I.O. Obi, K.G. Akpomie, A.C. Ofomatah, Application of response surface methodology for optimization of dissolved solids adsorption by activated coal, Appl. Water Sci. 9 (2019) 1–11. https://doi.org/10.1007/s13201-019-0943-7.

[128] H. Akçay, A.S. Anagün, Multi response optimization application on a manufacturing factory, Math. Comput. Appl. 18 (2013) 531–538. https://doi.org/10.3390/mca18030531.

[129] R.H. Myers, D.C. Montgomery, C.M. Anderson-Cook, Response surface methodology-process and product optimization using designed experiments, 3rd Ed., Wiley, 2009.

[130] D. Lendrem, M. Owen, S. Godbert, DOE (design of experiments) in development chemistry: Potential obstacles, Org. Process Res. Dev. 5 (2001) 324–327. https://doi.org/10.1021/op000025i.

[131] D.C. Montgomery, Design and analysis of experiments, 9th Ed., John Wiley & Sons, Inc., 2017.

[132] D.C. Montgomery, Response surface methods and designs, in: Des. Anal. Exp., 9th Ed., John Wiley & Sons, Inc., 2017: pp. 489–568.

[133] D.E. Coleman, D.C. Montgomery, A systematic approach to planning for a designed industrial experiment, Technometrics. 35 (1993) 1–12. https://doi.org/10.1080/00401706.1993.10484984.

[134] D.C. Montgomery, Introduction, in: Des. Anal. Exp., 9th Ed., John Wiley & Sons, Inc., 2017: pp. 1–22.

[135] B. Govaerts, B. Francq, R. Marion, M. Martin, M. Thiel, The Essentials on Linear Regression, ANOVA, General Linear and Linear Mixed Models for the Chemist, in: Ref. Modul. Chem. Mol. Sci. Chem. Eng., 2nd Ed., Elsevier Inc., 2020: pp. 431–463. https://doi.org/10.1016/b978-0-12-409547-2.14579-2.

[136] D.C. Montgomery, Experiments with a single factor: the analysis of variance, in: Des. Anal. Exp., 9th Ed., John Wiley & Sons, Inc., 2017: pp. 64–134.

[137] R.G. Brereton, The use and misuse of p values and related concepts, Chemom. Intell. Lab. Syst. 195 (2019) 1–7. https://doi.org/10.1016/j.chemolab.2019.103884.

[138] R.J.G. Halfens, J.M.M. Meijers, Back to basics: An introduction to statistics, J. Wound Care. 22 (2013) 248–251. https://doi.org/10.12968/jowc.2013.22.5.248.

[139] A.I. Khuri, J.A. Cornell, Response surfaces: designs and analyses, 2nd Ed., Dekker, New York, 1996. https://doi.org/10.1201/9780203740774.

[140] Z.B. Guzel-Seydim, A.K. Greene, A.C. Seydim, Use of ozone in the food industry, LWT - Food Sci. Technol. 37 (2004) 453–460. https://doi.org/10.1016/j.lwt.2003.10.014.

[141] T. Miyanishi, Theory and practice of ozone bleaching, Japan Tappi J. 72 (2018) 435–439. https://doi.org/10.2524/jtappij.1702.

[142] V. Prabha, R.D.E.B. Barma, R. Singh, A. Madan, Ozone technology in food processing : A review, Trends Biosci. 8 (2015) 4031–4047.

[143] M. Prabaharan, J.V. Rao, Study on ozone bleaching of cotton fabric-process optimisation, dyeing and finishing properties, Color. Technol. 117 (2001) 98–103. https://doi.org/10.1111/j.1478-4408.2001.tb00342.x.

[144] H.A. Eren, S. Eren, Ozone bleaching of cellulose, IOP Conf. Ser. Mater. Sci. Eng. 254 (2017) 1–3. https://doi.org/10.1088/1757-899X/254/8/082009.

[145] M.B. Roncero, M.A. Queral, J.F. Colom, T. Vidal, Why acid pH increases the selectivity of the ozone bleaching processes, Ozone Sci. Eng. 25 (2003) 523–534. https://doi.org/10.1080/01919510390481838.

[146] C.L. Chen, H.M. Chang, J.S. Gratzl, G.Y. Pan, Studies an Ozone Bleaching. I. The Effect of PH, Temperature, Buffer Systems and Heavy Metal-Ions on Stability of Ozone In Aqueous Solution, J. Wood Chem. Technol. 4 (1984) 367–387. https://doi.org/10.1080/02773818408070655.

[147] E.M. Cadena, T. Vidal, A.L. Torres, Influence of the hexenuronic acid content on refining and ageing in eucalyptus TCF pulp, Bioresour. Technol. 101 (2010) 3554–3560. https://doi.org/10.1016/j.biortech.2009.11.105.

[148] R. Chand, D.H. Bremner, K.C. Namkung, P.J. Collier, P.R. Gogate, Water disinfection using the novel approach of ozone and a liquid whistle reactor, Biochem. Eng. J. 35 (2007) 357–364. https://doi.org/10.1016/j.bej.2007.01.032.

[149] W. Ding, W. Jin, S. Cao, X. Zhou, C. Wang, Q. Jiang, H. Huang, R. Tu, S. Han, Q. Wang, Ozone disinfection of chlorine-resistant bacteria in drinking water, Water Res. 160 (2019) 339–349. https://doi.org/10.1016/j.watres.2019.05.014.

[150] A. Quederni, J.C. Mora, R.S. Bes, Ozone absorption in water : mass transfer and solubility, Ozone Sci. Eng. J. Int. Ozone Assoc. 9 (1987) 1–12.

https://doi.org/10.1080/01919518708552384.

[151] W.H. Glaze, Reaction products of ozone: A review, Environ. Health Perspect. 69 (1986) 151–157. https://doi.org/10.1289/ehp.8669151.

[152] M.D. Gurol, P.C. Singer, Kinetics of ozone decomposition: A dynamic approach, Environ. Sci. Technol. 16 (1982) 377–383. https://doi.org/10.1021/es00101a003.

[153] B.G. Ershov, P. a. Morozov, Decomposition of ozone in water at pH 4–8, Russ. J. Appl. Chem. 81 (2008) 1895–1898. https://doi.org/10.1134/S1070427208110048.

[154] F.J. Beltrán, Ozone reaction kinetics for water and wastewater systems, 1st Ed., Lewis Publishers, 2004.

[155] E. Cogo, J. Albet, G. Malmary, C. Coste, J. Molinier, Effect of reaction medium on ozone mass transfer and applications to pulp bleaching, Chem. Eng. J. 73 (1999) 23–28. https://doi.org/10.1016/S1385-8947(99)00011-X.

[156] T. He, M. Liu, X. Tian, Kinetics of ozone bleaching of eucalyptus kraft pulp and factors affecting the properties of the bleached pulp, BioResources. 13 (2018) 425–436. https://doi.org/10.15376/biores.13.1.425-436.

[157] A.K. Bin, M. Roustan, Mass transfer in ozone absorption, in: Int. Spec. Symp. IOA 2000, 2000: pp. 99–131.

[158] F. Arooj, N. Ahmad, I.A. Shaikh, M.N. Chaudhry, Application of ozone in cotton bleaching with multiple reuse of a water bath, Text. Res. J. 84 (2013) 527–538. https://doi.org/10.1177/0040517513499429.

[159] P. Bajpai, Green Chemistry and Sustainability in Pulp and Paper Industry, Springer, 2015. https://doi.org/10.1007/978-3-319-18744-0.

[160] J.R. Phillips, B.F. Greenwood, E. Funk, S. Dunn, Medium consistency pulp ozone bleaching, US 005411633A, 1995.

[161] Pulp and paper chemistry and technology Volume 2, n.d.

[162] P. Bajpai, Environmentally Friendly Production of Pulp and Paper, John Wiley & Sons, Inc., 2010. https://doi.org/10.1002/9780470649657.

[163] A. Lagorce-Tachon, T. Karbowiak, C. Loupiac, A. Gaudry, F. Ott, C. Alba-Simionesco, R.D. Gougeon, V. Alcantara, D. Mannes, A. Kaestner, E. Lehmann, J.P. Bellat, The cork viewed from the inside, J. Food Eng. 149 (2015) 214–221. https://doi.org/10.1016/j.jfoodeng.2014.10.023.

[164] A. Lagorce-Tachon, F. Mairesse, T. Karbowiak, R.D. Gougeon, J.P. Bellat, T. Sliwa, J.M. Simon, Contribution of image processing for analyzing the cellular structure of cork, J. Chemom. 32 (2017) 1–8. https://doi.org/10.1002/cem.2988.

[165] J. Staehelin, R.E. Buhler, J. Hoigné, Ozone decomposition in water studied by pulse

radiolysis. 2. Hydroxyl and hydrogen tetroxide (HO4) as chain intermediates, J. Phys. Chem. 88 (1984) 5999–6004. https://doi.org/10.1021/j150668a051.

[166] Z. Osawa, C. Schuerch, The action of gaseous reagents on cellulosic materials, TAPPI J. 46 (1963) 79–84.

Chapter 3

NATURAL CORK STOPPERS CHEMICAL COMPOSITION

Part of this chapter has been published in:

D.G. Branco, J.R. Campos, L. Cabrita, D. V. Evtuguin, Structural features of macromolecular components of cork from *Quercus suber* L., Holzforschung. 74 (2020) 625–633. https://doi.org/10.1515/hf-2019-0271.

D.G. Branco, C. Santiago, A. Lourenço, L. Cabrita, D. V. Evtuguin, Structural Features of Cork Dioxane Lignin from *Quercus suber* L., J. Agric. Food Chem. (2021). https://doi.org/10.1021/acs.jafc.1c01961.

Content

3.1 Introduction

The chemical processing/modification of natural cork stoppers need fundamental knowledge on structural features of its macromolecular components, which is far from being completely disclosed. The cork chemical composition has been studied over the past years by different scientists until reaching a consensus. The chemical composition of cork varies significantly and depends on many factors such as geographic position, climate, soil conditions, genetic origin, tree dimensions, age (virgin or reproduction), and growth conditions [1,2].

The cork cell walls are constituted by a set of structural and non-structural components. The structural components are macromolecules that provide support and stiffness to the cell wall, and, unlike non-structural components, they cannot be removed by simple extraction being frequently isolated through chemical reactions that transform them into smaller units much easier to be removed by extraction with an appropriate organic solvent [3].

Among structural components of cork, suberin plays a central role, followed by lignin and polysaccharides (cellulose and hemicellulose). Despite interest in using cork to produce various materials, detailed chemical and structural analysis of its components is far from exhaustive.

Previous chemical studies on bark planks from *Q. suber* L. included in-tree and between tree variations [4,5], differences between virgin and reproduction cork [6,7], and characterization of wetcork [8]. Besides this, the studies on the chemical analysis used mainly cork boards that still contain the scrape, which is the outer layer in cork that is in contact with the atmosphere. When performing the cork chemical analysis in cork boards the scrape is also grounded and stiffed which will have implications on the chemical analysis. On the other hand, using natural cork stoppers gives more accurate information about this material and helps to understand the behavior of natural cork stoppers during their processing.

More detailed studies on the chemical composition included mainly analysis of suberin contributing to *ca.* 33-48% of cork [1,9–15]. With regard to lignin, information about its structure is incomplete and sometimes contradictory [16–23]. This can be explained by the variable sources of cork and the differences in the isolation procedure and analysis methodology. The close structural association between the lignin and the suberin makes difficult its isolation and quantification [20]. Thus, the appropriate quantification of lignin (e.g., as Klason lignin) is possible only after exhaustive desuberinization of cork material. This removal of suberin and extractives may be incomplete, which makes it difficult to quantify lignin reliably and assess its structural characteristics [20–22,24]. Similar difficulties were reported for the analysis of lignin in different fruits and agriculture residues [25,26].

The lignin content reported in cork varies approximately between 15 and 29% [1], showing a significant discrepancy that is not justified by the variability of the cork source. The reported proportion between the main structural units, guaiacyl (G), syringyl (S), and *p*-hydroxyphenyl (H), also varies substantially, suggesting the type of lignin to be from typical G type [18–22] to more likely GS type [23,27]. However, it is commonly accepted that the lignin in cork is strongly condensed and structurally associated with suberin, hemicelluloses, and probably other cell components [1,18,20,23]. At the same time, the reported frequency of occurrence of different lignin condensed and noncondensed structures in cork varies substantially depending on the lignin isolation method and analytical and methodological approaches [17–24,27]. No quantitative assessment of lignin substructures per a phenol propane structural unit (PPU) has been reported. Few studies report the molecular weight of lignin isolated from cork, which can reach up to 8000 Da [18].

As far as cork hemicellulose concern, few studies were found with a brief characterization of hemicellulose isolated from *Quercus suber* L. [28–32] However, an emphasis towards the presence of xylose must be recognized revealing that cork hemicelluloses have some similarities with hardwood hemicelluloses. The major hemicellulose present hardwood is *O*-acetyl-(4-*O*-methylglucurono)-xylan, in other words is constituted by a backbone of β-(1→4)-linked xylopyranosyl units (Xylp) substituted at position C2 and/or C3 with O-acetyl group (degree of substitution between 0.5 and 0.6) and ramified with 4-O-methylglucuronic acid (MeGLcA) α-(1→2)-linked to the xylan chain, with an average relation of 1 to 10 xylopyranosyl residues[33–35]. There is also assigned as side group in the xylan main chain L-arabinofuranose (Araf), among other substitutions, however in less extent [35].

Accordingly, the main goal of this study presented in this chapter was the structural characterization of macromolecular components of natural cork stoppers with an emphasis on lignin and polysaccharides. Consequently, a careful detailed knowledge of the macromolecular components of natural cork stoppers is essential to better understand the behavior of natural cork stoppers during their processing and to develop new upgrading approaches.

3.2 Materials and Methods

Natural cork stoppers supplied by Amorim Cork, S.A (Santa Maria de Lamas, Portugal) were ground and sifted to obtain the fraction of 40-60 mesh. The cork stoppers have a single caliber of 49x24 mm (length x diameter) and belong to the 1st class (middle class).

3.2.1 Chemical characterization

3.2.1.1 Moisture content

The moisture content from 1 g of cork was determined on an oven at 105 ºC, in agreement with norm TAPPI T 412 om-11.

3.2.1.2 Ash content

Following procedure ***3.2.1.1***, the ash content was determined by calcination of the material at 525 ºC described in the standard procedure Tappi T 211 om-93.

3.2.1.3 Extractives

Extractive-free cork was obtained by exhaustive extraction of cork particles sequentially with dichloromethane (DCM), MeOH: water (50:50, v/v), and water. The extractive content in DCM was determined by Soxhlet extraction depicted in Tappi T 204 om-88. The determination of extractives in MeOH: water (50:50, v/v) and in hot water was performed for 2 h under reflux. The solvent was recovered on a rotary evaporator with a vacuum oven until constant weight and was stored in a desiccator. No attempt was made to analyze this fraction.

3.2.1.4 Suberin

Suberin extracts were obtained by alkaline methanolysis with sodium methoxide. About 7.0 g of extractive-free cork was treated under reflux with 700 mL of dry methanol with 2% of sodium methoxide ($NaOCH_3$) for 3 h. After filtration, the resulting residues were again refluxed in 100 mL of methanol for 15 min and filtered. The two methanol extracts were combined and acidified to pH 6 with 0.25 M sulfuric acid (H_2SO_4) and concentrated in a rotary evaporator. The resulting concentrate was suspended in 100 mL of water and extracted 3 times with chloroform solutions that were dried over anhydrous sodium sulfate. The solvent was evaporated to dryness and the product obtained was suberin.

3.2.1.5 Lignin

The lignin content in cork-free from extractives and suberin was determined by the Klason method described in Tappi standard T 222 om-88. Lignin was isolated by acidolysis from extractives-free and desuberized cork residue in a nitrogen atmosphere by the dioxane method adapted from a previously published, with some modifications.

About 3.5 g of cork was placed in a 0.5 L three-necked flask fitted with a reflux condenser, nitrogen bubbler, and dropping funnel. The solvent, 200 mL of dioxane/water (9:1, v/v) mixture containing 1.46 g of hydrogen chloride equivalent to 0.2 M, was added slowly from the funnel. The reaction mixture, under a nitrogen atmosphere, was heated with a heating mantle and refluxed for a period of 30 min. Then, the mixture was cooled to around 50℃. The liquid phase was decanted, and the solid residue was subjected to another extraction with 200 mL of an acidic dioxane/water solution for a period of 40 min. Three more extractions were performed in the same way with different extraction periods, more specifically 30, 30, and 20 min. The last (fifth) extraction was performed without the addition of hydrochloric acid in the dioxane/water mixture. Each portion of the extract was concentrated separately (200 mL to around 40 mL), then the concentrates were combined, and the lignin was precipitated by adding it to cold water (about 800 mL) under vigorous stirring, being kept further for 12h in the dark room at 4 ºC. Once the lignin was precipitated, the solution obtained was centrifuged and the solid residue was washed with water until pH 5 of the supernatant and again centrifuged. Finally, the solid residue was dried in a vacuum oven at 30 ºC, and the lignin was determined gravimetrically. The amount of extracted lignin was ca. 50% of Klason lignin.

3.2.1.6 Cellulose

The cellulose was determined by the Kürschner & Hoffer method which consisted of three consecutive treatments of extractive- and suberin-free cork sample (*ca.* 1g) with HNO_3: EtOH mixture (1:4, v/v) under reflux for 1 h each (3 x 50 mL). After every hour, the reaction mixtures were filtered off, and 50 mL of fresh nitric acid and ethanol solution (1:4, v/v) were added. The obtained final insoluble residue was filtered on a G3 glass filter, washed with hot water and acetone, and dried to constant weight at 105 ℃ [36].

3.2.1.7 Xylan

The cork holocellulose was obtained from extractive-free and desuberized cork residue by delignification with peracetic acid. About 5.0 g of extractive-free cork was treated with 10% (v/v) of peracetic acid solution (200 mL) at 80 ºC for 20 minutes. After delignification, the holocellulose was filtered off on a porous glass filter, washed with acetone and with warm water, and dried in an oven

at 40ºC. The holocellulose yield 74.2% (based on extractive and suberin free sample). The isolation of xylans was carried out by two consecutive extractions with Me_2SO (2.0 g of holocellulose with 50 mL of Me_2SO in each assay) at 50ºC for 12 h and further precipitation of resulted extract with 600 mL MeOH:EtOH solution (1:1, v/v) acidified with 20 mL of formic acid. After the complete precipitation, the xylans were isolated by centrifugation, washed three times with anhydrous MeOH, and dried under vacuum at room temperature [37].

3.2.2 Gas chromatography- mass spectrometry (GC-MS) analysis

Gas chromatography-mass spectrometry (GC-MS) analysis was performed with about 10 mg of isolated suberin that was dissolved in 500 μL of pyridine (p.a. grade, Fisher Bioreagents, Geel, Belgium) with internal standard (tetracosane, 1 mg/mL) (Sigma-Aldrich Chem. Comp., Steinheim, Germany), and the compounds containing free hydroxyl and carboxyl groups were converted into their trimethylsilyl (TMS) ethers and esters by adding 300 μL of N,O-bis-(trimethylsilyl)trifluoracetamide (BSTFA) (Sigma-Aldrich Chem. Comp., Steinheim, Germany). After reacting for 12 h under room temperature, the corresponding TMS derivatives were analyzed by GC-MS on a Trace GC 2000 series coupled with Thermo Scientific DSQII mass spectrometer (Thermo Fisher Scientific, Waltham, MA, USA) using a column capillary DB-1 J&W (30 m × 0.32 mm i.d. 0.25 μm) and helium as carrier gas (30 cm/s). The chromatographic conditions were as follows: initial temperature: 80 ºC for 5 min; temperature rate: 4 ºC/min; final temperature: 285 ºC for 10 min; injector temperature: 290 ºC; transfer-line temperature: 290 ºC; split ratio: 1:65. Compounds were identified as TMS derivatives by comparing their mass spectra with the Wiley-Nist spectral library (Nist MS search 2.0), with data from the literature and in some cases, by injection of standards.

3.2.3 Sugar analysis

Sugar analysis of desuberized residue and isolated xylan were carried out using hydrolysate obtained by Saeman hydrolysis (the residue was hydrolyzed for 3.0 h with 72% H_2SO_4 followed by 2.5 h at 100ºC with 4% H_2SO_4; internal standard - 1 mg/mL of 2-deoxyglucose). The desuberized residue was analyzed on a Dionex™ Integrion™ HPIC™ system (Thermo Fisher Scientific, Waltham, MA, USA). The sample was analyzed on a Dionex CarboPAC™ SA 10-4 μm (2x250 mm) column protected by Dionex CarboPAC™ SA 10G-4 μm (2x50 mm) guard column, and the chromatograms were processed with Thermo Scientific Dionex Chromeleon® software. The eluent was potassium hydroxide (KOH) 1 mM (0.38 mL/min). The same hydrolysate was used for the analysis of uronic acid content by colorimetric method with *m*-phenylphenol [38].

The released neural monosaccharides from the isolated xylan were determined as alditol acetate derivates by gas chromatography [39]. The quantitative analysis was carried out on a Varian 3350 gas chromatograph equipped with FID detector and with a DB-225 J&W column (30 m x 0.25 mm i.d. x 0.15 µm film thickness). The temperature program was started at 220 ºC with a 5 min hold, and then raised to a final temperature of 230 ºC at 2 ºC/min, and held for 5 min.

3.2.4 Fourier-transform infrared spectroscopy (FTIR)

FTIR spectra were obtained for dioxane lignin and cellulose and were recorded with a MATTSON 7000 spectrometer (Mattson Instruments, Madison, WI, USA) in KBr pellets (1 mg of sample to 300 mg of KBr). Spectra were obtained in transmittance mode, from 4000 to 400 cm^{-1}, with a resolution of 4 cm^{-1} and 128 scans/min.

3.2.5 Permanganate oxidation

Permanganate analysis was carried out according to the procedure described previously [40]. This method is comprised of five basic steps: (i) previous sample ethylation to protect phenolic units, (ii) lignin oxidation with potassium permanganate to aromatic aldehydes, (iii) oxidation of aromatic aldehydes with hydrogen peroxide to aromatic acids, (iv) methylation of oxidized products with diazomethane, and (v) gas chromatography analysis of methyl esters. Permanganate oxidation (PO) products were analyzed by gas chromatography coupled with a mass spectrometry detector (GC-MS) on a GC-MS-QP2010 Ultra instrument (Shimadzu, Kyoto, Japan) using a capillary column, 140 ºC; temperature gradient, 5 ºC/min; final temperature of the column, 270 ºC, injector temperature 230 ºC. Helium was the carrier gas with a total flow of *ca.* 1 mL/min. Pyromellitic acid tetramethyl ester was used as the internal standard.

3.2.6 NMR Analysis

The quantitative ^{1}H NMR and ^{13}C NMR spectra were registered on an AVANCE III 300 spectrometer (Bruker, Wissembourg, France) operating at 300.1 (298 K) and 75.2 MHz (303 K), respectively, with TMS as the internal reference. The ^{1}H NMR spectrum of acetylated dioxane lignin [41] chloroform ($CDCl_3$) solution, placed in a 5 mm diameter tube, was carried using the following acquisition parameters: 12 µs pulse width (90°), 2 s relaxation delay, and 300 scans. In the ^{1}H NMR spectrum of xylan, the isolated xylan was dissolved in D_2O (ca. 2% w/w) and sodium 3-(trimethylsylil) propionate-d_4 (TMSP, δ 0.00) was used as internal standard, the final solution was placed in 5-mm diameter tube. The acquisition parameters were as follows: 12 μs pulse width (90º), 18 s relaxation delay and 300 scans.

The quantitative ^{13}C NMR spectrum of dioxane lignin dissolved in deuterated dimethyl sulfoxide (DMSO-d_6) at a 25% (w/w) concentration was recorded acquiring 18 000 scans with a relaxation time of 12 s and a 90º flip angle. The phase-sensitive ^{1}H-detected heteronuclear single quantum coherence (HSQC) NMR spectra of dioxane lignin was acquired on an Ascend 500 spectrometer (Bruker, Wissembourg, France).

The HSQC NMR spectrums were acquired over a F1 spectral weight of 12000 Hz and a F2 width of 2000 Hz with a 2048 x 1024 matrix and 128 transients per increment. The delay between scans was 2 s and the HSQC experiment was optimized for a one-bond heteronuclear coupling constant ($^{1}J_{C-H}$) of 148 Hz.

The cork residue after lignin isolation was analyzed by solid-state ^{13}C CP-MAS NMR (cross-polarization-magic angle spinning nuclear magnetic resonance). The spectra were recorded on an Avance 400 spectrometer (Bruker, Wissembourg, France), where the samples were packed into a zirconia rotor sealed with Kel-F caps and spun at 12 kHz. The acquisition parameters were as follows: ca. 7000 scans with a 90º proton pulse, a 1 ms cross-polarization contact time, and a 2.5 s recovery delay.

The 2D ^{1}H-^{1}H TOCSY spectrum (τ_{mix}=0.050 s) of the isolated xylan was acquired using the MLEVST standard pulse program. A spectral width of 2185 Hz was employed in both dimensions. The relaxation delay was 1.5 s. For each FID, 128 transients were acquired, the data size was 1024 in t_1 x 512 in t_2.

3.2.7 Elemental analysis

Isolated dioxane lignin was characterized by elemental analysis, performed on a Truspec 630-200-200 instrument (LECO Corp., St. Joseph, MI, USA), in triplicate. The oxygen content was calculated from the C, H, and N content by difference: O % wt=100-(C % wt + H % wt + N % wt).

3.2.8 Molecular weight analysis

The molecular weight of dioxane lignin was assessed by size-exclusion chromatography (SEC) using PL-GPC 110 system (Polymer Laboratories, Shropshire, UK) equipped with two PLgel 5 μm MIXED D 300 mm × 7.5 mm columns protected by a PLgel 5 μm pre-column (Polymer Laboratories, Shropshire, UK). The column, injector system, and detector (RI) were maintained at 70 ºC during the analysis. The eluent (0.1 M LiCl in DMF) was pumped at a flow rate of 0.9 mL/min. The columns were calibrated with lignin model compounds and lignin samples (M_p=950-3200 Da) previously characterized by electrospray ionization ESI-MS [42].

3.2.9 Analytical pyrolysis

Analytical pyrolysis coupled with gas chromatography and mass spectrometry (Py-GC-MS) was performed as described previously [43]. Around 0.10 mg of lignin or cork material was pyrolyzed (550 ºC for 1 min) in a platinum coil Pyroprobe connected to a CDS 5150 valved interface linked to a gas chromatograph (Agilent 7890B) with a mass detector (5977B) and using a fused-silica capillary column (ZB-1701: 60 m x 0.25 mm i.d. x 0.25 μm film thickness). The chromatographic conditions used were as follows: 40 ºC, held for 4 min, 10 ºC/min to 70 ºC, 5 ºC/min to 100 ºC, 3 ºC/min to 256 ºC, held for 3 min, 5 ºC/min to 270 ºC, held for 9 min. The temperatures applied were as follows: 270 ºC (injector), 280 ºC (MS interface). The electron ionization energy was 70 eV. Helium was the carrier gas with a total flow of 1 mL/min. The compounds were identified by comparing their mass spectra with Wiley, the NIST2014 database, and the literature [43,44].

3.2.10 X-ray

X-ray diffraction scattering analysis of Kürschner & Hoffer cellulose was carried out on a Philipps X'Pert MPD diffractometer (Malvern Panalytical, Malvern, UK) using a Cu-*K*α source (λ=0.154 nm) in the 2Θ range 2–40° and scanning step width of 0.02 °/scan. The degree of crystallinity [DC%=Ic/(Ic+Ia) *100] was calculated as described elsewhere using the integral intensities from crystalline (Ic) and amorphous halo (Ia) regions of the diffractogram [45].

3.2.11 Methylation linkage analysis

The xylan was triggered with powdered NaOH and methylated CH_3I [46,47] followed by a methylation of the polysaccharides. The methylated xylan was hydrolyzed by treatment with 2 M trifluoroacetic acid for 1.5 h at 120 ºC, and the partial methylated sugars were reduced with sodium borohydride and acetylated [48,49]. Partially methylated alditol acetates (PMAA) were dissolved in dichloromethane and analyzed by GC-MS (Trace GC 2000 series coupled with Thermo Scientific DSQII mass spectrometer) using DB-1 capillary column (30 m x 0.32 mm i.d., 0.25μm film thickness). The chromatographic conditions were as follows: detector and injector at 280 and 220 ºC, respectively. Temperature program used was as follows: 10 min at 45 ºC with an increase of 10 ºC/min until 140 ºC and standby 5 min at 140 ºC; an increase of 0.5 ºC/min from 140 to 170 ºC and standby 1 min at 170 ºC; an increase from 170 to 280 ºC with a rate of 15 ºC/min and standby 5 min at 280 ºC.

3.3 Results and Discussion

3.3.1 Chemical composition of natural cork stoppers

The results on the general chemical composition of cork from natural cork stoppers are summarized in Table 3.1. The moisture content of powdered natural cork stoppers was 2.6%.

Table 3.1- Chemical composition of natural cork stoppers.[a]

Components	Rel. abundance (% dry sample± standard deviation)
Ash	1.0±0.0
Extractives (Total)	13.4±0.0
DCM	5.2±0.0
MeOH:Water (50:50, v/v)	6.0±0.0
Water	2.2±0.0
Suberin (2% sodium methoxide)	44.0±2.0
Klason lignin	16.2±0.3
Cellulose[b]	17.2±0.2
Hemicelluloses	6.6±0.1

[a]All analyses were carried out in duplicate.
[b]The value obtained as glucan after hydrolysis of desuberized residue.

The ash content (1.0%) obtained in this study was within the range of inorganics contents reported for the cork materials elsewhere (*ca.* 1-2%) [3,6,7]. The non-structural components of cork were characterized as extractives in three different media (Table 3.1). Among extractives, the major fraction was polyphenolics soluble in MeOH: water (50:50, v/v) solution (6.0%) followed by DCM-soluble non-polar extractives (5.2%) and the water-soluble compounds (2.2%), which include hydrolyzable tannins, water-soluble polysaccharides, and soluble salts.

In terms of the chemical composition, cork is dominated by the presence of suberin that was the most abundant macromolecular component of the cell wall (44.0%) followed by cellulose and lignin, which showed similar contents (17.2 and 16.2%, respectively). The content of lignin was obtained as acid-insoluble residue (Klason lignin) after two-step hydrolysis (72% and *ca.* 4% H_2SO_4) of extractives-free cork. The value of acid-insoluble residue (16.2%) was inferior to those (21.8%) reported previously [6] and usually reviewed in the literature between 20 and 27% [1,3–5]. This determined amount of Klason lignin is also lower than normally reported for oak woods [50].

The cellulose content (17.2%) was obtained via sugar analysis from extractive-free cork after the removal of the suberin (desuberized residue). The relatively low cellulose content in cork confirms the commonly accepted physiological role of the suberized cells in cork, which appears to be water retention [51]. Therefore, unlike in xylem cells, this hydrophilic macromolecular component of cork does not play a leading role in defining cell wall properties. The attempts to isolate the

relatively pure cellulose by the Kürschner & Hoffer method, from desuberized residue for the quantification needs, were not completely successful due to the significant amounts of contaminants of waxy nature.

The amount of hemicelluloses (6.6%) was rather moderate being inferior to extractives (13.4%). Aiming to expand the knowledge about the macromolecular components of cork, these were isolated, and a thorough structural characterization was carried out.

3.3.2 Analysis of suberin

The composition of suberin was assessed after its depolymerization by alkaline methanolysis. Isolated suberin-derived compounds were analyzed by GC-MS as partially methylated/TMS-derived depolymerization products, whose quantification is presented in Table 3.2.

Table 3.2- Identification of methyl ester/TMS ether derivatives of suberin monomers detected by GC-MS.

Retention time, min	Compounds, detected as methyl ester (Me) and/or TMS ester/ether (TMS) derivatives	Amount, % (w/w)
28.81	Ferulic acid (Me/TMS ester)	6.69
31.91	Hexadecanoic acid (TMS ester)	0.05
32.68	9-Octadecenoic acid (Me/TMS ester)	0.10
35.75	Tetradecanedioic acid (Mono Me)	0.75
36.86	16-hydroxyhexadecanoic acid (Me/TMS ester)	0.71
38.44	Octadecanedioic acid (Me/TMS ester)	1.15
39.14	Unknown compound	2.23
39.51	Tetracosane (internal standard)	7.36
40.14	18-hydroxyoctadec-9-enoic acid (Me/TMS ether)	13.57
40.82	Unknown compound	0.80
41.59	9,10-epoxy-18-hydroxyoctadecanoic acid (Me/TMS ether)	2.71
42.47	Octadec-9,12-enedioic acid (TMS ester)	7.24
42.72	9,10-epoxyoctadecanoic acid (Me)	5.61
43.58	9,10-epoxy-18-hydroxyoctadecanoic acid (Me/TMS ether)	11.44
44.96	9,10-epoxy-18-hydroxyoctadecanoic acid (Me/TMS ether)	7.26
45.70	9,10-epoxy-18-hydroxyoctadecanoic acid (Me/TMS ether)	4.30
45.91	9,10-dihydroxyoctadecanedioic acid (Me/TMS ether)	3.41
46.54	9,10,18-trihydroxyoctadecanoic (Me/TMS ether)	3.69
47.22	Docosanedioic acid (Me)	1.58
47.94	22-hydroxydocosanoic acid (Me/TMS ether)	13.07
49.28	Octadecanedioic (Me/TMS ester)	1.21
50.00	Unknown compound	5.08

The major monomeric units of suberin are aliphatic fatty acids, hydroxy fatty acids, and dicarboxylic acids including epoxy moieties with chain lengths of C_{14}-C_{26}, being the major aliphatic components with a chain length of C_{18}. The most relevant contributions to C_{18} chain length compounds are based on seven acids: 9-octadecenoic acid, 18-hydroxyoctadec-9-enoic acid, isomers

of 9,10-epoxy-18-hydroxyoctadecanoic acid, 9,10,18-trihydroxyoctadecanoic acid, 9-octadecenedioic acid, 9,10-epoxyoctadecanedioic acid, and 9,10-dihydroxyoctadecanedioic acid. It is noteworthy that the contribution of these monomeric acids in the suberin may vary, due to their biosynthetic routes as proposed by Holloway & Deas [52].

Epoxidized acid chains are commonly found among suberin monomers. This functionality arises from the epoxidation of a double bond on the aliphatic acid chains and is believed to limit the degree of crosslinking of the suberin macromolecule in a manner that may alter the physical properties of this polymer [13]. On the other hand, the presence of ferulic acid suggests that this compound serves as a linking point between the aliphatic monomers identified in suberin polymer and the lignin in the cork cell wall [9,11,51].

3.3.3 Analysis of lignin

3.3.3.1 Dioxane lignin from cork

The cork lignin was assessed as dioxane lignin (DL) isolated from the extractive-free and desuberized residue. The content of the acid-insoluble (Klason) lignin in the cork was 16.2%, which is relatively low, probably due to the removal of an easily extractable fraction under the conditions of suberin removal. The yield of dioxane lignin from extractive-free and desuberized cork residue was ca. 50%, which is almost 20 times greater than the yield of milled cork lignin (MCL) and almost 5 times greater than the yield of organosolv lignin previously used for characterization of cork lignin [17,18,20,22,27].

At the same time, the yield of cork DL (50%) was inferior to DL yields from hardwoods that can reach as high as 80% [41]. The main reason could be the strong structural association of cork lignin with polysaccharides and, probably, condensed tannins, as revealed from the analysis of the residue after cork DL isolation by solid-state ^{13}C NMR (Figure 3.1).

As can be seen in Figure 3.1, besides polysaccharides (cellulose and hemicelluloses), this residue still contained a significant amount of unremoved lignin, as follows from the intense peak at *ca.* 55-56 ppm (methoxy groups in lignin) and strong signals in the region of 105-160 ppm (aromatic carbons). The significant content of syringyl units in the residue is evidenced from the strong resonance at *ca.* 152 ppm assigned to C-3/C-5 in etherified S units. In addition, the strong carbon resonance at 114 and 122, the shoulder at 145, and the resonances centered at 173 ppm indicate the eventual presence of condensed tannins of catechin/gallocatechin types chemically modified under alkaline conditions during suberin removal from the cork material [26,53]. Only a small amount of suberin was detected (resonances at 20-30 ppm).

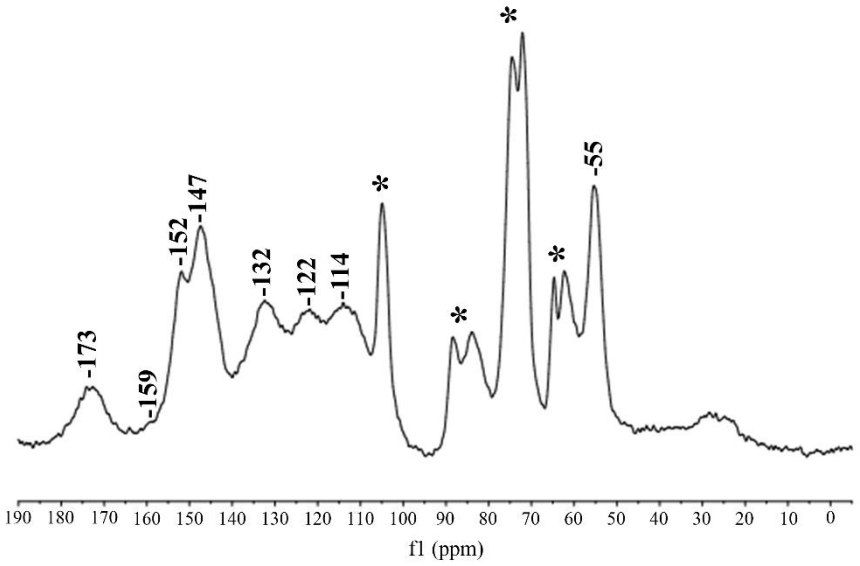

Figure 3.1- CP-MAS ^{13}C NMR spectrum of the desuberized cork residue after the isolation of dioxane lignin. Resonances belonging to polysaccharides denoted by an asterisk.

The isolated cork DL had a low content of concomitant polysaccharides (ca. 2%, mainly glucan), as revealed by ion chromatography analysis (Table 3.5), and suberin as revealed from the control FTIR spectrum (Figure 3.2). The latter did not show strong bands characteristic of suberin at 2980 (C-H stretching in aliphatic moieties) and 1740 cm^{-1} (C=O stretching in esters). Besides the characteristic lignin bands at 1603, 1512, and 1421 cm^{-1} (aromatic skeletal vibrations in G and S rings), the FTIR spectrum had a band at 1724 cm^{-1} from stretching vibrations of C=O in unconjugated ketone structures and in conjugated to aromatic ring carboxyl groups in lignin [54,55].

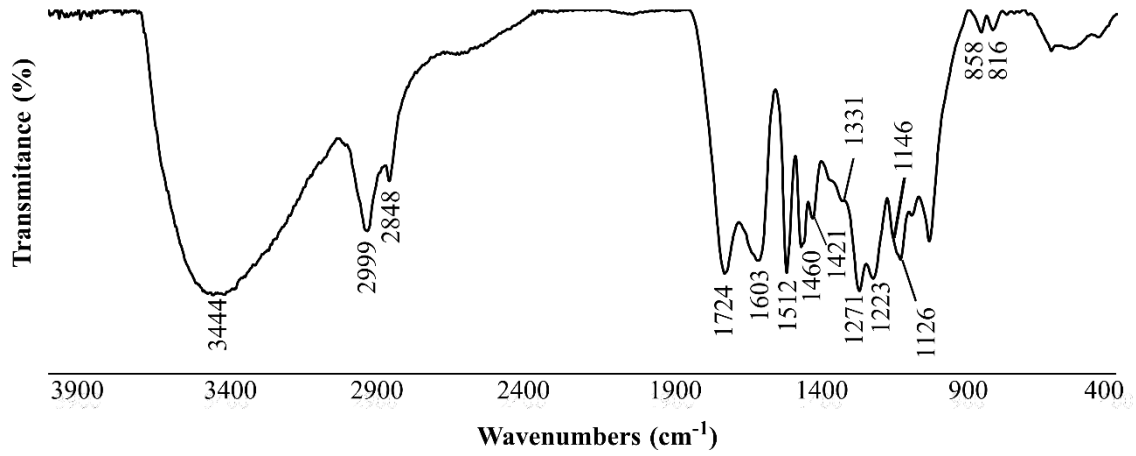

Figure 3.2- FTIR spectra in KBr of dioxane lignins isolated from natural cork stoppers.

According to the proposed lignin classification through FTIR spectroscopy (Figure 3.2), it can be suggested that the isolated lignin is of GS type since it respects the following conditions in terms

of bands intensity: 1603<<1512>>1460 cm^{-1} [56]. The FTIR spectrum also shows a strong peak at 1126 cm^{-1} with a typical shoulder at 1146 cm^{-1} characteristic of GS-type lignins.

3.3.3.2 Analysis by Py-GC-MS

Analytical pyrolysis is a degradative tool for the evaluation of lignin building blocks, which usually corroborates with results of chemical degradation techniques such as thioacidolysis or nitrobenzene oxidation [41]. This technique was applied to assess the ratio of the H, G, and S units in the cork lignin in situ without isolation from the cork and in the isolated DL.

The pyrograms of the extractives-free and desuberized cork and isolated cork DL are presented in Appendix A. A total of 94 compounds were released during pyrolysis and correspond to lignin-derived products as well as suberin, carbohydrates, and tannin-derived compounds, which were not considered for analysis. Cork DL and starting cork material without suberin showed a yield from total released pyrolysis product of nearly 58% and 38%, respectively. The identified pyrolysis products are listed in Table 3.3.

The cork material before isolation of DL showed a H:G:S molar ratio of 8:89:3, allowing the assignment to G-type lignin. However, the cork DL, assessed by the same technique, showed a H:G:S ratio of 5:82:13, which is more characteristic of GS-type lignin. Previously, a similar proportion of the H, G, and S structural units was reported for the MCL [17,18,21–23]. Taking into consideration the analysis of the residue after lignin isolation by solid-state ^{13}C NMR (Figure 3.1), the results on the H:G:S ratio obtained for cork DL looks more reliable than those obtained directly from the initial desuberized cork material. The obtained discrepancy in the H:G:S ratio of the cork lignin in situ and the isolated lignin could be explained by partial degradation of the cork DL, resulting in more abundant phenolic units contributing more to the yield of pyrolysis products (eventually higher volatile products/char ratio). This applies primarily to syringyl unit-built lignin molecules that are less ramified than guaiacyl unit-built lignin.

Table 3.3- Identities and relative molar abundance (% of Identified) of the lignin-derived compounds identified in Py-GC/MS of the cork lignin dioxane and cork after desuberinization process. (NI- non-identified)

Peak	RT	Compounds	Origin	Cork without suberin	Dioxane lignin
1	21.73	2-hydroxy-benzaldehyde	H	0.2	0.2
2	23.34	phenol	H	2.0	1.2
3	24.10	guaiacol	G	10.6	8.8
4	25.90	1-hydroxy-2,5-dimethylbenzene	H	0.0	0.1
5	26.74	4-methylphenol	H	0.8	1.1
6	26.93	2-methoxy-6-methylphenol	G	0.5	0.5
7	27.81	creosol	G	0.0	0.2
8	28.24	4-methylguaiacol	G	1.9	9.4
9	30.41	4-ethylphenol	H	0.3	0.2
10	30.46	NI and ethylguaiacol isomer	G	0.2	0.2
11	31.72	4-ethylguaiacol	G	3.0	2.7
12	34.11	4-vinylguaiacol	G	8.3	6.7
13	35.07	eugenol	G	0.5	0.9
14	35.19	4-propylguaiacol	G	0.4	0.5
15	36.29	syringol	S	0.5	1.7
16	37.34	*cis*-isoeugenol	G	0.5	0.7
17	37.91	3-methoxy-5-methylphenol	G	0.0	0.9
18	39.41	*trans*-isoeugenol	G	2.3	3.0
19	39.94	4-methylsyringol	S	0.0	1.8
20	40.43	vanillin	G	1.3	1.9
21	40.86	1-(4-hydroxy-3-methoxyphenyl)propyne	G	0.3	0.3
22	41.29	1-(4-hydroxy-3-methoxyphenyl)propyne	G	0.2	0.3
23	42.80	4-ethylsyringol	S	0.1	0.4
24	43.34	vanillic acid methyl ester	G	0.1	0.8
25	43.56	acetoguaiacone	G	1.5	1.4
26	45.02	4-vinylsyringol	S	0.2	1.0
27	45.47	guaiacylacetone	G	1.5	3.4
28	46.65	propioguaiacone	G	0.3	1.0
29	47.48	butyrovanillone	G	0.0	1.1
30	49.44	methyl dihydroferulate	G	0.0	0.4
31	49.72	*trans*-4-propenylsyringol	S	0.1	0.5
32	50.01	dihydroconiferyl alcohol	G	0.5	1.0
33	50.92	syringaldehyde	S	0.0	0.3
34	53.26	acetosyringone	S	0.0	0.3
35	54.68	syringylacetone	S	0.0	0.7
36	55.97	ferulic acid methyl ester	G	0.0	2.6
		H:G:S molar ratio		8:89:3	5:82:13

3.3.3.3 Permanganate Oxidation

Analysis of products arising from permanganate oxidation (PO) of cork DL allows obtaining information about "condensed" and "noncondensed" structures of the isolated lignin. Although only phenolic lignin units are accessible for analysis, it is usually assumed that they reflect the whole lignin structure [40]. Figure 3.3 shows 9 different aromatic carboxylic acid methyl esters that were identified as oxidation products and contributed to the total yield of *ca.* 8% (w/w) based on the lignin submitted to analysis. Product I, II, and III arise from oxidation of the noncondensed H, G, and S units, respectively, whereas products V, VI, VII, and IX arise from the so-called condensed units. The isohemipinic acid methyl ester (structure V) originates mainly from the phenylcoumaran (*β*-5') structure, whereas structure VI is assigned to G units condensed at the C6 position, such as dilignol *α*-6'-type structures [41,57–59]. Oxidation products VIII and IX are derived from biphenyl-type (5-5') and diaryl ether-type (4-O-5') structures, respectively. The diethylated structures IV and VII do not belong to lignin and are attributed to condensed tannins. Products IV and VII have already been identified as PO products in *Eucalyptus globulus* wood [41], *Acacia mangium* wood [57] and in grape stalks [26,53] and originate from procyanidins. The last finding confirms the eventual structural association of lignin and tannins proposed above based on the solid-state ^{13}C NMR results (Figure 3.1). However, it is not conclusive whether this association has already occurred in the cell wall or was acquired during the isolation procedure.

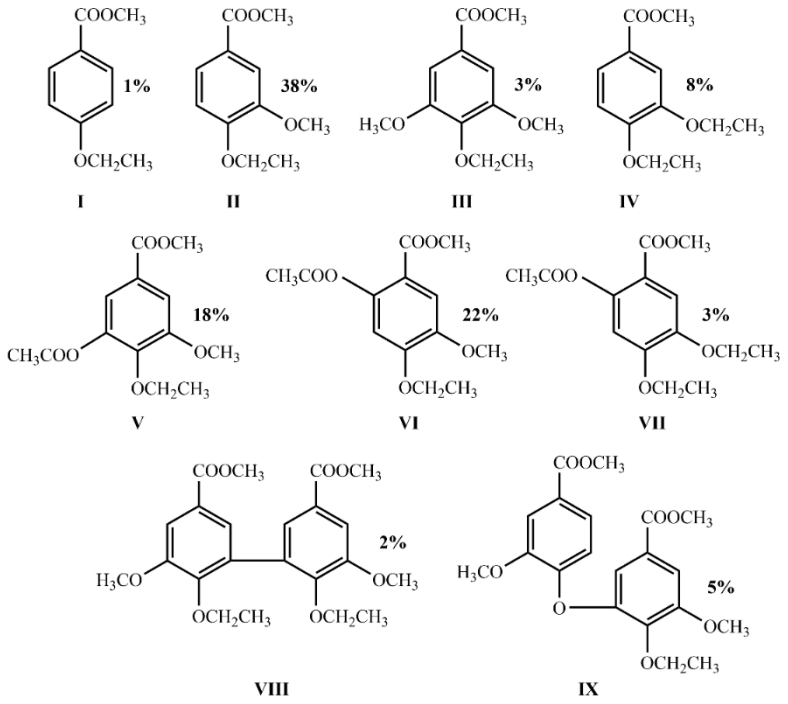

Figure 3.3- Carboxylic acid methyl esters obtained from permanganate oxidation analysis. Abundance of the structures is in molar percent.

Figure 3.3 shows the molar proportion of the obtained oxidation products with an approximate H:G:S ratio 1:95:4 (excluding IV and VII structures). This fact confirms the predominance of G-type over S-type terminal phenolic structures.

In general, the detected relative abundance of diaryl ether structures (IX) was similar to that previously reported for the cork lignin assessed in situ or after its isolation [21,27]. However, it is noteworthy that the relative abundance of the biphenyl structures (VIII) found among PO products in the present work is inferior and that the relative abundance of V and VI (Figure 3.3) superior to those reported previously either for isolated MCL/ organosolv or in situ cork lignin [21,27]. The plausible explanation could be that at least part of the biphenyl structures was etherified in lignin and not protected completely by previous ethylation before PO. In that case, part of the biphenyl structures will result in the methyl ester of isohemipinic acid (V structure). For example, the dibenzodioxocin structures reported in cork lignin [22,23] under PO analysis give product V (Figure 3.3).

The relatively high abundance of VI structures can be the result of lignin structural association with tannins due to the condensation reactions occurring either in the desuberizing of cork or in the isolation of DL. Previously, lignin reaction with procyanidins under alkaline or acidic conditions was considered the main obstacle to the delignification of agricultural wastes such as grape stalks. The possible condensation mechanism between lignin and procyanidins was discussed previously [26].

In fact, the molecular weight distribution (MWD) of cork DL was abnormal, showing a multimodal profile (Figure 3.4). The molecular weight of the low molecular fraction (depicted in black) was 2500 Da, very similar to that normally found for the hardwood dioxane lignins [41,57]. The higher molecular weight fraction >5000 Da can be assigned to lignin structural associations (depicted in red) with tannins and probably with suberin (Figure 3.4).

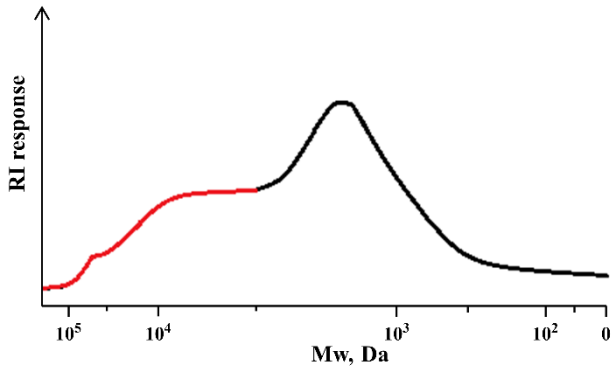

Figure 3.4- SEC molecular weight distribution profile of cork dioxane lignin.

3.3.3.4 Two-Dimensional NMR Spectroscopy

The structural features of cork dioxane lignin were confirmed by ^{1}H-^{13}C correlation NMR spectroscopy (HSQC). Figure 3.5 shows two principal regions of HSQC NMR spectra: the left image is related to the oxygenated aliphatic (δ 50-100/2.0-6.0) region, and the image on the right side corresponds to the aromatic (δ 100-155/5.0-8.0) region. The basic assignments of signals were made based on the results of previous work on the analysis of lignins from hardwoods, cork, and agricultural residues [22,23,41,53,58,59]. Thus, the *β*-O-4', *β*-5', *β*-1', and *β*-*β*' were unambiguously identified (Figure 3.5). The eventual presence of dibenzodioxocin structures was confirmed by characteristic cross-peaks detected at δ 83.4/4.80 and 85.2/3.85 assigned to the C_α and C_β atoms, respectively [22,23]. A small abundance of coniferyl alcohol structures (CA) was confirmed by detection of the cross-signal δ 61.6/4.12 assigned to C_γ/H_γ. No esterified CA structures were detected.

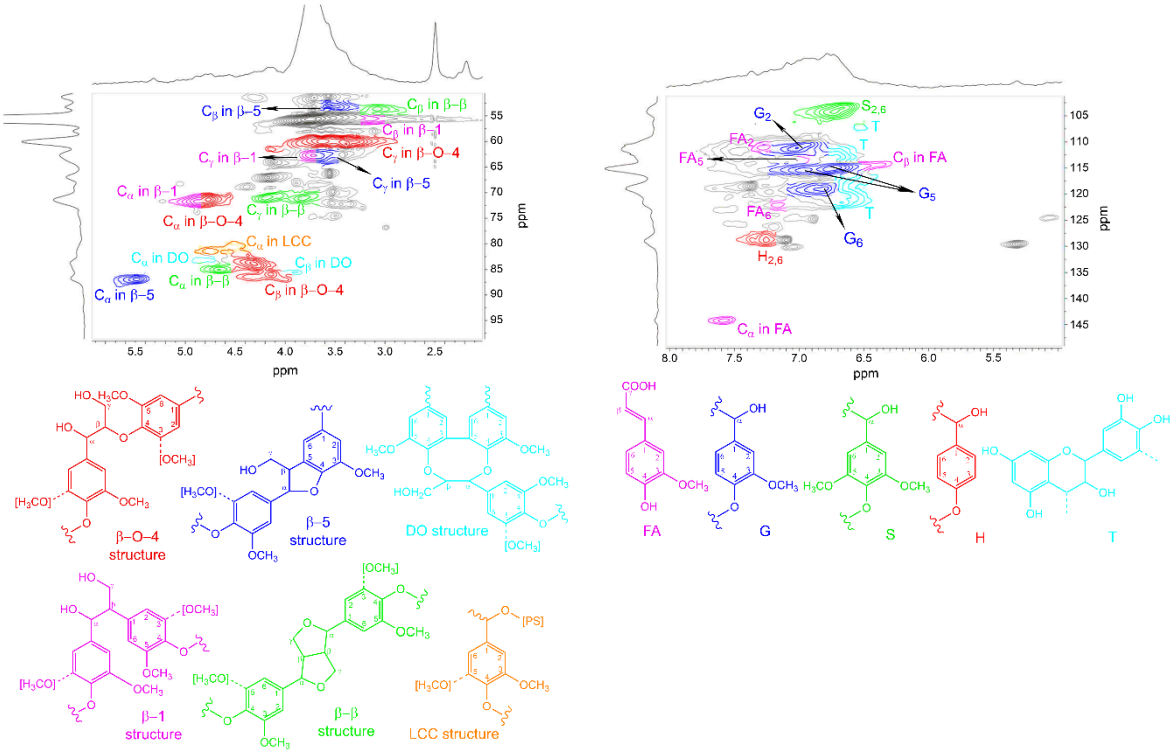

Figure 3.5- HSQC NMR spectra of the oxygenated aliphatic (left) and aromatic (right) regions of the cork dioxane lignin (308 K, DMSO-d_6).

Besides common signals from the S and G structural units in the aromatic region, the characteristic resonances from ferulic acid (FA)-type structures have been detected (Figure 3.5). FA structures are specific for cork lignin, being responsible for the structural association with other cell wall components, primarily with suberin [1,18,22].The cross-peak group of the tertiary aromatic carbons in the range of 110-125/6.5-6.8 ppm does not apply to lignin (Figure 3.5). These signals are

typical for the structurally associated procyanidins (T) [26]. This observation is in agreement with tannin-derived products detected in the PO analysis of cork DL. The presence of H units is evidenced by the cross peaks at δ 128.8/7.20-7.35 assigned to C2/H2 and C6/H6 in the corresponding structures [60]. The H2/H6 proton shifts in the H structures are of *ca*. δ -0.30 than those normally found in *p*-coumaric (Pc) acid-type structures [58] and fits to etherified H structures without electron acceptor groups in the propane chain [60]. Hence, the H structures in cork lignin are not of Pc origin. The oxygenated aliphatic region in the HSQC spectrum also showed cross-signals at δ 81.6/4.52-4.75 characteristic of benzylic carbon involved in ether linkage with glucans [61]. Since isolated cork DL still contained residual carbohydrates (mainly glucans), these are likely structurally associated with lignin via benzyl ether bonds.

3.3.3.5 Quantitative ^{1}H and ^{13}C NMR Spectroscopy

The quantitative ^{13}C NMR spectrum (Figure 3.6) of cork dioxane lignin permits detailed information on the abundance of different lignin structures. The matching of carbon chemical shifts was made base on the HSQC spectrum and available database in the literature [26,41,57–60].

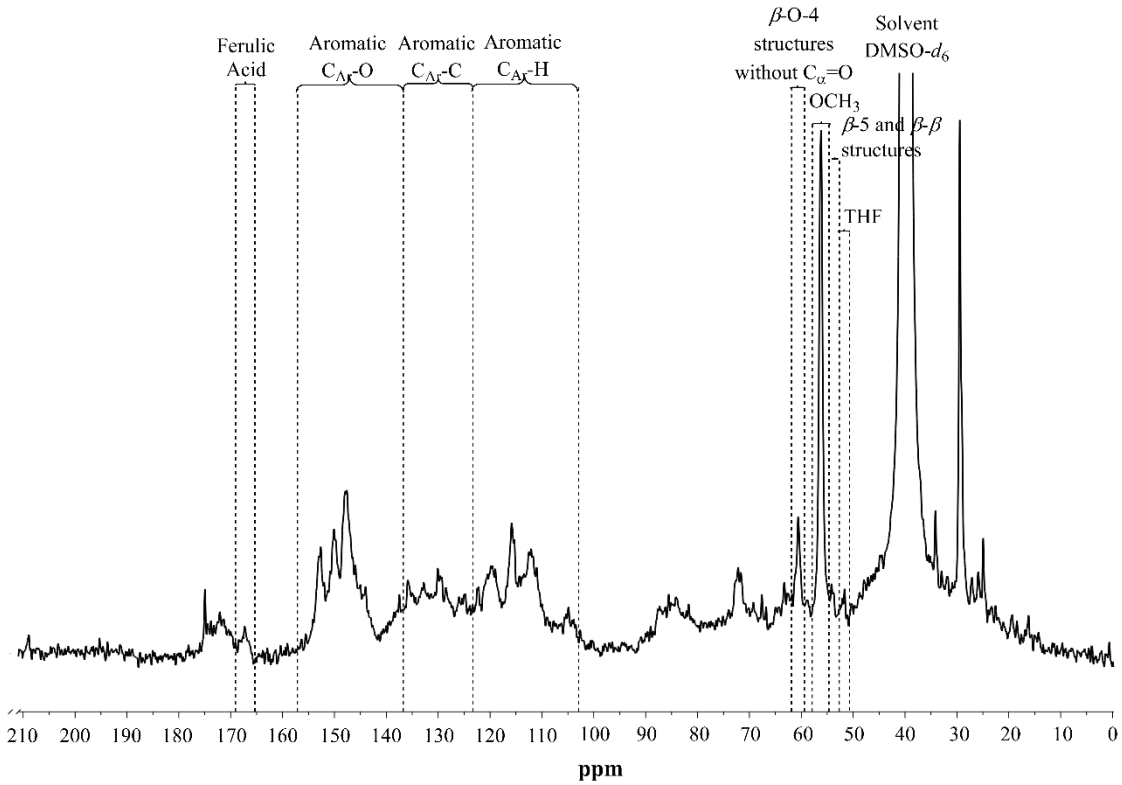

Figure 3.6- Quantitative ^{13}C NMR spectrum of cork dioxane lignin (308 K, DMSO-d_6).

Analysis results of the main structures in lignin are summarized in Table 3.4. The calculations have been carried out per one aromatic ring (C_6) by integration in the ^{13}C NMR spectrum the aromatic region (102.8-162.0 ppm), attributed to the six carbons in the aromatic ring of lignin structural units, in which the integral value one carbon allowed quantification of each structure based on the characteristic resonance [41].

Table 3.4- Quantification of the structures and functional groups of lignin as revealed by quantitative ^{13}C and ^{1}H NMR.

Lignin structures/functional groups	Amount (number/C_6)
β-5' and β-β' structures[a]	0.11
β-β' structures[b]	0.07
THF[b]	0.16
OCH_3[a]	1.08
β-O-4' structures without C_α=O[a]	0.38
Aromatic C_{Ar}-H[a]	2.29
Aromatic C_{Ar}-C[a]	1.43
Aromatic C_{Ar}−O[a]	2.28
Ferulic acid structures[a]	0.14
H:G:S ratio[a]	5:72:23
OH phen[b]	0.37
OH aliph[b]	0.82
CHO in cinnamaldehyde type units[b]	0.02
CHO in benzaldehyde type units[b]	<0.01
$C_\beta O$[a]	0.05

[a]Data from quantitative ^{13}C NMR ($n_x = (I_x \cdot 6)/I_{102.8-159}$).
[b]Data from quantitative ^{1}H NMR spectrum of acetylated lignin ($n_x = I_x/(I_{3.5-4.0} \cdot 3.24)$)

Thus, the H:G:S molar ratio was evaluated considering the characteristic signals from the tertiary aromatic carbons in the S (102.0-110.0 ppm) and G (110.0-122.0 ppm) units, while the amount of H units was assessed by signal integration at 159.0-162.0 ppm (C-4 in corresponding structures) [41]. The H:G:S proportion obtained was 5:72:23, which differs from other literature data that show a larger proportion of G unit values (80-98%) and, respectively, a lower abundance of S and H units [20,23]. This fact may be explained by the more representative dioxane lignin sample isolated in the present work (50% of the total cork lignin) in comparison to previously reported MCL and mild acidolysis of lignin (2-12% yield) [17,18,20,22,27]. The accessibility of S-type lignin appears to be the reason. This was confirmed by solid-state ^{13}C NMR analysis, which still showed considerable amounts of unremoved lignin rich in S units in the residue after isolation of cork DL (Figure 3.1). Assuming the importance of lignin heterogeneity in the cell wall, it is proposed that there is a higher proportion of S units in lignin occurring in the interior cell wall layers than in the

external layers and in the middle lamella, similar to the xylem cells [62]. Taking into consideration the fact that the secondary cork cell wall layer contains the lignin clusters embedded into the suberin laminae and cellulosic fibrils [1], its accessibility even after mechanical pretreatment must be compromised. The desuberized cork cells showed a much reduced and collapsed secondary cell layer with the remaining lignin huddled in the middle of the other cell wall components [63]. The H:G:S molar ratio calculated from the ^{13}C NMR spectrum (5:72:23) is somewhat different from that assessed by Py-GC-MS (5:82:13). One reason could be the much lower abundance of phenolic S than G units in lignin that could affected the yield of pyrolysis monomeric volatile products.

The amount of lignin structures linked by *β*-O-4' bonds (Table 3.4) was determined based on the integration of the signals at 59.2-61.8 ppm (C_γ resonance in *β*-O-4' structures). The abundance of the *β*-5' and *β*-*β*' structures and THF (tetrahydrofuran)-type structures (Table 3.4) was assessed using C_β resonances at 53.0-54.3 and 50.0-52.3 ppm, respectively [41]. On the basis of the data obtained, it could be assumed that cork lignin contains a moderate amount of aryl ether structures (*β*-O-4'-type structures) and is relatively condensed with a high content of quaternary carbons (C_6-C) in the aromatic ring (Table 3.4). Taking into consideration the common substitution of the aromatic ring with a propane chain, the estimated amounts of condensed structures of alkyl-aryl and aryl-aryl type might be 0.43 per PPU (1.43-1). A considerable part of the condensed structures might be related to lignin structural association with procyanidins. The value obtained is close to the abundance of condensed structures assessed by PO (Figure 3.3).

The group of resonances centered at 167.4 ppm is assigned to carboxyl or ester groups in etherified ferulates (FA), which is believed to be the linking point between suberin and lignin in the cork cell wall [51,64]. The presence of FA was also confirmed by the HSQC spectrum (Figure 3.5). The absence of a characteristic strong resonance at nearly 159 ppm (C4 in Pc) [58,60] confirms the absence of some significant amount of Pc structures in cork DL, as also suggested earlier by analysis of the HSQC spectrum. Figure 3.6 also shows resonances at 174.8 ppm and at 34.2, 29.5, and 24.9 ppm, which are assigned to the carboxyl groups (COOH) and aliphatic methylene (CH and CH_2) groups, respectively, in fatty, dicarboxylic, and hydroxyl acids arising from the degraded suberin [65]. The intensity of the carbon signals at 20-30 ppm in the cork DL (Figure 3.6) was superior to that in the residue after DL isolation (Figure 3.1). It cannot be excluded that these structures are structurally associated with the cork lignin by the same manner as in the neat cork material or by newly formed linkages during the isolation procedure.

The small quantity of ketone structures (C_β=O) evidenced from the resonance at 208.9 ppm (Figure 3.6) might be Hibbert-type substructures arising in lignin as a typical acidolytic byproduct [41]. Through the combination of elemental analysis (C, 59.9%; O, 34.8%; H, 5.3%) and quantitative analysis of the methoxy groups (based on the resonance centered at 56.2 ppm in the ^{13}C NMR

spectrum) it was calculated to be the average molecular mass of the C_9 empirical phenyl propane unit (201.9 g/mol). This empirical formula $C_9H_{7.46}O_{3.31}(OCH_3)_{1.10}$ is different from that previously reported in the literature $C_9H_{8.74}O_{2.82}(OCH_3)_{0.85}$ [18], which could be explained by the difference in the amount of detected syringyl units.

The quantitative ^{1}H NMR spectrum (Figure 3.7) of acetylated lignin was used to confirm quantitative estimations for some structural element done by ^{13}C NMR as well as to obtain additional structural information such as the amounts of aliphatic and phenolic hydroxyl groups. Quantification was carried out per one phenyl propane unit (PPU, $C_9H_{7.46}O_{3.31}(OCH_3)_{1.10}$) using the resonance of the methoxy groups at 3.6-4.0 ppm as an internal standard and integrating the proton intensities in the corresponding functionalities, as described previously [41].

The amount of aliphatic and phenolic hydroxyl groups is revealed by integration of the resonances at 1.7-2.2 and 2.2-2.5 ppm, respectively, in the ^{1}H NMR spectrum (Figure 3.7). The cork lignin contained 0.37 phenolic hydroxyl groups per PPU, which is slightly out of range with hardwood lignins (0.20-0.30) [41,56]. This can be explained, at least partially, by the detected tannin admixtures possessing a high content of phenolic groups. The amount of *β-β*' structures was assessed based on the specific resonance of H_β in the range of 2.8-3.1 ppm. Hence, the content of the *β*-5' structures was inferred by difference knowing the sum of *β*-5' and *β-β*' structures from quantitative ^{13}C NMR and the content of *β-β*' structures from quantitative ^{1}H NMR spectrum (Table 3.4).

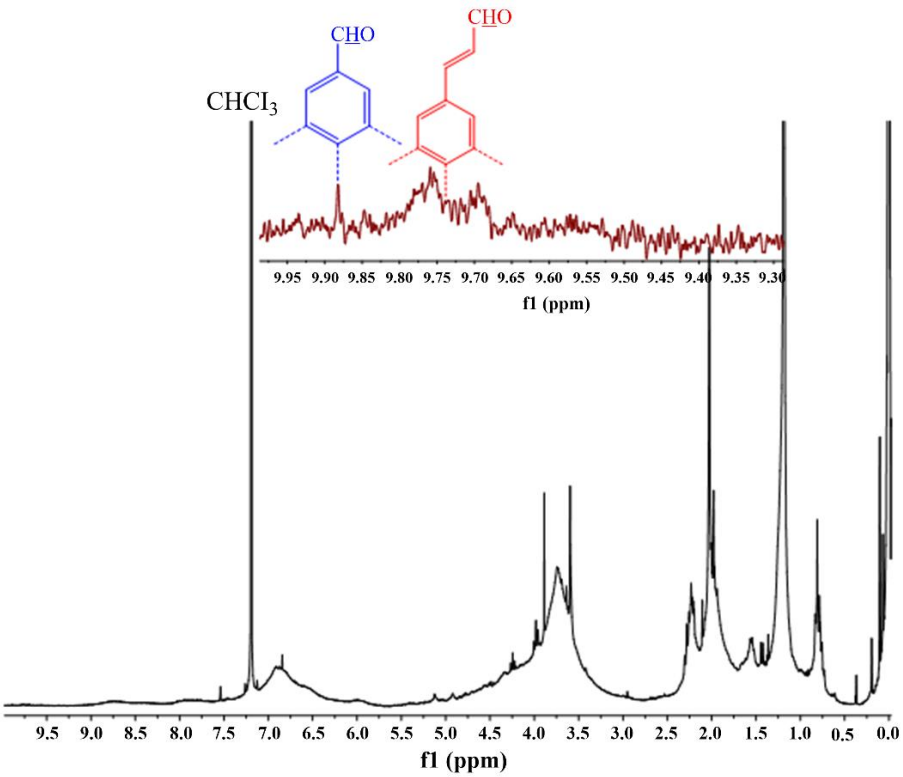

Figure 3.7- ^{1}H NMR spectrum of acetylated cork dioxane lignin (298 K, $CDCl_3$). Expanded formyl proton region shows benzyl- and cinnamaldehyde-type structures.

The region at 9.30-10.00 ppm of the ^{1}H NMR spectrum allows the determination of the amount of aldehyde groups; this region is assigned to formyl protons and reveals the content of aldehyde groups in cinnamaldehyde-type structures (Table 3.4). The signals between 0.8 and 1.6 ppm, assigned to CH_3 and CH_2 in saturated aliphatic compounds, respectively, suggest once more the presence of aliphatic compounds associated with lignin as already demonstrated by analysis of the ^{13}C NMR spectrum (Figure 3.6).

3.3.4 Analysis of cellulose

The supramolecular structure of isolated cellulose (Kürschner & Hoffer method) was analyzed by FTIR and X-ray diffraction (WAXS) as a textured sample. FTIR spectrum (Figure not presented) showed the typical pattern of functional groups and skeletal vibrations of glucopyranose units of cellulose. The relatively high crystallinity index of 0.82 (T_{1375}/T_{2990}) indicates cork cellulose as a relatively highly crystalline material [66].

The cork cellulose is a typical cellulose I polymorph possessing the characteristic reflections 110, 1-10, and 200 in the WAXS diffractogram (Figure 3.8). The degree of cristanility (DC) of cellulose, evaluated based on the ratio of crystalline reflexes and the amorphous halo [DC= Ic/(Ic+Ia)*100], was 70.3% and the average crystallite width (d_{200}), assessed in the 200 lattice plane of elementary cell, was 3.5 nm.

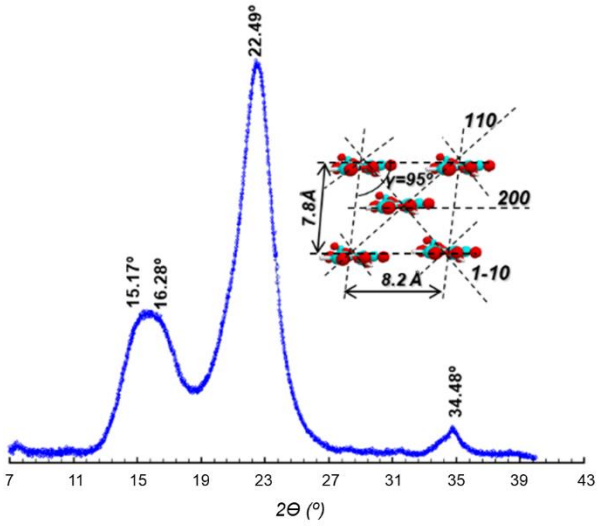

Figure 3.8- WAXS diffractogram of cork cellulose.

3.3.5 Analysis of hemicelluloses

The quantification of hemicelluloses was carried out based on the sugar analysis of the residue after the removal of extractives and suberin (Table 3.5), which showed that glucan accounts for 17.2% of dry cork, which represents 72.2% of all carbohydrates and it can be assumed that it belongs mainly to cellulose. In this way, the amount of hemicelluloses might be *ca*. 6.6%, where the composition of polysaccharides in relation to neutral sugars was the following: xylose (25.1%), arabinose (0.1%), mannose (0.7%), and galactose (2.0%). No detectable amount of rhamnose was found. When compared with literature data the values of each neutral sugar were lower, as glucose represents only 45.4% of total polysaccharides reported previously, instead of 72.2% [6]. Nevertheless, the results show that xylan still plays an important structural role in the cork cell wall.

Table 3.5- Polysaccharide composition of cork.

Polysaccharide	Rel. abundance (% dry cork sample ±standard deviation)
Glucan	17.2±0.2
Xylan	5.9±0.1
Mannan	0.2±0.0
Galactan	0.5±0.1
Arabinan	0.03±0.00

The structural analysis of xylan from cork was carried out after its extraction by DMSO from holocellulose obtained by delignification with peracetic acid of the desuberized and extractives-free cork residue. The obtained DMSO extract was purged into a mixture of ethanol and methanol and the precipitate was centrifuged and washed with absolute methanol before drying. The use of DMSO instead of alkaline solutions allows the intact xylan with labile substituents though the yield of the xylan is lower than after the alkaline extraction [37]. The yield of isolated xylan as about 50% as follow from the sugars analysis of the holocellulose before and after the extraction with DMSO.

Sugar analysis of the precipitated DMSO extract revealed the prevalence of xylose and uronic acids (Table 3.6), as might be expected from the preliminary analysis of the cork residue after extractives and suberin removal (Table 3.5), when assuming that the xylan should be the main hemicellulose. The proton spectrum of the isolated residue (Figure 3.9) also revealed the spectra patterns typically reported for the acetylated xylans from wood isolated by the similar procedure [67–69].

Table 3.6- Composition of monosaccharide's (% wt) in heteroxylan of cork.

Monosaccharides	Heteroxylan of cork
Xylose	77.5
Arabinose	2.9
Galactose	6.2
Glucose	4.8
Rhamnose	0.7
Mannose	traces
UA*	7.5

*Uronic acids (UA) were determined as the galacturonic acid

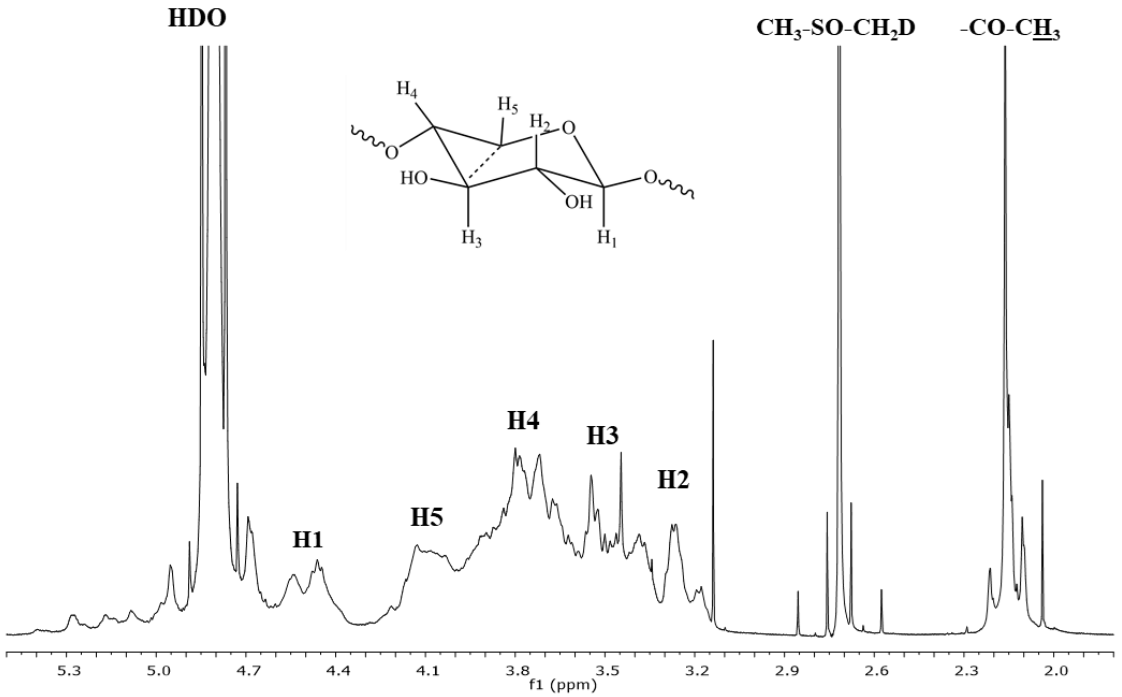

Figure 3.9- ^{1}H NMR spectrum (D_2O, 298K) of the residue isolated from DMSO extract of cork holocellulose. The extract of cork hemicellulose. The schematic representation of 1,4-anhydro-β-D-xylopyranose residue shows the proton assignments.

The presence of remarkable amounts of glucose, galactose and arabinose put in evidence the eventual concomitant polysaccharides co-precipitated with xylan from the DMSO extract (Table 3.6). These polysaccharides could be also structurally associated with xylan. In order to evaluate the type polysaccharides co-precipitated with xylan and the eventual types of interunit linkages, these were subjected to the methylation analysis, which results are summarized in Table 3.7. Based on these results, the concomitant polysaccharides can be characterized as glucan, arabinan and galactan typically present in the cell wall of xylem cells. In the previous works similar structural patterns of co-precipitated with xylan polysaccharides from its DMSO solution were assigned to amylose/amilopectin and rhamnoarabinogalactan in the composition of pectin [37,70,71].

Table 3.7- Results of the methylation analysis of cork xylan.

Methylated residue	Deduced structural unit	Relative abundance (mol.%)
Xyl-2,3,4	Xyl*p*-(1→	1.0
Xyl-2,3	→4)-Xyl*p*-(1→	84.5
Xyl-3	→2,4)-Xyl*p*-(1→	5.5
Xyl-2	→3,4)-Xyl*p*-(1→	traces
Ara-2,3,5	Ara*f*-(1→	1.8
Ara-2,5	→3)-Ara*f*-(1→	1.2
Ara-2	→3,5)-Ara*f*-(1→	0.4
Gal-2,3,4,6	Gal*p*-(1→	1.0
Gal-2,4	→3,6)-Gal*p*-(1→	2.4
Gal-2,3,6	→4)-Gal*p*-(1→	2.8
Gal-2,3	→4,6)-Gal*p*-(1→	0.4
Gal-2,3,4	→6)-Gal*p*-(1→	0.4
Glc-2,3,4,6	Glc*p*-(1→	0.9
Glc-2,3,6	→4)-Glc*p*-(1→	0.6
Glc-2,3	→4,6)-Glc*p*-(1→	4.0
Rha-2,4	→3)-Rha*p*-(1→	0.6
Rha-3	→2,4)-Rha*p*-(1→	0.3
Man-2,3,6	→4)-Man*p*-(1→	0.3

As regarding the substitution patterns in the xylan backbone, it can be suggested that the 1,4-anhydro-β-D-xylopyranose residues (→4)-β-D-Xyl*p*-(1→) in cork xylan possess the substitutions at *O*-2 position only, because the only *O*-3 methylated β-D-xylopyranose (Xyl*p*) adduct has been detected among methylated products (Table 3.7). The abundance of this methylated product (Xyl-3) was very similar to the relative abundance of uronic acids found under analysis of sugar composition of the precipitated xylan (Table 3.6). All these facts indicated that the xylan isolated from cork might be typical glucuronoxylan (heteroxylan). This proposition was further confirmed by exhaustive analysis of the obtained heteroxylan by a series of proton-proton and proton-carbon correlation NMR techniques.

The structural features of the xylan backbone were studied by single (COSY) and multiple (TOCSY) proton-proton correlation NMR techniques and single proton-carbon (HSQC) NMR while confirming the previously published corresponding correlations by multiple proton-proton (NOESY) and proton-carbon (HMBC) NMR [37,67–71]. The backbones of concomitant polysaccharides were identified based on the previously published 2D NMR data involving short and long-range proton-proton and proton-carbon correlations [70–74]. These results are summarised in Table 3.8 and confirm that the xylan from cork is a typical *O*-acetyl-(4-*O*-methyl-β-D-glucurono)xylan with random substitution of Xyl*p* residues at *O*-2, *O*-3 or at *O*-2,3. The Xyl*p* residues are substituted at *O*-2 by terminal 4-*O*-methyl-α-D-glucuronosyl (MeGlcA) and by α-D-glucuronosyl (GlcA) residues.

Table 3.8- Proton/carbon chemical shifts (ppm) in cork heteroxylan.

Structures unit	Assignments					
	H-1/C-1	H-2/C-2	H-3/C-3	H-4/C-4	H-5ax/C-5 H-5eq/C-5	H-6ax/C-6 H-6eq/C-6
Xyl (isol.)	4.47/102.7	3.27/73.5	3.53/74.3	3.78/77.1	3.40/63.7 4.09/63.7	n.r.
Xyl (Xyl-Ac)	4.43/103.4	3.18/73.5	3.50/74.4	3.72/77.3	3.36/63.8 4.06/63.8	n.r.
Xyl-3Ac	4.53/103.0	3.47/71.8	4.98/75.9	3.94/76.9	3.46/63.8 n.d./63.8	n.r.
Xyl-2Ac	4.68/100.8	4.68/74.2	3.79/72.5	3.86/77.0	3.45/63.8 n.d./63.8	n.r.
Xyl-2,3Ac	4.81/100.5	4.81/72.2	5.16/73.7	4.06/76.6	3.54/63.9 n.d./63.9	n.r.
Xyl-3Ac-2GlcA	4.72/102.0	3.67/75.3	5.07/74.6	3.99/77.1	3.50/n.d. n.d./n.d	n.r.
MeGlcA	5.28/98.8	3.54/72.2	3.87/73.6	3.18/83.0	n.d./n.d.	n.r.
GlcA	5.27/100.1	3.62/n.d.	3.84/n.d.	3.49/n.d.	n.d./n.d.	n.r.
GalA-2Rha	5.35/98.9	3.64/75.1	3.93 /n.d.	n.d./n.d.	n.d./n.d.	n.r.
t-Araf-1,3	5.25/110.2	4.21/82.2	3.95/77.6	4.13/85.2	3.82/62.3 3.71/62.3	n.r.
t-Araf-1,5	5.09/108.3	4.23/82.6	3.95/77.6	4.12/85.2	3.82/62.3 3.71/62.3	n.r.
Araf-1,3	5.24/110.1	4.12/82.0	4.24/83.4	4.09/84.7	3.82/62.3 3.80/63.4	n.r.
Gal-1,3,6	4.64/105.1	3.65/71.6	3.82/83.1	4.22/69.8	3.78/74.8	4.04;3.94/70.8
Gal-1,3a,6	4.54/105.1	3.66/71.6	3.70/81.5	4.12/69.8	3.82/74.8	4.04;3.93/70.2
Glc-1,4,6	4.94/99.5	3.53/n.d.	3.71/n.d.	3.56/n.d.	n.d./n.d.	3.88/n.d.
Glc-1,4	5.39/100.4	3.63/74.1	3.95/75.9	3.66/80.3	3.83/74.1	3.86;3.80/63.3

The following designations are used: Xyl (isol.), non-acetylated Xyl*p* in the backbone isolated from other acetylated Xyl*p* units; Xyl (Xyl-Ac), Xyl*p* linked with neighbouring acetylated Xyl*p*; Xyl-3Ac, 3-*O*-acetylated Xyl*p*; Xyl-2Ac, 2-*O*-acetylated Xyl*p*; Xyl-2,3Ac, 2,3-di-*O*-acetylated Xyl*p*; Xyl-3Ac-2GlcA, MeGlcA 2-*O*-linked and 3-*O*-acetylated Xyl*p*; GalA-2Rha, Rha*p* 2-*O*-linked Gal*p*A. t-Araf-1,3 and t-Araf-1,5 are terminal L-arabinofuranose structural units linked to the main backbone at *O*-3 and at *O*-5, respectively. Gal-1,3,6 are internal structural units →3,6)-β-D-Gal*p*-(1→ in the galactan. Glc-1,4,6 and Glc-1,4 are →4,6)-α-D-Glc*p*-(1→ and →4)-α-D-Glc*p*-(1→ units, respectively. n.d., non-determined. n.r., not relevant.

The quantitative evaluation of acetylation patterns in the heteroxylan backbone was carried out based on the characteristic assignments (Table 3.8) of anomeric protons in the quantitative proton NMR spectrum (Figure 3.10). The relative content of acetyl groups in the heteroxylan from cork is depicted in Table 3.9.

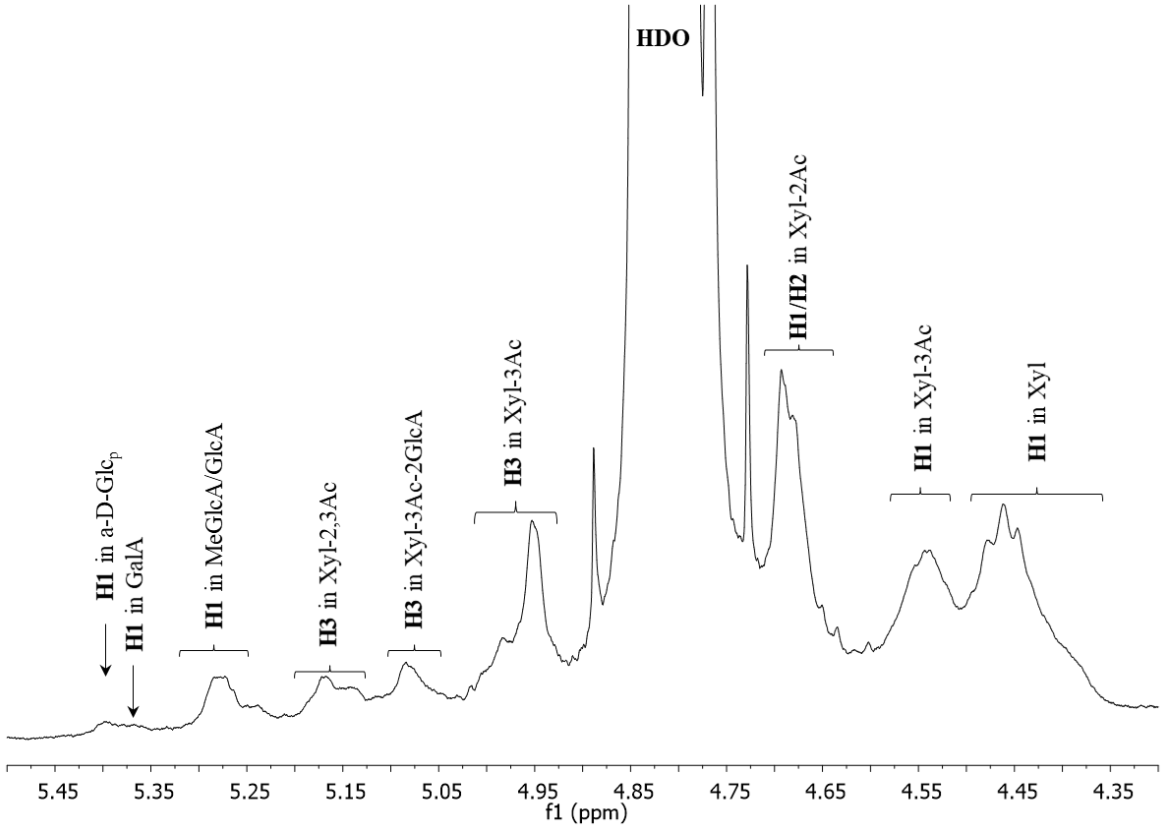

Figure 3.10- The expanded region of anomeric protons in the ^{1}H NMR spectrum (Figure 3.9) of *O*-acetyl-(4-*O*-methylglucurono)xylan from *Quercus suber* L. The designations are the same as presented in Table 3.8.

Table 3.9- Relative content of acetyl groups in structural units of xylan from cork.

Structural fragment (short designation)	Relative abundance (per 100 Xyl*p* units)
→4)-β-D-Xyl*p*-(1→ (Xyl)	44
→4)[3-*O*-Ac]-β-D-Xyl*p*-(1→ (Xyl-3Ac)	24
→4)[2-*O*-Ac]-β-D-Xyl*p*-(1→ (Xyl-2Ac)	16
→4)[3-*O*-Ac][2-*O*-Ac]-β-D-Xyl*p*-(1→ (Xyl-2,3Ac)	8
→4)[4-*O*-Me-α-D-Glc*p*A-(1→2)][3-*O*-Ac]-β-D-Xyl*p*-(1→ (Xyl-3Ac-2GlcA)	8
4-*O*- Me-α-D-Glc*p*A-(1→ (MeGlcA)	6
α-D-Glc*p*A-(1→ (GlcA)	2

It may be concluded that more than half of Xyl*p* units in the heteroxylan backbone are acetylated (DS 0.64). The highest frequency of the substitution occurs at *O*-3 with DS 0.40 (Table 3.9). About 25% of glucuronosyl residues linked at *O*-2 in Xyl*p* are not methylated (Glc*p*A). Practically all Xyl*p* units substituted at *O*-2 with uronic moieties are *O*-3 acetylated (Table 3.9). The molar ratio of Xylp to MeGlcA/GlcA residues in the heteroxylan backbone is about 13:1, which is higher than normally reported for the xylans in xylem of hardwoods (10:1) [37,57,75,76]. The low branching of cork

heteroxylan with uronic moieties and a relatively high degree of the substitution with acetyl groups makes this xylan more hydrophobic as normally found in hardwood xylem. The molecular weight of the xylan from cork is 26 kDa as revealed by size exclusion chromatography. It can be proposed that as in most of wood xylans, that the xylan of cork possesses the terminal structural fragment [→3)-α-L-Rha*p*-(1→2)-α-D-Gal*p*A-(1→4)-D-Xyl*p*] due to the presence of characteristic structural fragments found both by methylation analysis (Table 3.8) and by 2D NMR (Table 3.9).

As regarding the concomitant polysaccharides co-precipitated with xylan from DMSO solution, these can be classified as structural fragments of starch and pectin. The characteristic HSQC spectrum patterns are presented in Figure 3.11. The starch is a reserve polysaccharide localised in the parenchyma cells and is readily extracted by alkaline solutions and DMSO [70,71]. It draws attention the relatively high abundance of the ramified α-glucan chains at *O*-6 (α(1→ 6) bonding) from the amylopectin fragments (Table 3.7).

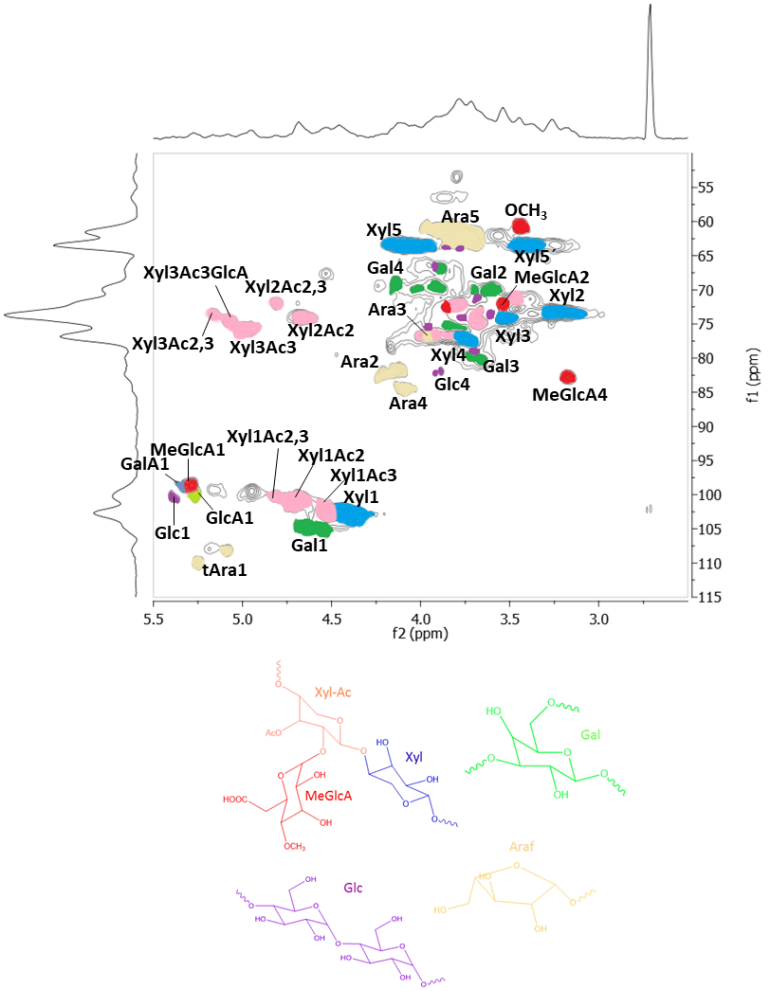

Figure 3.11- HSQC spectrum of the cork heteroxylan (D_2O, 303 K). The typical fragments of the heteroxylan and concomitant polysaccharides are depicted below the spectrum. The non-acetylated units are in blue, the acetylated ones in pink and the MeGlcA residues in red. The structural units belonging to galactan are shown in green and arabinan structural units in marron. The amylose fragments are in purple. All the designations are the same as Table 3.8.

The presence of β(1→ 4) and β(1→ 3)–linked galactans ramified by short arabinocyl chains was evidenced both by methylation and by 2D NMR analyses (Tables 3.7 and 3.8, Figure 3.11). These findings indicate the eventual fragments of pectin arabinogalactan (both type I and type II arabinogalactan). However, at the same time, the detection of β(1→ 6)-linked galactan chains with short rhamnoarabinoarabinocyl branches can indicate the presence of structural fragments from arabinogalactan-proteins (AGPs) [71,73]. AGPs are present in the cell wall and are implicated in many plant growth processes (e.g. in the lignification and cell expansion and differentiation). Being similar in nature to heteroxylan, these aforementioned structural fragments are difficult to separate by gradual precipitation in alcoholic solutions.

3.4 Conclusions

The results of this work allowed to evaluate and quantify the main chemical constituents of natural cork stoppers material and to clarify its structural features. Cork cell walls are mainly composed of suberin (44.0%), followed by cellulose (17.2%), lignin (16.2%) and hemicelluloses (6.6%).

The analysis of cork material from natural cork stoppers revealed that suberin is mainly composed of aliphatic fatty acids, hydroxy fatty acids, and dicarboxylic acids with the major aliphatic chain length of C_{18}.

Cork lignin is of GS type with a moderate proportion of S units. The H:G:S molar ratio of isolated cork dioxane lignin (cork DL) was 5:72:23. The H units are not of the *p*-coumaric acid type, and all of the cinnamic acid-type structures found in cork lignin are ferulates (14% mol). The molecular weight of cork DL is on the same order as that of lignin from hardwoods (M_w=2500 Da). The high molecular weight fractions detected in the 5000-50000 Da range belong to structural associations of lignin with procyanidins and probably with products derived from suberin and polysaccharides. The most abundant ether-linked structures in cork lignin are the *β*-O-4' (38 mol %) and 4-O-5' (5 mol %) structures. A particular characteristic of the lignin structure of cork is its high degree of condensation with an abundance of alkyl-aryl and aryl-aryl bonds of *ca.* 43 mol %. A significant part of the condensed lignin structures is related to the condensation between lignin and procyanidins, especially in the sixth position of the guaiacyl structural units. The contents of the *β*-5' and *β*-*β*' structures in cork lignin were 4 and 7 mol %, respectively. Among the terminal nonphenolic units, the coniferyl alcohol, ferulic acid cinnamaldehyde (2 mol %), benzaldehyde (<1 mol %), and Hibbert-type ketone structures (5 mol %) have been detected. The total content of hydroxyl groups was 1.19 per PPU with the major aliphatic hydroxyl groups located at C_γ and C_α (0.82 per PPU). The relatively high content of phenolic groups (0.37 per PPU) was explained by the presence of concomitant procyanidins in cork DL.

The cork cellulose is a typical cellulose I polymorph, with a degree of crystallinity of 70.3% and an average crystallite width of 3.5 nm. Among hemicelluloses, xylan is the most abundant contributing to 5.9% of cork weight. The xylan isolated is a typical *O*-acetyl-(4-*O*-methyl-β-D-glucurono)xylan(heteroxylan). More than half of Xyl*p* units in the heteroxylan backbone are *O*-3 acetylated (DS 0.64), and substituted at *O*-2 by terminal 4-*O*-methyl-α-D-glucuronosyl (MeGlcA) and by α-D-glucuronosyl (GlcA) residues (25%). The molar ratio of Xyl*p* to MeGlcA/GlcA residues in the heteroxylan backbone is about 13:1. Practically all Xyl*p* units substituted at *O*-2 with uronic moieties are *O*-3 acetylated. The molecular weight of the xylan from cork is 26 kDa. Xylan of cork possesses the terminal structural fragment [→3)-α-L-Rha*p*-(1→2)-α-D-Gal*p*A-(1→4)-D-Xyl*p*] due

to the presence of characteristic fragments found by methylation analysis and by 2D NMR. Starch and pectin were found as concomitant polysaccharides that co-precipitated with xylan from DMSO solution.

This information on the structural features of cork macromolecular components would help in a better understanding of the cork cell composition and the natural cork stoppers behavior during its chemical or chemo-mechanical processing.

3.5 References

[1] S.P. Silva, M.A. Sabino, E.M. Fernandes, V.M. Correlo, L.F. Boesel, R.L. Reis, Cork: properties, capabilities and applications, Int. Mater. Rev. 50 (2005) 345–365. https://doi.org/10.1179/174328005X41168.

[2] L. Yafang, J. Ting, S. Xiaozhou, Chemical composition of cork from *Quercus variablis*, Wood Fiber Sci. 44 (2012) 214–219.

[3] H. Pereira, Cork : Biology, production and uses, 1st ed., Elsevier B.V., Lisboa, 2007.

[4] H. Pereira, Variability of the chemical composition of cork, BioResources. 8 (2013) 2246–2256. https://doi.org/10.15376/biores.8.2.2246-2256.

[5] E. Conde, E. Cadahía, M.C. García-Vallejo, J.R. González-Adrados, Chemical characterization of reproduction cork from spanish *Quercus suber*, J. Wood Chem. Technol. 18 (1998) 447–469. https://doi.org/10.1080/02773819809349592.

[6] H. Pereira, Chemical composition and variability of cork from *Quercus suber* L., Wood Sci. Technol. 22 (1988) 211–218. https://doi.org/10.1007/BF00386015.

[7] H. Pereira, Studies on the chemical composition of virgin and reproduction cork of Quercus suber L ., An. Do Inst. Super. Agron. 25 (1981) 17–25.

[8] N. Parameswaran, W. Liese, H. Günzerodt, Characterization of wetcork in *Quercus suber* L., Holzforschung. 35 (1981) 195–199. https://doi.org/10.1515/hfsg.1981.35.4.195.

[9] M.F. Bento, H. Pereira, M.Á. Cunha, A.M.C. Moutinho, K.J. van den Berg, J.J. Boon, O. van den Brink, R.M.A. Heeren, Fragmentation of Suberin and Composition of Aliphatic Monomers Released by Methanolysis of Cork from *Quercus suber* L.,Analysed by GC-MS, SEC and MALDI-MS, Holzforschung. 55 (2001) 487–493. https://doi.org/10.1515/hf.2001.080.

[10] M.H. Lopes, A.M. Gil, A.J.D. Silvestre, C.P. Neto, Composition of suberin extracted upon gradual alkaline methanolysis of *Quercus suber* L. cork, J. Agric. Food Chem. 48 (2000) 383–391. https://doi.org/10.1021/jf9909398.

[11] J. Graça, H. Pereira, Methanolysis of Bark Suberins: analysis of glycerol and acid monomers, Phytochem. Anal. 11 (2000) 45–51. https://doi.org/10.1002/(SICI)1099-1565(200001/02)11:1<45::AID-PCA481>3.0.CO;2-8.

[12] N. Cordeiro, M.N. Belgacem, A.J.D. Silvestre, C. Pascoal Neto, A. Gandini, Cork suberin as a new source of chemicals. 1. Isolation and chemical characterization of its composition, Int. J. Biol. Macromol. 22 (1998) 71–80. https://doi.org/10.1016/S0141-8130(97)00090-1.

[13] M.C. García-Vallejo, E. Conde, E. Cadahía, B. Fernández De Simón, Suberin composition of reproduction cork from *Quercus suber*, Holzforschung. 51 (1997) 219–224.

https://doi.org/10.1515/hfsg.1997.51.3.219.

[14] E. Conde, M.C. García-Vallejo, E. Cadahía, Variability of suberin composition of reproduction cork from *Quercus suber* throughout industrial processing, Holzforschung. 53 (1999) 56–62. https://doi.org/10.1515/HF.1999.010.

[15] M.F.S. Bento, H. Pereira, M.Á. Cunha, A.M.C. Moutinho, K.J. Van Den Berg, J.J. Boon, A study of variability of suberin composition in cork from Quercus suber L. using thermally assisted transmethylation GC-MS, J. Anal. Appl. Pyrolysis. 57 (2001) 45–55. https://doi.org/10.1016/S0165-2370(00)00093-0.

[16] E. Zimmermann, W., Nimz, H. & Seemüller, H and ^{13}C NMR Spectroscopic Study of Extracts from Corks of Rubus idaeus, Solanum tuberosum, and Quercus suber., Holzforschung. 39 (1985) 45–49. https://doi.org/10.1515/hfsg.1985.39.1.45.

[17] A. V. Marques, H. Pereira, D. Meier, O. Faix, Quantitative analysis of cork (Quercus suber L.) and milled cork lignin by FTIR spectroscopy, analytical pyroiysis, and total hydrolysis, Holzforschung. 48 (1994) 43–50. https://doi.org/10.1515/hfsg.1994.48.s1.43.

[18] A. V. Marques, H. Pereira, D. Meier, O. Faix, Isolation and characterization of a guaiacyl lignin from saponified cork of *Quercus suber* L., Holzforschung. 50 (1996) 393–400. https://doi.org/10.1515/hfsg.1996.50.5.393.

[19] A.V. Marques, H. Pereira, Lignin monomeric composition of corks from the barks of Betula pendula, Quercus suber and Quercus cerris determined by Py-GC-MS/FID, J. Anal. Appl. Pyrolysis. 100 (2013) 88–94. https://doi.org/10.1016/j.jaap.2012.12.001.

[20] C.P. Neto, N. Cordeiro, A. Seca, F. Domingues, A. Gandini, D. Robert, Isolation and Characterization of a Lignin-Like Polymer of the Cork of Quercus suber L., Holzforschung. 50 (1996) 563–568. https://doi.org/10.1515/hfsg.1996.50.6.563.

[21] A. V. Marques, H. Pereira, D. Meier, O. Faix, Structural characterization of cork lignin by thioacidolysis and permanganate oxidation, Holzforschung. 53 (1999) 167–174. https://doi.org/10.1515/HF.1999.028.

[22] A. V. Marques, J. Rencoret, A. Gutiérrez, J.C. del Río, H. Pereira, Ferulates and lignin structural composition in cork, Holzforschung. 70 (2016) 275–289. https://doi.org/10.1515/hf-2015-0014.

[23] A. Lourenço, J. Rencoret, C. Chemetova, J. Gominho, A. Gutiérrez, J.C. del Río, H. Pereira, Lignin Composition and Structure Differs between Xylem , Phloem and Phellem in Quercus suber L ., Front. Plant Sci. 7 (2016) 1–14. https://doi.org/10.3389/fpls.2016.01612.

[24] A. V. Marques, H. Pereira, J. Rodrigues, D. Meier, O. Faix, Isolation and comparative characterization of a Björkman lignin from the saponified cork of Douglas-fir bark, J. Anal. Appl. Pyrolysis. 77 (2006) 169–176. https://doi.org/10.1016/j.jaap.2006.03.003.

[25] M. Bunzel, A. Schußler, G.T. Saha, Chemical Characterization of Klason Lignin Preparations from Plant-Based Foods, J. Agric. Food Chem. 59 (2011) 12506–12513. https://doi.org/10.1021/jf2031378.

[26] S.O. Prozil, D. V. Evtuguin, A.M.S. Silva, L.P.C. Lopes, Structural characterization of lignin from Grape Stalks (Vitis vinifera L.), J. Agric. Food Chem. 62 (2014) 5420–5428. https://doi.org/10.1021/jf502267s.

[27] M. Lopes, C. Pascoal Neto, D. Evtuguin, A.J.D. Silvestre, A. Gil, N. Cordeiro, A. Gandini, Products of the permanganate oxidation of cork, desuberized cork, suberin and lignin from Quercus suber L., Holzforschung. 52 (1998) 146–148. https://doi.org/10.1515/hfsg.1998.52.2.146.

[28] S.M. Rocha, M.A. Coimbra, I. Delgadillo, Demonstration of pectic polysaccharides in cork cell wall from Quercus suber L., J. Agric. Food Chem. 48 (2000) 2003–2007. https://doi.org/10.1021/jf991147g.

[29] A. Amparo, Structural studies of a hemicellulose B fraction (B-2) from the cork of *Quercus Suber*, Can. J. Chem. 66 (1988) 449–453.

[30] A. Asensio, Structural studies of a hemicellulose B fraction from the cork of *Quercus suber*, Carbohydr. Res. 165 (1987) 134–138.

[31] A. Asensio, Polysaccharides from the cork of *Quercus suber*, II. Hemicellulose, J. Nat. Prod. 51 (1988) 488–491.

[32] A. Asensio, Structural studies of the hemicellulose A from the cork of *Quercus suber*, Carbohydr. Res. 161 (1987) 167–170.

[33] A. Teleman, J. Lundqvist, F. Tjerneld, H. Stålbrand, O. Dahlman, Characterization of acetylated 4-O-methylglucuronoxylan isolated from aspen employing 1H and 13C NMR spectroscopy, Carbohydr. Res. 329 (2000) 807–815. https://doi.org/10.1016/S0008-6215(00)00249-4.

[34] T.M.P. Gomes, Y.I. Belenkiy, D. V Evtuguin, Xylan accessibility of bleached eucalypt pulp in alkaline solutions, Holzforschung. (2019) 1–8. https://doi.org/10.1515/hf-2019-0023.

[35] D. Morais de Carvalho, A.M. Abad, D. V. Evtuguin, J.L. Colodette, M.E. Lindström, F. Vilaplana, O. Sevastyanova, Isolation and characterization of acetylated glucuronoarabinoxylan from sugarcane bagasse and straw, Carbohydr. Polym. 156 (2017) 223–234. https://doi.org/10.1016/j.carbpol.2016.09.022.

[36] B.L. Browing, The isolation and determination of cellulose, in: Methods Wood Chem. Vol. II, Wiley-Interscience, New York, 1967: pp. 387–414.

[37] D. V. Evtuguin, J.L. Tomás, A.M.S. Silva, C.P. Neto, Characterization of an acetylated heteroxylan from *Eucalyptus globulus* Labill, Carbohydr. Res. 338 (2003) 597–604.

https://doi.org/10.1016/S0008-6215(02)00529-3.

[38] N. Blumenkrantz, G. Asboe-Hansen, New method for quantitative determination of uronic acids, Anal. Biochem. 54 (1973) 484–489. https://doi.org/10.1016/0003-2697(73)90377-1.

[39] R.R. Selvendran, J.F. March, S.G. Ring, Determination of aldoses and uronic acid content of vegetable fiber, Anal. Biochem. 96 (1979) 282–292. https://doi.org/10.1016/0003-2697(79)90583-9.

[40] G. Gellerstedt, Chemical Degradation Methods: Permanganate Oxidation, in: C.W. Dence, S.Y. Lin (Eds.), Methods Lignin Chem., 1st ed., Springer-Verlag Berlin Heidelberg, Berlin, 1992: pp. 322–333. https://doi.org/10.1007/978-3-642-74065-7.

[41] D. V. Evtuguin, C.P. Neto, A.M.S. Silva, P.M. Domingues, F.M.L. Amado, D. Robert, O. Faix, Comprehensive study on the chemical structure of dioxane lignin from plantation *Eucalyptus globulus* wood, J. Agric. Food Chem. 49 (2001) 4252–4261. https://doi.org/10.1021/jf010315d.

[42] D. V. Evtuguin, P. Domingues, F.L. Amado, C.P. Neto, A.J.F. Correia, Electrospray Ionization Mass Spectrometry as a tool for lignins molecular weight and structural characterisation, Holzforschung. 53 (1999) 525–528. https://doi.org/10.1515/HF.1999.086.

[43] J. Ralph, R.D. Hatfield, Pyrolysis-GC-MS Characterization of Forage Materials, J. Agric. Food Chem. 39 (1991) 1426–1437. https://doi.org/10.1021/jf00008a014.

[44] O. Faix, D. Meier, I. Fortmann, Thermal degradation products of wood. A collection of electron-impact (EI) mass spectra of monomeric lignin derived products, Eur. J. Wood Wood Prod. 48 (1990) 351–354.

[45] A. Figueiredo, D. Evtuguin, J. Saraiva, Effect of high pressure treatment on structure and properties of cellulose in eucalypt pulps, Cellulose. 17 (2010) 1193–1202. https://doi.org/10.1007/s10570-010-9454-2.

[46] I. Ciucanu, F. Kerek, A simple and rapid method for the permethylation of carbohydrates, Carbohydr. Polym. 131 (1984) 209–217. https://doi.org/10.1016/0008-6215(84)85242-8.

[47] A. Isogai, A. Ishfzu, J. Nakano, A new facile methylation method for cell-wall polysaccharides, Carbohydr. Res. 138 (1985) 99–108. https://doi.org/10.1016/0008-6215(85)85227-7.

[48] M.A. Coimbra, I. Delgadillo, K.W. Waldron, R.R. Selvendran, Isolation and Analysis of Cell Wall Polymers from Olive Pulp, in: H.F. Linskens, J.F. Jackson (Eds.), Mod. Methods Plant Anal., Springer Berlin Heidelberg, 1996: pp. 19–44. https://doi.org/10.1007/978-3-642-60989-3_2.

[49] P.J. Harris, R.J. Henry, A.B. Blekeney, B.A. Stone, An improved procedure for the methylation analysis of oligosaccharides and polysaccharides, Carbohydr. Res. 127 (1984)

59–73. https://doi.org/10.1016/0008-6215(84)85106-X.

[50] D. Fengel, G. Wegener, Wood-chemistry, ultrastructure, reactions, Walter de Gruyter, Berlin, 1989. https://doi.org/10.1515/9783110839654.

[51] M.A. Bernards, Demystifying suberin, Can. J. Bot. 80 (2002) 227–240. https://doi.org/10.1139/b02-017.

[52] P.J. Holloway, A.H.B. Deas, Epoxyoctadecanoic acids in plant cutins and suberins, Phytochemistry. 12 (1973) 1721–1735. https://doi.org/10.1016/0031-9422(73)80393-0.

[53] S.O. Prozil, D. V. Evtuguin, L.P. Cruz, Chemical composition of grape stalks of Vitis vinifera L . from red grape pomaces, Ind. Crop. Prod. 35 (2012) 178–184. https://doi.org/10.1016/j.indcrop.2011.06.035.

[54] O. Faix, Fourier Transform infrared spectroscopy, in: S.Y. Lin, C.W. Dence (Eds.), Methods Lignin Chem., Springer-Verlag, 1992: pp. 83–109. https://doi.org/10.1007/978-3-642-74065-7_3.

[55] H.L. Hergert, Infrared spectra, in: Lignins Ocurr. Form. Struct. React., John Wiley & Sons, Inc., New York, 1971: pp. 267–297.

[56] Faix O., Classification of lignins from different botanical origins by FT-IR spectroscopy, Holzforschung. 45 (1991) 21–27. https://doi.org/10.1515/hfsg.1991.45.s1.21.

[57] P.C. Pinto, D. V. Evtuguin, C.P. Neto, Chemical composition and structural features of the macromolecular components of plantation *Acacia mangium* wood, J. Agric. Food Chem. 53 (2005) 7856–7862. https://doi.org/10.1021/jf058081b.

[58] L. Oliveira, D. Evtuguin, N. Cordeiro, A.J.D. Silvestre, Structural characterization of stalk lignin from banana plant, Ind. Crops Prod. 29 (2009) 86–95. https://doi.org/10.1016/j.indcrop.2008.04.012.

[59] S. Magina, A.P. Marques, D. V. Evtuguin, Study on the residual lignin in *Eucalyptus globulus* sulphite pulp, Holzforschung. 69 (2015) 513–522. https://doi.org/10.1515/hf-2014-0218.

[60] S.A. Ralph, J. Ralph, L.L. Landucci, No Title, NMR Database Lignin Cell Wall Model Compd. (2004). http://ars.usda.gov/Services/%0A745 docs.htm?docid=10491 (accessed April 13, 2021).

[61] M. Balakshin, E. Capanema, H. Gracz, H.-M. Chang, H. Jameel, Quantification of lignin – carbohydrate linkages with high-resolution NMR spectroscopy, Planta. 233 (2011) 1097–1110. https://doi.org/10.1007/s00425-011-1359-2.

[62] N. Terashima, A new mechanism for formation of a structurally ordered protolignin macromolecule in the cell wall of tree xylem., J. Pulp Pap. Sci. 16 (1990) J150–J155.

[63] R.T. Teixeira, H. Pereira, Suberized cell walls of cork from cork oak differ from other species, Microsc. Microanal. 16 (2010) 569–575. https://doi.org/10.1017/S1431927610093839.

[64] M.A. Bernards, M.L. Lopez, J. Zajicek, N.G. Lewis, Hydroxycinnamic acid-derived polymers constitute the polyaromatic domain of suberin, J. Biol. Chem. 270 (1995) 7382–7386. https://doi.org/10.1074/jbc.270.13.7382.

[65] M.H. Lopes, C. Pascoal Neto, A.S. Barros, D. Rutledge, I. Delgadillo, A.M. Gil, Quantitation of aliphatic suberin in Quercus suber L. Cork by FTIR spectroscopy and solid-state 13C-NMR spectroscopy, Biopolymers. 57 (2000) 344–351. https://doi.org/10.1002/1097-0282(2000)57:6<344::aid-bip40>3.0.co;2-%23.

[66] V.W. Tripp, Measurement of cristallinity, in: N.M. Bikales, L. Segal (Eds.), Cellul. Cellul. Deriv., Wiley-Interscience, New York, 1971: pp. 305–323.

[67] V.M.F. Gonçalves, D. V. Evtuguin, R.M. Domingues, Structural characterization of the acetylated heteroxylan from the natural hybrid Paulownia elongata/ Paulownia fortunei, Carbohydr. Res. 343 (2008) 256–266. https://doi.org/10.1016/j.carres.2007.11.002.

[68] G. Marques, A. Gutiérrez, C. del R. José, D. V. Evtuguin, Acetylated heteroxylan from *Agave sisalana* and its behavior in alkaline pulping and TCF/ECF bleaching, Carbohydr. Polym. 81 (2010) 517–523. https://doi.org/10.1016/j.carbpol.2010.02.043.

[69] S.O. Prozil, E. V Costa, D. V Evtuguin, L.P. Cruz, M.R.M. Domingues, Structural characterization of polysaccharides isolated from grape stalks of *Vitis vinifera* L ., Carbohydr. Res. 356 (2012) 252–259. https://doi.org/10.1016/j.carres.2012.02.001.

[70] S.A. Lisboa, D. V. Evtuguin, C.P. Neto, B.J. Goodfellow, Isolation and structural characterization of polysaccharides dissolved in *Eucalyptus globulus* kraft black liquors, Carbohydr. Polym. 60 (2005) 77–85. https://doi.org/10.1016/j.carbpol.2004.11.024.

[71] S.A. Lisboa, D. V. Evtuguin, P.C. Neto, Characterization of non-cellulosic glucans in *Eucalyptus globulus* Labill. wood and kraft pulp, Holzforschung. 61 (2007) 478–482. https://doi.org/10.1515/HF.2007.110.

[72] L. Tan, F. Qiu, D.T.A. Lamport, M.J. Kieliszewski, Structure of a Hydroxyproline (Hyp)-Arabinogalactan Polysaccharide from Repetitive Ala-Hyp Expressed in Transgenic *Nicotiana tabacum**, J. Biol. Chem. 279 (2004) 13156–13165. https://doi.org/10.1074/jbc.M311864200.

[73] F.M. Nunes, A. Reis, A.M.S. Silva, M.R.M. Domingues, M.A. Coimbra, Rhamnoarabinosyl and rhamnoarabinoarabinosyl side chains as structural features of coffee arabinogalactans, Phytochemistry. 69 (2008) 1573–1585. https://doi.org/10.1016/j.phytochem.2008.01.021.

[74] S. Willfor, R. Sjoholm, C. Laine, B. Holmbom, Structural features of water-soluble arabinogalactans from Norway spruce and Scots pine heartwood, Wood Sci. Technol. 36 (2002) 101–110. https://doi.org/10.1007/s00226-001-0137-x.

[75] P.C. Pinto, D. V. Evtuguin, C.P. Neto, Structure of hardwood glucuronoxylans: modifications

and impact on pulp retention during wood kraft pulping, Carbohydr. Polym. 60 (2005) 489–497. https://doi.org/10.1016/j.carbpol.2005.03.001.

[76] P.C. Pinto, D. V. Evtuguin, C.P. Neto, Effect of structural features of wood biopolymers on hardwood pulping and bleaching performance, Ind. Eng. Chem. Res. 44 (2005) 9777–9784. https://doi.org/10.1021/ie050760o.

Chapter 4

CHANGES IN NATURAL CORK STOPPER SURFACE PROPERTIES UPON REACTIVE WASHING

This chapter was published in:

D.G. Branco, C.A. Santiago, F.J. Oliveira, L. Cabrita, D. V Evtuguin, Surface properties of cork in relation to reactive washing, Colloids Surfaces A Physicochem. Eng. Asp. 624 (2021). https://doi.org/10.1016/j.colsurfa.2021.126762

Content

4.1 Introduction

Cork morphology can be described as a homogeneous tissue of thin-walled cells grouped in a characteristic alveolar structure, resembling a honeycomb, usually without intercellular space (Figure 4.1). The cells look like rectangular prisms, placed parallel in the radial direction of the trunk [5,10–12]. The cell wall volume is about 10% of the total cell volume.

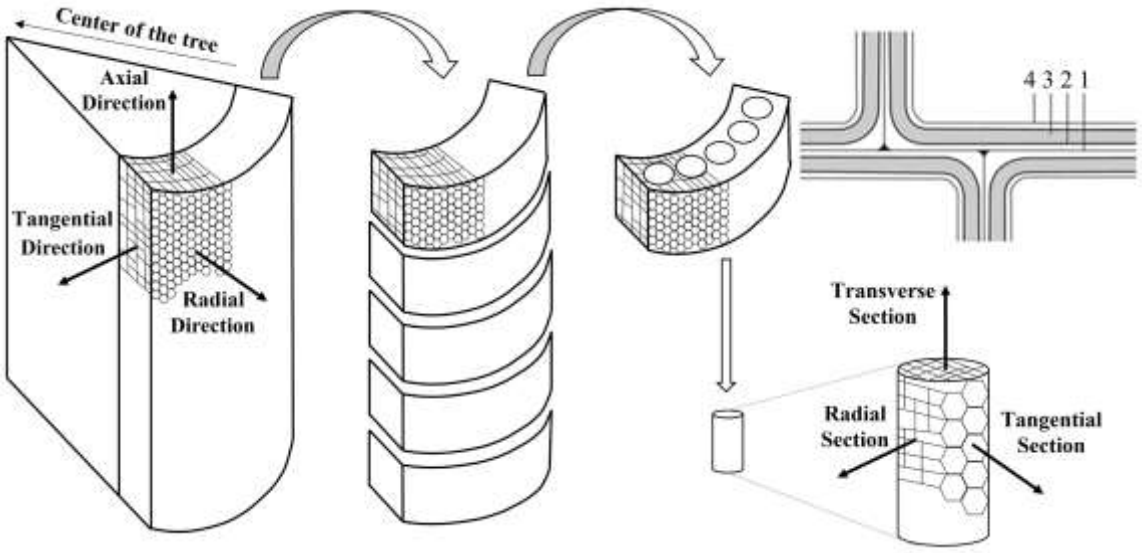

Figure 4.1- Schematic representation of the route from the cork layer of the *Quercus suber* L. to the natural cork stoppers: the extracted cork planks after being conditioned are cut into strips and the stoppers punched from a single piece of cork. Cork cells are radially oriented in the tree and lateral of a stopper represented essentially by macroscopic directions perpendicular to the axial direction. The tops of the stoppers are represented exclusively by the axial direction. The cork cell wall layers are depicted as follows: 1- Medium lamella; 2- Primary wall; 3- Secondary wall; 4- Tertiary wall [7].

In terms of chemical composition, suberin is the main macromolecular component of cork cell walls (*ca.* 44%) followed by lignin (*ca.* 16%), cellulose (*ca.* 17%), and hemicelluloses (*ca.* 7%) [7,8]. Suberin is an irregular natural 3D polyester constituted of inter-esterified long-chain fatty acids such as ω-hydroxyalkanoic acids and α, ω-dicarboxylic acids and, in less extent, of alkanoic acids, aliphatic alcohols, and glycerol [13,14]. Lignin, a 3D irregular aromatic polymer, is structurally associated with suberin in the layers assembled in a special way. Lignin-suberin matrix jointly with cellulose fibrils forms the multilayered cell wall with exceptional physical properties as concerns the compressibility, shock absorptivity, and elasticity [6–8,15]. Besides, the cork has such unsurpassed properties as impermeability, low thermal conductivity, and extraordinary lightness.

In the process of transforming the bark into cork stoppers for wine bottling, the raw material must pass through several industrial steps, where reactive washing (RW) plays the defining role in cleaning/disinfection and appearance (primarily color homogeneity and whiteness). RW consists of the multistage treatment of stoppers with hydrogen peroxide under strong alkaline conditions and

increased temperature. This causes changes in the surface of the cork material, leading to a deterioration in its receptivity to coating agents (silicone or paraffin emulsion and polymeric formulations) and in the sealing performance of bottles with spirits [16]. This is a very important factor since the treatment of the cork surface facilitates the insertion and extraction of the stopper in the bottle, in addition to improving its impermeability, which is essential in the wine aging process [16,17].

It is noteworthy that the modification of the cork surface is commonly considered a crucial prerequisite for the following targeted coating. Thus, the plasma treatment improves radically the adhesion properties [18] and the formation of iron oxide particles on the cork surface [19]. A chemical modification of cork by silanization [18,20] or by acetylation [21] improves the compatibility of the cork surface with specific polymer formulations. Although no relevant studies have been carried out to relate the RW and the surface properties of natural cork stoppers, the importance of this relationship has been recognized taking into account the effectiveness of subsequent surface coating operations and the performance of stoppers in the bottle [16,17].

In this chapter, for the first time, the surface properties of stoppers in different plane directions were evaluated and related to the changes in surface composition that occurred during the RW. The changes in the surface composition were analyzed by Fourier Transform Infrared-Attenuated Total Reflectance (FTIR-ATR) and by confocal Raman spectroscopy. The surface morphology was assessed by scanning electron microscopy (SEM) and 3D optical profilometry. The response of the modified cork surface to spirit solution with different levels of alcohol was evaluated by contact angles measurements with the liquid probes and consulting the wetting envelope in polar-dispersion energy coordinates.

4.2 Materials and Methods

Natural cork stoppers and reagents, namely hydrogen peroxide (35%, w/w), sodium hydroxide (9%, w/w), and sodium bisulfate (2.5%, w/w) were supplied by Amorim Cork, S.A (Santa Maria de Lamas, Portugal).

4.2.1 Reactive washing (RW) process in laboratory scale

Reactive washing (RW) of stoppers (49 x 24 mm) with a mixture of hydrogen peroxide and sodium hydroxide was performed on a laboratory rotation glass reactor (100 rpm) under controlled temperature (50 °C) following the timesheet protocol applied in the industry. In a typical trial, the oxidation reagents were added alternately to the reactor following the sequence used in the industry, respecting the reagent-to-stopper ratio. Once the oxidation step is completed, the stoppers were washed with water. Sodium bisulfate solution (2.5% w/w) was added to neutralize the surface of the stopper, which was washed again with water. Finally, the stoppers were dried at 40 °C in a ventilated oven for one hour.

4.2.2 Suberin and lignin isolation

Suberin and lignin were isolated from natural cork stoppers after they were ground and sieved in a 40–60 mesh fraction. Extractives-free cork was obtained by exhaustive sequential extraction of cork particles with dichloromethane, MeOH: water (50:50, v/v), and water. The extractives content in dichloromethane (DCM) was determined by Soxhlet extraction according to the Tappi T 204 om-88. The determination of extractives in MeOH: water (50:50, v/v) and in hot water was performed under reflux for 2 h. Suberin extracts were obtained after 3 h reflux of 7 g extractives-free cork particles in 700 mL of dry methanol containing 2% of sodium methoxide. After filtration, the resulting residues were again refluxed in 100 mL of methanol for 15 min and filtered. The two methanol extracts were combined and acidified to pH 6 with 0.25 M sulfuric acid (H_2SO_4) and concentrated in a rotary evaporator. The resulting concentrate was suspended in 100 mL of water and extracted three times with chloroform solutions that were dried over anhydrous sodium sulfate, the solvent was evaporated to dryness, and the suberin was dried in a vacuum oven at 35 ºC. Lignin was isolated using the dioxane method adapted from the procedure described elsewhere [23]. The isolated samples of suberin and lignin were used to analyze their location on the cork cell wall by confocal Raman spectroscopy.

4.2.3 SEM

The natural cork stoppers were cut into thin slices and covered by gold sputtering before SEM analysis. The images were acquired on a Hitachi TM 400 Plus SEM microscope (Hitachi High-Technologies, Tokyo, Japan) equipped with a BSE detector and operated at 15 kV under vacuum of 30 Pa.

4.2.4 3D optical profilometry

The surface texture analysis was carried out on a 3D optical profilometer Sensofar Metrology S neox (Sensofar, Terrassa, Spain) in Focus Variation mode by scanning within a vertical scanning range of 200 µm an area of 1750 x 1320 μm^2 using 10x optical microscope objective lenses (Nikon Corp., Tokyo, Japan). Focus Variation is a surface topography measurement method where the sharpness of the surface image in the optical microscope is used to determine the surface height at each position along the surface. For the objective used, the lateral optical resolution is 0.46 µm and the vertical resolution is about 0.3 µm. The SensoSCAN 6.2 software provided the correct course of the measurement process and the advanced analysis and visualization of the surface microtopography. The surface roughness analysis followed the standard ISO 25178, defined as Geometrical product specifications (GPS)- Surface texture: Areal.

4.2.5 FTIR-ATR spectroscopy

FTIR-ATR analyzes were performed on a Spectrum BX Perkin Elmer spectrophotometer (PerkinElmer, Waltham, Massachusetts, USA) with a resolution of 4 cm^{-1} and 128 scans in transmittance mode. All FTIR-ATR spectra were normalized at 1260 cm^{-1} using OriginPro 2015 software (OriginLab Corporation, Northampton, Massachusetts, USA).

4.2.6 Confocal Raman spectroscopy

Raman imaging was performed in a combined Raman-AFM-SNOM confocal microscope WITec alpha300 RAS+ (WITec, Ulm, Germany). A frequency-doubled Nd:YAG laser operating at 532 nm was used as an excitation source with the power of 15 mW at the sample. Raman imaging experiments were carried by raster-scanning the laser beam over the samples and accumulating fluorescence intensity signals over the Raman spectrum at each pixel. Raman images were built by integrating the fluorescence over specific Raman bands using WITec software for data evaluation and processing.

4.2.7 Contact angles

Contact angles were measured in an OCA20 of Data Physics Instruments goniometer (Data Physics, Filderstadt, Germany) equipped with a CCD camera using the sessile drop method and water, formamide, and diiodomethane as probe liquids, whose corresponding total surface energy and dispersive and polar components values are listed in Table 4.1.

Table 4.1- Polar and dispersive surface tension components of the liquid probes [24].

Liquid	Surface Tension (γ_L), mN/m	Dispersive component (γ_L^d), mN/m	Polar component (γ_L^p), mN/m
Water	72,8	21,8	51,0
Formamide	58,0	37,6	20,4
Diiodomethane	50,8	48,5	2,3

For each sample, 30 measurements were performed (10 measurements for each solvent used). The contact angle measurements were carried out at room temperature (21 ± 1 °C, RH 60%) and applying the drop volume of 1 µL with a velocity of deposition of 1 µL/s. Contact angles were measured as a function of time for 60 s and then extrapolated to zero time. The results of parallel measurements were averaged, and the standard deviation errors were evaluated. The obtained apparent contact angles (θ_{app}) were corrected (θ_0) for the surface topography using the Wenzel correction [25]:

$$cos\theta_{app} = rcos\theta_0 \quad (4.1)$$

where r is a rugosity factor defined as the ratio of true surface area (A) and the nominal area (A_{smooth}). The rugosity factor was calculated knowing the developed interfacial ratio (S_{dr}), $r = S_{dr}+1$. S_{dr} was obtained from 3D surface texture analysis using optical profilometry (according to ISO 25178).

The adhesion work (W_a) between a solid surface with a free surface energy of γs and a liquid with a surface tension of γ_L was elucidated as a function of a contact angle, θ, using the Young-Dupré equation for polymeric surfaces [26]:

$$W_a = \gamma_L(1 + cos\theta_0) \quad (4.2)$$

The evaluations of the free surface energy (FSE) of cork (γ_S) and its corresponding polar (γ_S^p) and dispersive (γ_S^d) components were performed using the series of liquid probes (Table 4.1) based on the Owens-Wendt-Rable-Kaeble (OWRK) model that satisfactorily describes the solid-liquid interfacial interactions in the air for the polymers [26] and lignocellulosic materials [27]:

$$\left(\frac{1+cos\,\theta}{2}\right)\left(\frac{\gamma_L}{\sqrt{\gamma_L^d}}\right) = \sqrt{\gamma_S^p} \times \sqrt{\frac{\gamma_L^p}{\gamma_L^d}} + \sqrt{\gamma_S^d} \tag{4.3}$$

where (γ_L), (γ_L^p), and (γ_L^d), represent the liquids superficial tension and the corresponding polar and dispersive components, respectively. Plotting $(1+cos\,\theta/2)\left(\gamma_L/\sqrt{\gamma_L^d}\right)$ *vs* $\left(\gamma_L^p/\gamma_L^d\right)^{1/2}$ allows the calculation of the parameters γ_S^d and γ_S^p. The free surface energy (FSE) comprises the polar and dispersive components $\left(\gamma_S = \gamma_S^p + \gamma_S^d\right)$, where the dispersion component (γ_S^d) correspond to London dispersion forces and the polar component (γ_S^p) refers mainly to hydrogen bonding.

4.2.8 Wetting envelope simulations

The wetting envelope is a tool that allows the visualization of the relationships between the polar and dispersive components of FSE with the surface wettability for different liquids. This simulation plot was built using the values of polar and dispersive components of FSE obtained for each sample analyzed. Wetting envelope uses two mathematical correlations, one dispersive (Equation 4.4) and another for polar component (Equation 4.5):

$$\gamma_L^d = R \times \cos\varphi \tag{4.4}$$

$$\gamma_L^p = R \times \sin\varphi \tag{4.5}$$

where R is a radial coordinate in the polar coordinate system and φ in an angular coordinate that varies between 0 and $\pi/2$ radians. These (γ_L^d) and (γ_L^p) from Equation 4.4 and Equation 4.5, respectively, were substituted in Equation 4.2 $\left(\gamma_L = \gamma_L^p + \gamma_L^d\right)$ and in Equation 4.6 from OWRK model.

$$W_a = 2\left(\sqrt{\gamma_s^d \times \gamma_L^d} + \sqrt{\gamma_s^p \times \gamma_L^p}\right) \tag{4.6}$$

Combining Equation 4.2 and Equation 4.6 and solving for the R as a function of φ and θ $(R(\varphi,\theta))$, the polar coordinates in the wetting envelope for the dispersion (x-coordinate) and polar (y-coordinate) coordinates (Equation 4.7 and Equation 4.8, respectively) can be presented as follows:

$$x = \gamma_L^d = \frac{4}{(1+cos\,\theta)^2}\left(\sqrt{\gamma_s^d}\cos\varphi + \sqrt{\gamma_s^p}\sin\varphi\right)^2 \cdot (\cos\varphi)^2 \tag{4.7}$$

$$y=\gamma_L^p=\frac{4}{(1+cos\,\theta)^2}\left(\sqrt{\gamma_s^d}\cos\varphi+\sqrt{\gamma_s^p}\sin\varphi\right)^2\cdot(\sin\varphi)^2 \quad (4.8)$$

To facilitate the understanding of the wettability characteristics of the samples, calculations were performed for four different θ angles: 0°, 45°, 60°, and 90°.

The wetting envelope allows relating the surface wetting curves to the polar and dispersive surface tension components of a specified liquid. Since the objective is to assess changes in the behavior of the cork stopper after reactive washing (RW), four solutions with different percentages of ethanol were selected to put on the wetting envelope (12%, 14%, 20%, and 40%), in order to evaluate the interfacial behavior of the cork surface towards different hydroalcoholic solutions. The polar and dispersive components for 12% and 14% solutions (Table 4.2), absent in the literature, were obtained by fitting to an exponential function (R^2=0.98) developed based on a known database [24,28].

Table 4.2- Polar and dispersive surface tension components of the ethanol solutions.

Solutions	**Surface tension (γ_L), mN/m**	**Dispersive component (γ_L^d), mN/m**	**Polar component (γ_L^p), mN/m**
EtOH/H_2O 12%	43.76	20.16	23.60
EtOH/H_2O 14%	42.38	20.08	22.30
EtOH/H_2O 20%	39.21	19.90	19.31
EtOH/H_2O 40%	33.05	19.55	13.50

4.3 Results and Discussion

4.3.1 Surface morphology and topology of a natural cork stopper

As revealed by scanning electron microscopy (SEM), the lateral and top of the untreated natural cork stopper showed a clear difference in terms of cork cells appearance (Figure 4.2). Thus, the lateral of the cork stopper shows the characteristic for radial direction alveolar structure, resembling a honeycomb, without intercellular space, in agreement with cell orientation on the cork layer (Figure 4.1). On the other hand, the top of the cork stopper exposes the cells as rectangles placed in parallel that correspond to the axial direction. Therefore, the lateral and the top part of the stoppers expose essentially the transverse and longitudinal sections of the cells, respectively. No significant differences were found in the SEM image analysis of the stoppers before and after the RW, though the stopper surface looks smoother after the RW (Figure B.1, Appendix B).

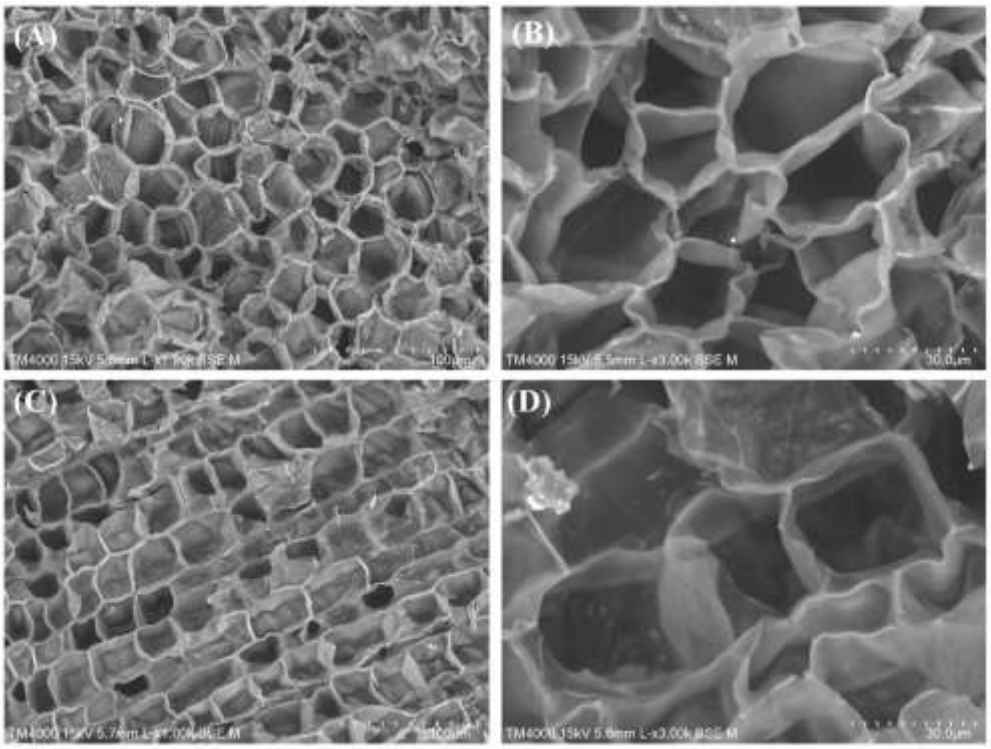

Figure 4.2- SEM micrograph images of the untreated cork stopper surface: the lateral at 800x (A) and at 3000x (B) magnification, and the top at 800x (C) and at 3000x (D) magnification.

It is noteworthy that on the lateral of the stoppers, the edges of the cell walls are crumped and the inner layers partially turned outward. Such a cell deformation is a result of punching/drilling of cork strips to obtain stoppers (Figure 4.1). Taken into attention the heterogeneity of the cell wall composition, this could affect the surface composition.

When compared the thickness of the cork cell wall with those of the xylem cells in oak (mainly libriforms), the former is almost five times inferior [29–31]. In addition, unlike libriforms, the areas rich in celluloses and suberin, but also by the rich in suberin inner layers of the cell wall partially turned outwards. At the same time, the top surface of the cork is exposed predominantly from the longitudinal section of the cell wall. In other words, the side and the top surfaces of the cork stoppers, which exhibit some different exposure to the layers of the cell wall, may have different surface properties.

The surface roughness of the lateral and top of the stoppers, given by the heigh parameter S_a, the arithmetical mean heigh of the surface, assessed by 3D optical profilometry, also revealed some differences. Thus, the lateral of the stoppers possessed *ca.* 30% less roughness when compared to the top surface (Table 4.3), where the parametric values of the maximum height of peaks (S_p) and valleys (S_v) are also included. Attention is drawn to the different nature of irregularities on the surface as revealed from the hybrid parameter S_{dr} data, the develop area ratio (Table 4.3), and the surface topology (Figure B.2, Appendix B): more slopping on the lateral and steeper on the top. This fact can be explained by the different nature of the cut of the cork surface at the top (with saw while cutting the strips) and on the lateral (with a hollow drill while punching the stoppers). After the RW, the surface roughness decreases, which is especially noticeable on the top of the stoppers (Table, Figure S2). This feature can probably be explained by a change in the composition of the cell wall, making it softer after treatment and shrinking after drying.

Table 4.3- Roughness parameters of the lateral and top surfaces of the natural cork stopper before and after RW as revealed by 3D optical profilometry according to ISO 25178.

Stopper sample	Lateral (μm)				Top (μm)			
	S_a	S_p	S_v	S_{dr}	S_a	S_p	S_v	S_{dr}
Before the RW	10.2 ±0.6	78.2 ±8.8	80.8 ±17.1	0.397 ±0.153	13.2 ±0.8	66.3 ±9.2	71.9 ±9.2	0.640 ±0.052
After the RW	10.6 ±0.5	55.8 ±2.6	80.3 ±6.6	0.209 ±0.073	11.1 ±0.9	59.3 ±11.6	77.2 ±7.1	0.098 ±0.067

4.3.2 Surface chemistry

The analysis of the cork surface elemental composition by energy-dispersive X-ray spectroscopy (EDS) revealed the major contribution of carbon (*ca*. 52%) and oxygen (*ca*. 42%) with a still noticeable amount of calcium (*ca.* 6%). The last is a part of inorganic and organic salts in the composition of cork. In particular, calcium oxalate is the most abundant organic salt presenting in the cork [32]. Some cork cells revealed the visible crystals of salts, which are silicates and inorganic and organic calcium salts according to the SEM-EDS analysis (Figure B.3, Appendix B).

The chemical composition of the stopper´s surface was assessed by FTIR-ATR spectroscopy, which showed similar features for the lateral and top (Figure 4.3). This can be explained by the relatively small depth (1-2 μm) of the analysis that allowed the assessment essentially the external cell wall sections. Hence, FTIR-ATR spectra reflect the presence of suberin, lignin, and polysaccharides (cellulose and hemicelluloses) occurring in the cell wall.

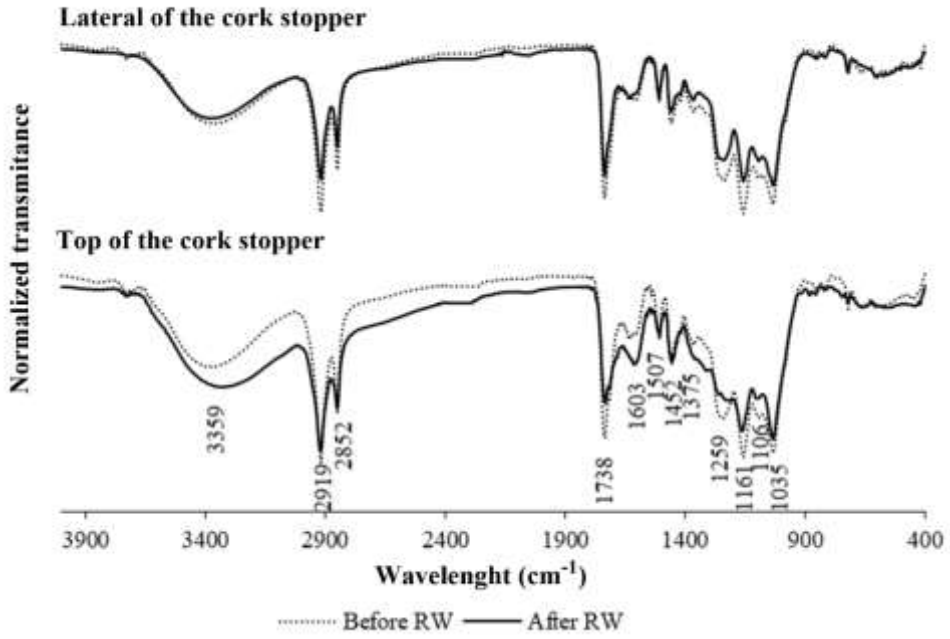

Figure 4.3- FTIR-ATR spectra of the lateral and top of the cork stopper before and after RW.

The noticeable differences were found in the surface composition of the lateral and top of the cork stopper before and after RW (Figure 4.3). The band at 3359 cm^{-1} is assigned to O-H stretching, the bands at 2919 and 2852 cm^{-1} to the asymmetric and symmetric stretching vibrations, respectively, of C-H bonds in CH_2 aliphatic structures, and the band at 1738 cm^{-1} is assigned to the stretching vibration of C=O bond in ester groups essentially from suberin [16,17,33]. The bands at 1603 (aromatic) and 1507 cm^{-1} relate to stretching vibrations of C=C bond in the aromatic ring of lignin, the bands at 1452 and 1375 cm^{-1} correspond to asymmetric and symmetric stretching vibrations of C-H bonds, respectively, the bands at 1259 and 1161 cm^{-1} represent the stretching vibrations of C-O bonds in esters and ethers, respectively. The bands at 1106 and 1035 cm^{-1} are assigned to stretching of C-OH and bending of C-H, respectively, mainly from polysaccharides and lignin [33].

The substantial decrease in the intensity of bands at 2919/2852 cm^{-1}, 1738, and 1259 cm^{-1} (Figure 4.3) indicates the eventual degradation of suberin as a result of the ester linkages saponification during RW carried out at high pH. On the other hand, the relative intensity of characteristic lignin signals at 1603/1507 cm^{-1} did not change significantly after RW. The inverse in

relative intensity of the signals at 1161 and 1035 cm^{-1} before and after the RW indicate the cleavage of some ether linkages with the formation of new OH groups [34]. The last fact is also confirmed by the relative increase of the band at 3359 cm^{-1} after RW. These cleaved ether bonds could belong to both suberin and lignin.

As the RW involved strong concentrations of hydrogen peroxide (35%,w/w) and NaOH (9%, w/w), both oxidative and hydrolytic mechanisms for the ether linkages cleavage could be proposed. It should be noted that the T_{2919}/T_{3359} ratio of the lateral was always higher than the top of both treated and untreated stoppers (Figure 4.3). This fact indicates higher exposure of suberin in the lateral than in the top of the stoppers in agreement with the SEM observations regarding the deformation of cell walls mentioned above.

Additionally, information for changes in the surface of the cork during RW was obtained using confocal Raman spectroscopy. The strong fluorescence of the cork material, due to the presence of a high concentration of lignin, tannins, and suberin, did not allow the acquisition of high-quality Raman spectra. To confirm this information, it was analyzed the fluorescence intensities of pure suberin, and lignin isolated from the cork material in the range of 200-4000 cm^{-1} (Figure 4.4).

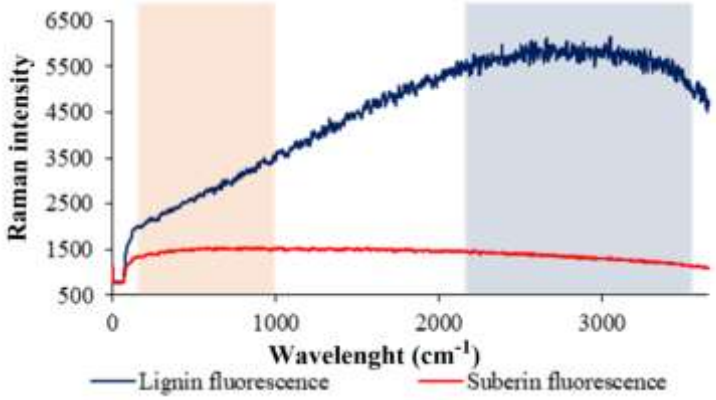

Figure 4.4- Raman fluorescence background obtained with @ 532 nm laser for lignin and suberin isolated from natural cork stoppers.

Thus, it was verified that both components contribute to the fluorescence of the sample, even though the fluorescence of suberin was much lower than that of lignin. Suberin had the highest fluorescence intensity at 250-1000 cm^{-1}, while lignin had the highest intensities at 2250-3500 cm^{-1}. Therefore, in the Raman imaging analysis of the cork stopper, the mapping was carried out to combine the images of fluorescence integral intensity from suberin acquired at 250-1000 cm^{-1} (red color) and from lignin at 2250-3500 cm^{-1} (blue color).

Thus, the Raman image (Figure 4.5) shows three different colors: blue for lignin, red for suberin, and pink that corresponds to the areas where lignin and suberin are combining. The small pink areas spread through the image strongly suggest that lignin and suberin are covalently linked in the cell

wall, probably by esterification of ferulates and hydroxyl groups of suberin monomers [35]. The image also shows that lignin is mainly deposited in the middle lamella and suberin is more abundant in the inner layers of the cell wall (Figure 4.5A). It should be noted that it was not possible to obtain high-quality images for the lateral of the cork stoppers due to the increased curvature of the surface, the intrinsic properties of cork in this area, and a relatively high mechanical damage to the cell walls that occurred during drilling.

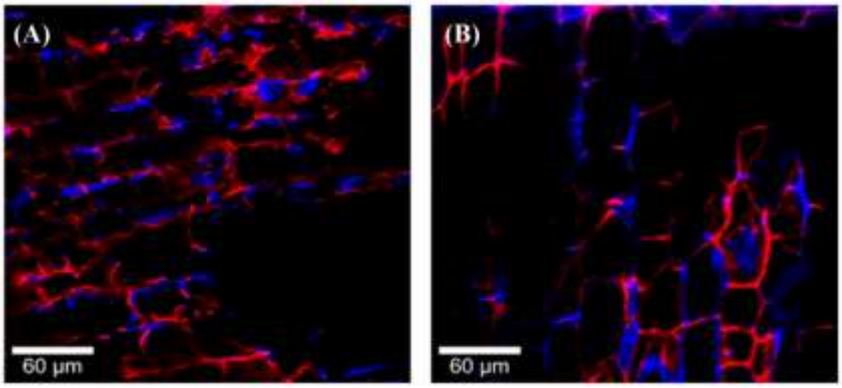

Figure 4.5- Confocal Raman images obtained by the combination of specific fluorescence zones from the lignin (blue color) and suberin (red color) on the top of the natural cork stopper before (A) and after (B) RW using @ 532 laser.

After reactive washing (Figure 4.5B), the color intensity of the Raman image decreases due to the greater crushing of the cell walls and the degradation of the structural polymers. However, there was a noticeable decrease in red and an increase in shades of blue and pink, thus confirming the detrimental effect of RW on suberin already pointed out by FTIR-ATR analysis.

4.3.3 Surface wettability

The measurement of contact angles with solvents of different polarities is one of the tools for the evaluation of free cork surface tension (γ_S), which is a key characteristic to predict its wettability [36]. Following this approach, the contact angles with three liquid probes of known surface tension (water, formamide, and diiodomethane) were measured for the lateral and top of the cork stoppers (Table 4.4). The evaluated FSE values with corresponding dispersion and polar counterparts (Figure 4.6) revealed cork stoppers as a material with a fairly low-energy surface similar to such hydrophobic polymers as polyethylene or polytetrafluoroethylene [36–39]. This feature is assigned primarily to the highly suberized cork cell walls poorly contributing to the polar component of FSE [36].

Table 4.4- Contact angles of the top and lateral surfaces of the cork stopper with water, formamide and diiodomethane.

Liquid probe	Measured contact angle (deg.)			
	Top of the cork stopper (TCS)		Lateral of the cork stopper (LCS)	
	Before the RW	After the RW	Before the RW	After the RW
Water	99.2±5.6	91.0±5.6	136.0±3.2	90.9±2.3
Formamide	101.2±5.2	99.3±3.1	115.1±5.0	90.0±5.3
Diiodomethane	77.7±5.0	76.0±5.2	81.3±6.2	76.0±2.3

The analysis of contact angles with liquid probes (Table 4.4) and the surface polarity index (γ_S^p/γ_S) showed a significant difference between the lateral and top of the stoppers (Figure 4.6). For instance, the top surface revealed a lower FSE (16.0 *vs.* 20.5 mN/m) and a higher polarity index (0.193 *vs.* 0.107) than the lateral one (Figure 4.6). Simultaneously, the contact angle with water was much lower on the top (99.2º) than on the lateral side (136.0º), which corresponds to a triple adhesion work (61.2 against 20.4 mN/m). These features must relate to the peculiarities in the composition of the surface of cork stoppers discussed above when the lateral surface exposes stronger the suberin-rich cell wall layers and less the cell wall section containing the polysaccharides.

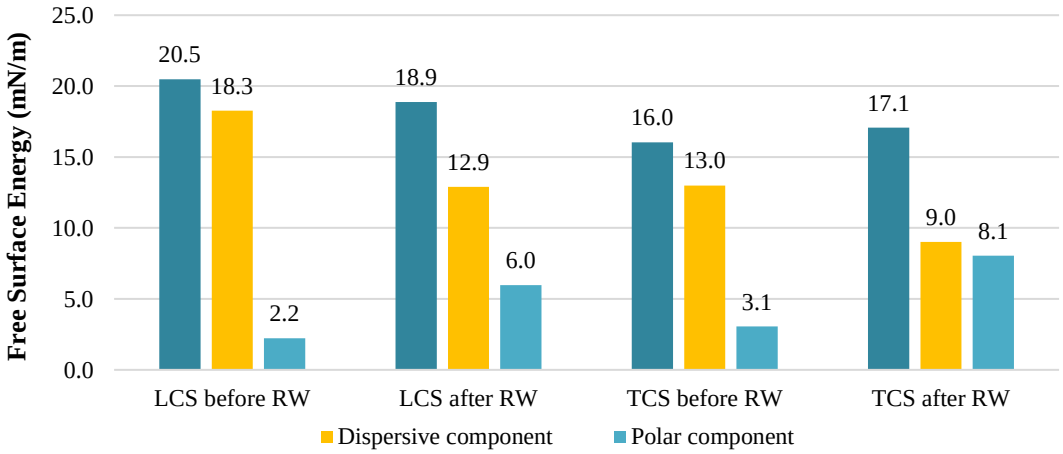

Figure 4.6- Contribution of polar and dispersive components to the total free surface energy of the lateral (LCS) and top (TCS) of the cork stopper before and after the RW.

The treatment of cork stoppers during RW changed remarkably its surface properties (Figure 4.6). Thus, the FSE of the top surface is slightly increased (from 16.0 to 17.1 mN/m) and the FSE of the lateral surface decreased (from 20.5 to 18.9 mN/m) with significant ricing of the polarity index from 0.193 to 0.474 for the top and from 0.107 to 0.317 for the lateral. Accordingly, the contact angles with the water fell both on top and on the lateral to similar values of nearly 91º, showing an improved affinity for aqueous solutions (Table 4.4). This improvement in surface wettability of the stoppers was assigned to the partial suberin degradation and enhanced exposure of hydrophilic cell wall components (e.g. cellulose and hemicelluloses) after the RW. It could be anticipated that the observed surface changes would alter the receipt of hydrophobic coating formulations and the stopper

sealing performance. The latter is particularly sensitive to capillary suction and surface wicking promoted by increased surface wettability.

In order to evaluate the critical effect of RW on the surface properties of cork stoppers under moistening with hydroalcoholic solutions mimicking alcoholic beverages, interaction models were carried out using a wetting envelope in polar-dispersive energy coordinates (Figure 4.7).

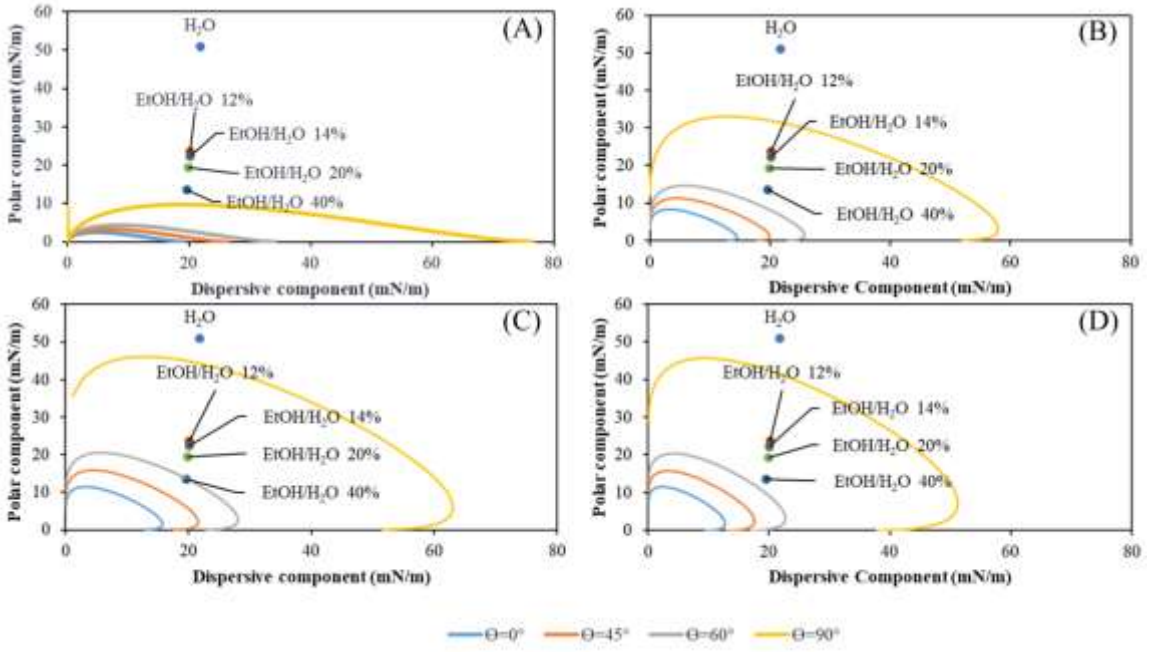

Figure 4.7- Wetting envelope of the lateral (A) and top (B) of the cork stopper surface before the RW and of the lateral (C) and top (D) of the cork stopper after the RW.

Such an approach allows reliable prediction of the interfacial behavior between the surface of various materials and liquids [40,41]. The simulations were done for the contact angles of 0, 45, 60, and 90º covering all the range of surface wetting, from completely wettable (0º) to non-wettable (90º). The wetting envelop area inside or outside the corresponding curves (e.g. 90°) represents contact angles below or higher than the simulated value, respectively. The lateral surface of cork stoppers is non-wettable with either water or with the examined hydroalcoholic solutions (12-40% ethanol v/v), while the top of stoppers is non-wettable only with water and the limited wetting occurred with hydroalcoholic solutions (contact angles of 60-90º). The wettability of cork stoppers increased gradually with the increase in the concentration of ethanol in the solution. The highest wettability was observed with the alcoholic solution containing 40% of ethanol (Figure 4.7).

The noticeable changes in cork stopper surface wettability were observed after the RW. Both the lateral and top surfaces became wettable withal examined hydroalcoholic solutions (Figure 4.7). In particular, the wettability of the lateral side of the stoppers inversed from non-wettable to wettable

after the RW, being the most critical for the high percentage ethanol solutions. This fact is explained by the increased FSE polar component of the cork being treated with aggressive chemical reagents (Figure 4.6). At the same time, the cork surface still maintained its hydrophobic nature, being non-wettable by water ($\theta > 90°$). It is worth mentioning that the wetting with hydroalcoholic solutions of the top surface of the cork stopper did not change as much after the RW, as was observed for the lateral surface (Figure 4.7). This can be explained by the increase in the polar component of the cork FSE after the RW (Figure 4.6) while the polar component of the surface tension in the hydroalcoholic solution gradually decreases with the increase in the concentration of the ethanol (Table 4.2). Hence, the wettability of the treated cork stopper with alcoholic solutions is not necessary declined straightforwardly with the increase of the polar component of the FSE. All depends on the balance between the polar and dispersion components of the FSE and its value. For instance, the relatively low FSE (17.1 mN/m) and high polarity index (0.474) of the top surface of treated stoppers allowed less wettability with hydroalcoholic solutions than the lateral possessing higher FSE (18.9 mN/m) and lower polarity index (0.317), as revealed by the wetting envelope simulations (Figure 4.7).

The increase in wettability of the cork stopper with hydroalcoholic solutions after the RW is indicative of the additional measures necessary to maintain its sealing capacity in the bottling of alcoholic beverages. This can be done by modifying the surface with different hydrophobizing agents (e.g food-grade paraffin) and polymeric formulations allowed in the industry. However, the efficiency of these surface modifications is also strongly dependent on the surface properties of cork stoppers [16,17] and must be considered.

4.4 Conclusions

This chapter envisages the anisotropy in the surface properties of the top and lateral of natural cork stoppers, resulting from the difference in the exposure of the cork cell wall layers and as a result of mechanical damage that occurred during the stopper production.

Image and surface chemical analyses revealed a greater exposure of the internal suberin-rich cell wall layers on the lateral than on top of the stoppers. At least partially, this is a result of the cork cell wall crumpling during the punching of the stoppers from strips. In addition, the lateral of the stoppers had *ca.* 30% less roughness compared to the top surface. These differences in the surface chemical composition and topology explain the higher polarity index of the top surface that predetermines its better wettability with water and hydroalcoholic solutions than the lateral surface of the stopper.

Reactive washing, being an aggressive treatment with hydrogen peroxide under strong alkaline conditions, impairs the surface properties of the cork stoppers regarding their wettability. The main changes occur due to the significant degradation of suberin on the cork surface. Consequently, the surface polarity index increases substantially due to the stronger exposure of the hydrophilic moieties of the degraded suberin and the more accessible hydrophilic structural polymers, such as polysaccharides. This leads to an increase in the wettability of cork stoppers, especially their lateral surfaces, which have turned from non-wettable to wettable with hydroalcoholic solutions after reactive washing. This is related to the balance of polar and dispersive components of the free surface energy and its absolute value. Indeed, the appropriate set of surface parameters, such as free surface energy value and the polarity index, can be inferred to achieve an acceptable wetting behavior for the cork stopper with certain solutions, according to simulations based on the Owens-Wendt-Rabel-Kaelble model.

The results in this chapter provide the fundamentals for the targeted modification of the cork stopper towards controlled wettability, also regarding the improvement of reactive washing operations and strategies of the surface coating.

4.5 References

[1] S.P. Silva, M.A. Sabino, E.M. Fernandes, V.M. Correlo, L.F. Boesel, R.L. Reis, Cork: properties, capabilities and applications, Int. Mater. Rev. 50 (2005) 345–365. https://doi.org/10.1179/174328005X41168.

[2] A. Costa, H. Pereira, A. Oliveira, Variability of radial growth in cork oak adult trees under cork production, For. Ecol. Manage. 175 (2003) 239–246. https://doi.org/10.1016/S0378-1127(02)00145-7.

[3] A. Caritat, M. Molinas, E. Gutierrez, Annual cork-ring width variability of *Quercus suber* L. in relation to temperature and precipitation (Extremadura, southwestern Spain), For. Ecol. Manage. 86 (1996) 113–120. https://doi.org/10.1016/S0378-1127(96)03787-5.

[4] J.F. Mano, Creep-recovery behaviour of cork, Mater. Lett. 61 (2007) 2473–2477. https://doi.org/10.1016/j.matlet.2006.03.157.

[5] M.A. Fortes, M. Emília Rosa, H. Pereira, The cellular structure of cork from *Quercus Suber* L., IAWA J. 8 (1987) 213–218. https://doi.org/10.1163/22941932-90001048.

[6] H. Pereira, Cork : Biology, production and uses, First edit, Elsevier B.V., 2007.

[7] H. Pereira, Variability of the chemical composition of cork, BioResources. 8 (2013) 2246–2256. https://doi.org/10.15376/biores.8.2.2246-2256.

[8] H. Pereira, Chemical composition and variability of cork from *Quercus suber* L., Wood Sci. Technol. 22 (1988) 211–218. https://doi.org/10.1007/BF00386015.

[9] E. Conde, E. Cadahía, M.C. García-Vallejo, J.R. González-Adrados, Chemical characterization of reproduction cork from spanish *Quercus suber*, J. Wood Chem. Technol. 18 (1998) 447–469. https://doi.org/10.1080/02773819809349592.

[10] L.J. Gibson, K.E. Easterling, M.F. Ashby, The structure and mechanics of cork, Proc. R. Soc. London A. (1981) 99–117. https://doi.org/doi:10.1086/303379.

[11] H. Pereira, E. Ferreira, Scanning electron microscopy observations of insulation cork agglomerates, Mater. Sci. Eng. A. 111 (1989) 217–225. https://doi.org/10.1016/0921-5093(89)90215-3.

[12] L.J. Gibson, Biomechanics of cellular solids., J. Biomech. 38 (2005) 377–99. https://doi.org/10.1016/j.jbiomech.2004.09.027.

[13] A.J.D. Silvestre, C.P. Neto, A. Gandini, Cork and suberins: Major sources, properties and applications, in: Monomers, Polym. Compos. from Renew. Resour., 2008: pp. 305–320. https://doi.org/10.1016/B978-0-08-045316-3.00014-4.

[14] M.A. Bernards, Demystifying suberin, Can. J. Bot. 80 (2002) 227–240. https://doi.org/10.1139/b02-017.

[15] A. V. Marques, H. Pereira, On the determination of suberin and other structural components in cork from *Quercus suber* L., An. Do Inst. Super. Agron. 42 (1987) 321–335.

[16] J.R. Gonzalez-Adrados, M.C. Garcia-Vallejo, M.J. Caceres-Esteban, J.L. Garcia De Ceca, F. Gonzalez-Hernandez, R. Calvo-Haro, Control by ATR-FTIR of surface treatment of cork stoppers and its effect on their mechanical performance, Wood Sci. Technol. 46 (2012) 349–360. https://doi.org/10.1007/s00226-011-0403-5.

[17] C. Ortega-Fernández, J.R. González-Adrados, M.C. García-Vallejo, R. Calvo-Haro, M.J. Cáceres-Esteban, Characterization of surface treatments of cork stoppers by FTIR-ATR, J. Agric. Food Chem. 54 (2006) 4932–4936. https://doi.org/10.1021/jf0529823.

[18] J. Abenojar, A.Q. Barbosa, Y. Ballesteros, J.C. del Real, L.F.M. da Silva, M.A. Martinez, Effect of surface treatments on natural cork: surface energy, adhesion, and acoustic insulation, Wood Sci. Technol. 48 (2014) 207–224. https://doi.org/10.1007/s00226-013-0599-7.

[19] J. Abenojar, S. López de Armentia, A.Q. Barbosa, M.A. Martínez, F. Velasco, L.F.M. da Silva, J.C. del Real Romero, Coating cork particles with iron oxide: effect on magnetic properties, Wood Sci. Technol. 54 (2020) 869–889. https://doi.org/10.1007/s00226-020-01191-4.

[20] F. Ben Abdallah, R. Ben Cheikh, M. Baklouti, Z. Denchev, A.M. Cunha, Effect of surface treatment in cork reinforced composites, J. Polym. Res. 17 (2010) 519–528. https://doi.org/10.1007/s10965-009-9339-y.

[21] C. Vilela, A.F. Sousa, C.S.R. Freire, A.J.D. Silvestre, C.P. Neto, Novel sustainable composites prepared from cork residues and biopolymers, Biomass and Bioenergy. 55 (2013) 148–155. https://doi.org/10.1016/j.biombioe.2013.01.029.

[22] T.-T.A. of the P. and P. Industry., TAPPI test methods T 204 om-88: solvent extractives of wood and pulp., (1996). https://doi.org/10.5772/916.

[23] D. V. Evtuguin, C.P. Neto, A.M.S. Silva, P.M. Domingues, F.M.L. Amado, D. Robert, O. Faix, Comprehensive study on the chemical structure of dioxane lignin from plantation *Eucalyptus globulus* wood, J. Agric. Food Chem. 49 (2001) 4252–4261. https://doi.org/10.1021/jf010315d.

[24] A.B. Figueiredo, D. V. Evtuguin, J. Monteiro, E.F. Cardoso, P.C. Mena, P. Cruz, Structure-surface property relationships of kraft papers: Implication on impregnation with phenol-formaldehyde resin, Ind. Eng. Chem. Res. 50 (2011) 2883–2890. https://doi.org/10.1021/ie101912h.

[25] J.C. Berg, Semi-empirical strategies for predicting adhesion, Elsevier B.V., 2002. https://doi.org/10.1016/b978-044451140-9/50001-9.

[26] D.K. Owens, R.C. Wendt, Estimation of the surface free energy of polymers, J. Appl. Polym.

Sci. 13 (1969) 1741–1747. https://doi.org/10.1002/app.1969.070130815.

[27] T. Nguyen, W.E. Johns, Polar and dispersion force contributions to the total surface free energy of wood, Wood Sci. Technol. 12 (1978) 63–74.

[28] B. Jańczuk, E. Chibowski, W. Wójcik, The influence of n-alcohols on the wettability of hydrophobic solids, Powder Technol. 45 (1985) 1–6. https://doi.org/10.1016/0032-5910(85)85053-1.

[29] D. Fengel, G. Wegener, Wood-chemistry, ultrastructure, reactions, Berlin, 1984. https://doi.org/10.1007/BF02608943.

[30] R.T. Teixeira, H. Pereira, Suberized cell walls of cork from cork oak differ from other species, Microsc. Microanal. 16 (2010) 569–575. https://doi.org/10.1017/S1431927610093839.

[31] H. Pereira, The rationale behind cork properties: A review of structure and chemistry, BioResources. 10 (2015) 1–23. https://doi.org/10.15376/biores.10.3.Pereira.

[32] F. Carvalho, M.L. Bastos, M.A. Remião, Determination of Oxalates in Cork Stoppers by HPLC with Electrochemical Detection, Am. J. Enol. Vitic. 46 (1995) 63–66.

[33] D.G. Branco, J.R. Campos, L. Cabrita, D. V. Evtuguin, Structural features of macromolecular components of cork from *Quercus suber* L., Holzforschung. 74 (2020) 625–633. https://doi.org/10.1515/hf-2019-0271.

[34] S. Omori, C.W. Dence, The reactions of alkaline hydrogen peroxide with lignin model dimers. Part 2. Guaiacylglycerol-b-Guaiacyl ether, Wood Sci. Technol. 15 (1981) 113–123. https://doi.org/https://doi.org/10.1007/BF00367858.

[35] R.G. Riley, P.E. Kolattukudy, Evidence for Covalently Attached p -Coumaric Acid and Ferulic Acid in Cutins and Suberins , Plant Physiol. 56 (1975) 650–654. https://doi.org/10.1104/pp.56.5.650.

[36] C.M.C.P.S. Gomes, A.C. Fernandes, B. de J.V.S. de Almeida, The surface tension of cork from contact angle measurements, J. Colloid Interface Sci. 156 (1993) 195–201. https://doi.org/10.1006/jcis.1993.1099.

[37] D. Bonn, J. Eggers, J. Indekeu, J. Meunier, Wetting and spreading, Rev. Mod. Phys. 81 (2009) 739–805. https://doi.org/10.1103/RevModPhys.81.739.

[38] M. Żenkiewicz, Methods for the calculation of surface free energy of solids, J. Achiev. Mater. Manuf. Eng. 24 (2007) 137–145.

[39] H. Kaelble, K.C. Uy, A Reinterpretation of Organic Surface Interactions, J. Adhes. 2 (1970) 50–60. http://dx.doi.org/10.1080/0021846708544579.

[40] S. Magina, J. Ferra, P. Cruz, H.I.S. Nogueira, I. Portugal, D. V. Evtuguin, Fluorinated polyhedral oligomeric silsesquioxane nanoparticles to boost the dirt repellence of high pressure laminates, Chem. Eng. J. 301 (2016) 362–370.

https://doi.org/10.1016/j.cej.2016.05.028.

[41] E. Neto, S. Magina, A. Camões, A. Begonha, D. V. Evtuguin, P. Cachim, Characterization of concrete surface in relation to graffiti protection coatings, Constr. Build. Mater. 102 (2016) 435–444. https://doi.org/10.1016/j.conbuildmat.2015.11.012.

Chapter 5

OPTIMIZATION OF REACTIVE WASHING OF NATURAL CORK STOPPERS EMPLOYING FRACTIONAL FACTORIAL DESIGN

This chapter was submitted as:

D.G. Branco, C.A. Santiago, L. Cabrita, D. V Evtuguin, Optimization of reactive washing of cork stoppers employing fractional factorial design

Content

5.1. Introduction

In the transformation process of the oak outer bark into the natural cork stoppers, this material must pass through several industrial steps, where the reactive washing (RW) plays a key role in disinfection, surface purification, and appearance (color homogeneity and brightness) of the final product. RW commonly consists in the treatment of stoppers with hydrogen peroxide (H_2O_2) under strong alkaline conditions and increased temperature [1,2].

Hydrogen peroxide evokes the disinfection and degradation of the chromophore structures on the surface of the cork with an increase in its brightness. The excess of reagents (H_2O_2 and NaOH) is washed away by sequential treatment with sodium bisulfate solution to neutralize alkalinity and with water. All reagents are of high-grade quality according to food safety requirements, whose costs are remarkably superior to corresponding ordinary quality technical products. Quite efficient and cost-effective chlorine-based reagents have been exempt from the practice of RW due to the formation of harmful chloro-organic derivatives, besides causing unpleasant odors and corrupting the flavor of the drinks with which they are in contact [2–4].

The active specie in cork stoppers´ bleaching, hydroperoxide anion (HO_2^-), is formed only under strong alkaline conditions (pH>11) [5]. At the same time, hydrogen peroxide and sodium hydroxide solutions form a relatively harsh reaction system towards main macromolecular cork components [6]. This leads to significant changes in surface properties of cork stoppers making them more hydrophilic that in turn affects negatively their subsequent receptivity towards various coatings, such as food-grade paraffin and silicon emulsions [6,7]. This coating with paraffin and silicon is essential to control the impermeability, sealing, and extraction properties of cork stoppers [7,8]. Thus, the overload of RW reagents is prejudicial not only for economic reasons but also negatively affects the consumption properties of cork stoppers.

Depending on the required final stopper brightness, different profiles of reagent addition are adjusted, and the process is evaluated through the measure of the final ISO brightness or L*a*b coordinates. Accordingly, the efficiency of the RW process must be tuned to achieve the lowest reagents consumption without compromise the cork stoppers final brightness. The optimization of the reagents profile along RW can be carried out while employing the experimental design techniques allowing the process analysis and modeling. The expected results contribute to a better understanding of the process variables and to reduction of its overall costs [9,10].

The response surface methodology (RSM) is a combination of mathematical and statistical approaches for experimental designs based on the adjustment of a polynomial equation to the experimental data, thus allowing the evaluation of the different factor' effects and seeking the optimal conditions for the desired process [9–12]. For example, if each factor has three levels to analyze and

for the four independent variables, the number of practical tests corresponds to 3^4 (or 81) experiments, which can be very time and labor-consuming. In this way, instead of applying a full factorial design experiment, a three-level and four-factor fractional factorial design can be employed. A fractional factorial design requires fewer experiments than the full factorial and still allows the analysis of the effects of each process variable at different levels as well as their interactions [13,14].

In the case of the RW process in study, before applying RSM, a well-designed experimental test program is required to determine the response of each factor, namely the hydrogen peroxide and sodium hydroxide concentrations, process time, and washing water volume applied.

The main objective of this study was to analyze the effect of operational variables, such as concentrations of hydrogen peroxide and sodium hydroxide, process time and volume of washing water applied, on the ISO brightness of the cork stopper surface and to evaluate how these interactions between different variables affect the response of interest. To achieve this goal, the RSM approach was used with a fractional factorial design of three levels and four factors that allowed the optimized process parameters to reach a defined ISO brightness target.

5.2. Materials and methods

Natural cork stoppers were supplied by Amorim Cork, S.A. (Santa Maria de Lamas, Portugal). The stoppers were from the same batch, *i.e.*, originated from the same industrial processing preceding RW, which reduces the variability of the stopper process before washing. Cork stoppers have a single caliber of 49x24 mm (length x diameter) and belong to the 1st class (middle class). Hydrogen peroxide (35%, w/w), sodium hydroxide (9%, w/w), and sodium bisulfate (2.5%, w/w), all of which are food grade and currently used in industry, were also supplied by the company Amorim Cork S.A. (Santa Maria de Lamas, Portugal).

5.2.1. Reactive washing (RW) process in laboratory scale

The reactive washing process was carried out on a laboratory rotation glass reactor (100 rpm) under controlled temperature (50 ℃). In a typical trial, the reagents ($NaOH + H_2O_2$) were added to the reactor containing 10 natural cork stoppers following the sequence and the timesheet protocol used in the industry, respecting the reagent-to-stopper ratio. In the sequence, firstly is added sodium hydroxide (3 mL), then hydrogen peroxide (5 mL), and at last is added 0.5 mL of distilled water. After 5 minutes of the reagents enter in contact with the stopper surface, they are removed to avoid cork swelling [2].

After the oxidation step that has a duration of 33 min, the stoppers were washed with distilled water. Sodium bisulfate solution (10 mL) was added further to neutralize the surface of the stoppers, which were washed again with distilled water (150 mL). The treated stoppers were dried in a ventilated oven at 40℃ for one hour. Afterward, the cork stoppers were allowed to stabilize for 24 hours before the evaluation of ISO brightness.

5.2.2. ISO brightness measurement

Brightness is the key parameter to evaluate the efficiency of reactive washing thus reflecting the stopper appearance. The ISO brightness corresponds to a numerical value of diffuse reflectance (% ISO) with respect to blue light of wavelength 457 nm. A similar process is also commonly used in the pulp and paper industry, according to norm Tappi T 525 om-06. The analysis was performed on the Konica Minolta cm700-d portable spectrophotometer (Konica Minolta; Tokyo, Japan) and was adapted from the internal procedure used in the company Amorim Cork S.A.

In general terms, all 10 stoppers used in the assays were evaluated through ISO brightness analysis, performing three random measurements on the top and the lateral surfaces. In this way,

each stopper ISO brightness value corresponds to the average of six measurements. The final ISO brightness assigned to each test is the ISO brightness mean value of the 10 stoppers used.

5.2.3. Response Surface Methodology (RSM)

The first task to apply the response surface methodology (RSM) is to establish the levels for each variable under study (hydrogen peroxide and sodium hydroxide concentrations, oxidation time, and water volume). To complete this task, a series of tests were carried out using the time one-factor-at-a-time methodology (OFAT). These pre-experimental tests provided information about the influence of each factor in the RW process through the ISO brightness obtained for each test. These assays are not shown in this chapter being not the main objective of this study. Although this methodology gives helpful information about the process, it does not consider the possibility of interactions between factors. Thus, the effect of different operating parameters on the reactive washing process was evaluated using a three-level four-factor fractional factorial experimental design approach [9,10,15,16]. The RW process variables (A, B, C, D) with their coded and actual levels are presented in Table 5.1.

Table 5.1- RW process variables and respective coded and actual levels.

Variables	Coded variables	Units	Type of variable	Real values of coded levels		
				-1	0	1
Hydrogen peroxide concentration	A	% (w/w)	Discrete	20	25	35
Sodium hydroxide concentration	B	% (w/w)	Discrete	5	7	9
Oxidation time	C	min	Discrete	20	25	33
Washing water volume	D	ml/10 stoppers	Discrete	100	125	150

-1: factor at low level; 0: factor at medium level; +1: factor at high level

Each coded variable (A, B, C and D) in study is associated with one of the process variables, as hydrogen peroxide concentration (%, w/w), sodium hydroxide concentration (%, w/w), oxidation time (min) and washing water volume (ml/10 stoppers), respectively. All the variables are discrete, which means that the variable has measurable characteristics, is either finite or countably infinite [9].

The actual values used for each variable correspond to the combination of all the higher levels assigned for each factor. This experimental design resulted in 25 assays with three replicates. These replications are essential to understand the process variability [17].

The experimental results were fitted to a second-order polynomial (Equation 5.1). The model characterizes the effects of process variables (A, B, C, and D) and their interactions on the response variable Y (ISO brightness).

$$Y = b_0 + b_1A + b_2B + b_3C + b_4D + b_{12}AB + b_{13}AC + b_{14}AD + b_{23}BC + b_{24}BD + b_{34}CD + b_{11}A^2 + b_{22}B^2 + b_{33}C^2 + b_{44}D^2 \quad (5.1)$$

where, Y is the predicted response, b_0 is model constant; b_1, b_2 b_3 and b_4 are linear coefficients; b_{12}, b_{13}, b_{14}, b_{23}, b_{24} and $b_{34}$are cross product coefficients and b_{11}, b_{22}, b_{33} and b_{44} are the quadratic coefficients. Statistical Stat-Ease *Design Expert* 11.0.5.0 software (Stat-Ease Inc., Minneapolis, MN, USA) was used to establish the validity of the models based on analysis of variance (ANOVA) and coefficient of determination (R^2).

5.3. Results and Discussion

5.3.1. The model equations and statistical evaluation

The effects of four process variables (hydrogen peroxide and sodium hydroxide concentrations, oxidation time, and water volume) of the reactive washing on the ISO brightness were evaluated using an experimental design of 3^4 fractional factorial experimental with three replications and the ANOVA analysis.

Table 5.2 shows the total of 25 tests generated randomly that were carried out during the experimental study, as well as the actual ISO brightness values obtained in each assay performed and response values predicted via *Design Expert* version 11.0.5.0 software. The tests include two replications for run 6 and one replication for run 5.

Table 5.2- Three-level and four-factor fractional factorial experimental design and associated response (actual and predicted ISO brightness (%)).

Run	A	B	C	D	ISO Brightness (%)[a]	
					Actual	Predicted
1	35	9	20	150	33.49	33.86
2	25	7	33	125	33.77	33.79
3	35	9	20	100	33.89	33.66
4	20	9	20	150	32.22	31.84
5	25	7	25	150	33.19	33.51
6	25	9	25	100	32.86	32.59
7	20	5	20	150	32.16	31.99
8	35	7	25	100	34.67	34.68
9	25	5	20	100	33.92	34.08
10	20	9	33	150	32.95	32.99
11	25	9	25	100	32.86	32.59
12	25	7	33	150	34.07	33.95
13	35	5	25	125	35.50	35.31
14	20	7	20	100	31.42	31.60
15	35	5	33	150	34.56	34.80
16	35	9	33	150	33.87	33.54
17	20	5	33	150	33.27	33.34
18	35	7	25	150	34.50	34.28
19	20	9	25	150	31.93	32.30
20	25	7	25	150	33.69	33.51
21	35	9	20	125	33.58	33.65
22	35	9	33	100	32.97	33.26
23	20	5	33	100	33.86	33.65
24	25	9	25	100	32.24	32.59
25	20	5	25	125	32.50	32.60

[a]The relative error in brightness determination was within 5%.

The predicted ISO brightness (Table 5.2) ranged from 31.60 to 35.31% depending on the combination of process parameters, while the actual ISO brightness has its minimum at 31.42% (run 14) and its maximum at 35.50% (run 13), with an average of 33.36% for the obtained response in the 25 runs. The differences between the actual and the model's predicted values of ISO brightness were relatively small, which indicates that the predicted values agree with the experimental results. The average ISO brightness of natural cork stoppers in RW trials under standard industrial conditions (35% H_2O_2 solution, 9% NaOH solution, 150 ml of water with a reaction time of 33 min) is 33.78%, which was considered as a target value.

The actual ISO brightness values acquired were fitted to an empirical model, in this case, a quadratic polynomial regression equation based on the coded parameters (Equation 5.2) that correlate the independent variables to the response:

$$Y = 33.86 + 1.04A - 0.67B + 0.24C - 0.024D - 0.23AB - 0.37AC - 0.17AD - 0.050BC + 0.32BD + 0.018CD - 0.57A^2 + 0.051B^2 - 0.021C^2 + 0.11D^2 \quad (5.2)$$

The coefficient of determination (R^2) acquired for the ISO brightness is 0.9381, implying that the regression has a significant value as is shown in Figure 5.1. Figure 5.1 also reveals the residual versus predicted values for ISO brightness, which suggests a uniform distribution.

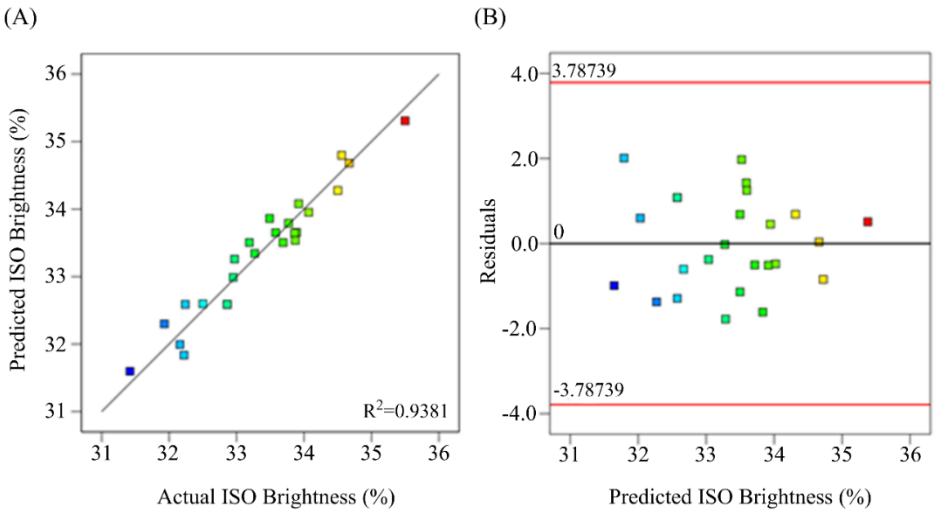

Figure 5.1- Model diagnostic plots: (A) ISO brightness predicted vs. actual plot; (B) Residual plot for predicted ISO brightness.

To evaluate the adequacy of fit of the model towards ISO brightness was used the analysis of variance (ANOVA), supplied by *Design Expert* 11.0.5.0 software (Table 5.3).

Table 5.3- Analysis of variance (ANOVA).

Source	Sum of squares	Degree of freedom	Mean Square	*F*-value	*p*-value
Model	21.01	14	1.50	10.83	0.0003
Residuals	1.39	10	0.1386		
Lack of fit	1.00	7	0.1436	1.13	0.5062
Pure error	0.39	3	0.1271		

The analysis of variance (ANOVA) is based on the sum of squares determination, thus the data such as the model sum of squares (21.01), degrees of freedom (14), and mean square (1.50) are the essential parameters for the model evaluation. The results implied that the model has significance since the *p*-value is less than 0.0500 and the *F*-value (10.83) has a value superior to the critical one ($F_{(0.05,14,10)}$=2.87), which means that the null hypothesis (H_0) is false, that is at least one of the model parameters b_i is non-zero [9].

Another approach to verify the adequacy of the model towards the ISO brightness actual values is analyzing the lack of fit, this value corresponds to the difference between the model prediction values and the average of the replicated runs performed at the same experimental conditions [18]. Lack of fit *F*-value has a value of 1.13 indicating that the lack of fit is not significant relative to the pure error since it has a value inferior to the critical one ($F_{(0.05,7,3)}$=8.89), besides the *p*-value of 0.5062 also characterizes this parameter as non-significant, thus approving the adequacy fitting of the model.

Table 5.4- Coefficient of determination for the model.

Statistics	Response: ISO brightness
Standard deviation	0.37
Adjusted R^2	0.8515
Predicted R^2	0.2950
R^2	0.9381

Table 5.4 presents the coefficients of the model determination statistics with a standard deviation of the predicted model of 0.37. Through the coefficient of determination analysis, it is showed that the predicted R^2 (0.2950) and the adjusted R^2 (0.8515) have a significant difference, this fact may indicate that could exist factors in the model that have no significance [19].

In this way, Table 5.5 demonstrates the model coefficient estimate, *F*-value, and *p*-value associated with each parameter of the empirical model.

Table 5.5-Estimated coefficients, *F*-value and *p*-value for each parameter of the empirical model.

Source	Coefficient Estimate	*F*-value	*p*-value
A	1.04	92.91	< 0.0001
B	-0.67	40.86	< 0.0001
C	0.24	4.98	0.050
D	-0.024	0.065	0.80
AB	-0.23	2.97	0.12
AC	-0.37	6.47	0.030
AD	0.17	2.04	0.18
BC	-0.050	0.12	0.74
BD	0.032	5.94	0.035
CD	0.018	0.021	0.89
A^2	-0.57	5.88	0.036
B^2	0.051	0.073	0.79
C^2	-0.021	0.0099	0.92
D^2	0.11	0.24	0.63

The *p*-value consists of the probability, under the assumption of no influence of one of the variables in the response, of obtaining a result equal to or more extreme than what was actually obtained [20]. *p*-values less than 0.05 indicate that the model terms are significant, in this case, A, B, C, AC, BD, and A^2 are significant terms in the model [21]. *p*-values greater than 0.1000 indicate the model terms are not significant, such as D^2, C^2, B^2, CD, BC, AD, AB, and D. Thus, the model was reduced in a hierarchical way of the parameters, considering the analysis of variance (ANOVA), when each of the equation terms of the empirical model was removed. This process of the elimination of insignificant terms helps to improve and simplify the model. Equation 5.3 is the equation of the empirical model, since the parameters that are not significant for the model (D^2, C^2, B^2, CD, and BC) are excluded, the removal of more parameters does not cause its noticeable improvement:

$$Y = 33.95 + 1.03A - 0.65B + 0.23C - 0.020D - 0.24AB - 0.39AC - 0.15AD + 0.30BD - 0.53A^2 \quad (5.3)$$

Since the model has been changed, all the assumed values obtained until now have been modified, such as the predicted values for each experimental combination of process variables, as well as the residuals (Figure 5.2).

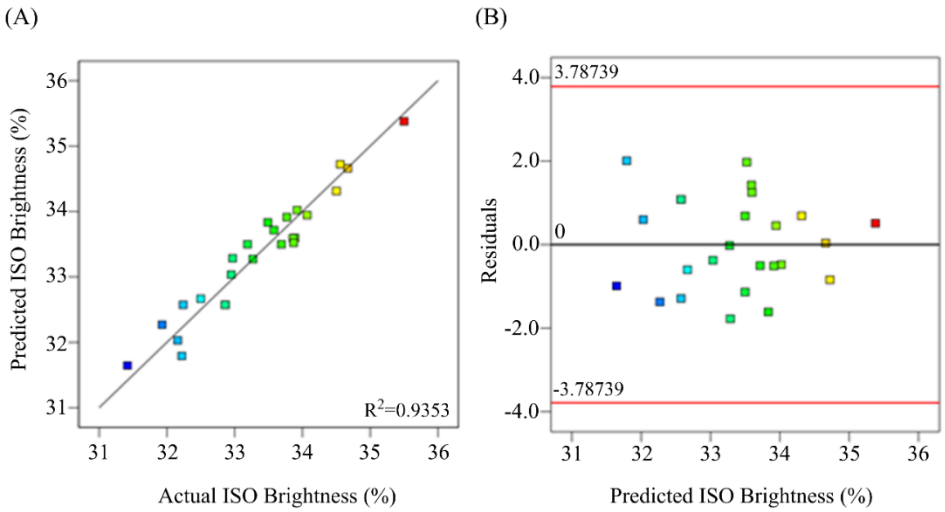

Figure 5.2- Model diagnostic plots for the reduced empirical model: (A) ISO brightness predicted vs actual plot; (B) Residual plot for predicted ISO brightness.

Figure 5.2 demonstrates that ISO brightness predicted plotted versus actual experimental values obtained fits well the regression with a coefficient determination (R^2) of 0.9353, although it has a slightly inferior value than the extended empirical model (R^2=0.9381). The residuals plot for predicted ISO brightness is uniformly distributed. Table 5.6 characterizes the ANOVA statistics for the reduced model.

Table 5.6- Analysis of variance (ANOVA) for ISO brightness in the reduced empirical model.

Source	Sum of squares	Degree of freedom	Mean Square	*F*-value	*p*-value
Model	20.95	9	2.33	24.11	<0.0001
Residuals	1.45	15	0.0966		
Lack of Fit	1.07	12	0.0889	0.70	0.7172
Pure error	0.38	3	0.1271		

The results (Table 5.6) showed a slight decrease in the model sum of square and the degree of freedom became 9, which directly implies an increase in the model mean square. The fact that *F*-value (24.11) has a much greater value than the critical value ($F_{(0.05,9,15)}$=2.59) and the *p*-value is less than 0.0001, also confirms the fitting adequacy of the model [9]. The lack of fit *F*-value in the reduced empirical model is inferior (0.70) to that in the initial model (1.13), which shows that this reduction improves the model prediction. Additionally, the *F*-value of the lack of fit (0.70) is lower than the critical one ($F_{(0.05,12,3)}$=8.74), which in combination with *p*-value (0.7172) shows that its value is acceptable in the overall model.

Table 5.7- Coefficients of determination statistics for the ISO brightness.

Statistics	Response: ISO brightness
Standard deviation	0.31
Adj R^2	0.8965
Pred R^2	0.7757
R^2	0.9353

The results of Table 5.7 show that the model reduction also slightly improves the standard deviation by decreasing from 0.37 in the initial model to 0.31 in the reduced one. The coefficient of determination (R^2) also decreases (0.9353), but the predicted R^2 (0.7757) and adjusted R^2 (0.8965) are in good agreement, as the discrepancy between these two values is less than 0.2, which reveals a model with adequate parameters (Table 5.8).

Table 5.8- Estimated coefficients, *F*-value and *p*-value for each parameter of the reduced empirical model.

Source	Coefficients estimated	*F*-value	*p*-value
A	1.03	141.23	< 0.0001
B	-0.65	63.26	< 0.0001
C	0.23	8.07	0.012
D	-0.020	0.071	0.79
AB	-0.24	7.02	0.018
AC	-0.39	17.57	0.00080
AD	-0.15	2.73	0.12
BD	0.30	9.53	0.0075
A^2	-0.53	9.56	0.0074

The data in Table 5.8 also indicate that there are still terms in the model that have no significance. However, the removal of such terms (AD and D) did not lead to the general improvement of the model. Consequently, the model that was previously considered most suitable for the experimental results of the real ISO brightness is the reduced empirical model described by Equation 5.3.

5.3.2. The effect of process variables on ISO brightness

The estimated coefficients for each model parameter that resemble the reactive washing process variables from Equation 5.3 (Table 5.8) indicate that factors A and C (concentration of the H_2O_2 and the oxidation time, respectively) have a positive effect on the ISO brightness. On the other hand, B factor (concentration of NaOH) has a negative effect. This is understandable since alkalinity favors the formation of chromophores due to the formation of quinone structures with lignin and tannins presenting on the surface of cork stoppers [6]. Accordingly, the excess of NaOH is strongly prejudicial to the brightness of the stoppers and must be corrected accordingly. In addition, D factor

(amount of water in the washing step) has no significant effect on the ISO brightness in the range of the parameter levels examined, but due to the design model hierarchical rules cannot be removed. Likewise, Equation 5.3 establishes the effects of each interaction studied in the model, which shows that all factors, with exception to BD, have a negative effect on ISO brightness. With the reduction of the empirical model, the only quadratic effect present in the equation is factor A, which has a negative effect on the response.

The predicted response of the process is represented in three dimensional (3D) form of the response surface in Figures 5.3-5.6 plotting the interaction between two variables. Figure 5.3 shows the effect of A (hydrogen peroxide concentration) and B (sodium hydroxide concentration) on ISO brightness at the center level of C (oxidation time) and D (washing water volume).

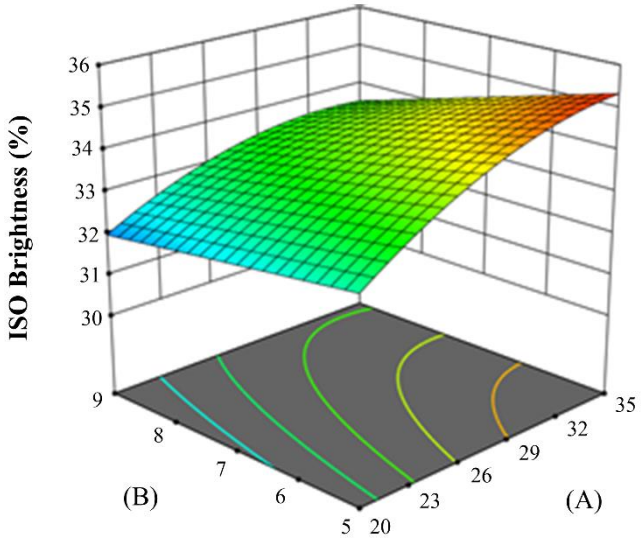

Figure 5.3- Response surface plot representing the effect of A and B on ISO brightness.

Figure 5.3 reveals that increasing factor A causes an improvement of ISO brightness. On the other hand, the alteration of factor B does not change in a significant way the ISO brightness. This can be explained by the excess of NaOH concentration in the reaction system. The best value of ISO brightness (35.34 %) is obtained when variable A is at the highest level and variable B in the lowest one (Figure 5.3). However, taking into consideration that the target ISO brightness is 33.78%, it is possible to reduce the factor A in the RW while keeping the other two variables (C and D) in the center point.

Figure 5.4 demonstrates the effect of hydrogen peroxide concentration (A) and oxidation time (C) variables on the ISO brightness at the center level of sodium hydroxide concentration (B) and washing water volume (D).

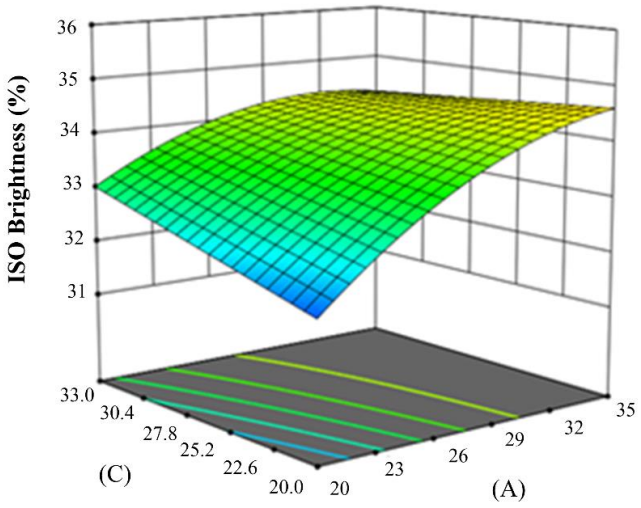

Figure 5.4- Response surface plot representing the effect of A and C on ISO brightness.

Noteworthy that for the maximum level of A, factor C has almost no significant effect on the ISO brightness for the levels examined. However, if factor A is at the minimum level, factor C has more influence on the response, and the lowest brightness value (31.78%) is less than the ISO brightness target (Figure 5.4). Apparently, when the chromophores of cork do not degrade extensively due to the lack of H_2O_2, their removal from the surface of the stoppers is more dependent on the reaction time.

Figure 5.5 illustrates the effects of A (hydrogen peroxide concentration) and D (washing water volume) factors on ISO brightness, keeping factors B (sodium hydroxide concentration) and C (oxidation time) at the center level.

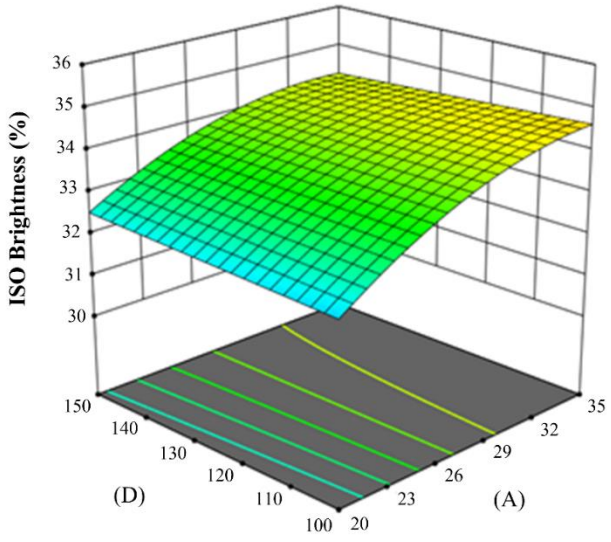

Figure 5.5- Response surface plot representing the effect of A and D on ISO brightness.

As stated before and confirmed by Figure 5.5, factor D has no significant effect on ISO brightness since does not cause noticeable changes in the response. If factor A is increased to the

highest levels examined, the response is improved, but for the lowest levels of A, the ISO brightness (32.27%) is less than the target value.

Figure 5.6 shows the effects of the last interaction present in the model, the factors B (sodium hydroxide concentration) and D (washing water volume), while the factors A (hydrogen peroxide concentration) and C (oxidation time) are in the center level.

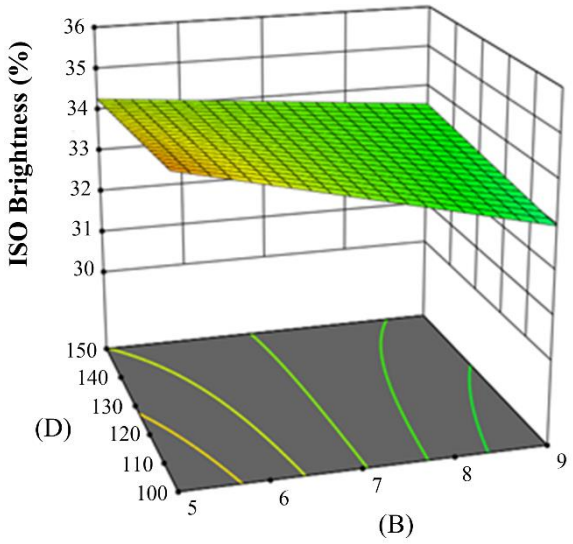

Figure 5.6- Response surface plot representing the effect of B and D on ISO brightness.

Considering the levels examined (Figure 5.6), it can be seen that the best value for ISO brightness is obtained for the lowest levels of B and D factors. This is in tune with the previous discussion when the lowest level of alkalinity provoked less formation of chromophores on the surface of stoppers and needs less water to wash out the reaction products. The variation of D factor for the highest or the lowest level of factor B does not imply any significant change in the response. From the response surface plot present in Figures 5.3-5.6 this empirical model allows the optimization of the RW process.

5.3.3. Model validation

To validate the model that predicts the ISO brightness after the reactive washing process applied, nine additional tests were performed using different levels of independent variables. Factor D was not modified and it was maintained at the lowest level because this does not have a significant influence on the response. The test results as well as the predicted and the actual responses are present in Table 5.9.

Table 5.9- Conditions of the validation tests and predicted and actual ISO brightness.

Run Number	Condition				ISO brightness (%)	
	A	B	C	D	Actual	Predicted
1	20	5	20	100	32.90	32.35
2			25		31.00	32.83
3			33		30.00	33.60
4	25	7	20		33.40	33.16
5			25		33.10	33.44
6			33		32.55	33.88
7	35	9	20		32.50	33.60
8			25		32.89	33.48
9			33		33.61	33.29

Figure 5.7 shows the relationship between the ISO brightness predicted by the model and the respective value obtained experimentally for each of the nine tests. The results obtained clearly indicate that it is possible to validate the model developed since the real experimental values are in accordance with the predicted, with a coefficient of determination (R^2) of 0.9211.

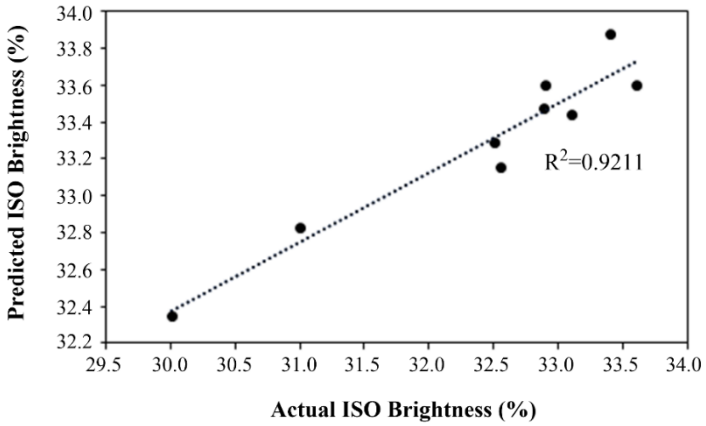

Figure 5.7- Relation between the actual and predicted ISO brightness.

5.3.4. Optimization results

Using the numerical option of the optimization module of the *Design Expert* software (version 11.0.5.0), it was possible to optimize the levels of the independent variables to obtain the target ISO brightness of 33.78%. The results obtained showed that natural cork stoppers with a target of 33.78% ISO brightness can be achieved with a value of 22 for variable A (% of H_2O_2 concentration), 6 for variable B (% of NaOH concentration), 33 for variable C (time of the oxidative treatment, min) and the lowest level of 100 for variable D (water consumption for the washing, ml/10 stoppers). This implies significant changes in the profile of the added reagents. Such an approach leads to a

significant improvement in the RW process, thus allowing a reduction of 37% for variable A and 33% for variables B and D, respectively, without deteriorating the final quality parameter of natural stoppers (ISO brightness).

After applying the reactive washing proposed by the *Design Expert* software, the ISO brightness was measured and it was obtained a value of 34.2 (±2.2)%, which implies that the optimized conditions were able to reach the target ISO brightness while reducing the operational variables.

5.4. Conclusions

The effect of four reactive washing process independent variables (hydrogen peroxide and sodium hydroxide concentrations, oxidation time, and washing water volume) on the ISO brightness of the natural cork stoppers on a laboratory scale was studied. Three-level and four-factor fractional factorial experimental design and response surface methodology were used to develop mathematical models for ISO brightness response, using experimental data and software *Design Expert* version 11.0.5.0. The experimental results were fit to a second-order polynomial equation and the model was optimized by elimination of several insignificant factors and validated.

The model developed revealed that variable A (H_2O_2 concentration) is the one that most influences the response (brightness of cork stoppers), followed by variable B (sodium hydroxide concentration). Variable C (time of oxidative treatment) had significance only at relatively low hydrogen peroxide concentrations (variable A). Variable D (volume of washing water) has no significance in the developed model. This was explained by the need to change the profile of the reagents in relation to the final brightness of the stoppers.

By applying the optimized reagent profiles with an ISO brightness target (33.78%), it was possible to obtain a significant improvement in the process in terms of reagent savings, with a reduction of 37% for variable A, and 33% for variables B and D, respectively.

5.5. References

[1] H. Pereira, The rationale behind cork properties: A review of structure and chemistry, BioResources. 10 (2015) 6207–6229. https://doi.org/10.15376/biores.10.3.Pereira.

[2] L. Liu, S.L. Cui, Hydrogen peroxide bleaching to wine corks with a novel catalyst, Adv. Mater. Res. 734–737 (2013) 2282–2286. https://doi.org/10.4028/www.scientific.net/AMR.734-737.2282.

[3] G. Zucchini, A. Donati, Process for bleaching and sterilizing cork articles, and cork articles bleached using the said process, US 005098447A, 1992.

[4] H. Pereira, Production of cork stoppers and discs, in: Cork Biol. Prod. Uses, 2007: pp. 263–288. https://doi.org/10.1016/b978-044452967-1/50014-5.

[5] H.U. Süss, N.F. Nimmerfrof, J.D. Kronis, The naked truth on hot peroxide bleaching, in: CPPA 1997 Annu. Meet., Montreal, 1997: pp. 1–13.

[6] D.G. Branco, C.A. Santiago, F.J. Oliveira, L. Cabrita, D. V Evtuguin, Surface properties of cork in relation to reactive washing, Colloids Surfaces A Physicochem. Eng. Asp. 624 (2021). https://doi.org/10.1016/j.colsurfa.2021.126762.

[7] J.R. Gonzalez-Adrados, M.C. Garcia-Vallejo, M.J. Caceres-Esteban, J.L. Garcia De Ceca, F. Gonzalez-Hernandez, R. Calvo-Haro, Control by ATR-FTIR of surface treatment of cork stoppers and its effect on their mechanical performance, Wood Sci. Technol. 46 (2012) 349–360. https://doi.org/10.1007/s00226-011-0403-5.

[8] C. Ortega-Fernández, J.R. González-Adrados, M.C. García-Vallejo, R. Calvo-Haro, M.J. Cáceres-Esteban, Characterization of surface treatments of cork stoppers by FTIR-ATR, J. Agric. Food Chem. 54 (2006) 4932–4936. https://doi.org/10.1021/jf0529823.

[9] D.C. Montgomery, Design and analysis of experiments, 9th Ed., John Wiley & Sons, Inc., 2017.

[10] F.C. Zimmer, A.H.P. Souza, A.F.C. Silveira, M.R. Santos, M. Matsushita, N.E. Souza, A.C. Rodrigues, Application of factorial design for optimization of the synthesis of lactulose obtained from whey permeate, J. Braz. Chem. Soc. 28 (2017) 2326–2333. https://doi.org/10.21577/0103-5053.20170083.

[11] J.U. Ani, U.C. Okoro, L.E. Aneke, O.D. Onukwuli, I.O. Obi, K.G. Akpomie, A.C. Ofomatah, Application of response surface methodology for optimization of dissolved solids adsorption by activated coal, Appl. Water Sci. 9 (2019) 1–11. https://doi.org/10.1007/s13201-019-0943-7.

[12] M.A. Bezerra, R.E. Santelli, E.P. Oliveira, L.S. Villar, L.A. Escaleira, Response surface methodology (RSM) as a tool for optimization in analytical chemistry, Talanta. 76 (2008)

965–977. https://doi.org/10.1016/j.talanta.2008.05.019.

[13] D.P. Obeng, S. Morrell, T.J. Napier-Munn, Application of central composite rotatable design to modelling the effect of some operating variables on the performance of the three-product cyclone, Int. J. Miner. Process. 76 (2005) 181–192. https://doi.org/10.1016/j.minpro.2005.01.002.

[14] A. V. Veličković, O.S. Stamenković, Z.B. Todorović, V.B. Veljković, Application of the full factorial design to optimization of base-catalyzed sunflower oil ethanolysis, Fuel. 104 (2013) 433–442. https://doi.org/10.1016/j.fuel.2012.08.015.

[15] V. Czitrom, One-factor-at-a-time versus designed experiments, Am. Stat. 53 (1999) 126–131. https://doi.org/10.1080/00031305.1999.10474445.

[16] N. Hamaidi-Maouche, S. Bourouina-Bacha, F. Oughlis-Hammache, Design of experiments for the modeling of the phenol adsorption process, J. Chem. Eng. Data. 54 (2009) 2874–2880. https://doi.org/10.1021/je800959k.

[17] N.R. Domagalski, B.C. Mack, J.E. Tabora, Analysis of Design of Experiments with Dynamic Responses, Org. Process Res. Dev. 19 (2015) 1667–1682. https://doi.org/10.1021/acs.oprd.5b00143.

[18] G.E.P. Box, N.R. Draper, Response Surfaces, Mixtures, and Ridge Analyses, 2nd Ed., Wiley-Interscience, 2008. https://doi.org/10.1198/jasa.2008.s238.

[19] R.H. Myers, D.C. Montgomery, C.M. Anderson-Cook, Response surface methodology-process and product optimization using designed experiments, 3rd Ed., Wiley, 2009.

[20] R.G. Brereton, The use and misuse of p values and related concepts, Chemom. Intell. Lab. Syst. 195 (2019) 1–7. https://doi.org/10.1016/j.chemolab.2019.103884.

[21] B. Govaerts, B. Francq, R. Marion, M. Martin, M. Thiel, The Essentials on Linear Regression, ANOVA, General Linear and Linear Mixed Models for the Chemist, in: Ref. Modul. Chem. Mol. Sci. Chem. Eng., 2nd Ed., Elsevier Inc., 2020: pp. 431–463. https://doi.org/10.1016/b978-0-12-409547-2.14579-2.

Chapter 6

IMPLEMENTATION OF OZONE AS A BLEACHING AGENT IN REACTIVE WASHING OF NATURAL CORK STOPPERS

Content

6.1. Introduction

Throughout the production process of the cork stoppers, reactive washing (RW) plays an important role to ensure the cleaning /disinfection, dust removal, and appearance, mainly color homogeneity and brightness. To increase the surface brightness, basic processes need to occur: (1) removal of the colored matter, and (2) transformation of the coloring matter into colorless. To achieve these goals it is necessary to remove, at least partially, chromophore-containing compounds that influence the cork color [1,2]. To reach the desired stopper surface brightness is necessary to apply bleaching chemicals, such as chlorine-based chemicals, hydrogen peroxide, oxygen, ozone, among others. The chlorine-based chemicals, despite being efficient and economic, leave small amounts of chlorine in the form of chloro-organic compounds that cause unpleasant smells and corrupt the taste of the drink with which the cork stoppers are in contact [3].

To fill this gap, nowadays, its used hydrogen peroxide under strong alkaline and increased temperature conditions in a multistage process, these conditions caused changes in the stopper surface that affect the receptivity of the surface to the coating agents (silicone or paraffin emulsion and polymeric formulations) [4,5]. This is a drawback for this process, that combined with the increasing environmental concern in the past decades leads to the study of new approaches that can achieve the main goals of RW, while not interfering negatively in the stopper surface properties and reducing environmentally hazardous effluents.

Ozone could be the alternative to the hydrogen peroxide treatment reagent. When comparing the oxidation potential of ozone (2.07 V, 25 °C) with that of hydrogen peroxide (1.77 V, 25 °C), it becomes clear that is a promising bleaching agent [6,7]. From the environmental point of view, ozone does not produce toxic conversion products, which makes this agent particularly interesting [8]. Additionally, it has been stated that the introduction of the ozone stage in ECF bleaching sequences of cellulosic pulps can reduce by 20-32% the conventional bleaching costs, and reach even higher brightness levels in the case of TCF bleaching sequences [9]**.**

Due to ozone electron deficiency, this oxidant reacts with a wide range of organic compounds, containing olefinic, aromatic, and phenolic structures, such as lignin [10–13]. Several studies have been presented that use ozone as a delignification agent with different types of biomass, such as cereal straw [14–16], wood pulp [17,18] and wood chips [19], cotton [7,20,21], among others, and even in wastewater treatments [22], but the action of ozone in cork materials have not been reported, yet.

Ozone is formed by adding free oxygen radical to the oxygen molecule, and is thermodynamically unstable and spontaneously reverts into oxygen, so must be generated “in situ” [21]. The efficiency of ozone bleaching is influenced by different parameters such as ozone

concentration, treatment time, temperature, mixing homogeneity, pH, and water content in the reaction medium.

Several studies involving the ozone as a bleaching agent in different raw materials showed that the increase of ozone concentration and reaction time causes an increase in brightness. However, for longer reaction times, cellulose degradation may occur, which causes a decrease in the material quality, in this case, the natural cork stoppers [11]. The brightness rise of the stopper surface will be more pronounced in the first moments, ranging from seconds up to several minutes, since ozone can react almost spontaneously with the double bonds of the functional groups of the chromophores [7,23]. The ozone reactive washing (ORW) temperature should be maintained between 30 °C and 60 °C by analogy with cellulosic pulp treatments [8,23,24]. However, temperatures as high as 60 ºC allow the increase in pulp delignification by 5-10%, without any negative impact on pulp strength and brightness [9,25]**.** As for the homogeneity of the pulp mixture with ozone, the better this variable, the higher interaction between ozone and the reaction sites, promoting higher levels of pulp brightness [9]**.**

The main goal of this study was to apply ozone in the natural cork stoppers reactive washing. Firstly, the different levels of process variables were applied, and the process was optimized using statistical tools to evaluate the final color of the stoppers (ISO brightness and CIE L*a*b* color parameters). Once the process is optimized, the changes in the surface stoppers composition were thoroughly analyzed by Ultraviolet-visible (UV/vis) and Fourier Transform Infrared-Attenuated Total Reflectance (FTIR-ATR) spectroscopy. The surface morphology was assessed by scanning electron microscopy (SEM) and roughness analysis. To evaluate the possible odors released by the cork stoppers after ozone treatment, a direct combination of the mass spectrometer and headspace solid-phase microextraction (HS-SPME/GC-MS) techniques were used. The response of the ozone modified stopper surface to spirits with different levels of alcohol was evaluated by contact angles measurements with liquid probes and constructing the wetting envelope in polar-dispersion energy coordinates.

6.2. Materials and Methods

Natural cork stoppers were supplied by Amorim Cork, S.A. (Santa Maria de Lamas, Portugal). The cork stoppers have a caliber of 49x24 mm (length x diameter) and belong to 1st class (medium class).

6.2.1. Ozone reactive washing

Ozone reactive washing (ORW) requires three essential components: the ozone generator, the reactor with ozone supply, and the ozone destroyer [26]. Ozone was generated by an ozone generator Fischer 502 (Fischer Group, Waldachtal, Germany) with pure oxygen (99.9%) source and an electrical discharge intensity of 0.7 A. All the trials were performed under a continuous supply of ozone. A round bottom flask was used as a reactor and two consecutive erlenmeyers with 10% potassium iodide solution were implemented as ozone destroyers. All the connections between the three essential components were dully established with teflon tubes to prevent any ozone leakages from the system. Each trial uses 10 natural cork stoppers, and all the trials were performed in the absence of water.

6.2.2. Ozone reactive washing optimization

In the cork reactive washing with ozone, the effect of the process variables, such as reaction time, temperature, rotation intensity (medium homogeneity), and oxygen flow, on the ISO brightness and CIElab color coordinates of the cork stopper surface, were evaluated.

ISO brightness corresponds to a numerical value of diffuse reflectance concerning blue light of wavelength 457 nm [27]. This procedure is common in the pulp and paper industry, properly described in Tappi T 525 om-06. This analysis was performed on the Konica Minolta cm700-d portable spectrophotometer (Konica Minolta, Tokyo, Japan), with the ISO brightness value of each stopper corresponding to the average of six measurements, as performed in the internal procedure of the company Amorim Cork, S.A.

The CIE-L*a*b* color coordinates, lightness (L* (D65)) and the chromaticity coordinates a* (D65) and b* (D65), which are cartesian coordinates were also determined on the same equipment. Coordinate a* determines redness (+a*) or greenness (-a*), and b* range from yellow (+b*) to blue (-b*), these parameters allow the evaluation more accurately of the stopper surface. Ideally, to achieve the highest levels of brightness is necessary to have an L* (D65) closer to 100 and the coordinates a*(D65) and b*(D65) approximately zero.

Firstly, was evaluated the ideal processing time for the ozone treatment by varying between 5, 10, 15, and 30 minutes, while maintaining the other process variables constants. The 50ºC external

heating that corresponds to 41 °C in the reaction medium was selected for the ORW temperature. Rotation was set at 30 rpm and inlet oxygen flow was 50 L/h allowing the production of 1.8 g/h of ozone. Afterward, the cork stoppers from each assay must stabilize for 24 hours before the ISO brightness and CIElab color coordinates are measured. The four assays were evaluated through analysis of variance (ANOVA) and Tukey test of the ISO brightness and CIElab color parameters.

Once the processing time is established, it was analyzed the influence of the temperature, rotation intensity, and oxygen flow on the efficiency of the process. Each process variable was ranged between two levels, which led to the application of 2^3 full factorial experimental design, where the reference assay corresponds to the best assay selected previously (Table 6.1). The temperature varied between 50 and 70 °C, the last being 55 °C in the reaction medium, the rotation took values of 30 or 120 rpm and the inlet oxygen flow ranged in the interval of 50 and 100 L/h (production of 5.0 g/h of ozone).

Table 6.1- Full factorial 2^3 assays.

Assay	Temperature (°C)	Rotation (rpm)	Oxygen flow (L/h)
Reference	50	30	50
1	70	30	50
2	50	120	50
3	50	30	100
4	70	120	50
5	50	120	100
6	70	30	100
7	70	120	100

The values of ISO brightness and CIElab color parameters of each assay were measured, and an ANOVA methodology was applied to verify if any of the assays performed, and respective process conditions changed significantly the surface color parameters. Additionally, the Tukey test was used to compare the assays and verify the efficiency of reactive washing. All the data were analyzed using SPSS computer software (Statistical Package for the Social Sciences, version 27.0, IBM, USA) and followed a normal distribution, the significance levels were set at $p \leq 0.05$.

6.2.3. SEM and surface roughness

The natural cork stoppers were cut into thin slices and covered by gold sputtering before SEM analysis. The images were acquired on a Hitachi TM 4000 Plus SEM microscope (Hitachi High-Technologies, Tokyo, Japan) equipped with a BSE detector and operated at 15 kV under a vacuum of 30 Pa.

The surface roughness analysis was carried out on a portable surface roughness tester SURFTEST SJ-210 (Mitutoyo America Corporation, Illinois, USA) with a speed of 0.5 mm/s and a

cut-off wavelength value of 2.5 mm. The surface roughness analysis followed the standard ISO 4287-1997 and the obtained values correspond to an average of 25 measurements.

6.2.4. Solid ultraviolet-visible (UV-vis) spectroscopy

UV-vis diffuse reflectance (UV-vis DR, k/s) spectra were recorded at room temperature (21±1 ºC, RH 60%) on a Thermo Scientific™ Evolution 220 spectrophotometer (Thermo Scientific, Massachusetts, USA) equipped with an ISA-220 reflectance accessory using $BaSO_4$ as background reference, at scan velocity of 200 nm/min. The studied range was 220-700 nm with a bandwidth of 5 nm. The lateral and the top were cut from the natural cork stopper before and after ORW obtaining a sample (10 x 10 mm and thickness about 1 mm). Two replicates were analyzed for each sample. The amount and type of light-absorbing materials or chromophores were characterized by the Kubelka-Munk light absorption coefficient (k/s) at different wavelengths. The reflectance spectra were also converted into k/s spectra using known Kubelka–Munk Equation 6.1 [28]:

$$\frac{k}{s} = \frac{(1-R)^2}{2R} \tag{6.1}$$

where R is the reflectance of the opaque sample, k is the specific absorption coefficient, and s is the specific scattering coefficient. A constant scattering coefficient among the studied samples was assumed for a comparative quantitative analysis of the changes in chromophores among the studied samples. The obtained spectra were treated using Thermo Scientific™ INSIGHT™ software (Thermo Scientific, Massachusetts, USA).

6.2.5. FTIR-ATR spectroscopy

Fourier transform infrared- attenuated total reflectance (FTIR-ATR) spectra were collected on a Spectrum BX Perkin Elmer spectrophotometer (PerkinElmer, Waltham, Massachusetts, USA) with a resolution of 4 cm^{-1} and 128 scans in a transmittance mode. The spectrums were normalized at 1260 cm^{-1} band using OriginPro 2015 software (OriginLab Corporation, Northampton, Massachusetts, USA).

6.2.6. HS-SPME/GC-MS

A total of 13 natural cork stoppers treated with ozone from the optimized assay were placed in a hermetically closed flask at room temperature (21±1 ºC, RH 60%) and in dark for 24 h in contact with the fiber carboxen-poly(dimethylsiloxane) (CAR-PDMS) (75 µm) (Supelco, Madrid, Spain). The volatile compounds present on the natural cork stoppers come in equilibrium with CAR-PDMS fiber by headspace solid-phase microextraction (HS-SPME).

Once the contact time is completed, the GC-MS analysis was performed on a Trace GC 2000 series coupled with a Thermo Scientific DSQII mass spectrometer (Thermo Fisher Scientific, Waltham, MA, USA) using a column capillary DB-1 J&W (30 m x 0.32 mm i.d. 0.25µm) and high purity helium as carrier gas at the constant flow of 1.2 mL/min. The GC injector was held at 285 ºC in splitless mode and the transfer-line temperature was also 285 ºC. An initial oven temperature of 35 ºC was held for 6 min then increased 10 ºC/min to 250 ºC (5 min). The mass range was 40-300 m/z, with a scan rate of 1.84 scan/s. The analysis was performed in full-scan mode. Before this methodology, the SPME fiber was conditioned according to the manufacture's recommendations (270 ºC for 2 h).

Compounds were identified by comparing their mass spectra with the Wiley-Nist spectral library (Nist MS search 2.0), with data from the literature and in some cases, by injection of standards.

6.2.7. Contact angles and interface interaction

Contact angles were measured in a Contact Angle System OCA20 goniometer (Data Physics, Filderstadt, Germany) that is equipped with a CCD camera and SCA20 software using the sessile drop method and water, formamide, and diiodomethane as probe liquids. For each sample, 30 measurements were performed (10 measurements for each solvent used). The contact angle measurements were carried out at room temperature (21±1 ºC, RH 60%) and applying the drop volume of 1 µL with a velocity of deposition of 1 µL/s. Contact angles were measured as a function of time for 60 seconds and then extrapolated to zero time. The results of parallel measurements were averaged, and the standard deviation errors were evaluated.

The evaluations of the free surface energy (FSE) of cork (γ_s) and its corresponding polar (γ_s^p) and dispersive (γ_s^d) components were performed using the series of liquid probes (water, formamide, and diiodomethane) based on the Owens-Wendt-Rable-Kaeble (OWRK) model that satisfactorily describes the solid-liquid interfacial interactions in the air for the polymers [29] and lignocellulosic materials [30]:

$$\left(\frac{1+\cos\theta}{2}\right)\left(\frac{\gamma_L}{\sqrt{\gamma_L^d}}\right)=\sqrt{\gamma_s^p}\times\sqrt{\frac{\gamma_L^p}{\gamma_L^d}}+\sqrt{\gamma_s^d} \tag{6.2}$$

where γ_L, γ_L^p, and γ_L^d represent the liquids superficial tension and the corresponding polar and dispersive components, respectively. Plotting $(1+\cos\theta/2)\left(\gamma_L/\sqrt{\gamma_L^d}\right)$ *vs* $(\gamma_L^p/\gamma_L^d)^{1/2}$ allows the calculation of the parameters γ_s^d and γ_s^p.

6.2.8. Wetting envelope simulations

Wetting envelope is a tool that allows the visualization of the relationships between polar and dispersive components, along with FSE, and helps to better understand the wettability of the surface towards different liquids. This simulation was built using the values of polar and dispersive components of FSE obtained for each sample analyzed. Wetting envelope was applied as described elsewhere [5]. To facilitate the understanding of the wettability characteristics of the samples, calculations were performed for four different angles (θ): 0°, 45°, 60°, and 90°.

The behavior changes of the cork stopper after ozone reactive washing (ORW) were assessed by evaluating the interfacial behavior of the cork stopper surface towards four solutions with different percentages of ethanol (12, 14, 20, and 40%) on the wetting envelope. The polar and dispersive components for each ethanol solution were imported from the literature [5].

6.3. Results and Discussion

6.3.1. Ozone reactive washing optimization

The introduction of ozone as an alternative to reactive washing in the natural cork stoppers started with some preliminary assays to identify the possible process conditions. In the first trial was analyzed the ozone reactive washing in the presence and absence of water. The presence of water difficult the increase of the brightness of the surface of the natural cork stoppers, mainly due to the limitation of the mass transference of the oxidizing species of ozone towards the reaction sites [31,32]. Hence, all the assays were performed in the absence of water.

Based on the literature of the bleaching of cellulosic pulp and on the preliminary assays, the reactive washing of natural cork stoppers with ozone was carried out at a temperature of 50°C, 30 rpm reactor rotation and an inlet oxygen flow of 50 L/h, allowing the ozone flow of *ca*. 1.8 g/h of ozone, for four different reaction times: 5, 10, 15, and 30 minutes (Table 6.2).

Table 6.2- CIElab color coordinates values and ISO brightness means before and after ORW and respective standard deviation (SD) for different reaction times (5, 10, 15, and 30 min) using the conditions of the reference assay.

Process time (min)	L* value (±SD)		a* value (±SD)		b* value (±SD)		ISO brightness (%) (±SD)	
	Baseline[a]	After ORW	Baseline[a]	After ORW	Baseline[a]	After ORW	Baseline[a]	After ORW
5	60.3±2.5	62.1±2.5	12.2±0.6	11.2±0.8	24.7±1.3	24.5±1.2	15.7±1.6	17.2±1.8
10	59.5±2.5	62.6±2.2	12.1±1.0	10.6±0.8	24.9±1.5	24.0±1.3	15.2±1.6	17.8±1.7
15	60.2±2.4	61.6±2.8	12.2±1.1	10.1±1.3	24.9±0.9	22.5±1.5	15.5±1.6	17.8±1.9
30	60.1±1.6	62.6±1.8	12.2±1.1	10.4±1.1	24.6±0.7	23.0±1.1	15.5±1.2	18.3±1.7

[a] levels corresponding to 0 min of the natural cork stoppers with ozone as a bleaching agent on the reactive washing

The values of the CIElab color coordinates and ISO brightness confirmed that ozone acts on the stopper surface, the baseline shows the natural color shadows before ozone treatment. Even though cork is a natural material and consequently has great variability within the raw material, the color parameters did not reveal this, since the baseline values (L*, a*, b* and ISO brightness) are very similar, which shows the color homogeneity of cork surface. After ORW, independently of the processing time, occurs an increase of L* and ISO brightness and a decrease of a* and b*, however, the differences between each process time are apparently small, in this way to understand whether all the experiments had the same mean responses (null hypothesis) or if there is at least one assay, in this case, one process time, with responses mean significantly different from the others (alternative hypothesis) was applied the ANOVA analysis, present in Table 6.3 [33].

Table 6.3- Color parameters ANOVA between groups (different ozone process time) after ORW.

Color parameter		Sum of squares	Degree of freedom	Mean square	*F*-value	*p*-value
ISO Brightness	Between groups	8.558	3	2.853	0.923	0.436
	Within groups	173.040	56	3.090		
	Total	181.598	59			
L * (D65)	Between groups	9.210	3	3.070	0.548	0.652
	Within groups	313.937	56	5.606		
	Total	323.148	59			
a * (D65)	Between groups	10.397	3	3.466	3.381	0.024
	Within groups	57.396	56	1.025		
	Total	67.793	59			
b * (D65)	Between groups	38.594	3	12.865	7.603	0.000
	Within groups	94.750	56	1.692		
	Total	133.344	59			

ANOVA analysis (Table 6.3) shows that independently of the ozone process time no significant differences were found in mean values of either ISO brightness or L*since the *p*-value for both responses is greater than 0.05, which means that the null hypothesis is accepted for these two responses. This fact is also confirmed by the *F*-value of 0.923 and 0.548 for the ISO brightness and L*, respectively, which is lower than the critical one (critical *F*-value=2.769) [34]. However, for the mean values of a* and b* color parameters *p*-values are 0.024 and 0.000, respectively, thus less than 0.05, and consequently there is at least one process time that significantly influences the value of coordinates a* and b*. Since the null hypothesis was rejected for these two color parameters, the Tukey test was used to determine which pairs of means between each process time had significant differences for a* and b* values (Table 6.4).

Table 6.4- Differences in a* and b* coordinate mean values for the different ozone process times pairs applying the Tukey test.

Colour parameter	Ozone process time pairs	Mean difference	95 % confidence interval of the difference		*p*-value
			Lower	Upper	
a*	5-10	0.581	-0.398	1.560	0.403
	5-15	1.126	0.147	2.105	0.018
	5-30	0.849	-0.130	1.828	0.111
	10-15	0.545	-0.434	1.524	0.459
	10-30	0.269	-0.710	1.248	0.886
	15-30	-0.277	-1.256	0.702	0.877
b*	5-10	0.537	-0.720	1.795	0.672
	5-15	2.049	0.792	3.307	< 0.001
	5-30	1.510	0.252	2.768	0.013
	10-15	1.512	0.254	2.770	0.012
	10-30	0.973	-0.285	2.230	0.183
	15-30	-0.539	-1.797	0.718	0.669

The mean difference value of coordinate a* changed significantly when the ozone was in contact with cork stoppers surfaces for 5 or 15 minutes (*p*-value = 0.018) (Table 6.4). Since the 15 minutes experiment allowed a lower mean value of a* coordinate than 5 minutes (Table 6.2), is concluded that 15 minutes is better than 5 minutes for the ozone process time in terms of a* coordinate. For the b* coordinate three different process time pairs differed significantly from each other (*p*-value <0.05). However, the lower *p*-value was reached for the mean difference value pair 5-15 minutes, which has a *p*-value less than 0.001 (Table 6.4). Looking at Table 6.2, it is confirmed that an ozone processing time lower than 15 minutes significantly impair the coordinate b* value.

The ANOVA (Table 6.3) and the Tukey test (Table 6.4) demonstrated that the cork stoppers should be preferably 15 minutes in contact with ozone. Thus, the study of the influence of the process variables (temperature, rotation, and inlet oxygen flow) using the 2^3 full factorial experimental design (Table 6.1) was performed with 15 minutes for the processing time. The ISO brightness and CIElab color parameters before and after ORW are summarized in Table 6.5.

Table 6.5- Mean values of coordinate L*, a*, b* and ISO brightness for the 2^3 full factorial design experiments.

Assay	L* value		a* value		b* value		ISO brightness (%)	
	Baseline	After ORW	Baseline	After ORW	Baseline	After ORW	Baseline	After ORW
Reference	60.2±2.4	61.6±2.8	12.2±1.1	10.1±1.3	24.9±1.0	22.5±1.5	15.5±1.6	17.8±1.9
1	59.6±2.7	62.0±2.3	11.0±1.4	9.4±1.1	23.6±1.6	21.5±1.1	15.9±1.7	18.5±1.9
2	60.6±2.0	62.0±2.1	12.1±0.7	10.3±1.0	24.7±0.9	22.5±1.1	16.1±1.3	18.0±1.6
3	59.5±2.6	61.0±1.5	11.7±1.2	10.6±1.1	24.0±1.1	23.1±1.1	15.4±1.6	16.8±1.0
4	60.7±2.0	65.1±1.7	11.9±1.0	9.7±1.1	25.0±1.4	22.7±1.4	15.8±1.3	20.8±1.6
5	59.6±2.7	61.4±3.1	11.3±1.0	10.4±0.9	23.7±1.4	22.8±1.1	15.6±1.7	17.4±2.3
6	59.9±2.4	61.2±3.0	11.9±0.8	10.4±1.1	24.5±0.9	23.1±1.1	15.5±1.7	17.1±2.3
7	59.2±2.6	62.1±2.3	11.5±1.1	10.1±1.4	24.2±1.3	23.0±1.4	15.1±1.5	17.9±1.8

Overall, the action of ozone on the cork stopper surface is proved by the increment on L* value and ISO brightness and the decrease of the mean value of coordinates a* and b*, however, the mean values of assays 3, 5, 6 and 7 are the less desirable (Table 6.5). The common factor between these four assays is the inlet oxygen flow, which is 100 L/h that corresponds to the higher ozone flow (5 g/h) in the reaction medium, this may indicate that in these assays the excess of ozone ends up entering and leaving the system without being consumed. Regardless of this information, the means values of each response variable are very similar between them, thus was applied the ANOVA analysis to better interpret the real significance of the obtained data and to verify if any of the assays and respective conditions imply a good efficiency of the process (Table 6.6).

Table 6.6- Color parameters ANOVA between assays from 2^3 full factorial experimental design after ORW.

Color parameter		Sum of squares	Degree of freedom	Mean square	*F*-value	*p*-value
ISO Brightness	Between groups	160.393	7	22.913	6.728	0.000
	Within groups	381.419	112	3.406		
	Total	541.812	119			
L*	Between groups	180.779	7	25.826	4.418	0.000
	Within groups	654.753	112	5.846		
	Total	835.532	119			
a*	Between groups	16.315	7	2.331	1.841	0.086
	Within groups	141.777	112	1.266		
	Total	158.092	119			
b*	Between groups	30.297	7	4.328	2.881	0.008
	Within groups	168.252	112	1.502		
	Total	198.548	119			

From the obtained color parameters analysis, it is shown that the color coordinate a* is the only one that did not change significantly between groups (assays), since it has a *p*-value higher than 0.05 (*p*-value=0.086) and an *F*-value (1.841) lower than the critical (2.092) (Table 6.6). However, the other color parameters (ISO brightness, L* and b* coordinates) demonstrated that at least one of the assays performed was significantly different from the others considering the *p*-value for these responses is lower than 0.05 and the *F*-value is higher than the critical one. In this way, it was applied the Tukey test on the response ISO brightness and the coordinates L* and b* (results not shown). The Tukey test demonstrated that assay 1 outstands in significance for the color coordinate b* from the assays 3, 6, and 7, on the other hand, ISO brightness and coordinate L* of assay 4 were significantly different from other experiments (reference, 1, 2, 3, 5, 6 and 7). According to Table 6.5, assay 4 achieved the best mean value of ISO brightness and coordinate L*, while maintaining a similar coordinate a* to that one obtained for assay 1, which means that assay 4 improved the values for the color parameters when compared with the other assays.

Assay 4 is performed at a higher level of external temperature (70 ºC, with an effective internal temperature in the reactor of 55 ºC) and rotation (120 rpm). As for the inlet oxygen flow is set on the lower level (50 L/h corresponding to 1.8 g/h of ozone flow), confirming that the increase of this process variable does not cause a significant positive impact on the color parameters. The temperature selected is within the ideal interval (30 to 60 ºC) for the medium reaction pointed out in the literature [8,32]. The higher level of rotation provides a greater movement of the natural stoppers, which promotes a better interaction between the natural cork stopper surface and ozone, thus improving the mass transfer of the oxidizing species and the chromophore and chromogens structures present on the stopper surface [9].

In this way, it was applied the paired-samples T-test (Table 6.7) in the values of the color parameters of assay 4 (Table 6.5) to verify if there are differences among them before and after the implementation of ozone on the surface of the stopper and thus evaluate the effectiveness of the experimental conditions.

Table 6.7- Differences on the color parameters values of assay 4 before and after ORW using paired-samples T-test.

Assay	Color parameters pairs	Paired differences			*t*	Degree of freedom	*p*-value
		Std. error mean	95% confidence interval of the difference				
			Lower	Upper			
4	**Brightness baseline-brightness after**	0.520	-6.086	-3.856	-9.563	14	<0.001
	L* baseline-L* after	0.641	-5.752	-3.005	-6.836	14	<0.001
	a* baseline-a* after	1.538	1.345	3.048	5.532	14	<0.001
	b* baseline-b* after	2.225	1.151	3.616	4.148	14	<0.001

The paired samples T-test confirmed that after using the conditions of assay 4 occurs a significant improvement of the color parameters since the p-value for all the studied responses are less than 0.001, hence the conditions used in assay 4 are the preferable ones, allowing the empowerment of ozone reactive washing efficiency. Noteworthy that even in assay 4 the brightness gain of stoppers did not exceed 5% ISO brightness, which is much inferior to that observed in the treatment with hydrogen peroxide.

6.3.2. Surface characterization

Although the color parameters used up until now for the characterization of cork stoppers surface provides the visible characteristics, they did not explain the surface chemical changes that occurred in reaction with ozone. Such an analysis can be done by UV-vis DR. UV-vis DR (k/s) spectra of lateral and top cork stopper before and after ORW were acquired to analyze the origin of chromophore/chromogen structures in natural cork stopper and to provide basic information on gaseous ozone effect on the stopper surface (Figure 6.1).

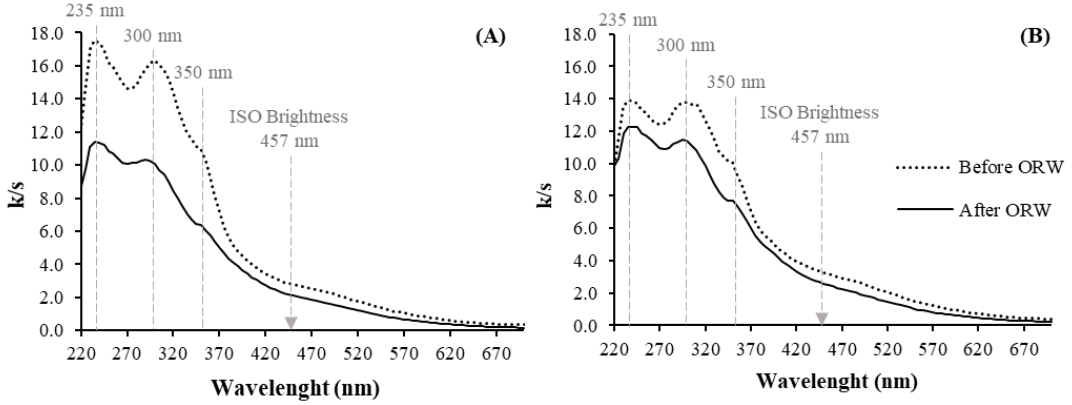

Figure 6.1- UV-vis DR (k/s) of the lateral (A) and top (B) of the natural cork stopper before and after ORW.

The lateral and top of the natural cork stopper revealed a distinct absorption intensity behavior through the wavelength. Before the ORW, the lateral surface possess higher absorption than the top in the range of 220-370 nm, at higher wavelength, the top shows more intensive absorption, which implies that the lateral surface is naturally brighter than the top since it has higher brightness values (looking k/s values at 457 nm), even though the lateral has much more chromogen structures (sharp bands at 235, 300, and 350 nm).

The DR spectra have two main peaks at 235 and 300 nm and a shoulder at 350 nm, that remain after ORW however a decrease in absorption intensity across the entire wavelength took place, which implies the removal of chromophore structures across the entire UV-vis spectrum. Ozone is a strong oxidant that can act directly on chromophore and chromogen structures. These structures arise mainly in pulp and wood from lignin (80-95%), carbohydrates (5-20%), and extractives (about 2%) that contribute to cork color and can induce the brightness reversion [35,36].

The first peak at 235 nm is assigned to double bonds conjugated with other electron-acceptor (COOH or CHO) functional groups arising, for example, from hexenuronic acid (HexA) groups that are formed from hemicelluloses under strong alkaline conditions [35–38]. In cork surface, the conjugated double bounds with electron-acceptor functional groups are in the composition of suberin, extractives of polyphenolic origin, and lignin. These structures are particularly abundant on the lateral of the cork stoppers (Figure 6.1). After ORW, this peak is significantly diminished which confirms the ozone effectiveness to remove such types of structures [37]. The reduction of these types of compounds translates into higher brightness stability of the stopper surface, hence lower brightness reversion, becoming an advantage of this procedure [9]**.** On the other hand, the peaks at 300 and 350 nm are associated with lignin structures and/or structures originated from lignin oxidation, and polyphenolics, such as quinones, α-carbonyl structures (coniferaldehyde, ferulic acid, p-coumaric acid, etc), nonconjugated phenolic groups, and aromatic conjugated structures, namely stilbenes, were also diminished after ozone action [36,38,39].

FTIR-ATR spectroscopy was used to assess the effect of ozone on the chemical composition of the stopper's surface, either on the lateral and top that reflected similar features as already been stated (Figure 6.2) [5]. The FTIR-ATR spectrum exhibits the typical peaks of the structural cork cell wall components, such as suberin, lignin, cellulose, and hemicelluloses. The intense band at 1735 cm^{-1} is characteristic in cork materials and is associated with the stretching vibration of C=O bond in ester groups mainly from suberin [5,40,41]. The band at 1634 cm^{-1} is assigned to stretching vibrations of C=C bond in conjugation with the aromatic ring of lignin or conjugated with COOH group, bands at 1605, 1511 and 1436 cm^{-1} belongs to the aromatic groups in lignin and polyphenolics, the bands at 1255 and 1162 cm^{-1} relates to the stretching vibrations of C−O bonds in esters and ethers,

respectively [40,42]. The bands at 1096 and 1031 cm^{-1} represent the stretching vibration of C−OH and bending of C−H, respectively, essentially from polysaccharides and lignin [5,42].

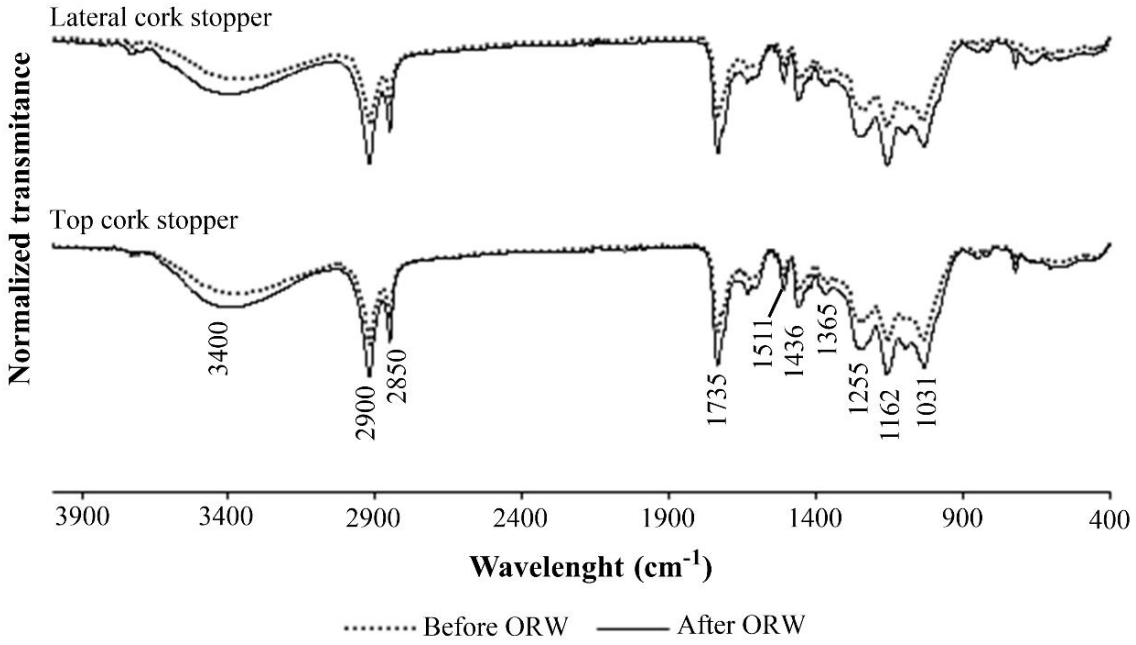

Figure 6.2- FTIR-ATR spectra of the lateral and top of the cork stopper before and after the ORW.

The main differences in the FTIR-ATR spectrum were found in the surface composition of the lateral and the top of the cork stopper after ORW. After ORW, an increase in intensity over almost all wavelengths took place. The peak at 1735 cm^{-1} attributed to the C=O stretching has increased after ORW. This could be due to lignin degradation and consecutively the formation of quinone and muconic acid type structures [43,44]. Additionally, the increase in the peak at 1735 cm^{-1} combined with the enhanced band assigned to the OH stretching vibrations at ca. 3400 cm^{-1} reveals the formation of new hydroxyl-containing functions (alcohol and carboxylic acid structures). The relative intensity of aromatic vibrations at *ca.*1605 cm^{-1} did not change significantly after ozone treatment [15,45]. Contrary to literature evidences in lignin reactions with ozone, the bands at 1511 cm^{-1} and 1463 cm^{-1} assigned to C=C groups in aromatic ring structure, increased in intensity, which shows that the lignin aromatic structures were not extensively degraded through aromatic ring opening, instead, it reveals a slightly higher number of aromatic rings that are in accordance with lignin condensation reactions [15,19,45,46]. One explanation may be drawn that along with the degradation of unsaturated structures, other structures of a similar nature could be formed upon oxidation with ozone.

On the other hand, an increase of absorbance in the peaks at 1365, 1255, 1162, 1096, and 1031 cm^{-1} occurred that can be associated with polysaccharides moieties, since lignin is degraded partially with ozone thus exposing better the cellulose and hemicelluloses for the analysis by ATR. Besides

this, the increase in the intensity of the signals at 1162 and 1035 cm^{-1} after ORW could also imply the cleavage of some ether linkages with the formation of new OH groups (evidenced at 3400 cm^{-1}) [47,48]. These cleaved ether bounds could belong either to suberin or lignin or hemicelluloses [4,41,49]. Anyway, the FTIR spectra indicated an increase in polar oxidized moieties on the surface of stoppers after the treatment with ozone.

6.3.3. Surface morphology and topology of the cork stopper

Scanning electron microscopy (SEM) shows the morphology of the lateral and the top of the stopper before and after ORW (Figure 6.3). Thus, the SEM micrograph images of the lateral were obtained in two different configurations, the lateral before ORW (Figure 6.3, A) was acquired at the tangential section with rectangles placed in parallel, while the lateral after ORW (Figure 6.3, B) shows the characteristic radial section with an alveolar structure, without intercellular space [5].

The top of the stopper reveals the conventional axial section with cells that resemble rectangles placed in parallel. After ORW, no significant changes can be observed which shows that the ozone action does not play a major modification on the stopper morphology.

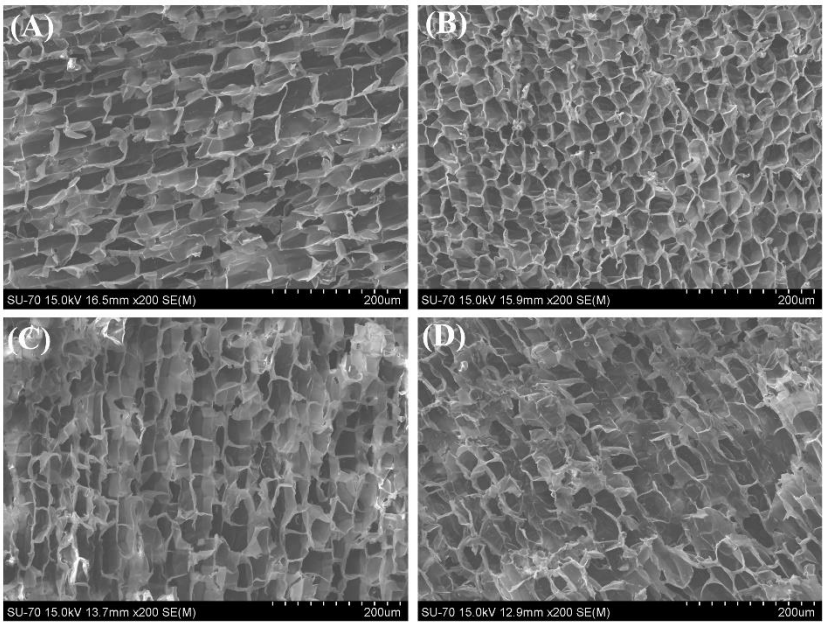

Figure 6.3- SEM micrograph images of the untreated cork stopper surface: the lateral (A) and top (C) at 200x, and lateral (B) and the top (D) at 200x after ORW.

The surface roughness of the lateral and top of the stoppers, given by the roughness average parameter R_a, the arithmetical average of the absolute values of the profile heights over the evaluation length, assessed by a surface roughness tester, also revealed some differences. As already revealed, the lateral of the stoppers has *ca.* 30% less roughness when compared to the top (Table 6.8), including the parametric values of the maximum profile heigh peak (R_p) and of valley depth (R_v) [5]. These

differences in the surface roughness of the lateral and the top can be explained by the different methodologies of cut in the two surface areas, the top is obtained with a saw while cutting the strips, whereas the lateral arises when using a hollow drill while punching the stoppers causing an increase in the roughness in the top.

Table 6.8- Roughness parameters of the top and lateral surfaces of the natural cork stopper before and after ORW as revealed by profilometry according to standard ISO 4287-1997.

Stopper sample	Lateral (μm)			Top (μm)		
	R_a (±SD)	R_p (±SD)	R_v (±SD)	R_a (±SD)	R_p (±SD)	R_v (±SD)
Before ORW	4.7±1.8	13.4 ±4.1	14.1±3.7	7.5±1.9	18.9±4.5	21.1±5.4
After ORW	4.6±1.3	12.4±2.5	14.5±3.2	7.9±1.4	19.7±2.5	21.3±3.4

After ORW, there are no significant changes in the surface roughness, since the values maintain their order of magnitude, however, it is observed that the overall standard deviation (SD) of each parameter has decreased which implies that after ORW the stopper surface gains roughness homogeneity.

6.3.4. HS-SPME/GC-MS odor evaluation

The analysis of aroma compounds in natural products that are in contact with alimentary products, as is the case of cork stoppers, is widely used to evaluate the eventual organoleptic effects [50,51]. The cork stoppers can release volatile compounds into a wine-like medium affecting its aroma, which may have repercussions on the final product and consequently to the wine quality. In this way, it was evaluated what type of compounds are capable to be released from the natural cork stoppers after ORW into the atmosphere at the ambient temperature and normal pressure. The volatile organic compounds released as well as the retention time and the percentual concentrations are depicted in Table 6.9.

Table 6.9- Volatile organic compounds released by natural cork stoppers before and after ORW: retention time (RT) and percentual analysis of each compound.

Compounds	RT (min)	Before ORW (%)	After ORW (%)
Alkanes		**2.04**	**1.92**
2,3,4-trimethyl-hexane	9.31	0.30	-
2,6,8-trimethyl-decane	13.23	0.21	-
Tridecane	18.81	0.64	-
2,6-dimethyl-heptadecane	22.64 /25.45	1.19	1.92
Aldehydes		**10.45**	**14.02**
Pentanal	5.86	0.32	0.71
2,3-dihidroxy-propanal	6.10	-	0.78
Hexanal	7.78	0.83	3.21

Heptanal	10.44	0.13	1.03
Benzaldehyde (lignin related)[52]	12.24	-	0.52
2-benzoyloxyl-R-Propanal	12.50	0.20	-
Octanal	13.44	0.28	0.99
Nonanal	16.38	2.73	2.42
Decanal	19.00	1.04	1.49
Undecanal	21.08	-	0.58
Vanillin (lignin related)	22.84	-	2.29
5-octadecenal	26.23	0.52	0.00
Acid carboxylic		**87.03**	**69.04**
Formic Acid	4.47	2.63	17.86
Acetic Acid	5.37	82.91	37.10
Formyl acetate	5.59	1.15	-
Propanoic acid	5.74	-	0.36
2,3-diacetyloxybutanedioic acid	6.36	-	0.10
Acetyl acetate	6.49	-	0.26
Acetoxyacetic acid	7.19	-	4.90
Dimethyl oxalate	8.59	-	1.74
4-hydroxy-butanoic acid	10.79	-	0.53
Hexanoic acid	13.18	-	1.97
Heptanoic acid	15.76	-	0.20
7-oxo-octanoic acid	17.67	-	0.18
Octanoic acid	18.34	-	0.65
3-tridecyl ester valeric acid	20.24	-	0.17
Nonanoic acid	20.53	-	2.60
Phthalic acid	28.66	0.34	0.27
Ketones		**0.00**	**13.49**
Acetone	4.22	-	6.08
2-hexanone	7.55	-	0.20
2-butanone	9.23	-	1.16
4-methyl-2-hexanone	6.72/10.06 /12.98	-	2.08
2-Nonanone	16.01	-	0.77
5-methyl-2-hepanone	17.14	-	0.19
3-decanone	18.55	-	0.21
2-decanone	18.67	-	0.80
2-Undecanone	20.82	-	1.62
Dodecalactone	22.18	-	0.38
Alcohols		**0.09**	**1.54**
3-methyl-1-butanol	8.41	-	0.09
2,7-dimethyl-1-octanol	15.44	-	0.39
6-methyl-1-heptanol	17.03	-	0.25
E-2-tetradecen-1-ol	24.33	-	0.66
2-hexadecanol	27.47	0.09	0.14
Furans		**4.40**	**-**
Furfural	8.67	4.40	-

The volatile organic compounds class present in the natural cork stoppers in greater amounts are the carboxylic acids (87.03%), followed by the aldehydes (10.45%) (Table 6.9). Within the acid carboxylic compounds is found acetic acid, which is the compound with a higher percentage on the overall (82.91%). This fact indicates that the odor released by the natural cork stoppers is influenced by the presence of acetic acid, which has a sour odor (Figure 6.4). Acid acetic was already found as a volatile compound present in cork [50,52] and, also in wine composition [53], this compound could be a product of the fungi activity and/or even a product of lipid oxidation. The second compound in higher percentage is furfural that is recognized by sweet, caramel, and almond notes (Figure 6.4). Furfural derives mainly from carbohydrate degradation products and may be a potential source of browning in natural products [51,54]. Among the aldehyde's compounds, nonanal and decanal are the compounds more representative with 2.73 and 1.04%, respectively. These compounds have already been recognized as cork volatile compounds [50,52], and are responsible for a sweeter and citrus odor (Figure 6.4). Alkanes (2.04%) have a higher odor threshold and do not represent a major role in odor impact [55], as for the alcohols with only 0.09% are associated with floral and grassy notes [55,56], but due to its low concentration do not represent a major influence in the overall odor pallet (Figure 6.4).

After ORW several differences can be observed, occurs a decrease of acid carboxylic and alkanes compounds accompanied by an increase of aldehydes, ketones, and alcohols compounds. However, the acid carboxylic compounds maintain the highest percentual value between the classes of compounds with 69.10%. The increase in carbonyl compounds, aldehydes, and ketones, could be explained by the degradation of fatty acids present in wax and suberin fraction of the cork by ozone action [51,55,57,58]. In fact, before ORW there was no ketones detected in the headspace, which after ORW has an expressive value (13.49%), as for the aldehydes it increases from 10.45 to 14.02%, as shown in Table 6.9. These types of compounds even in low amounts are responsible for strong aromas because of the low perception thresholds and sensory descriptors, increasing the odor perception of the natural cork stoppers after ORW (Figure 6.4) [51,59]. Among aldehydes, hexanal is the main linear aliphatic aldehyde (3.21%) followed by nonanal and decanal with 2.42 and 1.49, respectively. Hexanal is recognized by a green and grass odor, while nonanal and decanal have citrus and flowery notes [55,56]. Hexanal is the major product of oxidation of linoleic acid, while nonanal is a product of oxidation of oleic acid [51,57]. The presence of vanillin (2.29%) and benzaldehyde (0.52%) after ORW proves the action of ozone on the lignin structure and possesses vanillin and almond odor, respectively. In the ketone compounds group, the compound in higher percentage is the acetone (6.08%), followed by 4-methyl-2-hexanone (2.08%) and 2-undecanone (1.62%), which are responsible for the sweet, citrus, green, and fresh odors (Figure 6.4).

As for the alcohols compounds, it occurs an increase in the overall percentage (from 0.09 to 1.54%), increasing equally the diversity of volatile alcohols obtained, however, these values are consistently low with floral and grassy odor descriptors [55,56]. 3-methyl-1-butanol (0.09%) was already found as aliphatic alcohol in another cork samples studied and it has a slightly moldy odor [51,52]. Among the acid carboxylic compounds, acid acetic still is the compound that has higher importance in cork off-flavor, on the other hand formic acid is the compound that had the highest increment after ORW, which reveals the effectiveness of ozone oxidation over the cork compounds and it relates to a green odor [56].

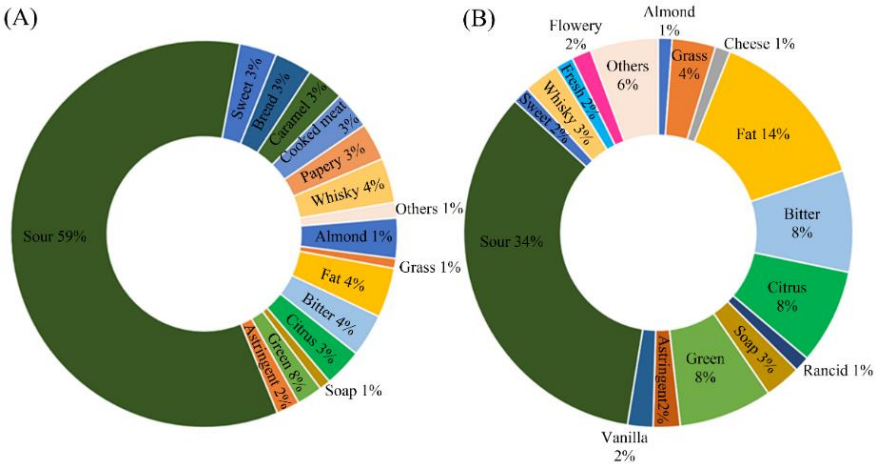

Figure 6.4- Odor perception of natural cork stoppers before (A) and after ORW (B).

Through Table 6.9 and Figure 6.4 it is recognized that the carbonyl compounds (aldehydes and ketones) and the acid carboxylic compounds in higher percentages are the major compounds responsible for the odors such as sour, fat almond, sweet, green, citrus, green, bitter. The other odors presented in Figure 6.4 are derived from other compounds of this group that are in lower concentration, but also contributed to the overall odor characteristics. From the odor descriptor point of view (Figure 6.4), both cork stoppers before and after ORW had the highest percentage to the sour odor descriptor that is justified by the amounts of acid acetic founded. However, after the ORW, the odor descriptors gain more diversity with more expressive percentages showing an enrichment of the odor after ORW.

6.3.5. Surface wettability

Contact angles with the three probe liquids (water, formamide, and diiodomethane) were measured in the two cork stopper areas (lateral and top) before and after ORW (Table 6.10). In turn, the free surface energy (FSE) was evaluated (Figure 6.5). The obtained values revealed that this material has a rather low-energy surface similar to hydrophobic polymers [60]. This is mainly to the

high content in suberin (44%) in cork cell walls poorly contributing to the polar component of FSE [42,61].

Table 6.10- Contact angles of the top and the lateral of the cork stopper with water, formamide and diiodomethane before and after ORW.

Liquid probe	Measured contact angle (deg.)			
	Top of the cork stopper (TCS)		Lateral of the cork stopper (LCS)	
	Before ORW	After ORW	Before ORW	After ORW
Water	99.2±5.6	96.1±3.2	136.0±3.2	137.4±2.2
Formamide	101.2±5.2	83.8±2.9	115.1±5.0	77.7±3.3
Diiodomethane	77.7±5.0	74.2±6.3	81.3±6.2	85.8±3.5

The lateral of the cork stopper before ORW showed higher values for the contact angles with the three probe liquids than the top of the cork stopper, with a greater FSE (20.5 *vs.* 16.0 mN/m). However, the top has a higher polarity index (γ_S^p/γ_S) than the lateral (0.193 *vs.* 0.107) (Figure 6.5). These features may be related to the fact that in the lateral surface the cell wall layers are richer in exposed suberin, and lower in polysaccharides content [5].

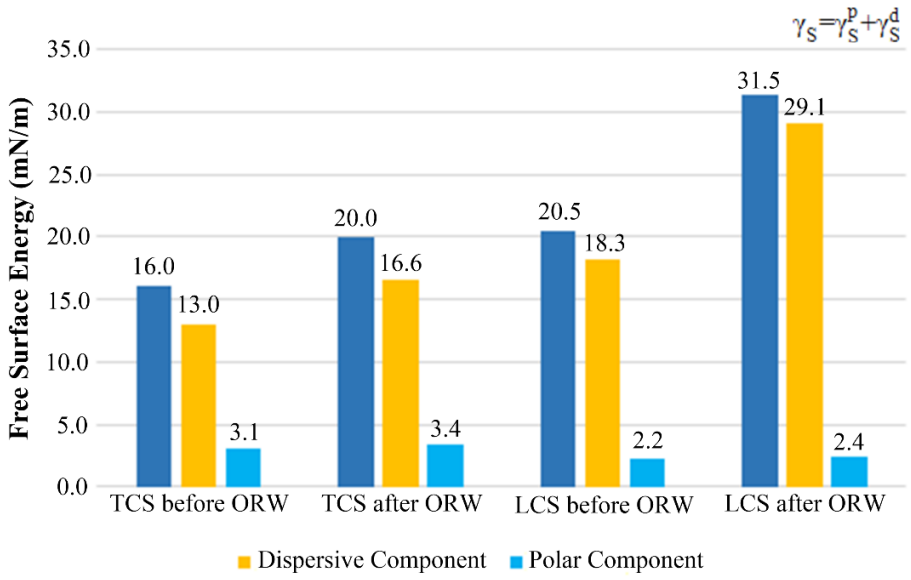

Figure 6.5- Contribution of polar and dispersive components to the total free surface energy of the lateral (LCS) and top (TCS) of the cork before and after ORW.

After ORW the FSE was increased for the top (from 16.0 to 20.0 mN/m) and the lateral (from 20.0 to 31.5 mN/m), being more pronounced for the lateral. This occurred with a significant decrease in polarity index from 0.193 to 0.170 for the top and from 0.107 to 0.076 for the lateral, which is in accordance with the contact angle values. Since the contact angle with water before and after ORW does not change significantly (Table 6.10), only a slight increase in the surface polar component (0.3 mN/m for the top and 0.2 mN/m for the lateral) took place, while the contact angles value with formamide and diiodomethane show considerable differences, which correspond to an increase in

the dispersive component for either the lateral (from 18.3 to 29.1 mN/m) or the top (from 13.0 to 16.6 mN/m), contributing to an improved wettability with apolar solvents.

The changes posterior to ozone treatment on the cork surface wettability towards hydroalcoholic solutions mimicking alcoholic beverages were assessed through the wetting envelope in polar-dispersive energy coordinates (Figure 6.6). Simulations were made for contact angles of 0, 45, 60, and 90°, allowing the study of surface wetting from completely wettable (0°) to non-wettable (90°). The hydroalcoholic solutions in the study comprise different ethanol percentages varying between 12, 14, 20, and 40% (v/v) and pure water. The wettability of such solutions increased gradually with the rise of ethanol in the solution, being the highest wettability observed for the solution containing 40% of ethanol (Figure 6.6). The lateral surface of the cork stopper before ORW is non-wettable with any of the solutions in the study (12-40% ethanol v/v) and water, on the other hand, the top surface of the cork stoppers is non-wettable only with water and partial wettable (contact angle of 60-90°) towards ethanol solutions.

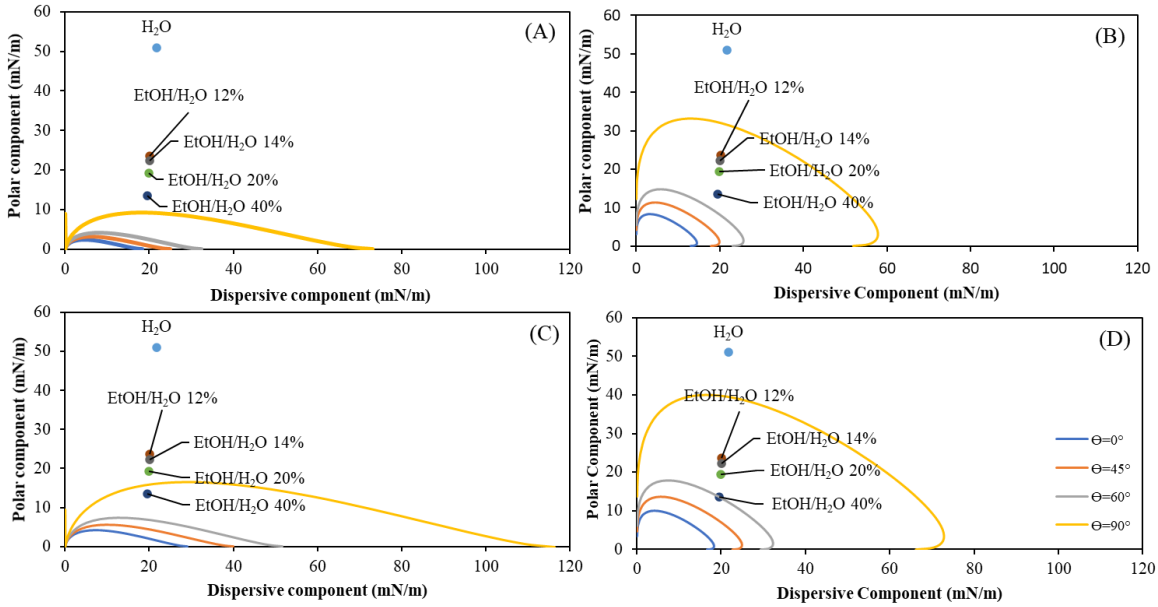

Figure 6.6- Wetting envelope of the lateral (A) and the top (B) of the cork stopper surface before ORW and of the lateral (C) and top (D) of the cork stopper surface after ORW.

After ORW, the cork stopper surface wettability suffers some changes (Figure 6.6). Both lateral and top are slightly more wettable, mainly for the high percentage ethanol solution (40% ethanol v/v). This is explained by the FSE polar and dispersive counterparts, in both surfaces occurs a notable increment of the dispersive component providing higher wettability with ethanol solutions. However, both lateral and top surfaces maintained their hydrophobic properties, because are non-wettable by water (θ>90º). The lateral surface of the cork stopper, even though it had the highest change in FSE

after ORW due to a significant increase in dispersive component did not show major differences in the wettability because the polar component was only slightly increased.

6.4. Conclusions

This study evaluates the implementation of ozone as a bleaching agent for natural cork stoppers. With only 15 minutes of ozone reactive washing, the ozone treatment allowed the best brightness gaining results with a temperature of 70ºC, a rotation velocity of 120 rpm, and an inlet oxygen flow of 50 L/h (production of 1.8 g/h of ozone), allowing the maximal increase of the coordinate L* and ISO brightness and the decrease of coordinates a* and b*. These results are, however, much moderated than the observed in reactive washing with hydrogen peroxide under alkaline conditions.

Ozone is a strong oxidant and is able to react with cork unsaturated compounds, as shown by the UV-vis analysis, revealing a decrease in absorption intensity across the entire spectrum range (220-700 nm) which confirms the action of ozone in the cork thus being capable to degrade both chromogen and chromophore structures. Additionally, FTIR-ATR analysis shows that ozone degrades cork components, in particular lignin, suberin, and polysaccharides with the formation on the surface of new oxidized moieties. FTIR-ATR analysis also reveals an increase of C=O groups belonging to ester, carbonyl and carboxyl-containing structures, which agrees with the HS-SPME/ GC-MS analysis that demonstrates the formation of volatile ketones and aldehydes after ORW and an increase of carboxylic acids. The formation of these compounds is associated with different odors, increasing the odor perception of natural cork stoppers after ORW. It was also proposed that the treatment with ozone lead to the formation of secondary chromophore structures that seal the development of stoppers brightness.

The increase of the free surface energy of the stoppers surface after the treatment with ozone increases its wettability, especially with hydroalcoholic solutions. The latter fact is due to the decrease in polarity index after the treatment with ozone. These surface changes occur mainly due to the polar components degradation, which leads to a greater exposure of suberin moieties, and consequently more hydrophobic surface. However, the surface of the stoppers maintains hydrophobicity, i.e., low wettability with water. The surface changes were moderate for the lateral showing a wettability with strong hydroalcoholic solutions only (40% EtOH/H_2O solution). The top surface of stoppers was wettable practically with all hydroalcoholic solutions examined (12-40% EtOH/H_2O solutions).

The results of this work provide fundamental knowledge for the implementation of ozone as a bleaching agent for natural cork stoppers.

6.5. References

[1] T.J. Dyer, Elucidating the formation and chemistry of chromophores during kraft pulping, 2004.

[2] D.N.S. Hon, W. Glasser, On Possible Chromophoric Structures in Wood and Pulps — a Survey of the Present State of Knowledge, Polym. Plast. Technol. Eng. 12 (1979) 159–179. https://doi.org/10.1080/03602557908067670.

[3] G. Zucchini, A. Donati, Process for bleaching and sterilizing cork articles, and cork articles bleached using the said process, US 005098447A, 1992.

[4] J.R. Gonzalez-Adrados, M.C. Garcia-Vallejo, M.J. Caceres-Esteban, J.L. Garcia De Ceca, F. Gonzalez-Hernandez, R. Calvo-Haro, Control by ATR-FTIR of surface treatment of cork stoppers and its effect on their mechanical performance, Wood Sci. Technol. 46 (2012) 349–360. https://doi.org/10.1007/s00226-011-0403-5.

[5] D.G. Branco, C.A. Santiago, F.J. Oliveira, L. Cabrita, D. V Evtuguin, Surface properties of cork in relation to reactive washing, Colloids Surfaces A Physicochem. Eng. Asp. 624 (2021). https://doi.org/10.1016/j.colsurfa.2021.126762.

[6] H.A. Eren, S. Eren, Ozone bleaching of cellulose, IOP Conf. Ser. Mater. Sci. Eng. 254 (2017) 1–3. https://doi.org/10.1088/1757-899X/254/8/082009.

[7] F. Arooj, N. Ahmad, I.A. Shaikh, M.N. Chaudhry, Application of ozone in cotton bleaching with multiple reuse of a water bath, Text. Res. J. 84 (2013) 527–538. https://doi.org/10.1177/0040517513499429.

[8] P. Bajpay, Hot peroxide bleaching, Can. Chem. News. 50 (1998) 15–17.

[9] E. Germer, A. Métais, J.C. Hostachy, Achievements in industrial ozone bleaching, Japan Tappi J. 65 (2011) 780–787. https://doi.org/10.2524/jtappij.65.780.

[10] R. Travaini, J. Martín-Juárez, A. Lorenzo-Hernando, S. Bolado-Rodríguez, Ozonolysis: An advantageous pretreatment for lignocellulosic biomass revisited, Bioresour. Technol. 199 (2016) 2–12. https://doi.org/10.1016/j.biortech.2015.08.143.

[11] M. Prabaharan, J.V. Rao, Study on ozone bleaching of cotton fabric-process optimisation, dyeing and finishing properties, Color. Technol. 117 (2001) 98–103. https://doi.org/10.1111/j.1478-4408.2001.tb00342.x.

[12] Z.B. Guzel-Seydim, A.K. Greene, A.C. Seydim, Use of ozone in the food industry, LWT - Food Sci. Technol. 37 (2004) 453–460. https://doi.org/10.1016/j.lwt.2003.10.014.

[13] T. Miyanishi, Theory and practice of ozone bleaching, Japan Tappi J. 72 (2018) 435–439. https://doi.org/10.2524/jtappij.1702.

[14] C. Li, L. Wang, Z. Chen, Y. Li, R. Wang, X. Luo, G. Cai, Y. Li, Q. Yu, J. Lu, Ozonolysis

pretreatment of maize stover: the interactive effect of sample particle size and moisture on ozonolysis process, Bioresour. Technol. 183 (2015) 240–247. https://doi.org/10.1016/j.biortech.2015.01.042.

[15] M. V Bule, A.H. Gao, B. Hiscox, S. Chen, Structural modification of lignin and characterization of pretreated wheat straw by ozonation, J. Agric. Food Chem. 61 (2013) 3916–3925. https://doi.org/10.1021/jf4001988.

[16] M.T. García-Cubero, L.G. Palacín, G. González-Benito, S. Bolado, S. Lucas, M. Coca, An analysis of lignin removal in a fixed bed reactor by reaction of cereal straws with ozone, Bioresour. Technol. 107 (2012) 229–234. https://doi.org/10.1016/j.biortech.2011.12.010.

[17] R.M.S. Simões, J.A.A.M. e Castro, Ozone delignification of pine and eucalyptus kraft pulps. 2. Selectivity, Ind. Eng. Chem. Res. 38 (1999) 4608–4614. https://doi.org/10.1021/ie980807o.

[18] A. Seisto, K. Poppius-Levlin, A. Fuhrmann, Effect of ozone bleaching on the fibre properties of pine and birch kraft pulp, Cellul. Pulps, Fibres Mater. (2000) 137–147. https://doi.org/10.1533/9781845698546.137.

[19] N.A. Mamleeva, S.A. Autlov, N.G. Bazarnova, V. V. Lunin, Delignification of softwood by ozonation, Pure Appl. Chem. 81 (2009) 2081–2091. https://doi.org/10.1351/PAC-CON-08-10-11.

[20] M. Prabaharan, R.C. Nayar, N.S. Kumar, J.V. Rao, A study on the advanced oxidation of a cotton fabric by ozone, Color. Technol. 116 (2000) 83–86. https://doi.org/10.1111/j.1478-4408.2000.tb00024.x.

[21] S.D. Perincek, K. Duran, A.E. Korlu, I.M. Bahtiyari, An investigation in the use of ozone gas in the bleaching of cotton fabrics, Ozone Sci. Eng. 29 (2007) 325–333. https://doi.org/10.1080/01919510701509578.

[22] G. Moore, C. Griffith, A. Peters, Bactericidal properties of ozone and its potential application as a terminal disinfectant, J. Food Prot. 63 (2000) 1100–1106. https://doi.org/10.4315/0362-028X-63.8.1100.

[23] J. Rounsaville, R.G. Rice, Evolution of ozone for the bleaching of paper pulps, Ozone Sci. Eng. 18 (1996) 549–566. https://doi.org/10.1080/01919512.1997.10382863.

[24] H. Sixta, H.-U. Suss, M. Schwanninger, A.W. Krotscheck, Pulp bleaching, in: H. Sixta (Ed.), Handb. Pulp, 1st Ed., WILEY-VCH Verlag GmbH & Co. KGaA, Lenzing, Austria, 2006: pp. 609–932. https://doi.org/10.1002/9783527619887.

[25] V. Gomes, J.L. Colodette, Um novo conceito de branqueamento de polpa kraft de eucalipto com ozônio em média consistência, Quim. Nova. 40 (2017) 54–59. https://doi.org/10.21577/0100-4042.20160149.

[26] R. Atav, A. Yurdakul, Effect of the ozonation process on the dyeability of mohair fibres, Color. Technol. 127 (2011) 159–166. https://doi.org/10.1111/j.1478-4408.2011.00293.x.

[27] P. Bajpai, Environmentally Friendly Production of Pulp and Paper, John Wiley & Sons, Inc., 2010. https://doi.org/10.1002/9780470649657.

[28] D.M. Hembree, H.R. Smyrl, Anomalous dispersion effects in diffuse reflectance infrared fourier transform spectroscopy: a study of optical geometries, Appl. Spectrosc. 43 (1989) 267–274. https://doi.org/10.1366/0003702894203057.

[29] D.K. Owens, R.C. Wendt, Estimation of the surface free energy of polymers, J. Appl. Polym. Sci. 13 (1969) 1741–1747. https://doi.org/10.1002/app.1969.070130815.

[30] T. Nguyen, W.E. Johns, Polar and dispersion force contributions to the total surface free energy of wood, Wood Sci. Technol. 12 (1978) 63–74. https://doi.org/10.1007/BF00390011.

[31] E. Cogo, J. Albet, G. Malmary, C. Coste, J. Molinier, Effect of reaction medium on ozone mass transfer and applications to pulp bleaching, Chem. Eng. J. 73 (1999) 23–28. https://doi.org/10.1016/S1385-8947(99)00011-X.

[32] G. Koch, Raw Material for Pulp, in: H. Sixta (Ed.), Handb. Pulp, 1st Ed., WILEY-VCH Verlag GmbH & Co. KGaA, Lenzing, Austria, 2006: pp. 21–68. https://doi.org/10.1002/9783527619887.

[33] B.A. Griffith, A.E.R. Westman, B.H. Lloyd, Analysis of variance. Part I- Variance, the F-test, and the analysis of variance table, Qual. Eng. 2 (1989) 195–226. https://doi.org/10.1080/08982118908962713.

[34] D.C. Montgomery, Design and analysis of experiments, 9th Ed., John Wiley & Sons, Inc., 2017.

[35] P.E.G. Loureiro, A.J.S. Fernandes, F.P. Furtado, M.G.V.S. Carvalho, D. V Evtuguin, UV-ressonance Raman micro-spectroscopy to assess residual chromophores in cellulosic pulps, J. Raman Spectrosc. 42 (2011) 1039–1045. https://doi.org/10.1002/jrs.2816.

[36] T. Tribulová, F. Kacík, D. Evtuguin, I. Cabalová, Assessment of chromophores in chemically treated and aged wood by UV-vis diffuse reflectance spectroscopy, Cellul. Chem. Technol. 50 (2016) 659–667.

[37] K.M.M. Eiras, J.L. Colodette, V.L. Silva, L.C.A. de Barbosa, New insights on brightness stability of eucalyptus kraft pulp, Nord. Pulp Pap. Res. J. 23 (2008) 102–107. https://doi.org/10.3183/npprj-2008-23-01-p102-107.

[38] A. Lähdetie, T. Liitiä, T. Tamminen, A.S. Jääskeläinen, Reflectance UV-Vis and UV resonance Raman spectroscopy in characterization of kraft pulps, BioResources. 4 (2009) 1600–1619. https://doi.org/10.15376/biores.4.4.1600-1619.

[39] J.-X. Sun, X.-F. Sun, R.-C. Sun, P. Fowler, M.S. Baird, Inhomogeneities in the chemical

structure of sugarcane bagasse lignin, J. Agric. Food Chem. 51 (2003) 6719–6725. https://doi.org/10.1021/jf034633j.

[40] C. Ortega-Fernández, J.R. González-Adrados, M.C. García-Vallejo, R. Calvo-Haro, M.J. Cáceres-Esteban, Characterization of surface treatments of cork stoppers by FTIR-ATR, J. Agric. Food Chem. 54 (2006) 4932–4936. https://doi.org/10.1021/jf0529823.

[41] M.H. Lopes, A.S. Barros, C. Pascoal Neto, D. Rutledge, I. Delgadillo, A.M. Gil, Variability of cork from portuguese quercus suber studied by solid-state ^{13}C-NMR and FTIR spectroscopies, Biopolymers. 62 (2001) 268–277. https://doi.org/10.1002/bip.1022.

[42] D.G. Branco, J.R. Campos, L. Cabrita, D. V. Evtuguin, Structural features of macromolecular components of cork from *Quercus suber* L., Holzforschung. 74 (2020) 625–633. https://doi.org/10.1515/hf-2019-0271.

[43] J. Gierer, The Chemistry of Delignification - A General Concept - Part II, Holzforschung. 36 (1982) 55–64. https://doi.org/10.1515/hfsg.1982.36.2.55.

[44] D. V. Evtuguin, G. Rocha, B.J. Goodfellow, Detection of muconic acid type structures in oxideised lignin using 2D NMR spectroscopy, Holzforschung. 63 (2009) 675–680. https://doi.org/10.1515/HF.2009.083.

[45] J. Liao, S. He, L. Mo, S. Guo, P. Luan, X. Zhang, J. Li, Mass-production of high-yield and high-strength thermomechanical pulp fibers from plant residues enabled by ozone pretreatment, J. Clean. Prod. 296 (2021) 1–9. https://doi.org/10.1016/j.jclepro.2021.126575.

[46] D. Areskogh, J. Li, G. Gellerstedt, G. Henriksson, Structural modification of commercial lignosulphonates through laccase catalysis and ozonolysis, Ind. Crops Prod. 32 (2010) 458–466. https://doi.org/10.1016/j.indcrop.2010.06.016.

[47] S. Omori, C.W. Dence, The reactions of alkaline hydrogen peroxide with lignin model dimers. Part 2. Guaiacylglycerol-β-Guaiacyl ether, Wood Sci. Technol. 15 (1981) 113–123. https://doi.org/10.1007/BF00367858.

[48] S. Omori, C.W. Dence, The reactions of alkaline hydrogen peroxide with lignin model dimers - Part 1: Phenacyl α-aryl ethers, Wood Sci. Technol. 15 (1981) 67–79. https://doi.org/10.1007/BF00366502.

[49] G. González-Gaitano, M.A.C. Ferrer, Definition of QC parameters for the practical use of FTIR-ATR spectroscopy in the analysis of surface treatment of cork stoppers, J. Wood Chem. Technol. 33 (2013) 217–233. https://doi.org/10.1080/02773813.2013.779715.

[50] N. Boudaoud, L. Eveleigh, A new approach to the characterization of volatile signatures of cork wine stoppers, J. Agric. Food Chem. 51 (2003) 1530–1533. https://doi.org/10.1021/jf025844b.

[51] S. Rocha, I. Delgadillo, A.J.F. Correia, GC-MS study of volatiles of normal and

microbiologically attacked cork from Quercus suber L, J. Agric. Food Chem. 44 (1996) 865–871. https://doi.org/10.1021/jf9500400.

[52] M. Careri, V. Mazzoleni, M. Musci, R. Molteni, Effects of electron beam irradiation on cork volatile compounds by gas chromatography-mass spectrometry, Chromatographia. 49 (1999) 166–172. https://doi.org/10.1007/BF02575280.

[53] E. Campo, V. Ferreira, A. Escudero, J. Cacho, Prediction of the wine sensory properties related to grape variety from dynamic-headspace gas chromatography-olfactometry data, J. Agric. Food Chem. 53 (2005) 5682–5690. https://doi.org/10.1021/jf047870a.

[54] A.-N. Yu, B.-G. Sun, D.-T. Tian, W.-Y. Qu, Analysis of volatile compounds in traditional smoke-cured bacon (CSCB) with different fiber coatings using SPME, Food Chem. 110 (2008) 233–238. https://doi.org/10.1016/j.foodchem.2008.01.040.

[55] B. Di Donfrancesco, K. Koppel, Sensory characteristics and volatile components of dry dog foods manufactured with sorghum fractions, Molecules. 22 (2017). https://doi.org/10.3390/molecules22061012.

[56] C.-Y. Qian, W.-X. Quan, Z.-M. Xiang, C.-C. Li, Characterization of volatile compounds in four different rhododendron flowers by GCxGC-QTOFMS, Molecules. 24 (2019). https://doi.org/10.3390/molecules24183327.

[57] N. Moreira, P. Lopes, M. Cabral, P. Guedes de Pinho, HS-SPME/GC-MS methodologies for the analysis of volatile compounds in cork material, Eur. Food Res. Technol. 242 (2016) 457–466. https://doi.org/10.1007/s00217-016-2636-x.

[58] M.C. Barreto, L.V. Boas, L.C. Carneiro, M. V. San Romão, Volatile compounds in samples of cork and also produced by selected Fungi, J. Agric. Food Chem. 59 (2011) 6568–6574. https://doi.org/10.1021/jf200560e.

[59] N. Moreira, S. Meireles, T. Brandão, P.G. de Pinho, Optimization of HS-SPME-GC-IT/MS method using a Central Composite Design for volatile carbonyl compounds determination in beers, Talanta. 117 (2013) 523–531. https://doi.org/10.1016/j.talanta.2013.09.027.

[60] H. Kaelble, K.C. Uy, A reinterpretation of organic liquid-polytetrafluoroethylene surface interactions, J. Adhes. 2 (1970) 50–60. http://dx.doi.org/10.1080/0021846708544579.

[61] C. Gomes, A. Fernandes, B. Almeida, The surface tension of cork from contact angle measurements, J. Colloid Interface Sci. 156 (1993) 195–201. https://doi.org/10.1006/jcis.1993.1099.

Chapter 7

INFLUENCE OF OZONE IN THE OPTIMIZATION OF THE CONVENTIONAL REACTIVE WASHING

Content

7.1. Introduction

Nowadays, RW uses hydrogen peroxide (H_2O_2) under strong alkaline conditions (pH>11), guaranteed by the addition of sodium hydroxide (NaOH), and increased temperature [1–3]. These conditions provide the formation of hydroperoxide anion (HO_2^-), which is the active specie that reacts with the chromophore structures in the cork stopper surface leading to an increase in its brightness, in addition to its disinfection [3]. The reagents that did not react (H_2O_2 and NaOH) are washed with water and consecutive sodium bisulfate solution to neutralize the alkalinity in the cork surface. Since the cork stoppers are in contact with beverages is mandatory the use of reagents of high-grade quality according to food safety requirements, which results in higher costs.

The reaction between hydrogen peroxide and sodium hydroxide solutions is exothermic and relatively harsh, that as already stated in another chapter may induce changes on the main macromolecular cork components and consequently, changes in the surface properties of the cork stopper making them more hydrophilic that in turn affects negatively their subsequent receptivity towards various coatings, such as food-grade paraffin and silicon emulsions [4,5]. The coating has as the main functions impermeability control, sealing, and extraction of cork stoppers [5,6]. Hence, the overload of reagents alters adversely the consumption properties of cork stoppers and is disadvantageous economically.

The demand for natural cork stoppers with different brightness shades leads to an adjustment on the reagent's addition, and the final product is properly evaluated through ISO brightness. Chapter 5 showed the optimization of RW that lead to a reduction of 37% of hydrogen peroxide concentration and 33% of the sodium hydroxide concentration and water washing volume while improving the physical properties of the natural cork stoppers and maintained the desired ISO brightness.

In chapter 6 it was applied ozone as a bleaching agent in the natural cork stoppers, which showed that only 15 minutes of treatment was able to slightly increase the ISO brightness of the cork stopper surface while enhancing the surface properties of the stopper, however the ISO brightness after ozone treatment did not reach the target value of 33.78%.

The challenge of the study presented in this chapter is combining these two reactive washings processes in a unique and sequential methodology, increasing the ISO brightness, while improving the surface properties of the stopper, reducing the consumption of reagents of the conventional reactive washing (hydrogen peroxide, sodium hydroxide, and water), and the process time.

The main purpose of the work displayed in this chapter is to conjugate the ozone reactive washing (ORW) with the conventional reactive washing (CRW), and in this way understand how the ORW in the preliminary stage can help on the optimization of the CRW by analyzing the effect of operational variables, such as concentrations of hydrogen peroxide and sodium hydroxide, process

time and volume of washing water applied, on the ISO brightness of the cork stopper surface. To achieve this objective, it was applied the RSM approach with a fractional factorial design of three levels and four factors that allowed the optimization of the CRW to reach a defined ISO brightness target.

7.2. Materials and Methods

Natural cork stoppers, as well as the reagents (hydrogen peroxide, sodium hydroxide, and sodium bisulfate), were supplied by Amorim Cork, S.A. (Santa Maria de Lamas, Portugal). Cork stoppers have a single caliber of 49x24 mm (length x diameter), belong to the 1st class (middle class), and came from the same batch. All the reagents are food grade and are currently used in the industry.

7.2.1. Reactive washing process in laboratory scale

Ozone reactive washing (ORW) was performed on a laboratory rotation round bottom glass reactor (120 rpm) under continuous supply of ozone, for 15 minutes, at a temperature of 70ºC, as described in Chapter 6. Each trial uses 10 natural cork stoppers that were placed in the reactor. Ozone was generated by an ozone generator Fischer 502 (Fischer Group, Waldachtal, Germany) with 50 L/h of the pure oxygen source and an electrical discharge of 0.7 A of intensity, which leads to a production of 1.8 g/h of ozone. The ozone that did not react with the cork stopper surface was destroyed in two consecutive erlenmayers with 10% potassium iodide (100% purity, VWR, analytical reagent) solution.

The conventional reactive washing (CRW) process was carried out on a laboratory rotation glass reactor, under 100 rpm of rotation and 50 ºC for the temperature. The 10 natural cork stoppers derived from ORW were treated with sodium hydroxide (NaOH) and hydrogen peroxide (H_2O_2) in an alternative mode following the arrangement and the timesheet protocol used in the industry and dully explained in Chapter 5. To avoid the stoppers surface swelling, the excess of reagents was withdrawn after 5 minutes in contact with the stoppers surface [2]. When the oxidation time was completed, the stoppers were washed alternatively with distilled water, sodium bisulfate solution (2.5% w/w), and distilled water. After this procedure, the stoppers were dried in a ventilated oven at 40 ºC for one hour. The ISO brightness of each stopper was measured after 24 hours, which is the necessary time for the cork stopper surface to stabilize.

7.2.2. ISO brightness assessment

The efficiency of the reactive washing was evaluated through ISO brightness, which is the numerical value of diffuse reflectance (% ISO) in respect to the blue light of wavelength 457 nm. This procedure is analogous to the one used in the pulp and paper industry, described in the norm Tappi T 525 om-06.

This analysis was executed on the Konica Minolta cm700-d portable spectrophotometer (Konica Minolta, Tokyo, Japan) and follows the internal procedure performed in the Amorim Cork S.A. The

10 stoppers of each trial were evaluated through ISO brightness analysis, performing three random measurements on the lateral and the top surfaces. The ISO brightness final value of each stopper corresponds to an average of six measurements. The final ISO brightness of each test is the ISO brightness mean value of the 10 stoppers used.

7.2.3. Response Surface Methodology (RSM)

To implement the response surface methodology (RSM) was settled the levels for each variable of the conventional reactive washing (CRW) under study (hydrogen peroxide and sodium hydroxide concentrations, oxidation time, and washing water volume). These levels were established by performing a series of tests using one-factor-at-a-time (OFAT) before applying the RSM, these preliminary tests are not disclosed in this chapter. In this way, it was used the three-level four-factor fractional factorial experimental design to evaluate the effect of the different process variables on the conventional reactive washing. Table 7.1 shows the coded and actual levels of the RW process variables (A, B, C, D).

Table 7.1- CRW process variables and respective coded and actual levels.

Variables	Coded variables	Units	Type of variable	Real values of coded levels		
				-1	0	1
Hydrogen peroxide concentration	A	% (w/w)	Discrete	15	25	35
Sodium hydroxide concentration	B	% (w/w)	Discrete	3	6	9
Oxidation time	C	min	Discrete	13	23	33
Washing water volume	D	ml/10 stoppers	Discrete	50	100	150

-1: fator at low level; 0: fator at medium level; +1: factor at high level

The conventional reactive washing corresponds to the combination of all the higher levels of each factor in the study. This experimental design resulted in 25 assays with five replicate pairs, which are crucial to comprehend the process variability [7].

The obtained results were fitted to a second-order polynomial (Equation 7.1), which relates the effects of process variables (A, B, C, D) and their interactions on the response variable Y (ISO brightness).

$$Y = b_0 + b_1A + b_2B + b_3C + b_4D + b_{12}AB + b_{13}AC + b_{14}AD + b_{23}BC + b_{24}BD + b_{34}CD + b_{11}A^2 + b_{22}B^2 + b_{33}C^2 + b_{44}D^2 \quad (7.1)$$

Where, Y is the predicted response, b_0 is model constant; b_1, b_2 b_3 and b_4 are the linear coefficients; b_{12}, b_{13}, b_{14}, b_{23}, b_{24} and b_{34} are the cross product coefficients and b_{11}, b_{22}, b_{33} and b_{44} are the quadratic coefficients. Statistical Stat-Ease *Design Expert* 11.0.5.0 software (Stat-Ease Inc., Minneapolis, MN, USA) was used to determine the authenticity of the models based on analysis of variance (ANOVA) and coefficient of determination (R^2).

7.3. Results and Discussion

7.3.1. The model equations and statistical evaluation

The conventional reactive washing process variables, namely hydrogen peroxide and sodium hydroxide concentrations, oxidation time, and water volume, were evaluated through ISO brightness using an experimental design of 3^4 fractional factorial experimental with five replications pairs and response surface methodology (RSM).

A total of 25 tests (Table 7.2) generated randomly, were carried out during the experimental study, where each assay shows the actual ISO brightness values obtained and response values predicted via *Design Expert* version 11.0.5.0 software. The five replication pairs correspond to tests 2 and 21, tests 5 and 12, tests 6 and 8, tests 16 and 19, and tests 17 and 22.

Table 7.2- Three-level and four-factor fractional factorial experimental design and associated response (actual and predicted ISO brightness (%)).

Run	A	B	C	D	ISO Brightness (%)[a]	
					Actual	Predicted
1	35	3	13	100	27.50	27.31
2	35	6	23	150	31.71	31.73
3	35	9	33	50	33.82	33.54
4	15	3	23	100	24.08	25.14
5	25	9	23	100	32.90	33.55
6	25	6	33	100	31.84	30.51
7	25	9	13	50	28.26	29.05
8	25	6	33	100	29.75	30.51
9	15	9	23	50	31.58	30.57
10	15	6	13	100	27.88	28.42
11	15	3	13	50	25.74	24.97
12	25	9	23	100	34.86	33.55
13	15	3	33	100	26.68	25.91
14	15	9	33	50	30.78	31.70
15	15	6	23	100	28.08	28.69
16	15	6	23	150	28.74	28.17
17	25	3	23	50	25.05	25.23
18	15	9	13	50	30.37	30.14
19	15	6	23	150	27.94	28.17
20	25	3	13	150	23.87	23.74
21	35	6	23	150	31.98	31.73
22	25	3	23	50	24.84	25.23
23	25	9	13	150	33.99	33.99
24	35	3	33	150	29.11	29.34
25	35	9	33	150	39.10	39.58

[a]The relative error in brightness determination was within 5%.

The actual ISO brightness values (Table 7.2) varied between 23.87% and 39.10% in tests 20 and 25 respectively. The predicted ISO brightness values were consistent with the actual ISO brightness values, maintaining the lower value for test 20 (23.74%) and the higher value for test 25 (35.86%), with an average of 29.62% for the actual response in the 25 runs.

The target value for the response was 33.78%. This value matched the value of ISO brightness of natural cork stoppers after conventional reactive washing (CRW) (35% H_2O_2 solution, 9% NaOH solution, 150 ml of washing water volume, and a reaction time of 33 min, without ozone reactive washing in the first stage).

The actual ISO brightness values acquired were fitted to a quadratic polynomial regression equation based on the coded parameters (Equation 7.2) that relate the independent variables to the response:

$$Y = 29.02 + 1.28A + 3.85B + 1.15C + 1.03D - 0.38AB + 0.53AC + 0.50AD + 0.19BC + 1.46BD + 0.025CD + 0.95A^2 + 0.68B^2 + 0.35C^2 - 1.04D^2 \quad (7.2)$$

The correlation established had a significant value, since the coefficient of determination (R^2) acquired for the ISO brightness was 0.9668 (Figure 7.1, A). The residual versus predicted values plot (Figure 7.1, B) for ISO brightness showed a uniform distribution.

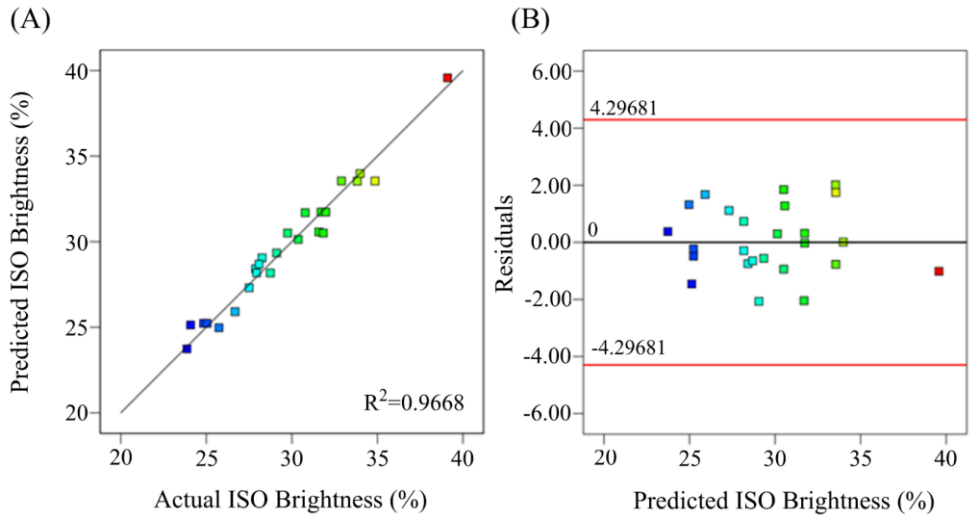

Figure 7.1- Model diagnostic plots: (A) ISO brightness predicted vs. actual plot; (B) Residual plot for predicted ISO brightness.

The adequacy of fit of the model towards ISO brightness was evaluated using the analysis of variance (ANOVA) supplied by *Design Expert* 11.0.5.0 software (Table 7.3).

Table 7.3- Analysis of variance (ANOVA) for ISO brightness.

Source	Sum of squares	Degree of freedom	Mean Square	*F*-value	*p*-value
Model	321.21	14	22.94	20.80	<0.0001
Residuals	11.03	10	1.10		
Lack of fit	6.55	5	1.31	1.46	0.3441
Pure error	4.48	5	0.89		

Table 7.3 shows the ANOVA parameters essential for the model evaluation such as the model sum of squares (321.21), degrees of freedom (14), and mean square (22.94). These results allowed the calculation of the *F*-value (20.80), which has a value superior in relation to the critical one ($F_{(0.05,14,10)}$=2.87), which means that the null hypothesis (H_0) is false, so there is at least one model parameter b_i that is non-zero [8], confirmed by the *p*-value (<0.0001) that shows that H_0 can be rejected at a 0.01% significance level, evidencing that the alternative hypothesis is true.

The lack of fit relates to the difference between the model prediction values and the average of the replicated runs [9]. The lack of fit *F*-value (1.46) demonstrates the adequacy of the model towards the ISO brightness since this value is inferior relative to the critical one ($F_{(0.05,5,5)}$=5.05) [8]. Additionally, the lack of fit *p*-value was 0.3441, which reinforced the non-significance of this parameter and, consequently the adequacy of the model.

Another approach to evaluate the goodness fit of the model was through the coefficient of the model determination statistics (Table 7.4).

Table 7.4- Coefficient of determination for the model.

Statistics	Response: ISO brightness
Standard deviation	1.05
Adjusted R^2	0.9203
Predicted R^2	0.1499
R^2	0.9668

The coefficient of determination R^2 (0.9668) indicates that the model was well adjusted to the data, nonetheless the adjusted R^2 (0.9203) and predicted R^2 (0.1499) have a considerable difference (Table 7.4), that reveal that may exist some model parameters b_i that are non-significant [10]. Hence, it was necessary to verify the *F*-value and *p*-value related to each parameter of the empirical model (Table 7.5).

Table 7.5- Estimated coefficients, *F*-value and *p*-value for each parameter of the empirical model.

Source	Coefficient Estimate	*F*-value	*p*-value
A	1.28	14.22	0.0037
B	3.85	186.36	< 0.0001
C	1.15	13.20	0.0046
D	1.03	9.12	0.0129
AB	-0.38	0.69	0.4250
AC	0.53	1.23	0.2933
AD	0.50	1.37	0.2691
BC	0.19	0.24	0.6370
BD	1.46	12.93	0.0049
CD	0.025	0.0026	0.9602
A^2	0.95	2.95	0.1167
B^2	0.69	1.43	0.2599
C^2	0.35	0.55	0.4767
D^2	-1.04	4.22	0.0672

Through the *p*-values evaluation the factors A, B, C, D, and BD were recognized as significant terms in the model since presented *p*-values lower than 0.05 [11]. On the other hand, factors with *p*-values higher than 0.1000 do not have significance for the model, such as C^2, B^2, A^2, CD, BC, AD, AC, and AB. In this way, the empirical model was reduced hierarchically, evaluating the analysis of variance (ANOVA) whenever a parameter is withdrawn. Once the non-significant parameters were removed, the empirical model was simplified (Equation 7.3).

$$Y = 29.78 + 1.36A + 3.77B + 1.14C + 0.83D + 1.14BD \quad (7.3)$$

Reducing the empirical model, the predicted values given by the model have changed, altering all the assumptions made up until now, including the residuals (Figure 7.2).

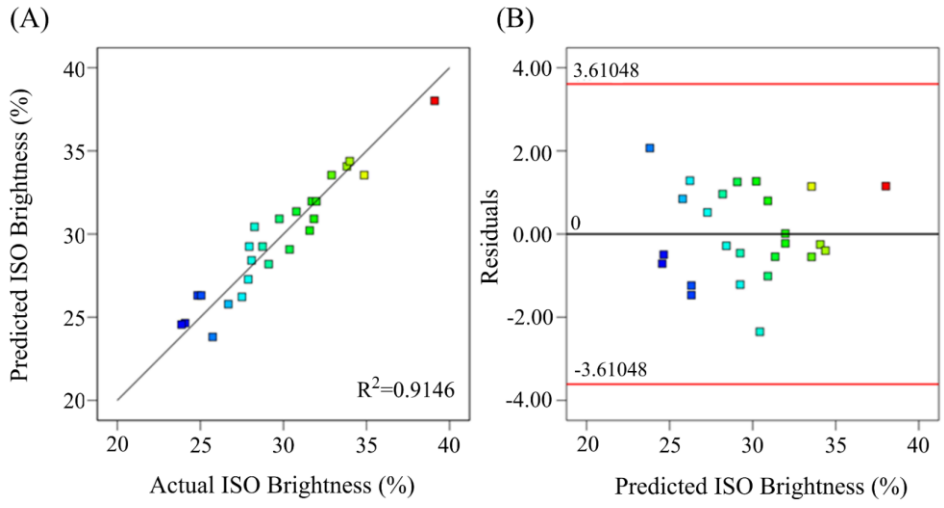

Figure 7.2- Model diagnostic plots for the reduced empirical model: (A) ISO brightness predicted vs. actual plot; (B) Residual plot for predicted ISO brightness.

The predicted ISO brightness for the reduced empirical model plotted versus the actual experimental values has a coefficient of determination (R^2) of 0.9146, which is inferior in relation to the extended empirical model (R^2=0.9668), however, the R^2 obtained in the reduced model still shows that the model fits well the regression (Figure 7.2, A).

The residuals versus the predicted ISO brightness (Figure 7.2, B) show that the data is uniformly distributed. In this way, it was evaluated the reduced model through analysis of variance (ANOVA), presented in Table 7.6.

Table 7.6- Analysis of variance (ANOVA) for ISO brightness in the reduced empirical model.

Source	Sum of squares	Degree of freedom	Mean Square	*F*-value	*p*-value
Model	303.86	5	60.77	40.68	<0.0001
Residuals	28.39	19	1.49		
Lack of Fit	23.90	14	1.71	1.90	0.2464
Pure error	4.48	5	0.90		

The ANOVA parameters for the reduced model reveal a slight decrease in the value of the sum of squares, and a reduction in the degree of freedom from 14 in the extended model to 5 in the reduced one, these modifications implied differences in the mean square (60.77) and *F*-value (40.68), that both showed higher values.

According to Table 7.6, it is recognized that the model is well fitted, since the *F*-value (40.68) is higher than the critical one ($F_{(0.05,5,19)}$=2.59), and the *p*-value is less than 0.0001. Additionally, the lack of fit *F*-value (1.90) is inferior to the critical *F*-value ($F_{(0.05,14,5)}$=4.64) and the *p*-value (0.2464) is higher than 0.05, which reinforces the adequacy of the model towards ISO brightness [8].

The coefficients of determination statistics of the reduced model are presented in Table 7.7

Table 7.7- Coefficients of determination statistics for the ISO brightness.

Statistics	Response: ISO brightness
Standard deviation	1.22
Adj R^2	0.8921
Pred R^2	0.8388
R^2	0.9146

Even though the coefficient of determination (R^2) of the model suffered a slight decrease in relation to the extended model, the adjusted R^2 (0.8921) and the predicted R^2 (0.8388) values showed a small difference, being inferior to 0.2, revealing that the model parameters b_i are satisfactory. In Table 7.8 is evaluated each model parameter by the *F*-value and *p*-value statistics.

Table 7.8- Estimated coefficients, *F*-value and *p*-value for each parameter of the reduced empirical model.

Source	Coefficients estimated	*F*-value	*p*-value
A	1.36	16.36	0.0007
B	3.77	147.26	< 0.0001
C	1.14	11.51	0.0031
D	0.83	6.49	0.0197
BD	1.14	9.32	0.0066

The *p*-values of all the model terms are inferior to 0.05, revealing that all the terms have significance to the model (Table 7.8). Therefore, the reduced empirical model (Equation 7.3) is considered the most adequate for the experimental ISO brightness values.

7.3.2. The effect of process variables on ISO brightness

The reduced empirical model, described by Equation 7.3 (Table 7.8), showed that all the linear coefficients of the model, A, B, C, and D (hydrogen peroxide concentration, sodium hydroxide concentration, oxidation time, and washing water volume, respectively), have a positive effect on the response, ISO brightness, factor B is the one with more significance. Additionally, the only cross product model parameter with significance, BD (sodium hydroxide concentration x water volume), also has a positive effect on the ISO brightness.

Figure 7.3 represents the effect of B (sodium hydroxide concentration) and D (washing water volume) on the ISO brightness with the model parameters A (hydrogen peroxide concentration) and C (oxidation time) on the center level in the form of the predicted response of the process in three dimensional (3D) plot of the response surface.

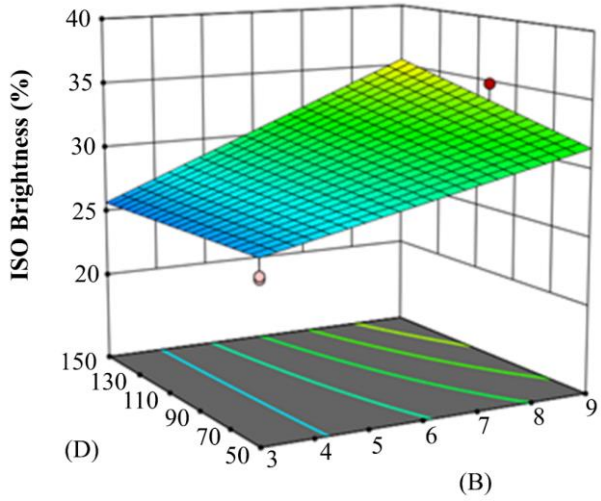

Figure 7.3- Response surface plot representing the effect of B and D on ISO brightness.

Figure 7.3 shows that at the center level for the model parameters A and B, the combination of an increase of the factors B and D allows the increase of the ISO brightness until (35.52%), however, the biggest differences are observed when altering the value of B (sodium hydroxide concentration), for example for the higher level of D (150 ml), increasing B from 3 to 9% translates into an ISO brightness of 25.70 and 35.52%, respectively.

The overall values of the ISO brightness showed in Figure 7.3 varies between 25.70 and 35.52%, and the target value (33.78%) is within the range, which means that some adjustments could be made into the original process to obtain the target ISO brightness.

7.3.3. Model validation

Nine extra tests were carried out to validate the model (Table 7.9), in these runs, factors C and D were kept at the lowest level since are the variables that were revealed to have less significance in the response. On the other hand, the independent variables A and B have more influence, hence the tests that were performed compile the combination of the three initial levels chosen for the initial study of the factorial fractional experimental design. The experimental ISO brightness values obtained, as well as the predicted response, are exposed in Table 7.9.

Table 7.9- Conditions of the validation tests and predicted and actual ISO brightness.

Run Number	Condition				ISO brightness (%)	
	A	B	C	D	Actual	Predicted
1	15	3	13	50	23.14	23.81
2		6			26.00	26.45
3		9			28.65	29.08
4	25	3			24.13	25.17
5		6			27.10	27.81
6		9			30.73	30.44
7	35	3			26.51	26.53
8		6			30.32	29.16
9		9			32.67	31.79

The predicted and actual ISO brightness values acquired reveal a good consistency, besides confirming the significance of the factors A (hydrogen peroxide concentration) and B (sodium hydroxide concentration), which showed that the higher the levels of each of these factors, the higher the ISO brightness achieved. This fact is more noticeable for factor B, which is in coherence with Equation 7.3. The natural cork stoppers before suffering the conventional reactive washing process pass through an ozone reactive washing that activates its surface, once they leave this first step the

stoppers are drier. When the sodium hydroxide is added to the reactor the natural stoppers absorb this reagent, creating the ideal conditions to form the hydroperoxide anion (HO_2^-) when the hydrogen peroxide is added. The higher the concentration of sodium hydroxide, the higher the capacity to produce the oxidative species.

The regression of the actual and predicted ISO brightness values for each test run is plotted in Figure 7.4.

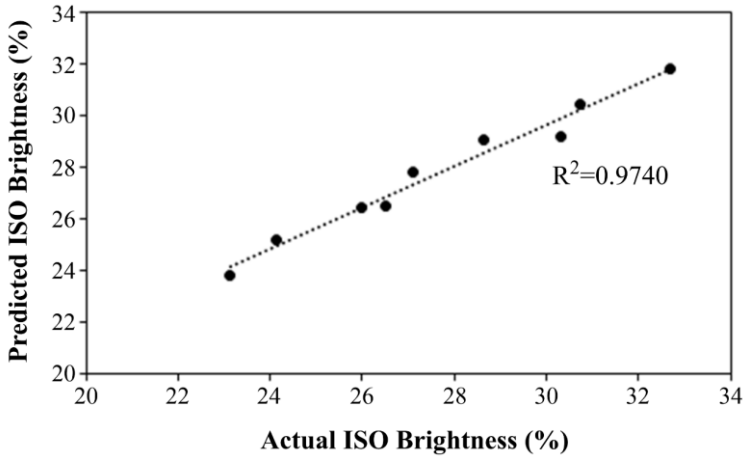

Figure 7.4- Relation between the actual and predicted ISO brightness.

Figure 7.4 confirms that the actual and predicted values of ISO brightness are in agreement, as is revealed by the coefficient of determination (R^2= 0.9740). These results confirmed the validation of the model developed.

7.3.4. Optimization results

The levels for each factor were optimized taking into account the target value of ISO brightness (33.78%), using the numerical option of the optimization module of the *Design Expert* software (version 11.0.5.0). This ISO brightness can be reached using 15 for variable A (% of H_2O_2 concentration), 9 for variable B (% of NaOH concentration), 18 for variable C (time of oxidation treatment, min), and 75 for variable D (water washing volume, ml/10 stoppers), which leads to a reduction of 57, 46 and 50 % for the variables A, C, and D, respectively.

Comparatively to the optimized conventional reactive washing present in Chapter 5, the preliminary stage of ozone reactive washing allows further reductions in the conventional reactive washing stage, such as 20% for variable A (% of H_2O_2 concentration), and 17% for variable D (water washing volume, ml/10 stoppers). As for the sodium hydroxide concentration (B), there is no reduction, since is the critical factor in this process. On the other hand, the time of oxidation has a reduction of 13% in relation to optimized conventional reactive washing, however as the ozone

reactive washing step has a duration of 15 min, the total process time of the reactive washing was 33 min, which in the overall process did not bring a reduction in this variable.

7.4. Conclusions

In this chapter it was evaluated the influence of the use of a preliminary stage of ozone reactive washing in the conventional reactive washing (CRW), by study the effect of this stage on the four independent variables of the CRW (hydrogen peroxide and sodium hydroxide concentration, oxidation time and washing water volume) on the response of interest, the ISO brightness. To achieve this goal, it was applied a three-level and four factor fractional experimental design and response surface methodology using experimental data and software *Design Expert* version 11.0.5.0.

Initially, the collected data was fitted to a second-order polynomial equation, however through statistical analysis was detected that some of the model parameters did not had significance, which led to a reduced model.

The model obtained that was validated reveals that only the variables A (hydrogen peroxide concentration), B (sodium hydroxide concentration), C (oxidation time), D (washing water volume), and BD have significance on the ISO brightness, being the factor B (NaOH concentration) the variable that most influence the response, followed by factor A (H_2O_2 concentration).

In this way, the model allows the optimization of the process with an ISO brightness target of 33.78%, by reducing the variable A from 35% to 15%, factor C from 33 min to 18 min and factor D from 150 to 75 ml, as in relation to the optimized conventional reactive washing in Chapter 5 this optimization reveals further reductions of 20% to factor A, and 17% for factor D.

7.5. References

[1] H. Pereira, The rationale behind cork properties: A review of structure and chemistry, BioResources. 10 (2015). https://doi.org/10.15376/biores.10.3.Pereira.

[2] L. Liu, S.L. Cui, Hydrogen peroxide bleaching to wine corks with a novel catalyst, Adv. Mater. Res. 734–737 (2013) 2282–2286. https://doi.org/10.4028/www.scientific.net/AMR.734-737.2282.

[3] H.U. Süss, D. Ag, D. Hanau, J.D. Kronis, The naked truth on hot peroxide bleaching, (1997) 1–13.

[4] D.G. Branco, C.A. Santiago, F.J. Oliveira, L. Cabrita, D. V Evtuguin, Surface properties of cork in relation to reactive washing, Colloids Surfaces A Physicochem. Eng. Asp. (2021). https://doi.org/10.1016/j.colsurfa.2021.126762.

[5] J.R. Gonzalez-Adrados, M.C. Garcia-Vallejo, M.J. Caceres-Esteban, J.L. Garcia De Ceca, F. Gonzalez-Hernandez, R. Calvo-Haro, Control by ATR-FTIR of surface treatment of cork stoppers and its effect on their mechanical performance, Wood Sci. Technol. 46 (2012) 349–360. https://doi.org/10.1007/s00226-011-0403-5.

[6] C. Ortega-Fernández, J.R. González-Adrados, M.C. García-Vallejo, R. Calvo-Haro, M.J. Cáceres-Esteban, Characterization of surface treatments of cork stoppers by FTIR-ATR, J. Agric. Food Chem. 54 (2006) 4932–4936. https://doi.org/10.1021/jf0529823.

[7] N.R. Domagalski, B.C. Mack, J.E. Tabora, Analysis of Design of Experiments with Dynamic Responses, Org. Process Res. Dev. 19 (2015) 1667–1682. https://doi.org/10.1021/acs.oprd.5b00143.

[8] D.C. Montgomery, Design and Analysis of Experiments, 9th ed., 2017.

[9] C.M. Anderson-Cook, Response Surfaces, Mixtures, and Ridge Analyses, 2008. https://doi.org/10.1198/jasa.2008.s238.

[10] R.H. Myers, D.C. Montgomery, C.M. Anderson-Cook, Response surface methodology-process and product optimization using designed experiments, Third Edit, 2009. https://www.m-culture.go.th/mculture_th/download/king9/Glossary_about_HM_King_Bhumibol_Adulyadej's_Funeral.pdf.

[11] B. Govaerts, B. Francq, R. Marion, M. Martin, M. Thiel, The Essentials on Linear Regression, ANOVA, General Linear and Linear Mixed Models for the Chemist, 2nd ed., Elsevier Inc., 2020. https://doi.org/10.1016/b978-0-12-409547-2.14579-2.

Chapter 8

CHANGES IN CORK STOPPER SURFACE AFTER OPTIMIZED REACTIVE WASHING

Content

8.1. Introduction

The reactive washing (RW) is applied to clean/disinfect the natural cork stoppers, and consequently improve the final appearance in terms of color homogeneity and whiteness. However, the RW process will have implications on the surface of the natural cork stopper, changing the receptivity towards coating agents (silicone, paraffin, and other functional formulations) and to hydroalcoholic solutions [1].

The conventional reactive washing (CRW) uses sodium hydroxide (9%, w/w) and hydrogen peroxide (35%, w/w), achieving the alkalinity required to activate the hydrogen peroxide, permitting the formation of hydroperoxide anion (HO_2^-), when combined with increased temperature. These harsh conditions lead to surface damage. In this way, the optimization of the CRW, and the introduction of ozone in the RW were pointed out as an alternative to the severe conditions applied currently, however, there are no relevant studies on the natural cork stoppers surfaces (lateral and top) concerning the changes after different applied RW processes.

Keeping the target value of 33.78% for the ISO brightness it was reached the optimized conventional reactive washing (OCRW) presented in Chapter 5 and the combination of ozone and optimized RW (RW+) demonstrated in Chapter 7. Both RW processes allowed the optimization of the reagents profile concentrations, oxidation time, and washing water volume. In this way, the main goal of this chapter was to evaluate the natural stopper surface after each of the optimized RW achieved in the previous chapters.

The study of the natural cork stopper surface properties after the application of different RW processes is of high importance since it has implications on the effectiveness of the subsequent treatment of the stoppers with coating formulations and the performance of the natural cork stoppers in the bottle [1,2].

The changes on the surface of the natural cork stopper in terms of color were assessed by ISO brightness, CIElab color parameters, and ultraviolet-visible (UV-vis) spectroscopy. On the other hand, the surface chemistry after each RW was evaluated through Fourier Transform Infrared-Attenuated Total Reflectance (FTIR-ATR). The surface wettability was analyzed by contact angles measurement, which allowed the evaluation of the free surface energy (FSE) and the respective dispersive and polar counterparts.

8.2. Materials and Methods

Natural cork stoppers, as well as the reagents (hydrogen peroxide, sodium hydroxide, and sodium bisulfate), were supplied by Amorim Cork, S.A. (Santa Maria de Lamas, Portugal). Cork stoppers have a single caliber of 49x24 mm (length x diameter), belong to the 1st class (middle class), and came from the same batch. All the reagents are food grade and are currently used in the industry.

8.2.1. Conventional reactive washing (CRW)

A total of 10 natural cork stoppers suffered the conventional reactive washing (CRW) with a mixture of hydrogen peroxide and sodium hydroxide, performed on a laboratory rotation glass reactor (100 rpm) under a controlled temperature (50 °C) following the timesheet protocol applied in the industry. In a typical trial, the oxidation reagents were added alternately to the reactor following the sequence used in the industry, respecting the reagent-to-stopper ratio. Once the oxidation time (33 min) is completed, the stoppers were washed with water (50 ml). Sodium bisulfate solution (2.5% w/w) was added to neutralize the surface of the stopper, which was washed again with water (150 ml). Finally, the stoppers were dried at 40 °C in a ventilated oven for one hour.

8.2.2. Optimized conventional reactive washing (OCRW)

The optimized conventional reactive washing (OCRW) was performed following the same guidelines of the CRW, however with small modifications. The oxidation reagents have been diluted from the reagents supplied by the industry, hydrogen peroxide (22%, w/w) and sodium hydroxide (6%, w/w) were added following the same timesheet as in CRW. The oxidation time maintains the 33 min, nevertheless, the volume of water of the second rinse is decreased from 150 ml to 100 ml, and the neutralize stage used 10 mL of sodium bisulfate (2.5%, w/w) then the cork stoppers are washed with water and then dried at 40 ºC in the ventilated oven for one hour.

8.2.3. Ozone reactive washing (ORW)

Ozone reactive washing (ORW) was performed on a laboratory rotation glass reactor under controlled rotation and temperature, 100 rpm and 70 ºC, respectively. The ozone was generated by the ozone generator Fischer 502 (Fischer Group, Waldachtal, Germany), with 50 L/h of pure oxygen as a source to produce 1.8 g/h of ozone, through an electrical discharge of 0.7 A of intensity. The ozone generator is dully linked to the reactor to prevent any type of ozone leakage of the process, all the ozone that did not react with the stoppers, was destroyed with a solution of potassium iodide

(10% w/w), which is found in two consecutive erlenmayers directly linked to the reactor. Each trial uses 10 natural cork stoppers and has a duration of 15 min.

8.2.4. Ozone reactive washing plus optimized reactive washing (RW+)

This process combines two of the methodologies presented before, the ozone reactive washing is applied exactly how is presented, the optimized reactive washing was performed taking into account that the ozone pre-washing stage alters the optimization of the conventional reactive washing. The cork stoppers that leave the ozone treatment are washed with sodium hydroxide (9% w/w) and hydrogen peroxide (15% w/w). After 5 minutes of the reagents entering in contact with the stopper surface, the reagents in excess are removed to avoid cork swelling [3]. The oxidation time is completed after 18 min, and the cork stoppers are washed with water (50 ml), sodium bisulfate (2.5% w/w), and water (50 ml). Once this process is finished, the cork stoppers are dried in a ventilated oven at 40 ºC over 1 hour.

8.2.5. ISO brightness and CIElab color parameters measurement

The stoppers deriving from the four reactive washing processes displayed above were evaluated through ISO brightness and CIElab color parameters once the cork stoppers completed one day of stabilization after each reactive washing process was performed.

ISO brightness corresponds to a numerical value of diffuse reflectance concerning blue light of wavelength 457 nm [4]. This procedure is already common in the pulp and paper industry, properly described in Tappi T 525 om-06. This analysis was performed on the Konica Minolta cm700-d portable spectrophotometer (Konica Minolta, Tokyo, Japan), with the ISO brightness value of each stopper corresponding to the average of six measurements, as performed in the internal procedure of the company Amorim Cork, S.A.

The CIE-L*a*b* color coordinates, lightness (L* (D65)) and the chromaticity coordinates a* (D65) and b* (D65), which are cartesian coordinates were also determined on the same equipment. Coordinate a* determines redness (+a*) or greenness (-a*), and b* range from yellow (+b*) to blue (-b*), these parameters allow the evaluation more accurately of the stopper surface. Ideally, to achieve the highest levels of brightness is necessary to have an L* (D65) closer to 100 and the coordinates a*(D65) and b*(D65) approximately zero.

8.2.6. Surface roughness

The surface roughness analysis was carried out on a portable surface roughness tester SURFTEST SJ-210 (Mitutoyo America Corporation, Illinois, USA) with a speed of 0.5 mm/s and a

cut-off wavelength value of 2.5 mm. The surface roughness analysis followed the standard ISO 4287-1997. The obtained values of R_a, R_p, and R_v correspond to an average of 25 measurements.

8.2.7. Solid ultraviolet-visible (UV-vis) spectroscopy

UV-vis diffuse reflectance (UV-vis DR, k/s) spectra were recorded at room temperature (21±1 ºC, RH 60%) on a Thermo Scientific™ Evolution 220 spectrophotometer (Thermo Scientific, Massachusetts, USA) equipped with an ISA-220 reflectance accessory using $BaSO_4$ as background reference, at scan velocity of 200 nm/min. The studied range was 220-700 nm with a bandwidth of 5 nm. The lateral and the top were cut from the natural cork stopper before and after ORW obtaining a sample (10 x 10 mm and thickness about 1 mm). Two replicates were analyzed for each sample. The amount and type of light-absorbing materials or chromophores were characterized by the Kubelka-Munk light absorption coefficient (k/s) at different wavelengths. The reflectance spectra were also converted into k/s spectra using known Kubelka–Munk (Equation 8.1) [5].

$$\frac{k}{s} = \frac{(1-R)^2}{2R} \tag{8.1}$$

where R is the reflectance of the opaque sample, k is the specific absorption coefficient and s is the specific scattering coefficient. A constant scattering coefficient among the studied samples was assumed for a comparative quantitative analysis of the changes in chromophores among the studied samples. The obtained spectra were treated using Thermo Scientific™ INSIGHT™ software (Thermo Scientific, Massachusetts, USA).

8.2.8. FTIR- ATR spectroscopy

Fourier transform infrared- attenuated total reflectance (FTIR-ATR) spectra were collected on a Spectrum BX Perkin Elmer spectrophotometer (PerkinElmer, Waltham, Massachusetts, USA) with a resolution of 4 cm^{-1} and 128 scans in a transmittance mode. The spectrums were normalized at 1260 cm^{-1} band using OriginPro 2015 software (OriginLab Corporation, Northampton, Massachusetts, USA).

8.2.9. Contact angle and interface interaction

Contact angles were measured in a Contact Angle System OCA20 goniometer (Data Physics, Filderstadt, Germany) that is equipped with a CCD camera and SCA20 software using the sessile drop method and water, formamide, and diiodomethane as probe liquids. For each sample, 30 measurements were performed (10 measurements for each solvent used). The contact angle

measurements were carried out at room temperature (21±1 ºC, RH 60%) and applying the drop volume of 1 μL with a velocity of deposition of 1 μL/s. Contact angles were measured as a function of time for 60 seconds and then extrapolated to zero time. The results of parallel measurements were averaged, and the standard deviation errors were evaluated.

The evaluations of the free surface energy (FSE) of cork (γ_s) and its corresponding polar (γ_s^p) and dispersive (γ_s^d) components were performed using the series of liquid probes (water, formamide, and diiodomethane) based on the Owens-Wendt-Rable-Kaeble (OWRK) model that satisfactorily describes the solid-liquid interfacial interactions in the air for the polymers [6] and lignocellulosic materials [7]:

$$\left(\frac{1+\cos\theta}{2}\right)\left(\frac{\gamma_L}{\sqrt{\gamma_L^d}}\right)=\sqrt{\gamma_s^p}\times\sqrt{\frac{\gamma_L^p}{\gamma_L^d}}+\sqrt{\gamma_s^d} \qquad (8.2)$$

where γ_L, γ_L^p, and γ_L^d represent the liquids superficial tension and the corresponding polar and dispersive components, respectively. Plotting $(1+\cos\theta/2)\left(\gamma_L/\sqrt{\gamma_L^d}\right)$ *vs* $(\gamma_L^p/\gamma_L^d)^{1/2}$ allows the calculation of the parameters γ_s^d and γ_s^p.

8.2.10. Wetting envelope simulations

Wetting envelope is a tool that allows the visualization of the relationships between polar and dispersive components, along with FSE, and helps to better understand the wettability of the surface towards different liquids. This simulation was built using the values of polar and dispersive components of FSE obtained for each sample analyzed. Wetting envelope was applied as described elsewhere [8]. To facilitate the understanding of the wettability characteristics of the samples, calculations were performed for four different angles (θ): 0°, 45°, 60°, and 90°.

The behavior changes of the cork stopper after each RW were assessed by evaluating the interfacial behavior of the cork stopper surface towards four solutions with different percentages of ethanol (12, 14, 20, and 40%) on the wetting envelope. The polar and dispersive components for each ethanol solution were present in the literature [8].

8.3. Results and Discussion

8.3.1. Surface color parameters

The measurement of ISO brightness and CIElab color parameters is a common way to monitor the reactive washing process. Accordingly, after each RW performed these characteristics were analyzed (Table 8.1).

Table 8.1- ISO brightness and CIElab color parameters of the natural cork stoppers surface before and after different optimized RW processes.

Reactive washing	L* value (±SD)	a* value (±SD)	b* value (±SD)	ISO brightness (%) (±SD)
Without RW	60.7±2.0	11.9±1.0	25.0±1.4	15.8±1.3
CRW industrial	74.8±1.5	3.5±0.7	20.7±1.3	30.8±2.0
CRW	75.6±1.2	3.3±0.4	21.1±1.3	33.2±1.8
OCRW	76.2±1.2	3.3±0.7	21.0±1.9	34.1±2.1
ORW	65.1±1.7	9.7±1.1	22.7±1.4	20.8±1.6
RW+	75.0±2.1	4.1±0.9	21.0±1.4	32.5±3.2

RW-Reactive Washing; CRW-Conventional Reactive Washing; OCRW-Optimized Conventional Reactive Washing; ORW-Ozone Reactive Washing; RW+-Ozone reactive washing plus optimized conventional reactive washing.

Table 8.1 shows that all the RW methodologies change positively the color parameters, since when compared the different RW with the surface of stoppers without any type of RW there is an increase of the ISO brightness and L* value, while a decrease in the a* and b* values. Among the distinct RW, the treatment of stoppers with ozone (ORW) was the one with the lowest color quality parameters. The conventional reactive washing (CRW), the optimized conventional reactive washing (OCRW), and the ozone reactive washing plus optimized reactive washing (RW+) may be considered similar in terms of color quality.

The UV-vis DR (k/s) spectra provides information about the chromophore/chromogen structures present in the natural cork stopper surface before any type of RW and show how the different RW processes implemented changed absorbance profiles (Figure 8.1).

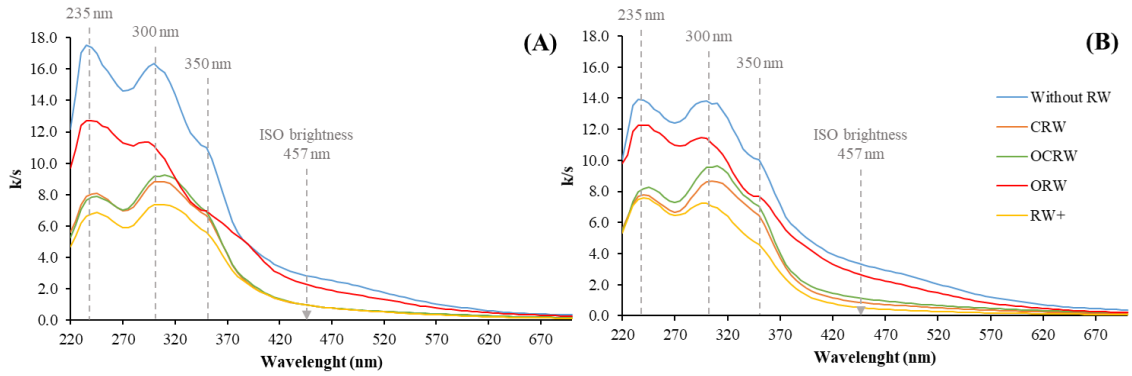

Figure 8.1- UV-vis DR (k/s) of the lateral (A) and top (B) of the natural cork stopper before and after different RW processes.

Figure 8.1 showed that the overall absorption behavior decreases in intensity following the sequence: stoppers without RW stoppers treated with ozone (ORW), stoppers with optimized conventional reactive washing (OCRW), stoppers with conventional reactive washing, and at last stoppers that combined the ozone reactive washing with the optimized reactive washing (RW+).

The CRW and OCRW revealed very similar spectra, being the major difference observed in the top surface of the cork stopper (Figure 8.1, B) that showed that after OCRW the top has a slightly superior absorbance intensity almost along all the studied wavelength, which is in accordance with the brightness values (looking k/s values at 457 nm). This fact affirms that even though in the OCRW process there is an optimization of the original CRW, including lower concentrations of the reagents applied (sodium hydroxide and hydrogen peroxide) and volume of washing water used, the final quality color parameters of the stopper surface are very similar to the CRW, saving the cork surface from more harsh conditions and decreasing the cost associated to the RW process.

The process with lower absorbance (k/s) intensity is the RW+, the first stage of washing with ozone allows an effective decrease of the chromophore/chromogen structures, mostly in the UV region, where the top of the cork stopper revealed a higher decrease of absorbance intensity between 280 and 370 nm, that englobes the peak at 300 nm and a shoulder at 350 nm, which are associated to lignin and polyphenolic structures and/ or structures arising from lignin oxidation, such as quinones, α- carbonyl structures (coniferaldehyde, ferulic acid, p-coumaric acid, etc), nonconjugated phenolic groups, and conjugated structures, namely stilbenes [9–11]. The introduction of ozone in the first stage of reactive washing complemented with hydrogen peroxide/sodium hydroxide RW could help the improvement of the brightness stability of the surface, since this RW is the one that showed inferior absorbance intensity in the ultraviolet region, implying that this RW is the one with lower chromogen groups capable to transform into chromophore structures and decrease the ISO brightness over time.

The other main peak at 235 nm, assigned to double bounds conjugated with other electron-acceptor functional groups (COOH or CHO), also decreases after the RW+, which implies that these structures are removed from the stopper surface, thus increasing brightness, as it is observed at the k/s values at 457 nm, and should also provide better brightness stability.

8.3.2. Surface chemistry

FTIR- ATR spectroscopy provides information about the changes on the chemical surface of the natural cork stopper after each RW applied. This evaluation was made either on the top and the lateral of the cork stopper (Figure 8.2).

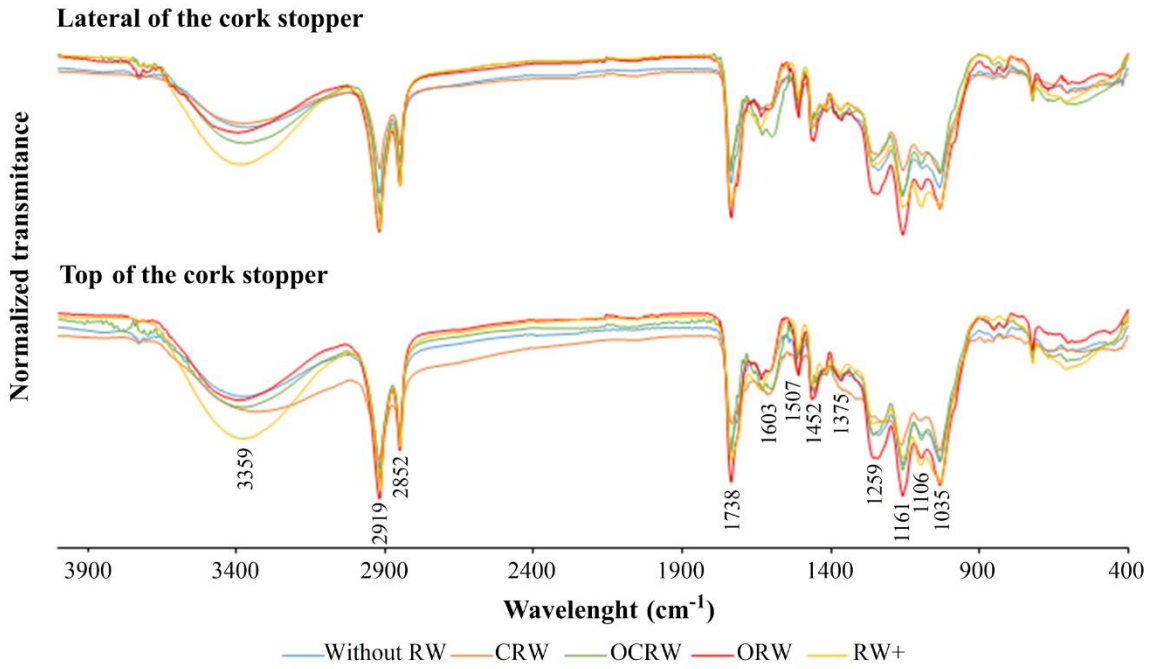

Figure 8.2- FTIR-ATR spectra of the lateral and top of the natural cork stopper before and after different RW processes.

Figure 8.2 shows that all the spectrums of the natural cork stopper surface after the different RW applied showed the characteristic peaks of the cork chemical components (suberin, lignin, hemicelluloses, cellulose, and extractives). The band at 3359 cm^{-1} is assigned to O-H stretching, the bands at 2919 and 2825 cm^{-1} correspond to the asymmetric and symmetric stretching vibrations, respectively, of C-H bonds in CH_2 aliphatic structures mostly from suberin [1,2,12]. The band at 1738 cm^{-1} is assigned to the stretching vibration of C=O bond in ester groups mainly from suberin, the bands 1603 and 1507 cm^{-1} are associated with C=C stretching vibrations from lignin aromatic rings, and the bands 1452 and 1375 cm^{-1} are assigned to asymmetric and symmetric stretching vibrations of C-H bonds, which are less specific peaks and can be associated with any chemical compound of cork [13,14]. The bands at 1259 and 1161 cm^{-1} are assigned to the stretching vibrations of C-O bonds in esters and ethers structures, respectively, while the bands at 1106 and 1035 cm^{-1} are assigned to stretching of C-OH and bending of C-H, respectively, principally from polysaccharides and lignin.

The major differences in the spectrums occur between the RW process employed, and the baseline of the natural cork stopper without RW. The band intensity at 3359 cm^{-1}, related to stretching in the OH groups, increased after all the RW processes applied, being more pronounced for the RW+. This increment implies that macromolecular components of cork degradation occurred with the formation of oxidized groups or simply the accessibility of OH groups was enhanced due to the degradation of protective suberin layer.

The CRW is, in overall, the process that shows the highest decrease in peaks intensity corresponding to suberin (2919, 2852, and 1738 cm^{-1}) in relation to the cork stoppers without RW either for the lateral and the top. As revealed in Chapter 4, the harsh conditions (pH, temperature, hydrogen peroxide concentration (35%, w/w) and sodium hydroxide concentration (9%, w/w)) in the CRW led to the eventual degradation of suberin and lignin.

The optimized conventional reactive washing (OCRW) follows the same patterns as CRW in the bands 2919, 2852, and 1738 cm^{-1}. However, the decrease in intensity is less pronounced than with CRW, which indicates less suberin degradation in this process, explained by the lower concentration of the reagents involved in RW, hydrogen peroxide (22%, w/w) and sodium hydroxide (6%, w/w). The effectiveness of this process is also revealed by the decrease in intensity of the band 1507cm^{-1} in the OCRW in relation to CRW that is associated with the lignin structure, indicating the reduction of C=C bonds in the aromatic structures of lignin, which may suggest a decrease of conjugated structures in lignin polymer and the reduction of the chromophore groups supported by the UV-vis analysis.

The ozone reactive washing plus optimized reactive washing (RW+) revealed some similarities with the ORW on the band's intensity of the peaks at 2919, 2856, 1738 cm^{-1}, where these two RW show the higher intensities either for the lateral or the top of the surface, which the higher exposure of suberin groups, that is accompanied by the OH band increase (3359 cm^{-1}) that may be from the acid carboxylic termination groups of suberin. On the other hand, the bands at 1603 and 1507 cm^{-1} at the RW+ are similar and lower than the respective bands of the stoppers without RW, respectively. This observation reveals that after RW+ lignin suffers degradation by aromatic opening ring [15–18], which ultimately led to a reduced chromophore conjugated groups revealed by the UV-vis lower absorbance (k/s) intensity (Figure 8.1). Figure 8.2 shows that the first stage of ozone in the RW+ process activates the surface of the cork stopper, which allows the bleaching of the natural cork stopper with lower concentration for the hydrogen peroxide (15%, w/w), lower oxidation time (from 33 min to 13 min) and lower washing water needs, allowing the degradation of lignin while increasing the exposure of characteristic moieties in suberin.

8.3.3. Surface wettability

The measurement of contact angles with the liquid probes (water, formamide, and diiodomethane) allowed the evaluation of free cork surface tension (γ_S) [19]. The contact angles were determined on the lateral and top of the surface, since as it has been demonstrated in Chapter 4 that these two areas have distinct behavior due to the different morphology of each area and consequently different exposure of cork chemical compounds.

The contact angles before and after each RW (Table 8.2) were used to calculate the polar and dispersive counterparts of the free cork surface tension (Figure 8.3) on the cork surface from each RW studied.

Table 8.2- Contact angles of the top and lateral of the natural cork stopper with water, formamide, and diiodomethane before and after different RW.

Natural cork stopper area	Measured contact angle (deg.)		
	Liquid probe		
	Water	Formamide	Diiodomethane
LCS before RW	136.0±3.2	115.1±5.0	81.3±6.2
LCS after CRW	90.9±2.3	90.0±5.3	76.0±2.3
LCS after OCRW	96.1±3.4	100.0±5.0	81.0±4.0
LCS after ORW	137.4±2.2	77.7±3.3	85.8±3.5
LCS after RW+	93.5±1.3	78.5±2.2	75.2±1.8
TCS before RW	99.2±5.6	101.2±5.2	77.7±5.0
TCS after CRW	91.0±5.6	99.3±3.1	76.0±5.2
TCS after OCRW	96.6±2.6	101.6±2.5	83.6±3.0
TCS after ORW	96.1±3.2	83.8±2.9	74.2±6.3
TCS after RW+	92.7±1.8	79.1±3.4	69.9±4.0

LCS-Lateral of the cork stopper; TCS- Top of cork stopper.

Based on the data of Table 8.2 it is possible to verify that, in overall the top of the cork stopper showed lower contact angles in relation to the lateral of the cork stopper, with exception to the CRW and OCRW. The contact angle with water were all superior to 90°, which evidenced that, independently of the RW applied, water does not wet the lateral or top of the natural cork stopper. Using the contact angles and the ORWK model, the dispersive and polar components of the cork FSE before and after RW were evaluated (Figure 8.3).

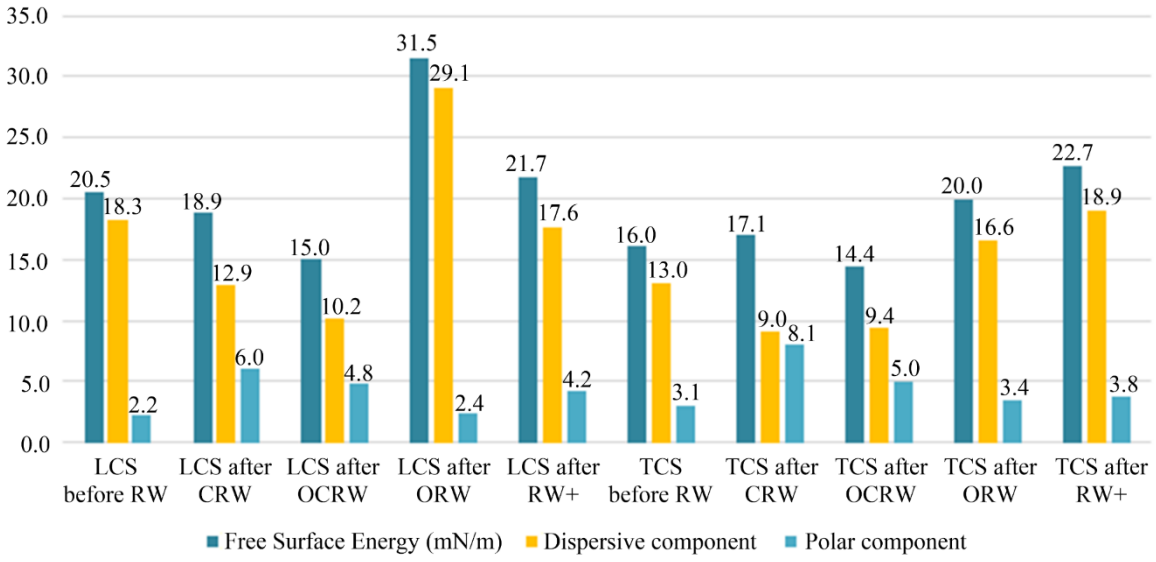

Figure 8.3- Contribution of polar and dispersive components to the total free surface energy of the lateral (LCS) and top (TCS) of the cork before and after different RW.

After the OCRW the free surface energy (FSE) decreased from 20.5 to 15.0 mN/m for the lateral, and from 16.0 to 14.4 mN/m for the top, which is values lower than the respective ones (18.9 and 17.1 mN/m) in the CRW. This fact shows that the decrease in reagent consumption in the OCRW caused much less pronounced degradation of the hydrophobic polymers (primary suberin) on the surface of natural stoppers when compared to stoppers after the CRW with higher reagent load. This was confirmed by obtained free surface energy (γ_s) values and its corresponding polar (γ_s^p) and dispersive (γ_s^d) components of the stoppers treated by OCRW, which were much closer in terms of gaining the polarity index (γ_S^p/γ_S) for untreated stoppers than for stoppers treated by CRW (Figure 8.3). Moreover, the known anisotropy in surface properties of the lateral and top of the natural cork stoppers [8] was leveled out to a significant extent after the OCRW reagents profile. In practice, this means better receptivity of hydrophobic coating formulations (e.g. paraffin emulsion or decorative polymeric formulations) by natural stoppers treated by the OCRW process than by the CRW process [8]. Consequently, the OCRW has not only saved reagents but also improved the processability of natural stoppers in relation to the targeted coatings.

The FSE after the RW+ in the lateral and top of the cork stopper (21.7 and 22.7 mN/m, respectively) are very similar, with a polarity index of 0.194 and 0.167, respectively. The RW+ process, when compared with the CRW showed higher FSE for the lateral (21.7 *vs.*18.9 mN/m) and the top (22.7 *vs.* 17.1) with a significant decrease in the polarity index from 0.317 to 0.194 for the lateral and from 0.473 to 0.167 to the top, combined with a slight increase of the contact angle with water, reveal the reduction of affinity with aqueous solutions (Table 8.2). This fact is in accordance with the FTIR-ATR analysis that revealed a higher exposure of hydrophobic groups of suberin after the RW+. In this way, the treatment with ozone in the first stage and the optimized CRW in the second stage of the CRW, thus altering the reagents profile by reducing the hydrogen peroxide concentration (15%, w/w), oxidation time and washing water volume, was effective in targeted reduction of lignin and polyphenolic chromophores, exhibiting better the suberin groups.

Since the roughness contributes to an increase in wettability of the cork stopper [20], the roughness of the lateral and top surfaces of the natural cork stopper were evaluated before and after each kind of RW. The roughness average (R_a) and the values of the maximum profile heigh peaks (R_p) and of valley depth (R_v) before and after each RW were evaluated (Table 8.3).

Table 8.3- Roughness parameters of the lateral and top of the natural cork stoppers before and after different RW.

Stopper	Lateral (μm)			Top (μm)		
sample	R_a (±SD)	R_p (±SD)	R_v (±SD)	R_a (±SD)	R_p (±SD)	R_v (±SD)
Without RW	4.7±1.8	13.4 ±4.1	14.1±3.7	7.5±1.9	18.9±4.5	21.1±5.4
After CRW	5.2±1.2	16.1±2.7	19.2±3.9	8.6±1.5	24.2±4.0	30.6±6.2
After OCRW	4.7±1.3	14.7±4.2	17.7±4.7	8.8±1.3	23.9±3.2	30.3±6.3
After ORW	4.6±1.3	12.4±2.5	14.5±3.2	7.9±1.4	19.7±2.5	21.3±3.4
After RW+	5.5±1.3	16.9±3.3	20.6±4.8	7.7±1.3	21.9±3.5	26.5±3.9

As already stated in Chapter 4, the lateral of the natural cork stoppers has *ca.* 30% less roughness than the top surface (Table 8.3). However, after the RW processing, several differences in surface roughness were observed. Thus, after CRW and RW+ in the lateral surface, an increase in all the three roughness parameters analyzed was detected. This fact is in accordance with the contact angle with water for the lateral after CRW and RW+ (90.9 and 93.5°, respectively), showing the higher wettability of the lateral surface. On the other hand, after OCRW and ORW, the differences between the roughness parameters are small for the lateral surface, indicating that these RW processes did not have a great influence on the roughness. In fact, after the ORW, the lateral surface of the natural stopper decreased in 0.1 and 1.0 μm for R_a and R_p, respectively, in relation to the lateral without RW.

In the top surfaces of the cork stoppers, the roughness average parameter (R_a), the parametric values of the maximum profile heigh peak (R_p), and of valley depth (R_v) showed higher values after each RW applied, outstanding the OCRW and CRW, followed by the RW+ process. This fact is in accordance with the contact angle of the top surface with water since after any of RW processes the contact angles with water decreased, revealing the higher wettability of this surface towards polar solutions.

To better understand the wettability behavior of the natural cork stoppers after each RW towards hydroalcoholic solutions and the hydrophobic coating formulations (e.g. paraffin and silicone) the wetting envelope simulations were performed (Figure 8.4). The hydroalcoholic solutions of 12, 14, 20, and 40% ethanol (v/v) to cover all the existing alcoholic solutions in beverages market were examined. In the wetting envelope simulations the hypothetical contact angles curves of 0, 45, 60, and 90° were introduced that allowed the evaluation of the surface from completely wettable (0°) to non-wettable (90°).

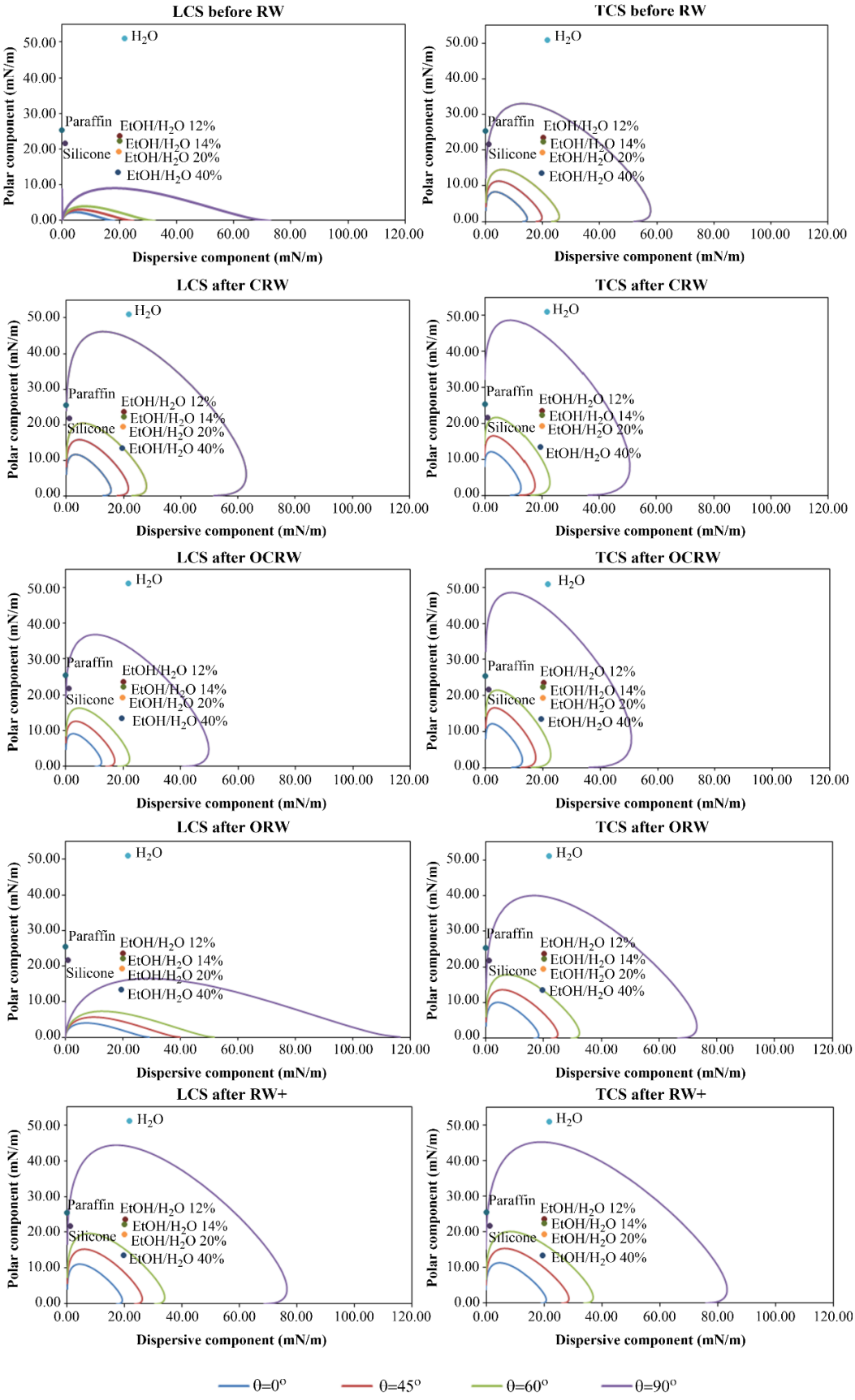

Figure 8.4- Wetting envelope of the lateral and top of the cork stopper before and after different RW.

As revealed from the contact angles measured with water none of the RW processes applied led to the wettability of the cork stopper surface with water, however, the increase of ethanol content in the hydroalcoholic solutions showed higher wettability by the cork stopper.

Figure 8.4 revealed that the OCRW in relation to the CRW improved the surface wettability of the natural cork stopper, in the lateral that is a decrease in both components (dispersive and polar) which still allows the wettability of the surface by paraffin and silicone formulations while decreasing the wettability of the 40% (v/v) hydroalcoholic for angles superior to 60°. As for the top, there is an increase in the polar component, however, the surface behavior towards the hydroalcoholic solutions remains the same.

After the RW+, the top and the lateral showed similar behavior towards the hydroalcoholic solutions and the paraffin and silicone formulations, which revealed higher wettability due to the increase in the dispersive component of the cork stopper surface.

8.4. Conclusions

The surface changes in the lateral and top of the natural cork stoppers after four reactive washing processes were studied. The RW carried out under different process conditions led to variable surface modifications. Conventional reactive washing (CRW) is the process currently applied in the industry and serves as a comparative term.

The surface color parameters evaluated through ISO brightness and CIElab color parameters demonstrated the better brightening efficiency of the optimized RW (OCRW and RW+) in relation to the CRW. This was also confirmed by the UV-vis spectroscopy that revealed the decrease in chromophore structures (vis-active compounds) and chromogen structures (vis-inactive compounds), eventually revealing greater brightness stability of these stoppers.

The surface chemistry evaluation by FTIR-ATR confirmed the CRW as the process with highest degradation of the suberin on the surface of stoppers. The modification of the reagents profile in the OCRW showed less degradation of the natural cork stopper surfaces. On the other hand, the RW+ revealed the best preservation of suberin on the surface of the stoppers and the highest degradation of lignin and polyphenolics.

The RW applied have implications on the surface wettability, where the main changes occur due to the suberin degradation, which can be related to an increase in the polarity index and a higher exposure of the hydrophilic structural polymers. After each RW, even though the lateral and top surfaces are non-wettable with water, there was an increase in wettability of the surfaces towards hydroalcoholic solutions, turning them from non-wettable to wettable. This evaluation performed in accordance with the balance between polar and dispersive counterparts of the free surface energy allowed the verification of the wettability of the surface towards coating formulations (food-grade paraffin and silicon) and providing reliable information for the improvement of the surface coating when applying the optimized RW (OCRW and RW+).

The results featured in this chapter allowed the evaluation of the natural cork stoppers surfaces after each optimized RW and provide information about its behavior regarding the surface chemical changes and wettability.

8.5. References

[1] J.R. Gonzalez-Adrados, M.C. Garcia-Vallejo, M.J. Caceres-Esteban, J.L. Garcia De Ceca, F. Gonzalez-Hernandez, R. Calvo-Haro, Control by ATR-FTIR of surface treatment of cork stoppers and its effect on their mechanical performance, Wood Sci. Technol. 46 (2012) 349–360. https://doi.org/10.1007/s00226-011-0403-5.

[2] C. Ortega-Fernández, J.R. González-Adrados, M.C. García-Vallejo, R. Calvo-Haro, M.J. Cáceres-Esteban, Characterization of surface treatments of cork stoppers by FTIR-ATR, J. Agric. Food Chem. 54 (2006) 4932–4936. https://doi.org/10.1021/jf0529823.

[3] L. Liu, S.L. Cui, Hydrogen peroxide bleaching to wine corks with a novel catalyst, Adv. Mater. Res. 734–737 (2013) 2282–2286. https://doi.org/10.4028/www.scientific.net/AMR.734-737.2282.

[4] P. Bajpai, Environmentally Friendly Production of Pulp and Paper, John Wiley & Sons, Inc., 2010. https://doi.org/10.1002/9780470649657.

[5] D.M. Hembree, H.R. Smyrl, Anomalous dispersion effects in diffuse reflectance infrared fourier transform spectroscopy: a study of optical geometries, Appl. Spectrosc. 43 (1989) 267–274. https://doi.org/10.1366/0003702894203057.

[6] D.K. Owens, R.C. Wendt, Estimation of the surface free energy of polymers, J. Appl. Polym. Sci. 13 (1969) 1741–1747. https://doi.org/10.1002/app.1969.070130815.

[7] T. Nguyen, W.E. Johns, Polar and dispersion force contributions to the total surface free energy of wood, Wood Sci. Technol. 12 (1978) 63–74. https://doi.org/10.1007/BF00390011.

[8] D.G. Branco, C.A. Santiago, F.J. Oliveira, L. Cabrita, D. V Evtuguin, Surface properties of cork in relation to reactive washing, Colloids Surfaces A Physicochem. Eng. Asp. 624 (2021). https://doi.org/10.1016/j.colsurfa.2021.126762.

[9] T. Tribulová, F. Kacík, D. Evtuguin, I. Cabalová, Assessment of chromophores in chemically treated and aged wood by UV-vis diffuse reflectance spectroscopy, Cellul. Chem. Technol. 50 (2016) 659–667.

[10] J.-X. Sun, X.-F. Sun, R.-C. Sun, P. Fowler, M.S. Baird, Inhomogeneities in the chemical structure of sugarcane bagasse lignin, J. Agric. Food Chem. 51 (2003) 6719–6725. https://doi.org/10.1021/jf034633j.

[11] A. Lähdetie, T. Liitiä, T. Tamminen, A.S. Jääskeläinen, Reflectance UV-Vis and UV resonance Raman spectroscopy in characterization of kraft pulps, BioResources. 4 (2009) 1600–1619. https://doi.org/10.15376/biores.4.4.1600-1619.

[12] G. González-Gaitano, M.A.C. Ferrer, Definition of QC parameters for the practical use of FTIR-ATR spectroscopy in the analysis of surface treatment of cork stoppers, J. Wood Chem. Technol. 33 (2013) 217–233. https://doi.org/10.1080/02773813.2013.779715.

[13] C.P. Neto, J. Rocha, A. Gil, N. Cordeiro, A.P. Esculcas, S. Rocha, I. Delgadillo, J.D.P. De Jesus, A.J.F. Correia, ^{13}C Solid-state nuclear magnetic resonance and Fourier transform infrared studies of the thermal decomposition of cork, Solid State Nucl. Magn. Reson. 2040 (1995) 143–151.

[14] M.H. Lopes, A.S. Barros, C. Pascoal Neto, D. Rutledge, I. Delgadillo, A.M. Gil, Variability of cork from portuguese quercus suber studied by solid-state ^{13}C-NMR and FTIR spectroscopies, Biopolymers. 62 (2001) 268–277. https://doi.org/10.1002/bip.1022.

[15] M. V Bule, A.H. Gao, B. Hiscox, S. Chen, Structural modification of lignin and characterization of pretreated wheat straw by ozonation, J. Agric. Food Chem. 61 (2013) 3916–3925. https://doi.org/10.1021/jf4001988.

[16] N.A. Mamleeva, S.A. Autlov, N.G. Bazarnova, V. V. Lunin, Delignification of softwood by ozonation, Pure Appl. Chem. 81 (2009) 2081–2091. https://doi.org/10.1351/PAC-CON-08-10-11.

[17] J. Gierer, The Chemistry of Delignification - A General Concept - Part II, Holzforschung. 36 (1982) 55–64. https://doi.org/10.1515/hfsg.1982.36.2.55.

[18] J. Liao, S. He, L. Mo, S. Guo, P. Luan, X. Zhang, J. Li, Mass-production of high-yield and high-strength thermomechanical pulp fibers from plant residues enabled by ozone pretreatment, J. Clean. Prod. 296 (2021) 1–9. https://doi.org/10.1016/j.jclepro.2021.126575.

[19] C. Gomes, A. Fernandes, B. Almeida, The surface tension of cork from contact angle measurements, J. Colloid Interface Sci. 156 (1993) 195–201. https://doi.org/10.1006/jcis.1993.1099.

[20] J. Abenojar, A.Q. Barbosa, Y. Ballesteros, J.C. del Real, L.F.M. da Silva, M.A. Martinez, Effect of surface treatments on natural cork: surface energy, adhesion, and acoustic insulation, Wood Sci. Technol. 48 (2014) 207–224. https://doi.org/10.1007/s00226-013-0599-7.

Chapter 9

EVALUATION OF THE QUALITY PARAMETERS OF NATURAL CORK STOPPERS FROM DIFFERENT REACTIVE WASHING PROCESSES

Content

9.1. Introduction

Natural cork stoppers are widely used in the wine industry as a sealant for bottles due to their unique physical and chemical properties, which guarantee the maintenance of the liquid tightness with minimal cork-wine interaction [1–3].

The natural cork stopper after the reactive washing (RW) procedure must pass through subsequential processual steps before reaching the winery industry, such as branding and surface treatment with coating agents (food-grade paraffin and silicone formulations). All these stages belong to the finishing process of the stopper. The branding on the natural cork stoppers is done accordingly to the customer's specifications and could be performed by heat, laser, induction, or ink approved by FDA. In the surface treatment, the natural cork stoppers are treated with silicone and paraffin formulations, that remain deposited in the form of a thin layer (~50 μm thick) on the surface of the stopper [4,5].

The RW changes the surface of the cork stopper by reducing its hydrophobicity and increasing the surface wettability, which occurs due to the increase in the exposure of the hydrophilic moieties in the stopper surface [6,7]. The treatment of the natural cork stoppers with silicone and paraffin emulsions bridges the changes caused by the RW, where it acts as a surface smoother, reducing the friction, and consequently improving the insertion into and extraction from the bottle of the stopper. Additionally, the treatment of stoppers also prevents wine leaks and act as a barrier against stopper absorption [3] and migration. The silicone and paraffin have distinct roles on the surface, while the silicone reduces the friction index, paraffin blocks the oxidation, capillary progression, and the potential wine leaks [5].

Due to the increased demand for quality in the market, Amorim Cork, S.A. performs several industrial quality tests in each of the natural stopper final production flow that allows answering the quality requirements. The tests contemplate pH measurement, humidity analysis, the residual content of hydrogen peroxide, dust content, color migration through absorbance measurement, capillarity progression, visual appearance, absorption in the bottle, and extraction forces. The compliance with the specified limit values of each quality test assures the overall quality of the natural cork stoppers. Although the efficiency of the treatment is evaluated through extraction forces and capillarity progression, which are indirect methods to analyze the overall coating of the surface, these tests did not allow the identification of the agent coats (silicone and paraffin) on the stopper surface. Since the different RW procedures induce distinct changes on the surface of the stopper, the wettability of the surface towards the agents could be different for the silicone or paraffin, leading to accumulations of the treatment formulations in specific areas or a thin and irregular treatment layer. In this way, some authors used FTIR spectroscopy with attenuated total reflectance (ATR) to evaluate the

efficiency of the treatment on the natural cork stoppers [4,5,7]. This methodology does not require sample preparation, and it is an expeditious method that allows the distinction between silicon and paraffin, which allows the optimization of the treatment formulation either the surface is more wettable for the silicone or paraffin. In this way, the FTIR-ATR analysis of the natural cork stopper after the treatment process in stoppers with different RW provides information for the targeted modification of the dosage of the treatment formulations.

The main goal in this chapter was to evaluate the stoppers through the industrial quality tests in every stage in the final process flow of the production of the natural cork stopper, as well as understand the efficiency of the treatment on the surface of the stoppers from different RW.

9.2. Materials and Methods

Natural cork stoppers were supplied by Amorim Cork, S.A. (Santa Maria de Lamas, Portugal). The cork stoppers have a caliber of 49x24 mm (length x diameter) and belong to 1st class (medium class). The natural cork stoppers were washed on a laboratory scale with four different RW: conventional reactive washing (CRW), optimized conventional reactive washing (OCRW), ozone reactive washing (ORW), and ozone reactive washing plus optimized reactive washing (RW+). All the RW implemented were already dully described in Chapter 8.

After the RW, 106 natural cork stoppers from each RW batch were branded by heat, and then 100 natural cork stoppers suffered treatment with the coating formulations (industrially prepared food-grade silicone and paraffin emulsions). The branding and treatment of the cork stoppers were performed on a pilot scale in Amorim Cork, S.A. Once these procedures were completed 12 natural cork stoppers from each RW were bottled. In each step of the final natural cork stopper production (RW, branding, treatment, and stopper in bottle) were performed the common industrial quality tests, featured in Figure 9.1.

Figure 9.1- Final natural cork stoppers flow steps and industrial quality tests performed in each step.

Even though, the extraction forces are one of the quality tests to perform on the stage of the stopper in bottle that provides useful information about the treatment process efficiency, this analysis was not accomplished. Instead, after the treatment of the natural cork stoppers the surfaces (lateral and top) were evaluated through FTIR-ATR revealing the efficiency of the treatment step.

9.2.1. Industrial quality tests

According to Figure 9.1, the industrial quality tests englobe pH measurement, humidity analysis, hydrogen peroxide content, dust content, color migration through absorbance measurement, capillarity progression, visual appearance, liquid absorption by natural cork stoppers in bottle, and the extraction force evaluation.

9.2.1.1. pH measurement´

In a flask were placed 5 stoppers, in which was added 200 mL of distilled water. The flask was stirred for a period of 30 minutes, and the pH of the water solution obtained was measured.

9.2.1.2. Humidity

A total of 25 stoppers of each reactive washing batch were randomly chosen to measure its humidity, after a cool-down period of about 2 h. This analysis was performed in the center of the lateral cork stopper, using an Aqua-Boy analog moisture meter (KPM Moisture Meters ltd, New York, USA). From the industrial point of view, cork humidity must range between 4 and 8%, for values lower than this the stopper may lose its mechanical properties and values higher than 8% that can provide conditions for microbiological growth [8,9], and brightness reversion [10]. This test method is disclosed in ISO 9727-3:2007 [11].

9.2.1.3. Residual content of hydrogen peroxide (H_2O_2)

The residual content of hydrogen peroxide is measured in an RQflex 20 Reflectoquant instrument (Merck, Darmstadt, Germany). For this analysis, 3 stoppers were placed in a flask with 100 ml of distilled water, that were stirred for 1 h at 120 rpm. Then a Reflectoquant strip was dipped in the aqueous solution and put in the instrument that gives L value (Equation 9.1).

$$\text{Hydrogen peroxide residual content} = \frac{L \times 0.1}{3} \tag{9.1}$$

The result was an average of three measurements, and ideally, the hydrogen peroxide content must be lower than 0.1 mg/stopper. Levels of residual hydrogen peroxide higher than 0.1 mg/stopper may impact adversely on the level of sulfur dioxide in the wine [12]. This methodology is presented in ISO 21128:2006.

9.2.1.4. Dust content

Dust content corresponds to the solid residues that can leave the stopper surface and may transfer into wine when in the bottle. To measure the amount of powder released by the stoppers, 8 stoppers were placed in a flask with 200 ml of distilled water, which were left to stir for 30 min at 120 rpm. Once this time is completed, the cork stoppers were withdrawn, and the solution suffered vacuum filtration passing through a membrane filter (1.2 μm). The membrane filter was then dried in the oven at 103 ºC for 2 hours. Finally, the filters were transferred to a desiccator for the cool down and weighted. The dust content was determined gravimetrically and should not go over 3 mg/stopper. This procedure is established by the ISO 9727-7:2001.

9.2.1.5. Color migration- absorbance measurement

In this quality test, to 5 stoppers in a flask was added 250 mL of distilled water, which was left to stir for 1 hour at 120 rpm. When the stirring period was completed, the stoppers were removed from the liquid and the macerates were filtered to retain the suspended solids. The remaining solution is analyzed in a UV-vis spectrophotometer with a 10 mm cell, at 420 nm for the wavelength. The result of this parameter corresponds to an average of three measurements, and this value should be equal or inferior to 0.1 [11]. This methodology is disclosed in the standard ISO 10106:2003.

9.2.1.6. Capillarity progression

In a tray was poured red wine with a height of approximately 3 mm, in this tray were placed 6 stoppers chosen randomly with the cork stoppers tops in contact with the wine. After 24 h at 20 ºC, the cork stoppers are removed from the tray and the point where the wine reaches its highest high is measured from the contact line with the liquid. The capillarity progression is presented as an average of the percentage of the lateral surface of the six stoppers that was covered with wine.

9.2.1.7. Absorption in bottle

Bottles (750 mL capacity) were filled with red wine. The bottling process was carried out under routine industrial conditions. All bottles have a CETIE (Centre Technique International de l'Enbouteillage et du Conditionnement) neck with standardized inner dimensions. Cork stoppers were conditioned to 20 ºC and 65% relative humidity (RH) and weighted before bottling. After bottling, bottles were laid down and stored in a horizontal position at room temperature until the natural cork stopper was removed. Measurements were made after one week of cork-liquid contact. Absorption in the bottle was determined in all bottles by measuring the difference in weight of the natural cork stopper before bottling and after extraction. Each RW procedure used 12 bottles and the final value of absorption in the bottle corresponds to the average of the 12 natural cork stoppers.

9.2.2. FTIR-ATR spectroscopy

Fourier transform infrared- attenuated total reflectance (FTIR-ATR) spectra were collected on a Spectrum BX Perkin Elmer spectrophotometer (PerkinElmer, Waltham, Massachusetts, USA) with a resolution of 4 cm^{-1} and 128 scans in a transmittance mode. The spectrums were normalized at 1260 cm^{-1} band using OriginPro 2015 software (OriginLab Corporation, Northampton, Massachusetts, USA).

9.3. Results and Discussion

The industrial quality tests were performed in the steps of the final natural cork stoppers formation flow, such as reactive washing, branding, treatment, and stopper in the bottle.

9.3.1. Reactive washing

After each RW process were evaluated the pH, humidity, hydrogen peroxide residual content, dust content, color migration through absorbance measurement, and capillarity progression, being all the results from each analysis presented in Table 9.1.

Table 9.1- Industrial quality tests after each RW procedure implemented.

RW procedure	pH	Humidity (%)	H_2O_2 residual content (mg/stopper)		Dust content (mg/stopper)	Color migration Absorbance	Capillarity progression (%)
			24 horas	48 horas			
Without RW	5.6	5.5	0.00	0.00	0.77	0.08 ± 0.008	16.9
CRW	5.7	6.8	0.73	0.94	0.26	0.07 ± 0.014	43.2
OCRW	5.5	5.8	0.84	1.07	0.16	0.06 ± 0.022	48.6
ORW	4.0	5.0	0.00	0.00	0.76	0.14 ± 0.023	34.4
RW+	5.3	5.4	0.90	0.94	0.23	0.22 ± 0.035	30.0
Allowed range of values	n.d.	4.0-8.0	<0.1	<0.1	<3.00	≤0.10	≤25.0

According to Table 9.1, after RW the natural cork stoppers were slightly acidic, being the ORW bleached stoppers the ones with lower pH (4.0), this is due to the reaction between ozone and the structural components of cork, leading to the formation of carboxylic acids that may remain unbounded or loosely bounded in the surface of the cork stopper and when in contact with water released themselves, giving rise to a water solution slightly acidic [13].

All the stoppers were in range with the allowed values for the humidity levels. On the other hand, the residual content of hydrogen peroxide revealed higher values than those allowed, with the exception of the stoppers without RW and ORW (both with 0.00 mg/stopper), which could be expected because these RW processes did not use hydrogen peroxide. The higher content of the hydrogen peroxide in the stoppers could be due to the lower centrifugation power of the laboratory reactor, and in this way the hydrogen peroxide may remain on the stopper surfaces capillaries, being released when in contact with water and forced stirring.

The dust content showed that all the RW applied guaranteed values inferior to 3.00 mg/stopper, which is the limit value allowed. The dust content in stoppers without RW and ORW was very similar

(0.77 and 0.76 mg/stopper) and higher than the other RW, which is explained by the absence of any type of water washing in both RW.

The color migration is established by the absorbance measurement at 420 nm, which is related to the violet in the visible spectrum. Table 9.1 showed that ORW and RW+ had absorbance values (0.14 and 0.22, respectively) superior to the value allowed (0.10), revealing that the stoppers from these RW when in contact with water may release some colored compounds. As for the capillarity progression, all the RW procedures revealed values higher than the limit value stipulated (25.0%), the only stoppers that respect the range values allowed for the capillarity progression are the ones without RW, and this is due to the high suberin content on the surface of the natural stopper that did not suffer a change in its content [2,14,15].

9.3.2. Branding

Once all the stoppers suffered the different RW procedures, the natural cork stoppers were branded. During this procedure, no major difficulties were found by the specialized operator, which indicates good surface stability for this type of process step. In this stage of the production of natural cork stoppers two industrial quality tests were applied: the visual appearance (Figure 9.2), and hydrogen peroxide residual content (Table 9.2).

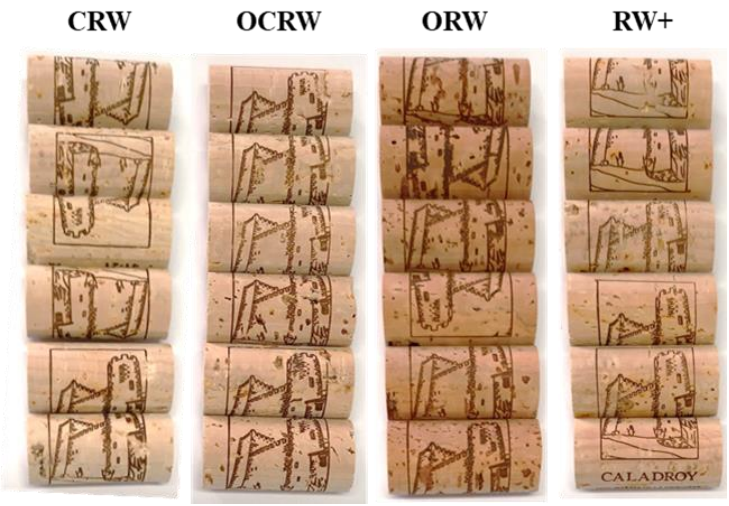

Figure 9.2- Visual appearance of natural cork stoppers after CRW, OCRW, ORW, and RW+, and subsequent branding by heat.

Figure 9.2 revealed that there is no significant difference in terms of the branding quality, the surface of the natural cork stoppers showed a good branding homogeneity in stoppers from the same RW, but also between stoppers from different RW.

Table 9.2- Residual content of hydrogen peroxide of natural cork stoppers after different RW procedures and subsequent branding by heat.

RW procedure	H_2O_2 residual content (mg/stopper)
CRW	0.03
OCRW	0.02
ORW	0.00
RW+	0.08

According to Table 9.2, in this step of the production occurs a significant decrease in the residual content of hydrogen peroxide in relation to values obtained after RW, this is due to the period of stabilization of the stoppers between the RW and the branding. In fact, all the stoppers from the different RW procedures had values inferior to 0.1 mg/stopper (Table 9.2), respecting the quality parameters of the industry.

9.3.3. Treatment

The treatment step in the natural cork stopper production flow is essential to guarantee the insertion and extraction of the cork stopper in the bottle, and at the same time minimize the wine-cork stopper interactions. In the industry after the treatment step, the stoppers are evaluated through pH measurement, humidity evaluation, dust content, color migration, and capillarity progression (Table 9.3).

Table 9.3- Industrial quality tests performed after the treatment step in stoppers with different RW.

RW procedure	pH	Humidity (%)	Dust content (mg/stopper)	Color migration Absorbance	Capillarity progression (%)
CRW	5.9	4.9	0.12	0.07 ± 0.009	12.5
OCRW	5.9	5.0	0.21	0.06 ± 0.004	15.3
ORW	5.2	4.5	0.61	0.13 ± 0.038	3.5
RW+	5.3	4.8	0.13	0.20 ± 0.026	2.1
Allowed range values	n.d.	4.0-8.0	<3.00	≤0.10	≤25.0

The pH values ranged from 5.2 to 5.9, occurring a slight increase for the CRW, OCRW, and ORW, while maintaining the pH value of the RW+. On the other hand, the humidity, even though continued in the range of the values allowed, suffered a small decrease. This could be explained by the period of time between the steps of the process that allowed the evaporation of the water present in the natural stoppers and the stabilization of the humidity.

The dust content (Table 9.3) in all the RW was inferior to the limit value specified (3.00 mg/stopper). Comparing the values obtained with the dust content after the RW step, it is observed a decrease in this value for almost all the RW, with an exception for the OCRW, which could indicate

lower wettability of the stopper surface towards silicone and paraffin that could be loosely placed on the stopper surface, then in contact with water under stirring leaves the surface and lead to a higher value of dust content.

The absorbance values were very similar to the ones obtained after RW, only with a slight decrease for the ORW and RW+, which may indicate that the application of the coating agents did not significantly influence this evaluation. In terms of capillary progression, all the samples revealed values lower than the limit required, providing information about the good efficiency of the treatment process. The results obtained may suggest that the stoppers from the RW+, followed by the ORW were the ones with greater treatment efficiency, since these are the stoppers with lower capillarity progression, with 2.1 and 3.5%, respectively.

9.3.4. Stopper in the bottle

The stage of the stopper in the bottle is essential to evaluate the efficiency of the treatment with the coating agents (silicone and paraffin of food grade). In this step, it is commonly analyzed the extraction forces and absorption of liquid by the stopper (Figure 9.3).

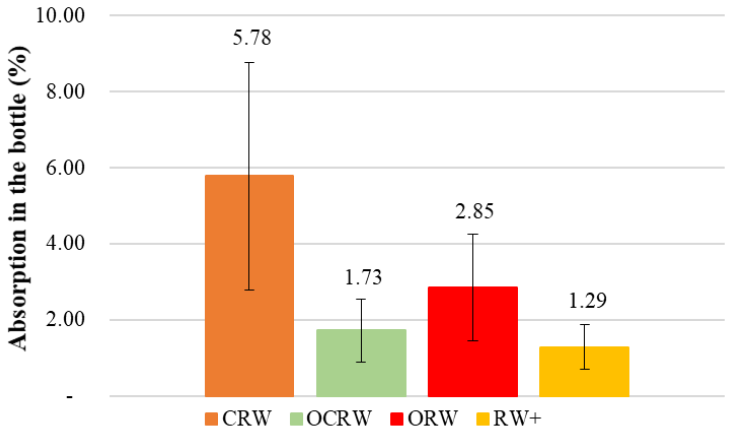

Figure 9.3- Average values obtained for absorption of wine by natural cork stoppers with different RW.

According to Figure 9.3, the stoppers with higher absorption in the bottle were the ones coming from the CRW (5.78%), on the other hand, the stoppers that suffered the optimized RW such as OCRW and RW+, revealed the lower values of absorption in the bottle (1.73 and 1.29%, respectively). The treatment stage is especially important to reduce the absorption in the bottle since the natural cork stopper, the direction of the fluid flow matches with the longitudinal axis of the cork tissue, being parallel to the growth layers and perpendicular to the lenticels channels [4]. The absorption values obtained for the CRW revealed the same tendency as the ones found in the literature, however, the absorption values from the others RW procedure had a lower absorption tendency, which may indicate a greater treatment efficiency in these stoppers [3,16].

Although this test can analyze indirectly the efficiency of the surface coating, it did not distinguish between the content of the two components applied, silicone and paraffin. Hence, to complement the information obtained by the absorption of liquid by the stopper, it was used surface analysis by FTIR-ATR, displayed in Figure 9.4.

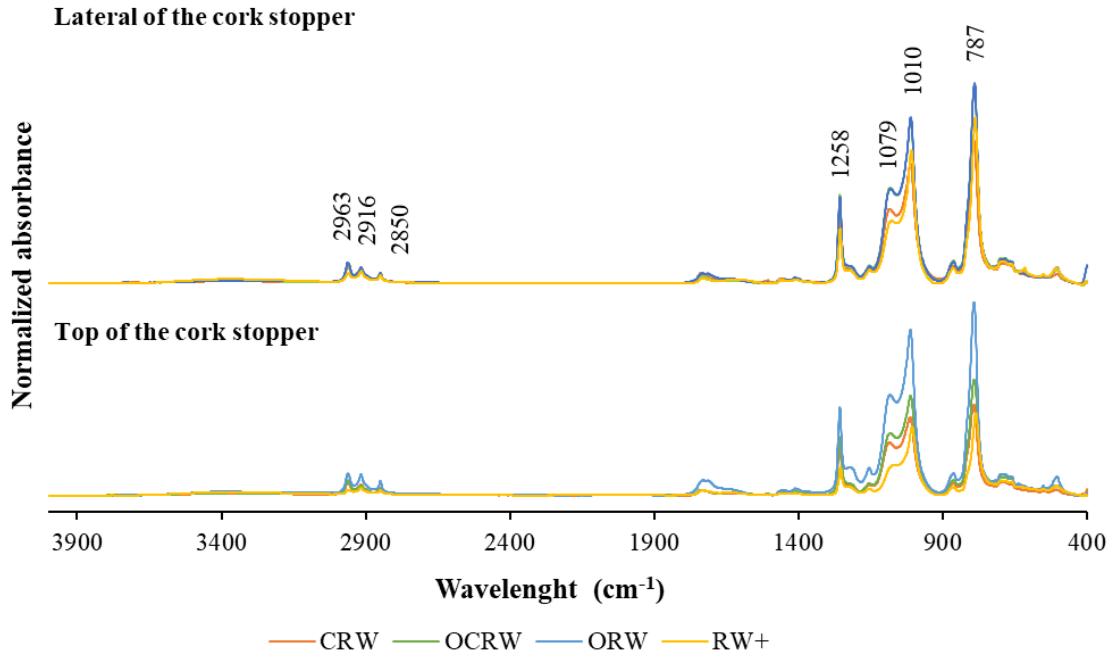

Figure 9.4- FTIR-ATR spectra of the lateral and top of the cork stoppers after the treatment with coating agents (food-grade silicone and paraffin formulations) in natural cork stoppers with different RW procedures.

The spectrums presented in Figure 9.4 is distinguished seven main peaks that are related to the coating agents. The bands at 2963, 2916, and 2850 cm^{-1} are less specific bands related to C-H asymmetric stretch in CH_3, C-H asymmetric stretch in CH_2, and C-H symmetric stretch in CH_2, respectively. However, the bands 2916 and 2850 cm^{-1} are more dominant for the paraffin [4]. On the other hand, the bands at 1258 cm^{-1} ($Si(CH_3)_nO$ symmetric stretch), 1079 cm^{-1} (Si-O-Si symmetric stretch), 1010 cm^{-1} (Si-O stretch), and 787 cm^{-1} (Si-C bonding) are associated with the groups of silicone.

Contrary to what was found in the literature the FTIR-ATR spectrum did not show the typical bands of the cork structural components with significant absorbance, which may indicate a thick, regular and non-fractured treatment layer since the FTIR-ATR analysis has a profundity of 0.5 to 5 µm [4,5,7].

To better understand the quality of the treatment process it was analyzed the values of absorbance in the main seven bands already identified, associating the absorbance of the bands 2916 and 2850 cm^{-1} (Abs2916 and Abs2850, respectively) to paraffin and the others to silicone (Table 9.4).

Table 9.4- Absorbance values for the selected bands of the FTIR-ATR spectrum of stoppers with distinct RW.

RW procedure		Abs2963	Abs2916	Abs2850	Abs1258	Abs1079	Abs1010	Abs787
Lateral of the cork stopper	**CRW**	0.0745	0.0680	0.0516	0.2473	0.2634	0.4140	0.4827
	OCRW	0.0797	0.0579	0.0408	0.3040	0.3276	0.5540	0.6677
	ORW	0.0754	0.0617	0.0412	0.2950	0.3198	0.5586	0.6718
	RW+	0.0477	0.0552	0.0420	0.1938	0.2209	0.4511	0.5559
Top of the cork stopper	**CRW**	0.0610	0.0525	0.0406	0.1814	0.1898	0.2716	0.3053
	OCRW	0.0602	0.0437	0.0322	0.2064	0.2158	0.3394	0.3921
	ORW	0.0757	0.0759	0.0505	0.2966	0.3368	0.5501	0.6317
	RW+	0.0214	0.0305	0.0226	0.0947	0.1011	0.2193	0.2592

According to Table 9.4, independently of the band, the lateral of the cork stopper has higher values of absorbance than the top of the cork stopper for the stoppers that came from CRW, OCRW, and RW+. All these RW have in common the use of hydrogen peroxide as a bleaching agent in at least one stage, revealing that in these RW occurs a greater degradation of the lateral when compared with the top of the cork stopper, increasing the exposure of the hydrophilic structural polymers (polysaccharides), which leads to an increase of the wettability of the lateral towards the coating agents [6]. Contrarily, the stoppers from the ORW had higher values of absorbance for the top than for the lateral, except for the bands 1010 and 787 cm^{-1}.

The bands associated with paraffin (2916 and 2850 cm^{-1}) were the ones with lower absorbance values when compared with the bands related to silicone. This fact may reveal a greater wettability of the surface of the stoppers with silicone than with paraffin. The values of absorbance showed the same tendency for the lateral and the top of the cork stopper, being highest for the ORW, followed by OCRW, CRW, and at last the RW+. However, as revealed by the capillarity progression and the absorption in the bottle, the stoppers with lower values are the ones from the RW+, which may indicate that even though this RW is the one with lower absorbance values associated with paraffin and silicone, the treatment efficiency was better for this RW. On the other RW, the absorbance values are higher, but the dust content is also higher, which may indicate that the quantities of the treatment applied were than necessary, creating a thicker treatment layer than what is required that when in contact with water may be released. In this way, the treatment in RW could be optimized, by diminishing the quantities used, reducing the cost associated.

Since the stoppers from the different RW processes respect the industrial quality requirements while reducing costs and time associated with RW and may allow the optimization of the treatment subsequent process, the reactive washings in the study are in conditions to be studied on a higher scale (pilot scale), increasing the number of stoppers from 15 to 500 stoppers. The pilot-scale reactor

was built especially for this effect and can perform the RW with ozone and the conventional reagents in the same equipment (Figure 9.5).

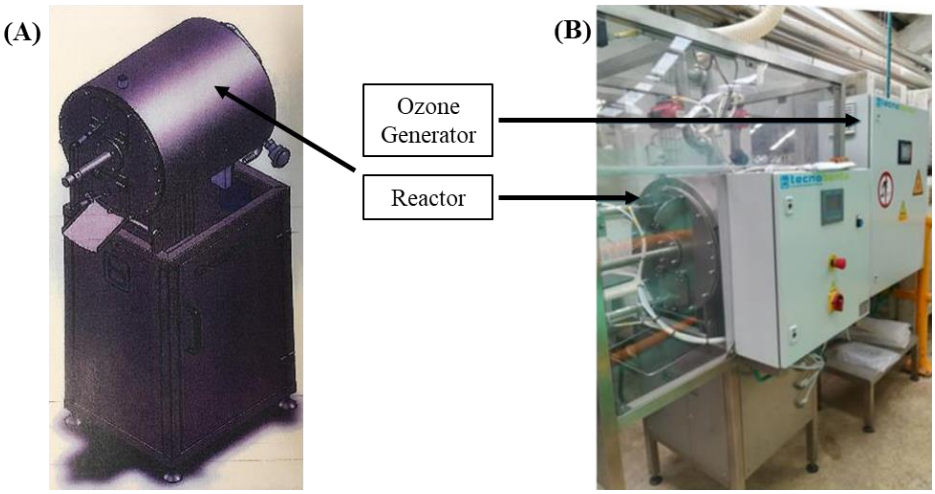

Figure 9.5-Equipament in pilot scale (500 stoppers) for the optimized RW procedures. (A) Preliminary reactor design; (B) Equipment for the RW implement in the industry.

Before starting the study of the optimized RW procedures on a pilot scale it was necessary to verify the instrument conditions in terms of temperature and flow profiles, as well as the centrifugal capacity, dry capacity, and ozone destruction, among other factors. However, the preliminary results obtained in the pilot-scale showed promising paths for the optimization of the RW.

9.4. Conclusions

The natural cork stoppers after completing the RW in the flow production have subsequential processual steps, such as branding and the surface treatment. To guarantee the quality of the stoppers in all the final steps of the production flow the industry implemented the analysis of several quality tests. These quality tests measure the pH, humidity, residual content of hydrogen peroxide, dust content, color migration, capillarity progression, absorption of wine by the stoppers, and extraction forces, depending on the production stage where the stoppers come from.

After the RW, the quality tests demonstrated that the optimized RW had similar values with CRW, having values higher than the allowed for the residual content of hydrogen peroxide, color migration, and capillarity progression. However, after the branding, all the stoppers from the different RW showed a decrease in the residual content of hydrogen peroxide to values inferior to the limit allowed (0.1 mg/stopper). The treatment of the surface revealed a thick and regular layer of the coating agents (food-grade silicone and paraffin formulations), since the FTIR-ATR spectrum there was not present the characteristic bands of the cork, and the absorption of wine by the cork stoppers revealed better values for the optimized RW than for the CRW.

The FTIR-ATR analysis allowed to verify that the lateral is more wettable for the agent coats than the top of the stoppers, independently of the RW procedure that they come from, in addition, it was also proven that silicone has a higher surface coverage than the paraffin. These facts may indicate that on the optimized RW, the treatment formulation could be optimized, reducing the costs involved in this step.

The assurance of the quality parameters showed promising results to go forward and study the optimized RW on a pilot scale, increasing from 15 to 500 natural cork stoppers. This study still is in a preliminary phase, however, shows promising pathways for the RW.

9.5. References

[1] H. Pereira, Variability of the chemical composition of cork, BioResources. 8 (2013) 2246–2256. https://doi.org/10.15376/biores.8.2.2246-2256.

[2] H. Pereira, Chemical composition and variability of cork from *Quercus suber* L., Wood Sci. Technol. 22 (1988) 211–218. https://doi.org/10.1007/BF00386015.

[3] J.R. González-Adrados, F. González-Hernandez, J.L. García de Ceca, M.J. Cáceres-Esteban, M.C. García-Vallejo, Wine absorption by cork stoppers, Spanish J. Agric. Res. 6 (2008) 645–649. https://doi.org/10.5424/sjar/2008064-356.

[4] C. Ortega-Fernández, J.R. González-Adrados, M.C. García-Vallejo, R. Calvo-Haro, M.J. Cáceres-Esteban, Characterization of surface treatments of cork stoppers by FTIR-ATR, J. Agric. Food Chem. 54 (2006) 4932–4936. https://doi.org/10.1021/jf0529823.

[5] G. González-Gaitano, M.A.C. Ferrer, Definition of QC parameters for the practical use of FTIR-ATR spectroscopy in the analysis of surface treatment of cork stoppers, J. Wood Chem. Technol. 33 (2013) 217–233. https://doi.org/10.1080/02773813.2013.779715.

[6] D.G. Branco, C.A. Santiago, F.J. Oliveira, L. Cabrita, D. V Evtuguin, Surface properties of cork in relation to reactive washing, Colloids Surfaces A Physicochem. Eng. Asp. 624 (2021). https://doi.org/10.1016/j.colsurfa.2021.126762.

[7] J.R. Gonzalez-Adrados, M.C. Garcia-Vallejo, M.J. Caceres-Esteban, J.L. Garcia De Ceca, F. Gonzalez-Hernandez, R. Calvo-Haro, Control by ATR-FTIR of surface treatment of cork stoppers and its effect on their mechanical performance, Wood Sci. Technol. 46 (2012) 349–360. https://doi.org/10.1007/s00226-011-0403-5.

[8] J.M.C. Pires, H. Pereira, M. V. San-Romão, Study of humidity and water activity of cork slabs during cork stopper manufacturing process- Preliminary results, Ciência Téc. Vitiv. 22 (2007) 15–20.

[9] J.A. Considine, E. Frankish, Microbiology and Methods, in: A Complet. Guid. to Qual. Small-Scale Wine Mak., Academic Press, 2014: pp. 79–95. https://doi.org/10.1016/B978-0-12-408081-2.00006-8.

[10] P.E.G. Loureiro, M.R.M. Domingues, A.J.S. Fernandes, M.G.V.S. Carvalho, D. V. Evtuguin, Discriminating the brightness stability of cellulosic pulp in relation to the final bleaching stage, Carbohydr. Polym. 88 (2012) 726–733. https://doi.org/10.1016/j.carbpol.2012.01.024.

[11] Confédération Européenne Du Liège, Código internacional das práticas rolheiras, (1999) 1–22.

[12] L. Filipe-Ribeiro, S. Rodrigues, F.M. Nunes, F. Cosme, Reducing the negative effect on white wine chromatic characteristics due to the oxygen exposure during transportation by the

deoxygenation process, Foods. 10 (2021). https://doi.org/10.3390/foods10092023.

[13] M. Ek, G. Gellerstedt, G. Henriksson, Pulping Chemistry and Technology, 3rd Ed., De Gruyter, 2009.

[14] H. Pereira, Studies on the chemical composition of virgin and reproduction cork of Quercus suber L ., An. Do Inst. Super. Agron. 25 (1981) 17–25.

[15] E. Conde, E. Cadahía, M.C. García-Vallejo, J.R. González-Adrados, Chemical characterization of reproduction cork from spanish *Quercus suber*, J. Wood Chem. Technol. 18 (1998) 447–469. https://doi.org/10.1080/02773819809349592.

[16] M.E. Rosa, M.A. Fortes, Water absorption by cork, Wood Fiber Sci. 25 (1993) 339–348.

Chapter 10

CONCLUSIONS AND PERSPECTIVES

Content

10.1.Conclusions

The main goals of this work were related to the study on the reactive washing of natural cork stoppers aiming to contribute both to the fundamental and applied aspects of this process. Accordingly, this study envisaged the study of the structural features of macromolecular components in natural cork stoppers, as well as the changes on the surface properties of natural cork stoppers during the reactive washing. These studies provided fundamental knowledge for the critical analysis of the conventional reactive washing and the evaluation of ozone as a new bleaching agent for the reactive washing.

This study revealed that the natural cork stoppers are mainly composed of suberin (44.0%), followed by cellulose (17.2%), lignin (16.2%), and hemicelluloses (6.6%). Suberin is mainly composed of aliphatic fatty acids, hydroxy fatty acids, and dicarboxylic acids. Cork lignin is of SG type, with a H:G:S molar ratio of isolated cork dioxane lignin (cork DL) of 5:72:23, and a moderate molecular weight of 2500 Da being structurally associated with procyanidins and probably with products derived from suberin and polysaccharides. The most abundant ether-linked structures in cork lignin are the *β*-O-4' (38 mol %) and 4-O-5' (5 mol %). Cork cellulose is a typical cellulose I polymorph, with a degree of crystallinity of 70.3% and an average crystallite width of 3.5 nm. Among hemicelluloses, xylan is the most abundant contributing to 5.9% of cork weight. The xylan isolated is a typical *O*-acetyl-(4-*O*-methyl-β-D-glucurono)xylan(heteroxylan) with randomly acetylated backbone (DS 0.64) and substituted at *O*-2 by terminal 4-*O*-methyl-α-D-glucuronosyl (MeGlcA) /α-D-glucuronosyl (GlcA) residues with a Xyl*p*:UA molar ratio of 13:1.

The anisotropy in the surface properties and the roughness of the top and lateral of natural cork stoppers was explained by the difference in the exposure of the phellogen cell wall layers and as a result of mechanical damage that occurred during the stopper production. Image and surface chemical analyses revealed a greater exposure of the internal suberin-rich cell wall layers on the lateral than on the top of the stoppers. At least partially, this is a result of the cork cell wall crumpling during punching of the stoppers from strips. In addition, the lateral of the stoppers had *ca.* 30% less roughness compared to the top surface. These differences in the surface chemical composition and topology explain the higher polarity index of the top surface that predetermines it better wettability with water and hydroalcoholic solutions than the lateral surface of the stopper. The harsh conditions of the conventional reactive washing leads to the significant degradation of suberin on the cork surface. Consequently, the surface polarity index increases due to the greater exposure of the hydrophilic moieties of the degraded suberin and hydrophilic structural polymers. These findings provided the fundamentals for the targeted modification of the cork stopper towards controlled

wettability, also regarding the improvement of reactive washing operations and strategies of surface coating.

The optimization of the conventional reactive washing was carried out using a three-level and four-factor fractional factorial experimental design and response surface methodology to develop mathematical models for ISO brightness response while evaluating the effect of four reactive washing process independent variables (hydrogen peroxide and sodium hydroxide concentrations, oxidation time, and washing water volume). The results revealed that hydrogen peroxide concentration is the one that most influences the response (brightness of cork stoppers), followed by sodium hydroxide concentration. The evaluation of the model allowed the optimization of the reagents profile, with a reduction of 37% for hydrogen peroxide, and 33% for NaOH and washing water volume, respectively, without changing the final appearance of the cork stoppers.

The first systematic study on the implementation of ozone as a bleaching agent for natural cork stoppers was performed. With only 15 minutes of ozone reactive washing, the ozone treatment allowed the best brightness gaining results with a temperature of 70ºC, a rotation velocity of 120 rpm, and an inlet oxygen flow of 50 L/h (production of 1.8 g/h of ozone). Ozone is effective on the degradation of chromogen and chromophore structures, as revealed by UV-vis DR analysis. FTIR-ATR analysis showed that ozone degrades cork components (mainly lignin, polyphenolics and polysaccharides) with the formation of new oxidized moieties. HS-SPME/GC-MS analysis demonstrated the formation of volatile ketones, aldehydes, and carboxylic acids after ozone treatment, increasing the odor perception. After ozone reactive washing, the free surface energy was increased, but the polarity index decreased leading to a greater wettability of the surface with hydroalcoholic solutions. This is a consequence of the degradation of unsaturated structures in lignin and polyphenolics and a greater exposure of suberin moieties.

The combination of ozone treatment and the conventional reactive washing with H_2O_2 was proposed to improve the economic feasibility and the quality performance of cork stoppers. The effect of the preliminary ozone stage on the conventional reactive washing (CRW) was studied and the novel reactive washing sequence was optimized on a laboratory scale. The response (ISO brightness) was evaluated using three-level and four factorial fractional factorial experimental design and response surface methodology involving four independent variables of CRW (hydrogen peroxide and sodium hydroxide concentration, oxidation time and washing water volume). The validated model revealed that the sodium hydroxide is the one with higher significance on the response. The model allowed the optimization of the reactive washing by reducing the hydrogen peroxide concentration from 35% to 15% (*ca.* 60% reduction), oxidation time from 33 min to 18min (*ca.* 45% reduction), and washing water volume from 150 to 75 mL per 10 stoppers (50% reduction).

The surface changes in the lateral and top of the natural cork stoppers after the conventional reactive washing (CRW), optimized conventional reactive washing (OCRW), ozone reactive washing (ORW), and ozone reactive washing plus optimized conventional reactive washing (RW+) were compared. The surface color parameters (ISO brightness and CIElab color parameters) demonstrated the better brightening efficiency of the optimized RW (OCRW and RW+) in relation to the CRW. UV-vis DR spectroscopy revealed the decrease in chromophore structures (vis-active compounds) and chromogen structures (vis-inactive compounds) in optimized RW trials. The FTIR-ATR spectroscopy confirmed the highest degradation of suberin on the surface of the stoppers with CRW, while the optimized RW, OCRW and RW+, showed less degradation and preservation of suberin on stopper surfaces, respectively. All the surface modifications lead to an increase in the surface wettability towards hydroalcoholic solutions.

The stopper behavior from the reactive washing process and the subsequent industrial steps, branding and treatment with food grade silicone and paraffin formulations, in terms of quality parameters commonly used in the industry was evaluated. After the RW, the quality parameters demonstrated that the optimized RW had similar values with CRW. However, after the branding, all the stoppers from the different RW showed a decrease in the residual content of hydrogen peroxide to values inferior to the limit allowed (0.1 mg/stopper). The treatment of the surface revealed a thick and regular layer of the coating agents (food-grade silicone and paraffin formulations), since the FTIR-ATR spectrum there was not present the characteristic bands of the cork, and the absorption of wine by the cork stoppers revealed better values for the optimized RW than for the CRW. In general, similar results were obtained when comparing basic quality parameters of the stoppers from optimized RW to the conventional RW at the lower consumption of reagents, less process time and better functional performance of stoppers.

10.2.Perspectives

As referred above the main goals of this thesis were the study of the conventional reactive washing and the implementation of ozone as a bleaching agent for the natural cork stoppers. In this way it would be interesting:

1. The study of the optimized reactive washing processes in pilot scale (500 stoppers).
2. The implementation of the optimized reactive washing processes in industrial scale (20000 and 100000 stoppers).
3. The analysis of the compounds that have the ability to migrate from the natural cork stoppers to hydroalcoholic solutions mimicking the alcoholic beverages from the market and study the influence of reactive washing on the quantity and quality of the compounds.
4. The application of the optimized reactive washing process in other types of cork stoppers.

Appendices

A. Cork pyrograms

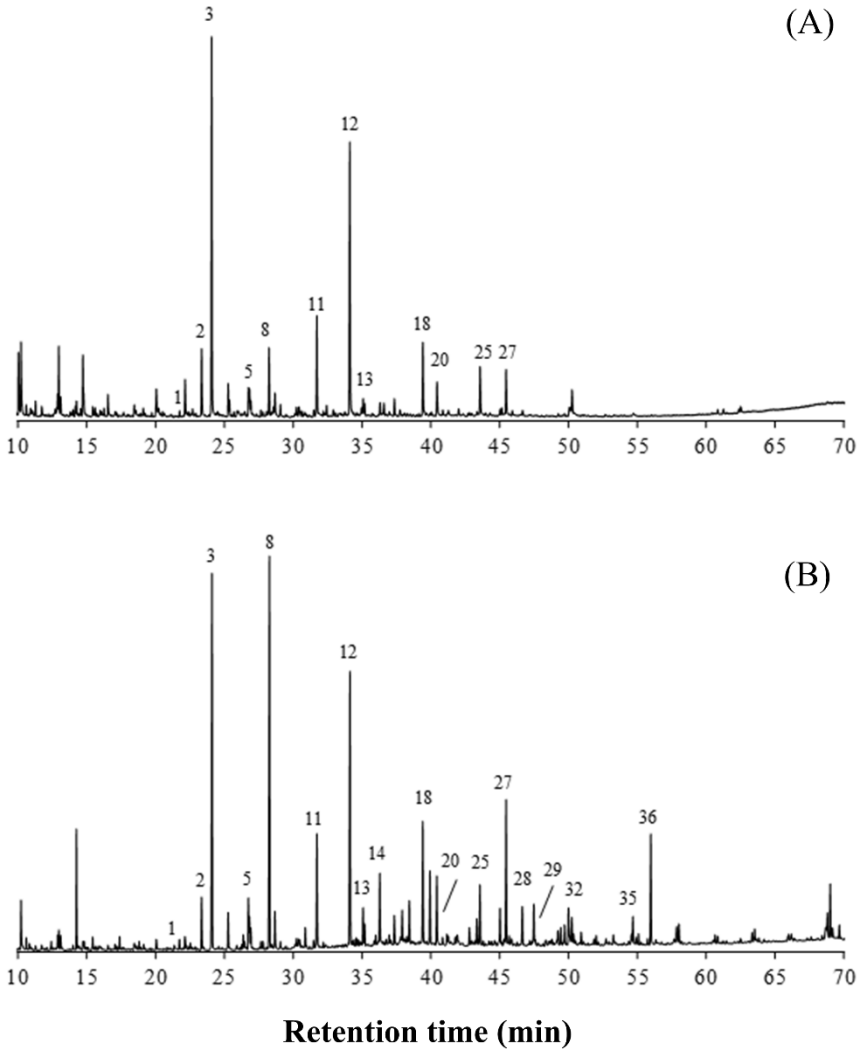

Figure A.1 - Py-GC/MS chromatogram of the dioxane lignin isolated from *Quercus suber* L.(B) and desuberized cork (A). The designations and relative abundances of the released lignin-derived compounds are listed in Table 3.3.

B. Supplementary material of Chapter 4

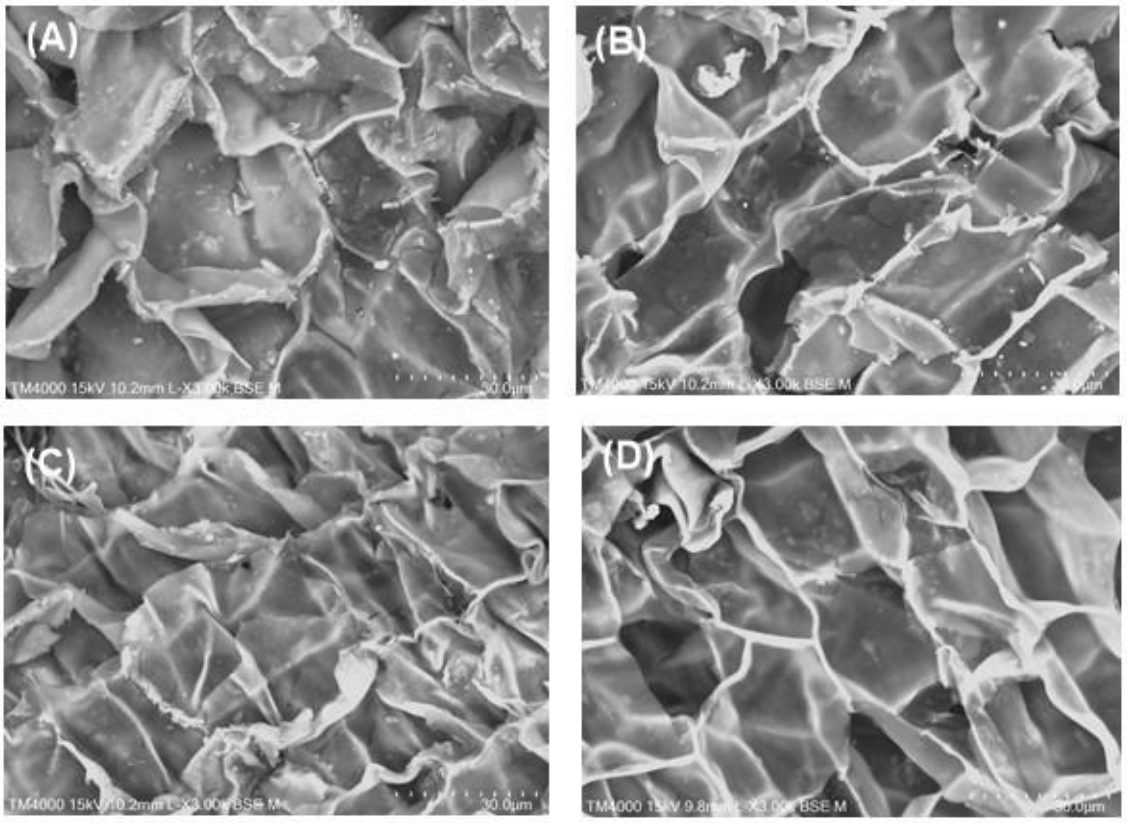

Figure B.1- SEM micrograph images (3000x) of the lateral and top of cork stopper surfaces before (A and C, respectively) and after (B and D, respectively) the RW.

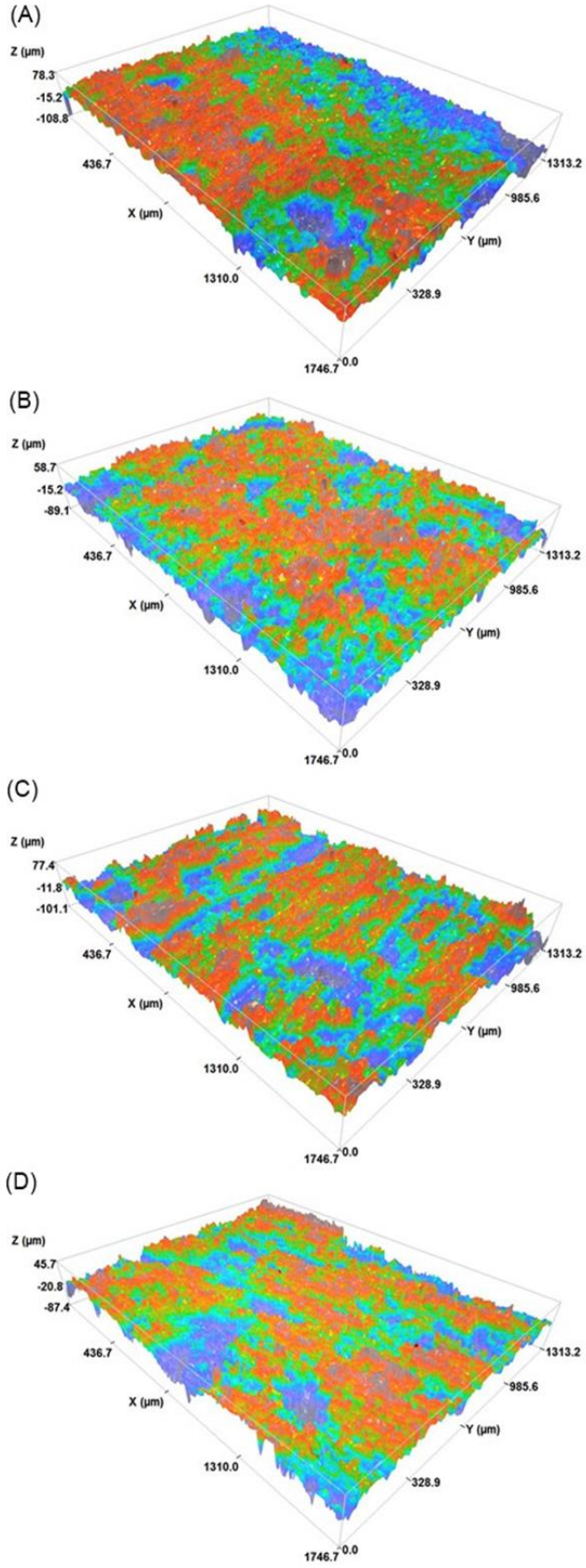

Figure B.2- 3D surface topology profiles of the lateral and top surface of the stopper before (A and C, respectively) and after (B and D, respectively) the RW.

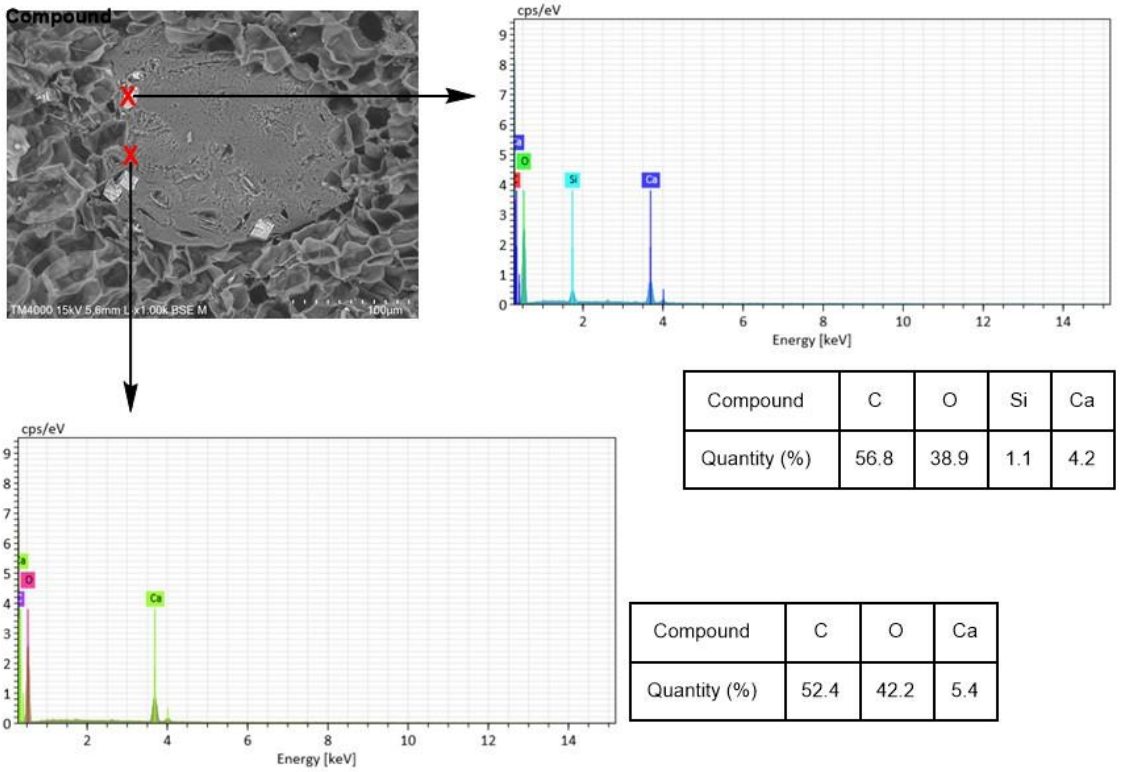

Compound	C	O	Si	Ca
Quantity (%)	56.8	38.9	1.1	4.2

Compound	C	O	Ca
Quantity (%)	52.4	42.2	5.4

Figure B.3- SEM-EDS analysis of cork stopper surface.